The Dissertation Committee for Alireza Mollaei Certifies that this is the approved version of the following dissertation:

Forecasting of Isothermal Enhanced Oil Recovery (EOR) and Waterflood Processes

Committee:

Larry W. Lake, Supervisor

Mojdeh Delshad, Co-Supervisor

Tadeusz W. Patzek

Thomas F. Edgar

Leon S. Lasdon

Forecasting of Isothermal Enhanced Oil Recovery (EOR) and Waterflood Processes

by

Alireza Mollaei, B.S.; M.S.

Dissertation

Presented to the Faculty of the Graduate School of

The University of Texas at Austin

in Partial Fulfillment

of the Requirements

for the Degree of

Doctor of Philosophy

The University of Texas at Austin

December 2011

Dedication

To God, for all of his bounties, blessings and lights he spread in my life,

To my family, for their permanent support and passion,

To whoever finds this work useful.

Acknowledgements

I would like to first acknowledge my supervisors, Dr. Larry W. Lake and Dr. Mojdeh Delshad for their guidance, encouragement, support and advice. I also thank the graduate committee members, Dr. Thomas F. Edgar, Dr. Leon S. Lasdon and Dr. Tadeusz W. Patzek for their helpful comments and suggestions.

I am grateful to Chevron-UT EOR alliance for financial and technical support of this work. Additionally, I would like to acknowledge faculty and staffs of the University of Texas at Austin and department of petroleum and geosystems engineering for providing services and supports. I extend my acknowledgment to CMG Simulation Company, UTCHEM simulator developers for reservoir simulations, Dr. Garry A. Pope for providing laboratory coreflooding data and Panos Andonyadis for providing EOR field/pilot data.

I appreciate all of the people who helped me in any ways during this work. My special thanks to my family who inspired and encouraged me to better accomplish my graduate studies.

Forecasting of Isothermal Enhanced Oil Recovery (EOR) and Waterflood Processes

Alireza Mollaei, Ph.D.

The University of Texas at Austin, 2011

Supervisors: Larry W. Lake

Co-Supervisor: Mojdeh Delshad

Oil production from EOR and waterflood processes supplies a considerable amount of the world's oil production. Therefore, the screening and selection of the best EOR process becomes important. Numerous steps are involved in evaluating EOR methods for field applications. Binary screening guides in which reservoirs are selected on the basis of reservoir average rock and fluid properties are consulted for initial determination of applicability. However, quick quantitative comparisons and performance predictions of EOR processes are more complicated and important than binary screening that are the objectives of EOR forecasting.

Forecasting (predicting) the performance of EOR processes plays an important role in the study, design and selection of the best method for a particular reservoir or a collection of reservoirs. In EOR forecasting, we look for finding ways to get quick quantitative results of the performance of different EOR processes using analytical model/s before detailed numerical simulations of the reservoirs under study. Although numerical simulation of the reservoirs is widely used, there are significant obstacles that restrict its applicability. Lack of necessary reservoir data and time consuming

computations and analyses can be barriers even for history matching and/or predicting EOR/waterflood performance of one reservoir.

There are different forecasting (predictive) models for evaluation of different secondary/tertiary recovery methods. However, lack of a general purpose EOR/waterflood forecasting model is unsatisfactory because any differences in results can be caused by differences in the model rather than differences in the processes. As the main objective of this study, we address this deficiency by presenting a novel and robust analytical-base general EOR and waterflood forecasting model/tool (UTF) that does not rely on conventional numerical simulation. The UTF conceptual model is based on the fundamental law of material balance, segregated flow and fractional flux theories and is applied for both history matching and forecasting the EOR/waterflood processes. The forecasting model generates the key results of isothermal EOR and waterflooding processes including variations of average oil saturation, recovery efficiency, volumetric sweep efficiency, oil cut and oil rate with real or dimensionless time.

The forecasting model was validated against field data and numerical simulation results for isothermal EOR and waterflooding processes. The forecasting model reproduced well ($R^2 > 0.8$) all of the field data and reproduced the simulated data even better.

To develop the UTF for forecasting when there is no injection/production history data, we used experimental design and numerical simulation and successfully generated the in-situ correlations (response surfaces) of the forecasting model variables. The forecasting model variables were proven to be well correlated to reservoir/recovery process variables and can be reliably used for forecasting. As an extension to the abilities of the forecasting model, these correlations were used for prediction of volumetric sweep efficiency and missing/dynamic pore volume of EOR and waterflooding processes.

Table of Contents

List of Tables xii

List of Figures xiv

Chapter 1: INTRODUCTION 1

1.1- Statement of the Problem 1

1.2- Research Objectives 4

Chapter 2: LITERATURE REVIEW 6

2.1- Recovery Stages 6

2.1.1- Primary 6

2.1.2- Secondary 7

2.1.3- Tertiary 8

2.2- Isothermal Enhanced Oil Recovery Processes 10

2.2.1- Chemical EOR Processes 14

2.2.1.1- Polymer Flooding 14

2.2.1.2- Surfactant-Polymer (SP) Flooding 16

2.2.1.3- Alkaline Surfactant-Polymer (ASP) Flooding 18

2.2.2- Gas (Solvent) Flooding EOR Processes 19

2.2.2.1- CO2 Flooding 20

2.2.2.2- Hydrocarbon Gas Flooding 21

2.2.2.3- N2, Flue Gas Flooding 23

2.3- Predictive Models 24

2.3.1- Waterflooding Predictive Models 24

2.3.2- Chemical Flooding Predictive Models 25

2.3.3- Gas (Solvent) Flooding Predictive Models 26

2.4- Sensitivity/Uncertainty Analysis 27

Chapter 3: DEVELOPMENT OF GENERAL ISOTHERMAL ENHANCED OIL RECOVERY (EOR) AND WATERFLOOD FORECASTING MODEL (UTF) 29

3.1- Introduction 29

3.2- Flow-Storage Capacity (F-C) 31
3.3- Application of Conservation of Mass and Momentum 33
3.4- Application of Frontal Advance Theory....36
3.5- Description and Application of Koval's Method 43
3.6- UTF Mathematical Formulation....46
3.6.1- Model Assumptions....46
3.6.2- One-Front and Multi-Front Displacement Processes 48
3.6.3- Evaluation of the Forecasting Model at Different Times....56
3.6.4- Simplified Approach to the Forecasting Model 59
3.7- Main Equations for Waterflood/EOR Performance Evaluation 65
Chapter 4: SENSITIVITY ANALYSIS....68
4.1- Introduction 68
4.2- Preliminary Sensitivity Analysis Using CFPM....69
4.2.1- Mathematical Formulation of Chemical Flood Predictive Model....69
4.2.2- Field Screening and Forecasting of SP Flood Using CFPM 73
4.3- Advanced Sensitivity Analysis....79
4.3.1- Fundamentals of Sensitivity Analysis 79
4.3.2- Sampling....80
4.3.3- Mathematical Formulation of Winding Stairs Sensitivity Analysis Method....82
4.3.4- CFPM Sensitivity Analysis Results....85
4.4- Discussions 96
Chapter 5: VALIDATION OF THE GENERAL ISOTHERMAL EOR AND WATERFLOOD FORECASTING MODEL 99
5.1- Model Validation Process....100
5.1.1- Required Field Data....100
5.1.2- Processing of the Field Data....100

5.2- History Matching 102
5.2.1- Waterflood History Matching Results 103
5.2.2- EOR History Matching Results 107
5.2.2- EOR History Matching Results 107
5.2.2.1- Chemical EOR 107
5.2.2.2- Solvent (Gas) Flooding/WAG EOR 115
5.2.3- Coreflood History Matching Results 121
5.3- Discussions 122

Chapter 6: EOR/WATERFLOOD FORECASTING AND NUMERICAL SIMULATION 124
6.1- Objectives 124
6.2- Experimental Design 125
6.3- Reservoir Modeling and Numerical Simulation 128
6.3.1- Reservoir Model Description 128
6.3.2- Reservoir Fluid Properties 131
6.3.3- Initial Conditions 132
6.3.4- Numerical Simulation Resulta and History Matching 133
6.4- The EOR/Waterflood Forecasting Model In-Situ Correlations 140
6.4.1- Response Surface Modeling (RSM) 140
6.4.2- Mathematical Description/ Visualization of In-Situ Correlations and Response Surfaces 140
6.5- Volumetric Sweep Efficiency and Missing Pore Volume 149
6.5.1- Definition of the Missing and Dynamic Pore Volume Concepts 149
6.5.2- Prediction of Missing Pore Volume and Final Volumetric Sweep Efficiency 151
6.6- Summary and Discussins 157

Chapter 7: SUMMARY, CONCLUSIONS AND RECOMMENDATIONS FOR FUTURE RESEARCH 159
7.1- Summary of the Research 159
7.2- Concluding Remarks 160

7.3- Recommendations For Future Research 162

Appendices 164

Appendix A: Derivation of the Injected Pore Volume at a Given Storage Capacity 164

Appendix B: EOR and Waterflood History Matching Results 165

Appendix B.1- Waterflood History Matching 165

Appendix B.2- EOR History Matching 165

Appendix B.2.1- Polymer Flooding 174

Appendix B.2.2- Surfactant-Polymer (SP) Flooding 178

Appendix B.2.3- Alkaline-Surfactant-Polymer (ASP) Flooding 188

Appendix B.2.4- Solvent/WAG Flooding 190

Appendix B.2.5- Coreflooding Experiments 194

Appendix C: Tables Of Numerical Simulation Runs Generated By Experimental Design 197

Appendix C.1- Waterflooding 197

Appendix C.2- Chemical Flooding 198

Appendix C.3- Solvent/WAG Flooding 199

Nomenclature 201

References 204

Vita 215

List Of Tables

Table 2-1: Summary of enhanced oil recovery processes 10

Table 3-1: Summary of main equations for EOR/Waterflood performance evaluation.....67

Table 4-1: Input parameters and output results of CFPM.....74

Table 4-2: Influence of different input parameters on ultimate recovery efficiency and peak oil rate based on average fluid and rock properties of the TORIS reservoir database.....78

Table 4-3: CFPM stochastic input parameters and range of variations 87

Table 4-4: Results of CFPM sensitivity analysis.....89

Table 5-1: Summary of fitted Koval factor (K_W) for history match of waterflooding.....106

Table 5-2: Matching parameters for Daqing field, pilot PO polymer flooding.....110

Table 5-3: Matching parameters for Wilmington SP flooding pilot.....113

Table 5-4: Matching parameters for Daqing ASP flooding, pilot XF 114

Table 5-5: Summary of matching parameters for SACROC 4PA CO_2/WAG flooding 118

Table 5-6: Summary of Field/pilot history matching variables for different EOR processes 119

Table 5-7: History matching parameters for coreflood laboratory experiments.....121

Table 6-1: Range of variations of reservoir/process variables used for Experimental Design of waterflooding 127

Table 6-2: Range of variations of reservoir/process variables used for experimental design of chemical EOR processes. 127

Table 6-3: Range of variations of reservoir/process variables used for experimental design of solvent (gas) flooding/WAG EOR processes 128

Table 6-4: Correlation coefficients (R^2) for response surfaces of the general isothermal EOR forecasting model (UTF) for polymer floods.....142

Table 6-5: Correlation coefficients (R^2) for response surfaces of the general isothermal EOR forecasting model (UTF) in case solvent flooding/WAG 144

Table 6-6: Correlation coefficients (R^2) for response surfaces of the general isothermal EOR and waterflood forecasting model (UTF) in case of waterflooding.....145

List of Figures

Figure 2-1: Schematic of injection-production operation of an EOR project (SNF-FLOERGER Co.) 8

Figure 2-2: Schematic of average oil saturation and recovery efficiency curves during different recovery stages 11

Figure 2-3: Schematic of capillary desaturation curve (CDC) 13

Figure 2-4: Ideal cross section of a typical SP flood showing injected slugs 17

Figure 2-5: Schematic of WAG process (Kinder Morgan Co.) 21

Figure 3-1: Typical flow-storage capacity curve 32

Figure 3-2: Fractional Flow construction for waterflood 38

Figure 3-3: Fractional Flow construction for polymer flood 40

Figure 3-4: Fractional Flow construction for surfactant-polymer flood 41

Figure 3-5: Fractional Flow construction for solvent (WAG) flood 42

Figure 3-6: Solvent cut as function of dimensionless time for different Koval factors (Koval, 1963) 45

Figure 3-7: Schematic of segregated flow, (a) without oil bank, (b) with oil bank 48

Figure 3-8: Typical storage capacity profile for a one-front displacement after breakthrough of displacing agent (F=Final, I=Initial) 49

Figure 3-9: Schematic of F^* vs t_D plot 54

Figure 3-10: Typical storage capacity profile for a two-front displacement after breakthrough of displacing agent 56

Figure 3-11: Typical output of general isothermal EOR and waterflood forecasting tool (UTF) 59

Figure 3-12: Schematic oil saturation profile for a two-front displacement.....61
Figure 4-1: Comparison between predicted and observed oil-rate-time responses.....73
Figure 4-2: Results of SP flood oil rate prediction for two cases with different injection rates.....76
Figure 4-3: Main and total sensitivity indices of ultimate recovery efficiency (E_R) for SP floods in pressure-constrained mode. 92
Figure 4-4: Main and total sensitivity indices of ultimate recovery efficiency (E_R) for SP floods in rate-constrained mode.....93
Figure 4-5: Main and total sensitivity indices of peak oil rate for SP floods in pressure-constrained mode.....94
Figure 4-6: Main and total sensitivity indices of the peak oil rate for SP floods in rate-constrained mode 95
Figure 5-1: Production history results of Salem SP flooding pilot.....101
Figure 5-2: Waterflooding history match for whole reservoir (Sand-B) 105
Figure 5-3: Waterflooding oil cut history match for a single well (A-2) in the reservoir (Sand-A) 105
Figure 5-4: Location of polymer flood pilots and wells in Daqing oil field.....110
Figure 5-5: Polymer flooding history match of Daqing PO pilot using general isothermal EOR and waterflood forecasting tool.....111
Figure 5-6: Location of Wilmington field in Los Angeles basin.....112
Figure 5-7: History match of Wilmington SP flooding pilot using general isothermal EOR and waterflood forecasting tool.....113

Figure 5-8: Alkaline surfactant-polymer (ASP) flooding history matching of Daqing XF pilot using general isothermal EOR and waterflood forecasting tool....115
Figure 5-9: Map of SACROC unit in Kelly-Snyder field showing 4 and 17 pattern areas....117
Figure 5-10: CO_2/WAG flooding history matching of SACROC-Four Pattern (4PA) using the general isothermal EOR and waterflood forecasting tool....118
Figure 5-11: ASP coreflood history matching of Core#B using the general isothermal EOR and waterflood forecasting tool (UTF)....122
Figure 6-1: The reservoir pilot used for simulation of secondary and EOR processes with surrounding and center vertical injectors and central vertical producers....129
Figure 6-2: Heterogeneous permeability field generated for V_{DP}=0.8 and λ=10....134
Figure 6-3: History match of Polymer flooding numerical simulation results (M^o= 3, V_{DP}= 0.8, λ_x= 10) using UTF....134
Figure 6-4: Numerical simulation recovery efficiency (E_R) results for polymer flood with different M^o, V_{DP} and λ....136
Figure 6-5: History match of WAG numerical simulation results using UTF....138
Figure 6-6: History match of Waterflooding numerical simulation results using UTF....139

Figure 6-7: Response surfaces for (a) chemical front Koval factor (K_C) correlation, (b) oil bank front Koval factor (K_B) and (c) final average oil saturation correlation (S_{oF}) correlation at λ_x= 10 vs. VDP and M^0 141

Figure 6-8: Solvent front Koval factor (K_S) correlation , (b) oil bank front Koval factor (K_B) correlation and (c) final average oil saturation (S_{oF}) correlation at λ=10 and BHP=2800 psi 146

Figure 6-9: Water front Koval factor (K_W) and final average oil saturation (S_{oF}) correlations at λ=10 vs. VDP and M^0.....148

Figure 6-10: 3D schematic of displacement process with swept and unswept regions.....150

Figure 6-11: Correlation of dynamic pore volume fraction for waterflood at λ=5 154

Figure 6-12: Correlation of dynamic pore volume fraction for polymer flood at λ=5.....154

Figure 6-13: Correlation of dynamic pore volume fraction for solvent flooding/WAG at P=2800 psi and λ=10.....156

Chapter 1: INTRODUCTION

Primary recovery (recovery with natural reservoir energy such as water drive or gas cap drive) usually produces a small portion of oil (10-15%) and reaches to its economic productive limit when the reservoir pressure is too low or the non-oleic phase (water or gas) production is too high. The second stage of the recovery is usually either wterflooding or gas injection to raise or maintain the reservoir pressure and keep the oil producing. However, oil production rate decline is unavoidable in the secondary recovery stage as it was for primary recovery. After a limited time of water or gas injection, the oil rates start to decline because of high water cut or gas oil ratio (GOR) and secondary recovery enters its mature phase. To increase the recovery efficiency and produce a considerable amount of oil remaining in the reservoir after secondary (or primary) recovery (usually about 60% of initial oil in place), tertiary recovery methods are applied. Enhanced oil recovery (EOR) is defined as oil recovery by the injection of materials not normally present in the reservoir (Lake, 1989). This definition does not restrict EOR to a particular stage (primary, secondary or tertiary) in the producing life of a reservoir although majority of EOR projects have been done in a tertiary recovery mode.

1.1- STATEMENT OF THE PROBLEM

Oil production from EOR processes supplies a considerable amount of the world's oil production. Therefore, the screening and selection of the best EOR process becomes important. Numerous steps are involved in evaluating EOR methods for field applications. Binary screening guides in which reservoirs are selected on the basis of reservoir average rock and fluid properties are consulted for initial determination of

applicability. However, quick quantitative comparisons and performance predictions of EOR processes are more complicated and important than screening that are the objectives of EOR forecasting.

In EOR forecasting, we look for finding ways to get quick quantitative results of the performance of different EOR processes before detailed numerical simulations of the reservoirs under study. Forecasting the performance of EOR processes plays an important role in the study, design and selection of the best method for a particular reservoir or a collection of reservoirs. Although numerical simulation of the reservoirs is widely used, there are significant obstacles that restrict its applicability. Lack of necessary reservoir data and time consuming computations and analyses can be barriers even for history matching and/or predicting EOR/waterflood performance of one reservoir. The fact of existence of intrinsic uncertainty in input data and the necessity for multiple realizations to study a problem under uncertainty is another limitation with the use of comprehensive numerical simulations.

In most cases, there is uncertainty with data and the input variables have a range of variations introduced with statistical distributions. The uncertainty of input variables and the relevant sensitivity of output results to changes in input variables make it necessary to study the problem in stochastic situation as well as deterministic. For that reason, sensitivity analysis is performed to gain a better understanding of the influence of different variables on the distributions of uncertainty in output results. This helps to characterize the key variables that govern the performance (efficiency) of each secondary/tertiary recovery process.

The main factors that affect the forecasting of the performance of an isothermal EOR/waterflood process are volumetric sweep efficiency, oil saturation at the start of a process (S_{oR}), the final average oil saturation after the process (S_{oF}) and the reservoir

heterogeneity. These parameters not only affect the EOR/waterflood process individually but also interact with each other such that they can have significant influence on the results and must be considered in modeling.

Estimation of volumetric sweep efficiencies is one of the most challenging parts of the forecasting of the performance of secondary/tertiary recovery projects. Some authors tried to predict the areal and vertical sweep efficiencies (Craig, 1955; Dyes, 1953; Claridge, 1971; Dietz, 1952). Prediction of the non-swept fraction of the reservoir (pilot) pore volume, named as missing pore volume in this dissertation, is a great challenge for any EOR/waterflood processes.

To get to these goals and answer to these requirements we need fast and robust forecasting of the EOR performance using analytical predictive models that include the relevant aspects of the process and also shows the relative advantages of various design scenarios. There are different predictive models for evaluation of different secondary/tertiary recovery methods. However, lack of a general purpose EOR/waterflood forecasting model is unsatisfactory because any differences in results can be caused by differences in the model rather than differences in the processes. We want to address this deficiency by presenting a novel analytical-base general EOR forecasting model that does not rely on conventional numerical simulation.

Developing a forecasting model as a tool to predict the performance of EOR/waterflood processes is conditioned to validation of the tool against real field or numerical simulation data. Numerous field/simulation data are necessary to validate and calibrate the forecasting tool.

1.2- RESEARCH OBJECTIVES

In this work we try to develop a novel general isothermal EOR and waterflood forecasting model to address the problems discussed in the previous section. The required steps to reach to this goal are described as follow:

1.2.1- Developing a novel general purpose forecasting (predictive) model

Developing an analytical, novel and general purpose EOR/waterflood forecasting model using the fundamental law of material balance, segregated flow and fractional flux concepts is the first step in this work. The model should include the relevant aspects of the EOR/waterflood processes and also show the relative advantages of various design scenarios. In addition, it should be fast, robust and accurate to history match and predict the performance including variations of average oil saturation, recovery efficiency, volumetric sweep efficiency, oil cut and oil rate with real or dimensionless time. Sensitivity analysis study helps to characterize the most influential reservoir/process variables for better designing of the forecasting model.

1.2.2- Validating the model against field/numerical simulation results

The next step is validating the general EOR/waterflood forecasting model against actual field and numerical simulation results of isothermal EOR and waterflood processes. This helps to evaluate the forecasting model abilities for history matching when injection/production history data are available.

1.2.3- Developing the forecasting model for performance prediction purposes

The main purpose of the forecasting model is to predict the EOR/waterflood performance when there is no or limited injection/production history data. This goal is accomplished by developing the in-situ correlations of the forecasting model through systematic comprehensive numerical simulation study based on the experimental design.

This ability helps in screening/forecasting of the EOR/waterflood processes before any comprehensive numerical simulations and can create a base for economical and portfolio analysis of EOR/waterflood processes.

1.2.4- Predicting the final volumetric sweep efficiency and missing pore volume

The subject of this step is developing the forecasting model to predict the volumetric sweep efficiency and unswept fraction of total pore volume (missing pore volume) of isothermal EOR/waterflood processes. This is achieved by generating the correlations of volumetric sweep efficiency as function of reservoir/process variables such as heterogeneity and mobility ratio.

To show the progress through the objectives of the research in a simpler way, the layout of the dissertation is arranged similar to the arrangement of the objectives described above. In chapter two, a literature review on different recovery stages, predictive models and sensitivity analysis is presented. Chapter three explains the development of the general isothermal EOR/waterflood forecasting model. In chapter four, we present the method and results of the sensitivity analysis. Chapter five is about the validation of the forecasting model against actual field and numerical simulation results. Chapter six presents the development of the forecasting model for prediction of EOR/waterflood results. The last chapter summarizes the discussions, final conclusions and recommendations for future works.

Chapter 2: LITERATURE REVIEW

As countries develop, industry and higher living standards drive up energy use, most often of oil. This justifies the world's increasing demand for crude oil and motivates the oil producers to increase the oil recovery or explore for new oil fields. Exploration of new oil resources has not found enough hydrocarbons to compensate for the depletion of the producing fields and increasing demand of world crude oil. Therefore, increasing the oil recovery using EOR methods is vital to meet the increasing world crude oil demand and counterbalance the inevitable oil production decline rate.

In this chapter we start with an overview of different stages of recovery during life of a reservoir. Then, isothermal EOR methods including chemical and gas flooding processes are reviewed. Predictive models and their applications for different recovery stages are discussed next. Finally, a brief review of sensitivity analysis as a method to characterize the effect of uncertainty of input variables on variations of output results is presented.

2.1- RECOVERY STAGES

Any reservoir around the world experiences at least one or maybe all of the stages of the recovery known as primary, Secondary and tertiary. Following this we review each recovery stage.

2.1.1- Primary Recovery

The primary recovery stage is characterized by one or combination of natural recovery (drive) mechanisms. These recovery mechanisms include:

Water drive: the natural existing aquifer forces the oil to flow towards the production wells

- Gas cap drive: the expansion of existing gas cap above the oil provides the reservoir energy for production.
- Solution gas drive: expansion of initially dissolved gas in the crude oil supplies the energy for oil production.
- Rock and liquid expansion: oil production comes from the expansion of reservoir rock and liquids.
- Gravity drainage: results from differences in the densities of the reservoir fluids.
- Compaction and reservoir subsidence: the considerable change in reservoir rock volume during the production and pressure depletion provides some energy for oil production.

When the reservoir pressure is not sufficient to produce the oil or gas/water production is too high, primary production reaches its economic limit. The recovery factor of primary stage usually is in the range of 5 to 15 % (Tzimas, 2005).

2.1.2- Secondary Recovery

The second stage of recovery is usually applied when the reservoir pressure is not high enough for spontaneous (natural) production. Secondary recovery relies on supplying reservoir energy from external sources for pressure maintenance. The main secondary recovery processes are waterflooding and gas injection where water or gas is injected into the reservoir to increase the reservoir pressure.

Although secondary recovery processes increase the oil production rate but, similar to primary stage, this is not permanent and after a certain time secondary recovery enters its mature phase by too high water or gas production making it uneconomical to continue. At this time, tertiary recovery processes can be applied to increase the oil

recovery but it's conditional to the profitability of the process (oil price and the cost of the tertiary recovery process).

2.1.3- Tertiary Recovery

Tertiary recovery processes increase the oil recovery by increasing sweep or displacement efficiencies or combination of both. In all of the EOR processes a fluid is injected into reservoir (a displacing fluid) to sweep the non-swept areas of the reservoir (unswept during secondary recovery) or increase the displacement efficiency of already swept areas by mobilizing the trapped oil. Figure 2-1 shows a schematic of injection-production for an EOR project with a cross section of one of the quarters of the five spot pattern.

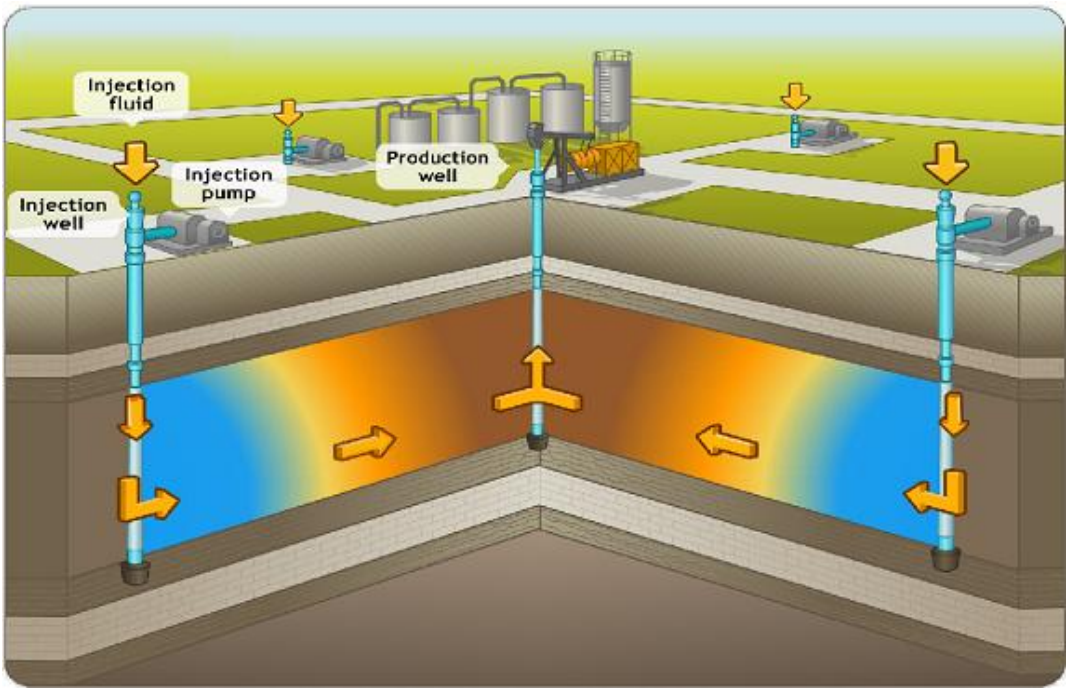

Figure 2-1: Schematic of injection-production operation of an EOR project (SNF-FLOERGER Co.).

EOR processes are classified by their mechanism and the injected material(s). There are four main categories of EOR processes as Table 2-1 shows:

- Gas flooding processes: in these types of EOR processes, the oil is displaced by injecting gas (as displacing agent). The injected gas can be miscible (for example rich hydrocarbon gas or CO_2) or immiscible (such as N_2 or lean hydrocarbon gases) with the reservoir oil. More recovery of oil is achieved by developed miscibility and reducing interfacial tension (capillary forces) or swelling and viscosity reduction.
- Chemical EOR processes: These EOR processes rely on injecting chemicals to improve the sweep of the oil or decrease the interfacial tension to effectively increase the oil production. Polymer flooding is a type of chemical EOR in which a water-soluble polymer is injected with water to increase the viscosity of water (as displacing agent) and increase the sweep efficiency by lowering the mobility ratio. Surfactant-polymer (SP) flooding is another type of chemical EOR process where dilute solutions of surfactants are injected to decrease the capillary forces by lowering the interfacial tension between phases. Another type of chemical EOR processes is alkaline-surfactant-polymer (ASP) flooding in which an alkaline (or caustic solution) is injected into reservoir to create in-situ soap with reservoir oil that has naturally occurring organic acids. This results in lowering the interfacial tension (reducing capillary forces) and increasing the oil recovery by mobilizing the trapped oil.
- Thermal processes: Heating the reservoir crude oil to reduce its viscosity and increasing the recovery has been successfully done. Steam flooding, cyclic steam stimulation, hot water flooding and in-situ combustion are different types of thermal EOR processes that improve both sweep and displacement efficiencies.

- Microbial EOR: MEOR is classified as a biological based technology where the structure or function of microbial environment existing in reservoir fluids is manipulated. It works by injecting bacteria or growing the naturally existing bacteria in the reservoir oil. The bacteria in the reservoir fluids will produce natural surfactants through their natural metabolism. The produced surfactants reduce the interfacial tension and mobilize the oil (Lazar et al., 2007).

Table 2-1: Summary of enhanced oil recovery processes.

Enhanced Oil recovery Processes			
Thermal	Gas	Chemical	Microbial
Steam Cyclic Steam Stimulation Hot Water In-situ Combustion	CO_2 Hydrocarbon Gas Nitrogen Flue Gas	Polymer Surfactant-Polymer Alkaline-Surfactant-Polymer	

2.2- ISOTHERMAL ENHANCED OIL RECOVERY PROCESSES

The oil remaining in the reservoir after previous recovery stages is either trapped in very small pores by capillary forces or it is bypassed by water. These remaining oils (trapped or unswept) are the target for EOR processes. In current research we only address isothermal EOR processes. Therefore our focus is on chemical EOR and gas flooding processes.

Recovery efficiency (E_R) of an EOR process is product of its volumetric sweep (E_v) and displacement (E_D) efficiencies as described in Equation 2-1:

$$E_R = E_V E_D \tag{2-1}$$

Volumetric sweep efficiency is the ratio of the volume of oil contacted to the volume of oil originally in place, i.e. the fraction of pore volume swept by the EOR

process (displacing fluid). Displacement efficiency is the ratio of the amount of oil displaced to the amount of oil contacted, i.e. the fraction of original oil saturation produced from the swept volume of the reservoir.

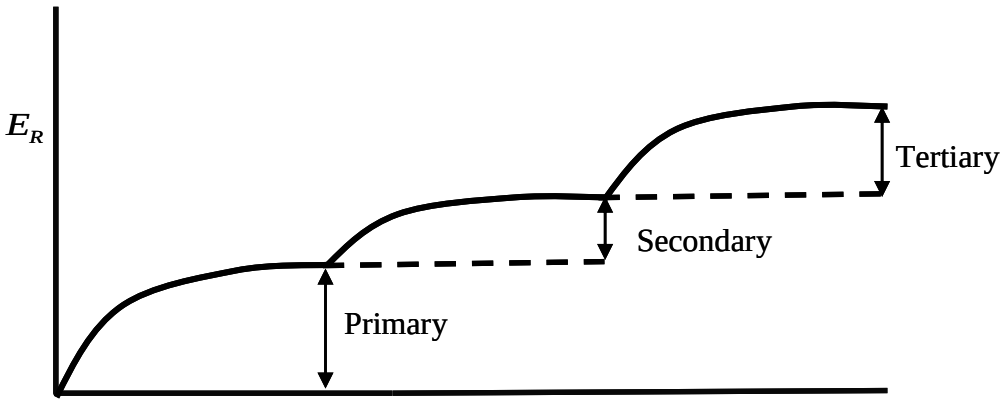

(a)

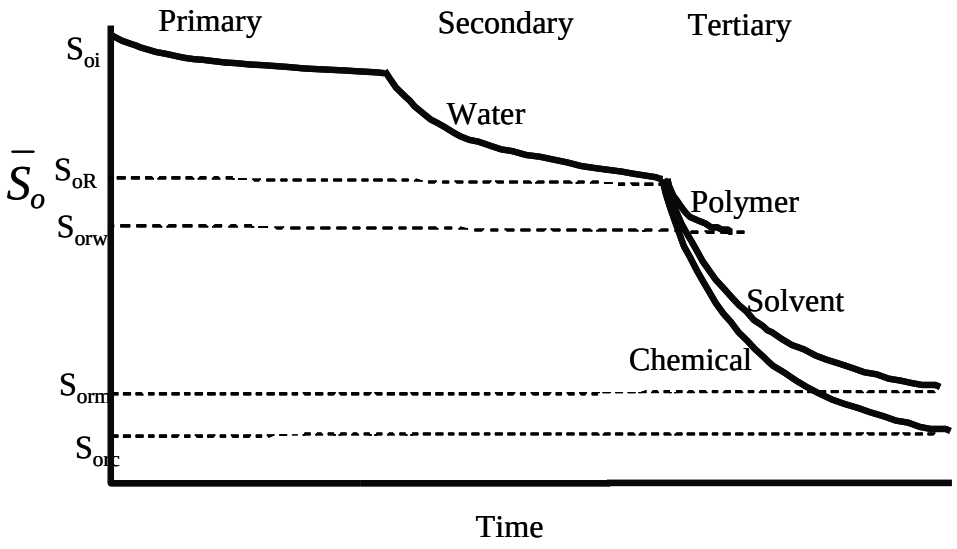

(b)

Figure 2-2: Schematic of average oil saturation and recovery efficiency curves during different recovery stages.

Figure 2-2 a and b show schematic recovery efficiency and average oil saturation curves during primary, secondary and tertiary recovery.

E_v measures the ability of the EOR process to contact the reservoir (both areally and vertically) while E_D represents the strength of the EOR process in mobilizing the trapped oil by capillary forces. Claridge (1971), Dietz (1952), Dykstra-Parsons (1950), Crane (1963), Stiles (1949), and Johnson (1965) discussed and developed models to predict volumetric sweep efficiencies (areal or vertical).

Enhanced oil recovery (EOR) processes increase the oil recovery either by increasing volumetric sweep or displacement efficiencies or a combination of both. Volumetric sweep efficiency increases by reducing the mobility of displacing fluid to decrease the mobility ratio of phases (ratio of the mobility of displacing to displaced fluid). Equation 2-2 defines the mobility ratio where M is mobility ratio, k is effective permeability and μis the viscosity of displacing or displaced (oil) fluid.

$$M = \frac{\left(\frac{k}{\mu}\right)_{displacing}}{\left(\frac{k}{\mu}\right)_{displaced}} \tag{2-2}$$

Displacement efficiency increases by reducing capillary forces against viscous forces. Therefore E_D is controlled by ratio of viscous to capillary forces called capillary number (N_{ca}).

$$N_{ca} = \frac{\mu_{ing} v}{\sigma} \tag{2-3}$$

where μ_{ing} is the viscosity of displacing fluid, v is Darcy velocity and σ is the interfacial tension between oil and water phases. For low capillary numbers (a rule of thumb says less than 10^{-5}), flow in porous media is dominated by capillary forces. The

variation of residual oil saturation (S_{or}) with capillary number is not strictly monotonic as shown in Figure 2-3. In fact, when capillary number (N_{ca}) exceeds the critical capillary number, $(N_{ca})_c$, the trapped oil is mobilized. To increase the capillary number, either the displacing fluid viscosity and velocity must increase or interfacial tension must decrease. The second, decreasing interfacial tension, is more practical and realistic as is done in chemical EOR and miscible gas (solvent) flooding. Increasing capillary number by increasing the displacing fluid velocity and/or viscosity is not practical since very large (orders of magnitude) viscosity and/or velocity is required to pass the critical capillary number and mobilize the residual oil. These can not occur because enormous pressure gradient is required. Therefore, the trapped oil remains unrecoverable for waterflooding.

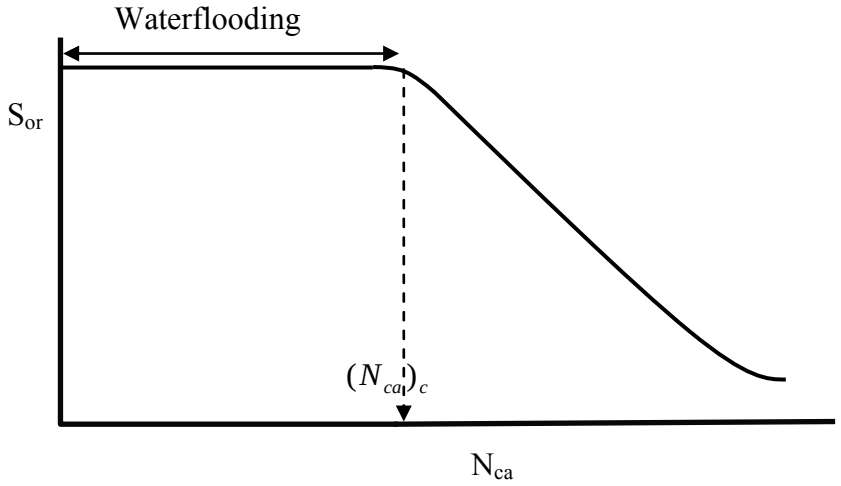

Figure 2-3: Schematic of capillary desaturation curve (CDC).

2.2.1- Chemical EOR Processes

Chemical EOR processes can increase both sweep and displacement efficiencies to recover oil. They use polymer for mobility control (increasing volumetric sweep

efficiency) and surface active agents (surfactants) for reducing the interfacial tension (increasing capillary number) and so decreasing the residual oil saturation. As explained in section 2.1.3, there are three types of chemical EOR methods: polymer, surfactant-polymer (SP) and alkaline-surfactant-polymer (ASP) flooding in common use.

2.2.1.1- Polymer Flooding

Waterflood is usually subject to fingering and channeling as result of unfavorable mobility ratio and reservoir heterogeneity. Typically, waterfloods with mobility ratio greater than five experience these effects (Sorbie, 1991). Polymers are used to achieve favorable mobility ratio during water, surfactant or alkaline flooding.

Polymer flooding consists of injection of a dilute solution of a water-soluble polymer to increase the viscosity of the injected water. The resulting increase in viscosity, as well as a decrease in aqueous phase permeability that occurs with some polymers, cause a lower mobility ratio (Lake, 1989). Therefore, polymer flooding is a mobility-controlled EOR process. It is suitable when water-oil mobility ratio is high for waterflooding and/or the reservoir is highly heterogeneous. Reservoirs with evidence of geological heterogeneity, extensive stratification and high permeability contrast between layers are potential candidates for polymer flooding (Sorbie, 1991). Lowering the mobility ratio delays the breakthrough and increases the sweep efficiency of the flood to achieve higher recovery. The oil rate also increases as a result of created oil bank ahead of polymer.

There are several purposes and applications of polymer in oil fields:

- Increasing volumetric sweep efficiency of the flood by reducing water mobility

- As polymer gelation for well profile control, in-depth profile control and colloidal dispersed gels (Krumrine et al., 1985).
- Drilling fluids
- Decreasing residual oil saturation (S_{or}), if the increase in viscosity (and so capillary number) is high enough as was reported in polymer flooding of Daqing because of polymer elasticity (Chen et al, 2011).

Use of polymer for EOR is often limited to increasing sweep by lowering the mobility.

Commercial polymers are either biopolymers (such as Xanthan gum) or synthetic (such as hydrolyzed polyacrylamide (HPAM), polyacrylamide (PAM) and polyacrylic acid). HPAM is the most commonly used polymer for EOR purposes. Adsorption, salinity, hardness, non-Newtonian effects (shear thinning or thickening), inaccessible pore volume, permeability reduction and degradation of polymer molecules (chemical, mechanical and thermal) and injectivity are the most important factors that should be considered in proper selection of polymer type (Lake, 1989). The injectivity (ratio of injection rate to injector-reservoir pressure difference) must be considered and tested in every EOR process that uses polymer since it is possible for a project to fail just because of loss of injectivity at start or during the project life. The Coalinga polymer flood is an example of such failure (Duane, 1983).

2.2.1.2- Surfactant-Polymer Flooding

Surfactant-polymer (SP, also known as micellar-polymer, microemulsion, soluble oil or low tension polymer flooding) flooding involves the injection of a surface-active agent (surfactant) to increase oil production by lowering the interfacial tension between oil and water resulting to mobilization of the trapped oil (Lake, 1989). SP flooding targets

both volumetric sweep efficiency (E_V) by using polymer and displacement efficiency (E_D) using surfactant. It is therefore expected that SP flooding has a larger recovery efficiency (E_R) than polymer flooding. However the costs, complexities and the risk involved with SP flooding are much more than polymer flooding that restricts the application of SP flooding.

The injection design of SP flood includes several steps to reach and maintain the ideal condition for reducing the interfacial tension by surfactant and also control the mobility during the flood.

Figure 2-4 illustrates the ideal steps existing in a typical SP flood. As one can see, the injection starts with *preflush,* which is injected in front of chemical slug (micellar solution) to provide proper conditions for the micellar solution (chemical slug) and to prevent loss of interfacial activity of surface active agents. Preflush is done by adjusting the brine salinity, pH and reducing adsorption of surfactant on the reservoir rock by adding some adsorbent into preflush.

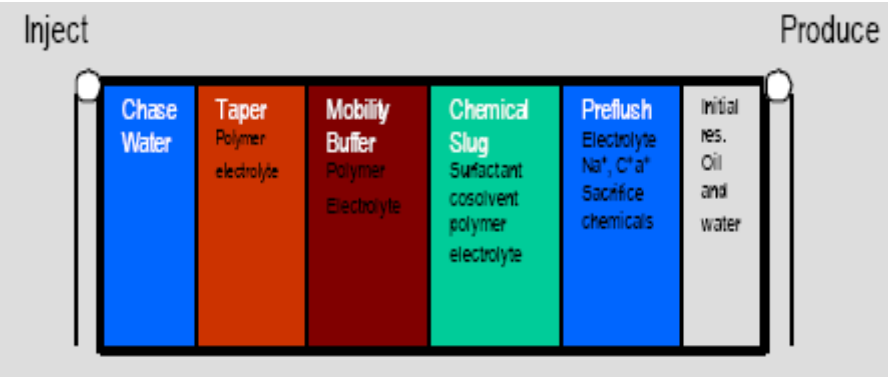

Figure 2-4: Ideal cross section of a typical SP flood showing injected slugs.

The next slug is a mixture of surfactant and polymer. Surfactant is expensive; therefore a small slug of surfactant (typically less than 0.25 PV with surfactant concentration between 0.5 to 1 percent) is injected. This is the slug that lowers interfacial tension and makes microemulsion (an equilibrium phase containing surfactant, brine and oil) to mobilize the trapped oil. The polymer injected with the surfactant is to control the mobility of the chemical slug. Sometimes alcohols are added also as co-solvent to improve the viscosity of the slug.

The next two slugs (the mobility buffer and mobility buffer taper) are used to move the chemical slug in the reservoir with a less expensive fluid but in a mobility-controlled manner to increase the sweep efficiency. Water is not proper to move the chemical slug directly because of its unfavorable mobility ratio. Finally, chase water (that is cheaper than polymer) is injected to displace the mobility buffer and make the process more economical by reducing the amount of injected polymer (Lake, 1989; Green and Wilhite, 1998).

SP flood is more successful in the laboratory than in field because of its complexities and non-ideal field conditions compared to laboratory. It requires small well spacing, large initial investment and large amount of chemicals. In addition, oil production from SP flood is delayed, which impacts the rate of investment return.

2.2.1.3- Alkaline- Surfactant-Polymer Flooding

The alkaline-surfactant-polymer (ASP) flooding increases the oil recovery by increasing both volumetric sweep and displacement efficiency as SP does. In fact, these two chemical EOR processes are very similar. The only major difference is that in ASP flooding in addition to surfactant and polymer, alkaline is also injected to generate in-situ surfactant by reacting with existing organic acids of crude oil. Some ASP pilot tests

achieved to incremental oil recovery of 23% of OOIP and about 60% of OOIP (original oil in place) ultimate recovery efficiency including previous primary recovery and secondary waterflood (Clark, 1988).

The injection steps involved in ASP flood are similar to SP. ASP starts with injection of preflush and then chemicals (including a mixture of alkaline, surfactant and polymer) are injected. The chemical slug is followed by polymer and chase water to increase the sweep and reduce the costs of the process. For crude oils containing organic acids the alkali has dual purposes: it generates natural surfactants, soap, upon reaction with the acid and reduces the adsorption of the injected surfactants by inducing a negative charge on the rock surface (Farajzadeh, 2011; Hirasaki, 2004).

ASP flooding is more sensitive to reservoir conditions (specially salinity) than SP flooding. After reaction of alkaline with the organic acids, the in-situ generated soap molecules accumulate at the oil-water interface and can considerably reduce the interfacial tension providing that the reservoir conditions, in particular the salinity, are optimal or close to optimal (Nelson, 1982). However, in most reservoirs the salinity of the formation brine is too large, making the alkaline flooding inefficient and uneconomic. To solve this problem, a synthetic hydrophilic surfactant is added to the chemical slug in the ASP process (Farajzadeh, 2011).

The success of ASP flood depends on the simultaneous propagation of injected (synthetic) and in-situ generated surfactants. If the in-situ generated surfactant moves faster than the injected surfactant, the phase behavior becomes over optimum and in-situ generated surfactant partitions into the trapped oil (Mohammadi, 2008).

Regarding that alkaline is inexpensive (Wyatt, 2008), the chemical costs of ASP flood is less than SP since less synthetic surfactant is required for injection. As a result, if

the reservoir conditions (rock and fluid) are proper, ASP is a more cost effective alternative to the SP flood.

2.2.2- Gas (Solvent) Flooding EOR Processes

Gas flooding is a widely used EOR method. Gas flooding EOR processes increase oil recovery mostly by decreasing residual oil saturation by attaining miscibility. Two fluids that mix together in all proportions within a single-fluid phase are miscible. Most practical miscible agents exhibit only partial miscibility toward the crude oil itself. Therefore, the term "solvent flooding" is used for all gas flooding processes (Lake, 1989).

Since the displacing fluid is gas, large density difference and adverse mobility ratio between displacing (gas) and displaced fluid (oil) can result in poor sweep efficiency and need to use water or foam for mobility control. Propane or liquid petroleum gas (LPG) are the solvents used for first contact miscible floods while CO_2, N_2, CH_4 or mixture of hydrocarbon gases are used for multi contact miscibility. In this research, we focus more on CO_2 flooding as the most common gas flooding EOR process.

2.2.2.1- CO_2 Flooding

CO_2 flooding (miscible or immiscible) is the second most common tertiary recovery method (the first is thermal EOR). The history of performed CO_2 flooding projects worldwide shows incremental oil recovery of 7% to 15% of OOIP. CO_2 flooding has proven to be among the most promising EOR methods, especially in the US where it takes advantage of available, naturally occurring CO_2 reservoirs and pipelines. Carbon dioxide is known to be highly soluble in crude oils, and in water, causing reduction in oil viscosity and also an appreciable swelling of crude oil (Simon, 1965).

The main advantages of CO_2 compared to other gases used in EOR are (Mathiassen, 2003; Martin, 1992):

- Swelling of the oil
- Reduction of oil viscosity
- Lower minimum miscibility pressure (MMP, 100 to 300 bar)
- Solubility in water and reducing water density to have less gravity instabilities
- Vaporizing heavier components of the oil resulting to easier miscibility

These advantages make CO_2 a favorable gas for EOR. However the mobility of CO_2 is high resulting in poor volumetric sweep efficiency because of fingering and gravity instabilities. CO_2 has a density like liquid but a viscosity more like a gas, this is because CO_2 in reservoir condition is often supercritical. This problem can be improved by alternating the injection of gas with a less mobility fluid such as water or foam. The purpose of water alternative gas (WAG) injection is to improve the poor sweep efficiency of gas flooding by injection of water and gas in alternate or simultaneous way. WAG significantly reduces the impact of viscous fingering by reducing the mobility of gas (Caudle, 1959). Figure 2-5 is a schematic of WAG process showing alternative slugs of injected gas and water with created miscible and oil bank zones ahead.

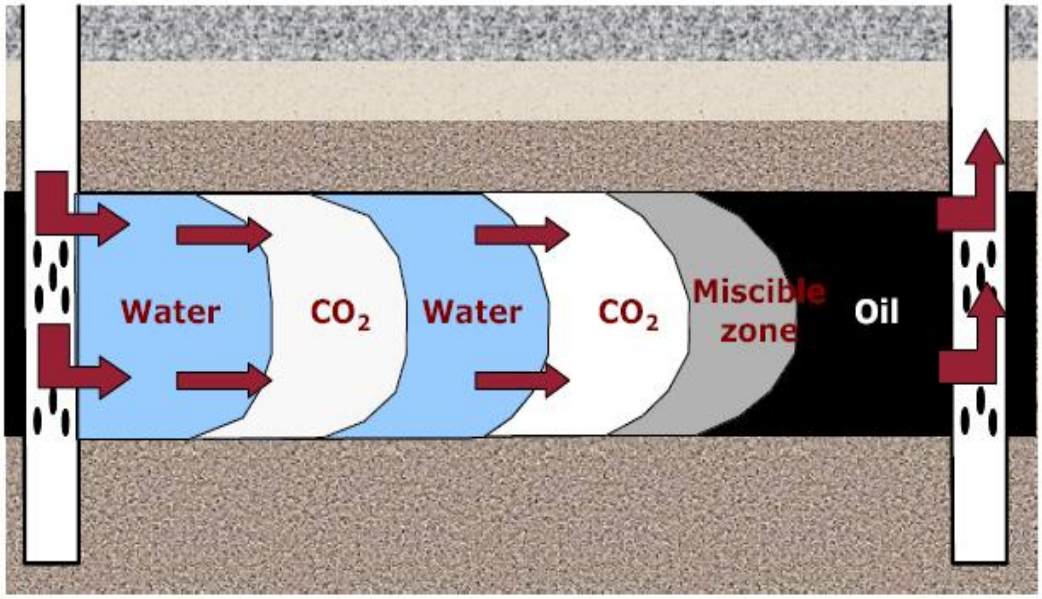

Figure 2-5: Schematic of WAG process (Kinder Morgan Co.).

The main factors affecting the WAG injection process are the reservoir heterogeneity, miscibility conditions, rock wettability, fluid properties, trapped gas, injection technique and WAG parameters such as slug size, WAG ratio and injection rate (Sanchez, 1999).

WAG has been successfully applied in field projects. A wide variety of gases have been used in WAG projects but about 90% of the projects have used CO_2 and hydrocarbon gases (Jarrel, 2002).

2.2.2.2- Hydrocarbon Gas Flooding

Similar to CO_2, hydrocarbon (HC) gases are used for EOR in both miscible and immiscible conditions. Most HC gases require a higher MMP to develop miscibility with reservoir oil than CO_2. An injected gas becomes miscible with oil when oil and gas have enough light to intermediate components (C_2-C_6) to develop miscibility through either vaporizing or condensing mechanisms. When a lean gas (a gas with little intermediate

components) is injected, the miscibility is achieved by vaporizing some intermediate components of oil into gas, making gas properties closer to oil until the miscibility occurs. If the injected gas is rich enough (having enough intermediate components), miscibility can be achieved through a condensing mechanism where intermediate components are condensed from gas into oil making oil lighter and closer to gas until miscibility is reached. In fact, miscibility occurs when there is no difference between gas and oil phases and they become indistinguishable. The outcome of miscibility is very low interfacial tensions (high capillary number) resulting in the recovery of residual oil saturation and enhancing displacement efficiency. In terms of the pressure required for efficient miscible displacement, hydrocarbon gases rank between the very high pressures required for nitrogen and the more modest range of pressures for CO_2 (Taber et al., 1997).

HC gases suffer from high mobility and sweep efficiency problems similar to CO_2. The volumetric sweep efficiency of a miscible flood depends on mobility ratio, viscous-to-gravity ratio, transverse mixing, well configuration, and heterogeneity in general (Doa, 2005). WAG has been successfully applied with HC gases to improve the sweep of hydrocarbon gas flooding. 42% of total WAG projects have been done by HC gases. Percentage of CO_2 WAG projects is a little more than HC gases and stands on 47% of all WAG projects (Christensen, 1998).

Availability of gas resources is as important as applicability. In offshore fields, it is recommended to use produced HC gases. A good example of this is Ekofisk field in the North Sea where, although studies showed CO_2 WAG yields higher incremental recovery, miscible hydrocarbon WAG was suggested to be more suitable (Jensen, 2000).

2.2.2.3- N_2, Flue Gas Flooding

Hydrocarbon gas and CO_2 flooding are the most favorable gas flooding processes but the high costs and availability of these sources encouraged use of nitrogen and flue gas for EOR purposes. Nitrogen has the advantages of being widely available, cost-effective, and environmentally clean. It is also an often proposed alternative to natural gas injection for deep, high-pressure volatile oil reservoirs (Boersma, 1992). The composition of flue gas (exhaust gas or inert gas) depends on its source. The produced flue gas from natural gas has different mole percent of Nitrogen and carbon dioxide than the flue gas produced from propane (Anada, 1980). Because of their low costs, large volumes of these gases can be injected and they can be used even as chase gas in miscible hydrocarbon gas and CO_2 flooding. However, nitrogen and flue gas flooding need very high pressure for miscibility with oil and so they are used in deep reservoirs with light oil (depth > 6,000 ft and ^{o}API >35, Taber, 1997).

If the pressure is large enough N_2/flue gas vaporize the lighter components of the oil and generate miscibility. The can enhance the gravity drainage in dipping reservoirs either miscible or immiscible. The reservoir should be steeply dipping to be proper for gravity stabilization during displacement, which has an unfavorable mobility ratio.

Analysis of costs associated with different gases for solvent flooding shows that nitrogen and flue gas injection costs compare very favorably with CO_2 injection costs and they are 30% to 60% cheaper than CO_2. In addition, flue gas is only recommended in regions close to industrial plants (Anada, 1980) and it is substituted with nitrogen in recent years (Taber et al., 1997).

2.3- PREDICTIVE MODELS

Predictive models (PMs) have been used as fast and robust tools to forecast the waterflood and EOR processes (Koval, 1963; Paton, 1969; Paul, 1982 and 1984; Giordano, 1987; Lake, 1978; Sayarpour, 2008). Each process is modeled analytically such that it includes the important aspects and variables of the process/reservoir (such as mobility ratio, reservoir heterogeneity, injection rate, etc.) and also represents the relative advantages of various design scenarios. Compared to binary screening, PMs not only can rank the reservoirs for a secondary/tertiary recovery process but also generate quantitative prediction of reservoir performance under a secondary/tertiary recovery process. In comparison with numerical simulation, PMs are much faster, less expensive and need much less input data.

PMs have been developed as analytical models that do not rely on numerical simulation to forecast EOR and waterflooding performance such as production rates, recovery efficiency and economic evaluation. Following this we review some of the PMs, each developed to predict a secondary/tertiary recovery process.

2.3.1- Waterflooding Predictive Models

Many authors tried to develop fast methods to predict waterflood performance using empirical correlations or analytical methods. Buckley-Leverett (1942) frontal advance theory and its extension, the Welge (1952) tangent method, is the first analytical model introduced for predicting the waterflood performance. It was developed for steady state, linear flow in homogeneous permeable media to find the outlet and average saturation.

Stiles (1949) presented a method to predict water cut considering permeability variation. Dykstra and Parsons (1950) identified the mobility ratio, permeability variations, initial oil saturation as the key variables influencing the performance of

waterflooding and developed a method to predict the recovery efficiency as function of these variables. Craig (1955) used areal sweep efficiency and mobility ratio concepts to predict the water-oil ratio of waterflooding in uniform sands. Bush (1968) used a large database of waterflooding projects to predict the oil production rate using some empirical parameters.

With recent advances in computational abilities, predictive models could be successfully developed to apply analytical models for history matching and predicting waterflooding in large fields. An example of such PMs is the Capacitance-Resistive Model (CRM, Sayarpour, 2008) that uses injection/production data for evaluation of reservoir performance.

2.3.2- Chemical Flooding Predictive Models

Chemical flooding methods inject chemicals (polymer, surfactant or alkaline) to reduce the mobility ratio and/or decrease interfacial tension between phases (water and oil). The PMs developed for EOR processes are not as many as those developed for waterflooding. One reason could be the higher level of complexity associated with chemical EOR methods and the relative less experience and knowledge compared to waterflooding.

Patton (1971) presented an analytical model to predict polymer flood performance (incremental oil recovery), which also provides quick estimate of additional oil recovery by polymer flood. Jones (1984) developed a predictive model for water and polymer flooding by combining a two-dimensional cross sectional model with areal sweep correlations and injectivity functions to predict the oil production rate versus time.

Paul (1982) developed a predictive model to forecast chemical (surfactant-polymer) flood EOR performance, which was used by the Department of Energy (DOE)

for identifying candidate reservoirs for chemical flooding. The model predicts recovery efficiency and oil rate as functions of relevant reservoir and fluid properties. Giordano (1987) studied the effect of pattern type, surfactant slug size, heterogeneity and process timing on surfactant-polymer flood using a simple model developed based on streamlines and distribution of velocities in the pattern.

2.3.3- Gas (Solvent) Flooding Predictive Models

Gas (solvent) flooding is one of the earliest methods applied to increase ultimate oil recovery. It involves injection of hydrocarbon or non-hydrocarbon gases into underground oil reservoirs to recover the residual oil saturation typically after waterflooding. They usually have good displacement efficiency but poor sweep efficiency because of an unfavorable mobility ratio. The lack of sweep efficiency is usually improved significantly by injecting water or foam as lower mobility agents with gas.

Koval (1963) presented a method that predicts recovery and solvent cut of unstable miscible displacements as a function of pore volumes of solvent injected. The model showed a good agreement with the experimental data. Claridge (1972) used a apparent pore volumes method to develop new correlation for predicting oil recovery in unstable miscible flooding by combining areal and displacement efficiency correlations.

Dake (1979) presented an analytical approach to evaluate the recovery efficiency of unstable immiscible displacement with the effect of gravity. The model is based on segregated flow condition that assumes there is no mobile oil behind the front. Paul et al. (1984) presented a PM for evaluation of CO_2 miscible flooding. Their model predicts oil, water and CO_2 production rates and was used to evaluate candidate reservoirs for CO_2

flooding based on economic criteria while preserving technical features, which affect flood performance.

Fayers (1988 and 1994) and Todd-Longstaff (1972) studied the unstable miscible displacement and developed models to describe viscous fingering that will be discussed more in chapter 3.

2.4- SENSITIVITY/UNCERTAINTY ANALYSIS

Often, the data (input variables) have ranges (because of uncertainty) that form statistical distributions. The uncertainty of input variables and the relevant sensitivity of output results to changes in the input make it necessary to study the problem stochastically as well as deterministically. Sensitivity analysis (SA) helps to quantitatively determine the influence of input variables or parameters on the distributions of uncertainty in output results by systematically changing the input variables. Generally, SA helps understand:

1. How the variation in the output of a model can be apportioned, qualitatively or quantitatively, to different sources of variations.
2. How the given model depends on the information that is fed into it.

SA is a method to ascertain how each of the model input parameters influences the variations in the model outputs and characterize the most influential variables. The results of SA provide information to increase understanding and quantification of the system for model development.

From a technical point of view, it is important to choose the most accurate and robust SA method that provides both reliable sensitivity measures, is independent of model type, and gives global results. Regression, correlation and variance decomposition

are examples of global SA methods that determine input-output sensitivity relationships across the entire specified ranges of the input variables. However, regression and correlation are model-dependent and therefore biased to the model they have fitted to data. We use variance decomposition SA method, which is model-free and global. Chapter four provides more details of sensitivity analysis.

Chapter 3: DEVELOPMENT OF GENERAL ISOTHERMAL ENHANCED OIL RECOVERY (EOR) AND WATERFLOOD FORECASTING MODEL (UTF)

3.1- INTRODUCTION

To study an object or phenomenon, generally a model (prototype or similitude) is constructed for feasible and more convenient analysis. The term *model* refers to physical representation of an object or an abstraction (for example a conceptual or mathematical model). Fundamentally, models are developed in an effort to explain how things in nature work. Forging new science depends on the development of models. Basically, a model is a scaled-down version of a natural object or system with details omitted by assumptions. The details that are left out depend on the goals and level of sophistication. If too much is left out, the model may be almost worthless. If too many details are included, the model may become too complicated to be useful.

From above, it is easy to understand why models lack some features of the real system. Often, it is impossible to directly observe the objects of a scientist's attention and certain features may be unknown. For instance, the system might be too small or inaccessible for direct visual study, such as the underground reservoirs or the surface of a distant galactic object. Gravity or magnetism can be studied through their effects on matter. However, neither gravity nor magnetism can be seen directly. Therefore, it is necessary for scientists and researchers to develop models as they probe the secrets of nature (Anonymous, Genesis Journal).

A variety of model types are developed to address different requirements. A core in the laboratory used for flooding experiments is an actual physical model. Logging and seismic are imaging models used to represent the invisible reality of the underground

reservoir. Darcy's law, the Buckley-Leverett equation and predictive models (PM) are mathematical models to describe the fluid flow phenomena using algebraic statements.

As said George E.P. Box (1987) "all models are wrong, but some are useful", models usually evolve and improve as new evidence or advances in science are made. Sometimes there are different models to describe one thing. All can be useful and the choice depends on our goals and level of sophistication required in a special project.

Analytical modeling of secondary or tertiary recovery processes and predicting the performance is another example of mathematical modeling known as predictive model (PM, as explained in Chapter 2). PM is very useful in selection, study and better design of EOR/waterflooding projects specially when comprehensive numerical simulation is impossible because of lack of time, necessary data or fully understanding of the reservoir/recovery process. Developing PMs is generally a difficult task involving in-depth understanding of the reservoir/recovery processes, strong mathematical skills and lots of efforts for validation. This is a reason for much fewer research on PMs compared to numerical simulation.

Several authors developed different PMs to predict the performance of different EOR/waterflooding processes. However, lack of a general purpose EOR/waterflooding forecasting model is unsatisfactory. This deficiency becomes more important in cases such as selection of EOR processes for one or several reservoirs because any differences in performance comparison of various EOR methods may be related to differences in the models used for the analysis rather than the EOR methods themselves. We address this deficiency by presenting a novel analytical-base general EOR/waterflooding forecasting model that uses numerical simulation only for calibration.

3.2- FLOW-STORAGE CAPACITY (F-C)

The fractional flux (fraction of the displacing agent crossing a cross-section at given position between injector and producer) for a constant mobility displacement in a uniformly layered reservoir with the same layer length and parallel flow is given by:

$$F_n = \frac{\sum_{i=1}^{i=n} (kh)_i}{\sum_{i=1}^{i=N_L} (kh)_i} \tag{3-1}$$

where F_n is the flow capacity. The storage capacity is defined in similar way as:

$$C_n = \frac{\sum_{i=1}^{i=n} (\phi h)_i}{\sum_{i=1}^{i=N_L} (\phi h)_i} \tag{3-2}$$

In these equations, k_i, ϕ_i and h_i are the permeability, porosity and thickness of the i^{th} layer. n is the layer in which the displacing agent is just breaking through at the cross-section and N_L is the total number of layers. If N_L becomes very large, the F-C plot approaches the continuous distribution as shown in Figure 3-1.

The figure below shows a typical flow-storage capacity plot (F-C or Lorenz curve) that is the most basic representation of heterogeneity in a reservoir. F-C may be calculated from core data, or from correlations of permeability from log data as described below.

As presented here, the permeabilities are arranged in order of decreasing permeability/porosity. The F-C curve is, in fact, a cumulative distribution function of the velocities in a reservoir and may apply to any reservoir, uniformly layered or not. If the reservoir is uniformly layered, the F-C curve directly related to sweep. One of the

contributions of this work is to parameterize the F-C curve, which without restrictions has N_L degrees of freedom, to only one parameter, the Koval factor.

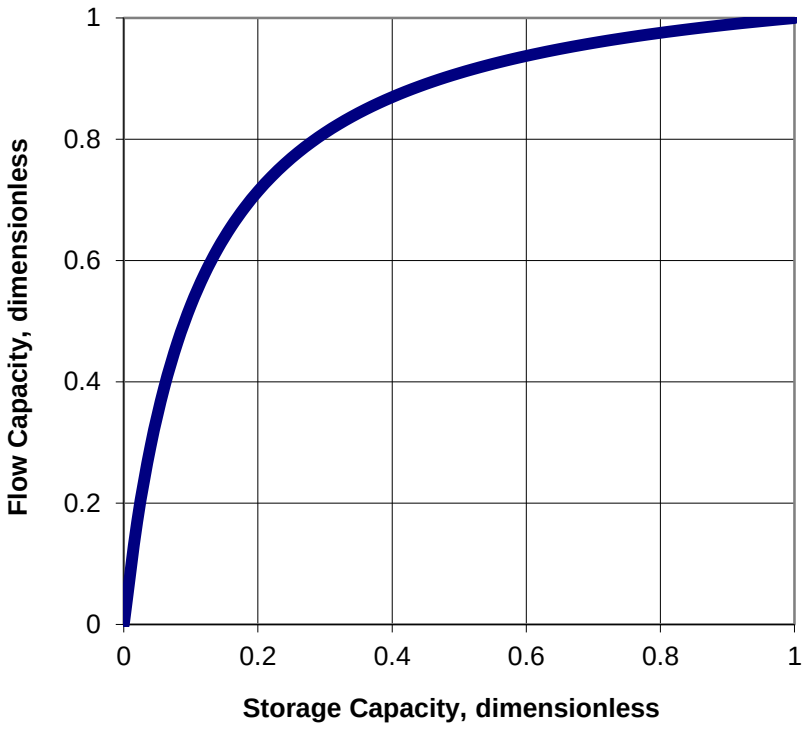

Figure 3-1: Typical flow-storage capacity curve.

It is obvious from Darcy's law that the interstitial velocity (the ratio of Darcy velocity to porosity) of the single-phase flow in each layer is proportional to the ratio of permeability to porosity (k_i/ϕ_i) of that layer. Therefore, F_n in Equation 3-1 is the fraction of total flow of velocity v_n or faster and C_n is the volume (pore volume) fraction. From the definitions of F and C, the slope of F-C curve at any C is equal to ratio of interstitial velocity at that point to the average interstitial velocity as described in Equation 3-3, (Lake, 1989):

$$\frac{dF}{dC} = \frac{\nu_n}{\bar{\nu}} \tag{3-3}$$

3.3- APPLICATION OF CONSERVATION OF MASS AND MOMENTUM

The bases of the forecasting model are the fundamental laws of conservation of mass and momentum. The mass balance (also called material balance) is applied in both macroscopic and microscopic (differential) scales. In the macroscopic scale, a material balance is applied to drive the basic equations of recovery, volumetric sweep and displacement efficiencies. In differential form, the material balance is applied along with momentum balance (Darcy's law) to derive the Buckley-Leverett equation, which will be used in frontal advance and fractional flow theories.

The oil material balance is described by the following equation:

$$\text{Pr}\,esent\,Oil \;-\; Initial\,Oil \;=\; Cumulative\,Oil\,In \;-\; Cumulative\,Oil\,Out \tag{3-4}$$

Using the sweep efficiency concept defined in Chapter 2, Equation 3-4 can be written as:

$$V_P \left[E_V \bar{S}_o + \left(1 - E_V\right) S_{oR}\right] - V_P S_{oR} = 0 - N_P \tag{3-5}$$

where N_P is the cumulative oil produced, V_P is the reservoir pore volume, E_v is volumetric efficiency, $\bar{S}_o$ is average oil saturation and S_{oR} is the initial oil saturation at start of the EOR (or waterflooding) process. After simplification, Equation 3-5 can be written as:

$$\Rightarrow \quad N_P = E_V \left(S_{oR} - \bar{S}_o\right) V_P \tag{3-6}$$

dividing by the original oil in place ($V_P S_{oi}$) gives:

$$\frac{N_P}{V_P S_{oi}} = E_V \frac{(S_{oR} - \bar{S}_o)}{S_{oi}} = E_V E_D = E_R = \text{Recovery Efficiency} \tag{3-7}$$

where E_D is the displacement efficiency (defined in chapter 2) and E_R is the recovery efficiency or cumulative oil produced divided by the original oil in place.

The material balance equation in differential form for one dimensional (1D) and incompressible flow of displacing phase is described in Equation 3-8:

$$\phi A \frac{\partial S_w}{\partial t} + \frac{\partial q_w}{\partial x} = 0 \tag{3-8}$$

where subscript *w* stands for displacing fluid, ϕ is porosity, A is cross sectional area, t is time, x is location and q is volumetric flow rate obtained from momentum balance (Darcy's law). The equation is more useful in dimensionless form described in Equation 3-9 using x_D and t_D as dimensionless location and time defined in following equations.

$$\frac{\partial S_w}{\partial t_D} + \frac{\partial f_w}{\partial x_D} = 0 \tag{3-9}$$

$$x_D = \frac{\int_0^x A\phi d\zeta}{\int_0^L A\phi d\zeta} \tag{3-10}$$

$$t_D = \frac{\int_0^t q d\zeta}{\int_0^L A\phi d\zeta} \tag{3-11}$$

where L is length of the permeable media and f_w is fractional flow of displacing fluid defined as:

$$f_w = \frac{q_w}{q} = \frac{q_w}{q_w + q_o} \tag{3-12}$$

where q is the total flow rate and q_o is oil phase flow rate. Equation 3-9 describes the relationship between fractional flow and saturation, which is the base of fractional flow theory and analysis. Using the chain rule, one can write:

$$\frac{\partial S_w}{\partial t_D} + \frac{df_w}{dS_w}\frac{\partial S_w}{\partial x_D} = 0 \tag{3-13}$$

where

$$\frac{df_w}{dS_w} = v_w \tag{3-14}$$

is the specific velocity (dimensionless interstitial velocity) calculated from analysis of fractional flow theory.

f_w in general is a complicated function of saturation derivative making Equation 3-13 a second order, nonlinear and parabolic that can not be solved analytically. Buckley-Leverett (1941) used the simplified definition of fractional flow as:

$$f_w = \frac{1}{1 + \frac{1}{M}} \tag{3-15}$$

where M is the mobility ratio defined in Equation 2-2 which is a function of saturation (S_w). Equation 3-13 with simplified definition of fractional flow is called Buckley-Leverett equation, which is now a first order, nonlinear, hyperbolic equation that can be solved analytically.

The solution of the Buckley-Leverett equation is of the form:

$$x_D = t_D \frac{df_w}{dS_w} \tag{3-16}$$

which gives the dimensionless distance travelled by a given saturation at time t_D (Peters, 2009). Equation 3-16 along with Welge tangent construction (Welge, 1952) is used in fractional flow analysis and frontal advance theory application (Lake, 1989 and Peters).

3.4- APPLICATION OF FRONTAL ADVANCE THEORY

Substituting Equation 3-14 into Equation 3-13 gives:

$$\frac{\partial S_w}{\partial t_D} + v_w \frac{\partial S_w}{\partial x_D} = 0 \tag{3-17}$$

which is called the convective mass balance equation (Siddiqui et al., 1995). Solving this equation results in the saturation at any location and time where v_w as described above is the dimensionless interstitial velocity (also called specific velocity) of the saturation defined in Equation 3-18.

$$\frac{df_w}{dS_w} = v_w = \frac{dx_D}{dt_D} \quad \Rightarrow \qquad x_D = t_D \frac{df_w}{dS_w} \tag{3-18}$$

Solving Equation 3-17 for the front of the displacing fluid (where the saturation change is maximum) is the subject of frontal advance theory. v_w is found from

construction and analysis of fractional flow curves. Welge (1952) and Pope (1980) performed this analysis for waterflood and EOR applications.

Figure 3-2 shows the application of frontal advance theory for waterflooding. As explained above, the slope of the fractional flow curve at any saturation gives the specific velocity of the saturation. The saturation points behind the front show higher velocity that results in overtaking of the front and having multiple saturations at one point. This is not true and the problem is solved by defining a shock at the front of the displacing fluid. Therefore all of the saturations behind the front travel with front velocity that is the slope of the tangent drawn from initial condition (I) to the water-oil fractional flow curve. The tangent point shows the saturation and fractional flow of the front of the flood and the slope is front velocity ($v_{\Delta S}$). The intersection of the tangent line and the line of f_w=1 gives the average oil saturation after break through. The saturations ahead of the front have lower velocity (lower slope, Lake, 1989).

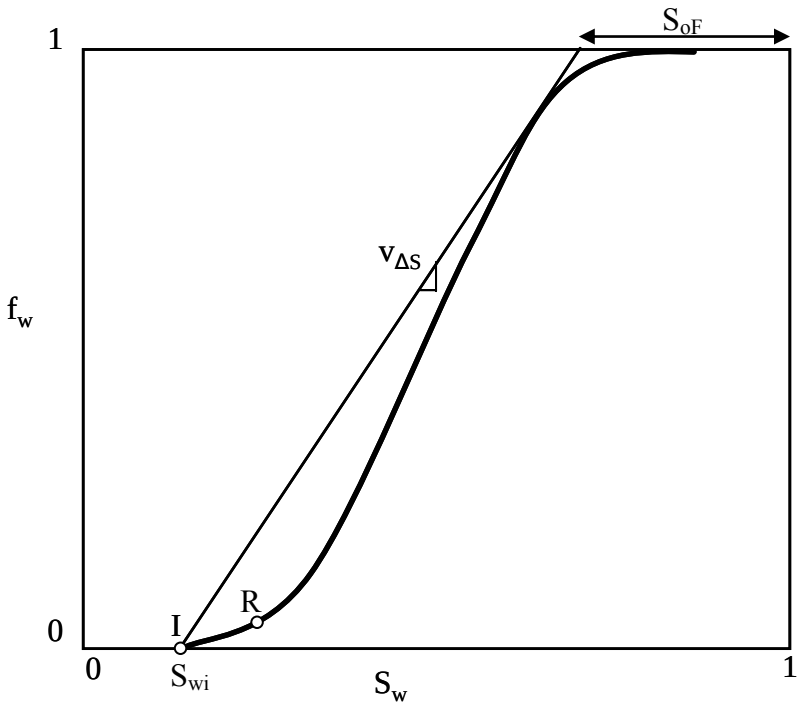

Figure 3-2: Fractional Flow construction for waterflood.

S_{oF} is the final average oil saturation representing the average oil saturation at final condition of the flood after injecting so many pore volumes of displacing fluid. For 1-D (one dimensional) piston-like displacement it is equal to average oil saturation after break through since the volumetric sweep is one. In case of 3-D (three dimensional) flow some portions of the reservoir remains unswept because of heterogeneity, viscous fingering and channeling. However, S_{oF} will be very close to the tangent point and facilitates the use of S_{oF} in calculation of front velocity for 3-D displacement. As explained later, S_{oF} is a key parameter in developing the forecasting model to account for the unswept oil. The front velocity for waterflooding is therefore given by Equation 3-19:

$$v_{\Delta S} = \frac{1}{1 - S_{oF} - S_{wi}} \tag{3-19}$$

If the initial condition is different than I (f_w=0, S_w=S_{wi}) and it has some movable water saturation with $f_w \neq 0$ (like point R on Figure 3-2), then Equation 3-20 describes the front velocity:

$$v_{\Delta S} = \frac{1 - f_{wR}}{S_{oR} - S_{oF}} \tag{3-20}$$

where S_{oR} is the oil saturation and f_{wR} is the fractional flow at start of waterflooding.

For EOR processes there is always another fractional flow curve in addition to water-oil fractional flow to represent the displacing fluid-oil bank flow. Figure 3-3 shows the fractional flow construction for polymer flooding. The left curve is water-oil and the right curve is polymer (displacing fluid)-water fractional flow curve. Ignoring the polymer adsorption (that is very small) and inaccessible pore volume and regarding that polymer is soluble with water, the tangent line to find the chemical front velocity (v_C) is plotted from origin to polymer-oil fractional flow curve. The oil bank region is between initial and displacing fluids, therefore it contacts with both and the intersection of the tangent line with oil-water curve shows the oil bank saturation (point B). The velocity of oil bank front will then be equal to the slope of the line between oil bank and initial fluid condition (point I) as shown in Figure 3-3.

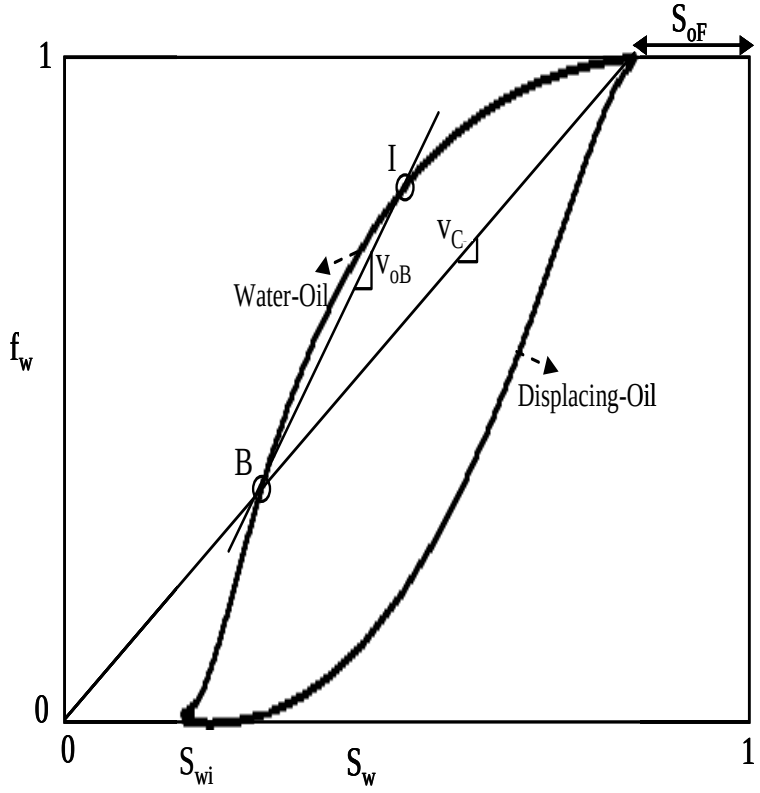

Figure 3-3: Fractional Flow construction for polymer flood.

Equations 3-21 and 3-22 describe the chemical and oil bank front velocities.

$$v_C = \frac{1}{1 - S_{oF}} \tag{3-21}$$

$$v_B = \frac{f_{wI} - f_{wB}}{S_{wI} - S_{wB}} = \frac{f_{wI} - v_C(1 - S_{oB})}{S_w^I - (1 - S_{oB})} \tag{3-22}$$

Figure 3-4 shows fractional flow construction for surfactant-polymer flooding. The major difference from polymer flooding is the enlarged saturation window (S_{wi} to (1-S_{oF})) for displacing fluid-oil curve. This is because of interfacial tension reduction and

mobilization of residual oil, which results in less S_{oF} (higher ultimate recovery). The procedure for analysis of fractional flow curves and calculation of chemical and oil bank fronts velocities are the same as polymer flooding.

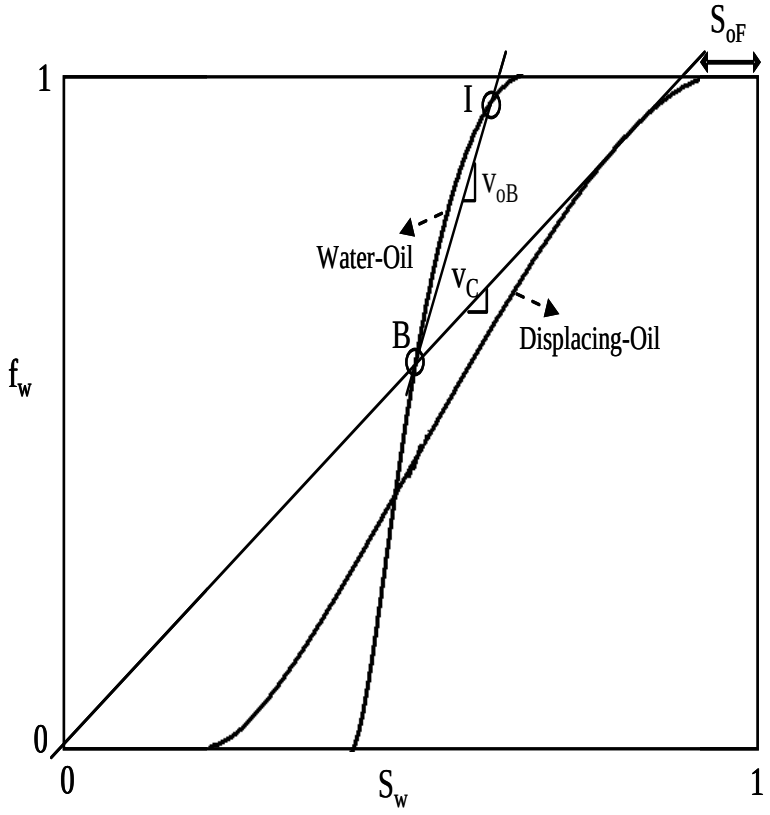

Figure 3-4: Fractional Flow construction for surfactant-polymer flood.

Modeling solvent (gas) flood EOR processes needs the water-solvent fractional flow curve in addition to water-oil curve. As explained in Chapter 2, solvent flooding is usually done as WAG (water alternating gas) to increase the volumetric sweep of the flood. The analysis of WAG fractional flow is based on the method presented by Walsh and Lake (1988). Figure 3-5 shows the fractional flow construction for solvent flooding

(WAG). Point J represents the injection condition. Knowing the WAG ratio, the ratio of water to solvent injection rate, the fractional flow corresponding to point J, f_{wJ}, is give by:

$$f_{wJ} = \frac{W_R}{1+W_R} \tag{3-23}$$

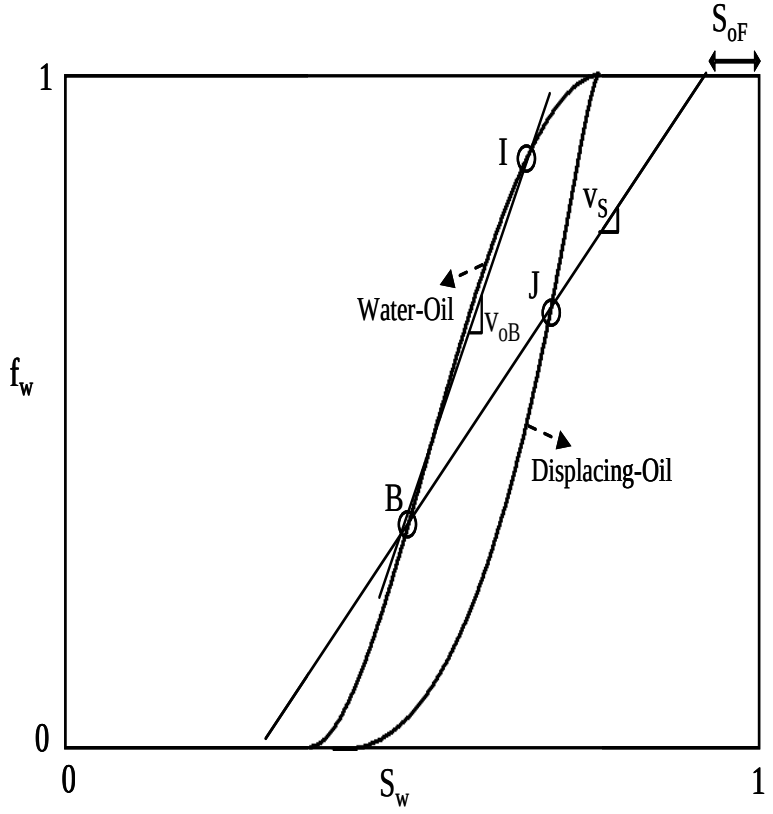

Figure 3-5: Fractional Flow construction for solvent (WAG) flood.

The line that gives the solvent velocity (v_S) is plotted from S_{oF} in upper right to the point J (injection point). The intersection of this line and water-oil curve shows the oil bank (point B) which flows between solvent and initial fluids (point I). The oil bank front velocity is given by the slope of the line drawn between points B and I. Equation 3-24 and 3-25 describe the solvent and oil bank front velocities.

$$v_s = \frac{1 - f_{wJ}}{(1 - S_{oF}) - S_{wJ}} \tag{3-24}$$

$$v_B = \frac{f_{wI} - f_{wB}}{S_{wI} - S_{wB}} = \frac{f_{wI} - (v_s S_{wB} + f_{wJ} - v_s S_{wJ})}{S_{wI} - S_{wB}} \tag{3-25}$$

where f_{wI} is the initial water cut ($f_{wI} = 1 - f_{oI}$) at initial water saturation (S_{wI}), S_{wJ} and f_{wJ} are the injection point water saturation and water cut on water-solvent fractional flow curve. S_{wB} and f_{wB} are oil bank saturation and water cut. See Lake (1989) for more details of fractional flow construction for different EOR processes.

3.5- DESCRIPTION AND APPLICATION OF KOVAL'S METHOD

Miscible displacement in heterogeneous media is much more difficult to model than immiscible displacement because it is less tractable physically and invariably does not lend itself to a simple mathematical formulation especially in the case of unstable miscible displacement (M> 1), which is accompanied by viscous fingering. Koval (1963) presented a method, analogous to the Buckley-Leverett method, for immiscible displacement, to predict the recovery and solvent cut as functions of pore volumes of solvent injected.

Buckley-Leverett frontal advance equation was described in Equation 3-18. The analogous equation for solvent (as displacing fluid) is:

$$\frac{df_s}{dS_s} = \frac{dx_D}{dt_D} \tag{3-26}$$

where subscript *s* stands for solvent.

The analogous equation for fractional flow described in Equation 3-15 is obtained by assuming linear relationship for relative permeability as function of saturation for solvent and oil during miscible flooding (first contact) as described in Equations 3-27 and 3-28:

$$k_{rs} = k^o S_s \tag{3-27}$$

$$k_{ro} = k^o (1 - S_s) \tag{3-28}$$

In addition, Koval modified the viscosity ratio to account for heterogeneity and transverse mixing by introducing a factor, Koval factor (K), into fractional flow equation.

$$K = H_K . E \tag{3-29}$$

where H_K is the heterogeneity factor estimated from experimental data and E is effective viscosity ratio defined as:

$$E = \left[0.78 + 0.22\nu^{1/4}\right]^4 \tag{3-30}$$

where the viscosity ratio is $\nu = \mu_o / \mu_s$.

Equation 3-31 is the solvent (displacing fluid) fractional flow proposed by Koval:

$$f_s = \frac{1}{1 + \left(\frac{1 - S_s}{S_s}\right)\left(\frac{1}{H_K}\right)\left(\frac{1}{E}\right)} = \frac{KS_s}{1 + S_s\ K - 1} \tag{3-31}$$

Taking the derivative of f_s with respect to S_s, $\frac{df_s}{dS_s}$, substituting into Equation 3-26 and eliminating the S_s (which is more difficult to determine than solvent cut) results in solvent cut (f_s) as a function of Koval factor, K, for ant time (t_D) and position (x_D):

$$f_s(x_D,t_D)=\begin{cases}0 & t_D<\dfrac{x_D}{K}\\[2ex] \dfrac{K-\left(\dfrac{Kx_D}{t_D}\right)^{1/2}}{K-1} & \dfrac{x_D}{K}<t_D<x_DK\\[2ex] 1 & t_D>x_DK\end{cases}$$

(3-32)

At the outlet, $x_D=1$, $t_D=1/K$ is the break through time and $t_D=K$ is the sweep out time (where all the oil is displaced by solvent). Figure 3-6 is the original plot of solvent cut versus pore volume injected for different Koval factors. As one can see, the higher the Koval factor (larger heterogeneity and/or viscosity ratio), the earlier solvent breakthrough and the later sweep out that causes less recovery efficiency.

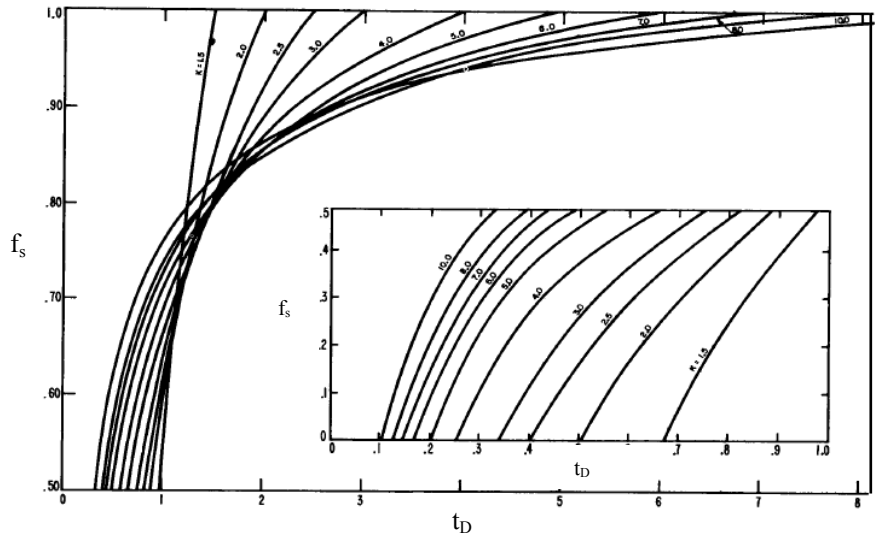

Figure 3-6: Solvent cut as function of dimensionless time for different Koval factors (Koval, 1963).

Knowing that oil cut = f_o = 1-f_s, the cumulative oil recovery is calculated by Equation 3-33:

$$N_{PV} = t_D^{bt} + \int_{t_D^{bt}}^{t_D} f_o dt_D = \frac{2(Kt_D)^{1/2} - 1 - t_D}{K-1} \tag{3-33}$$

where N_{PV} is the cumulative oil recovery as a fraction of total pore volume of the reservoir and t_D^{bt} is the break through time.

Koval's method has been successfully applied for both homogeneous and heterogeneous permeable media. Yang (2002) compared different analytical models like Koval (1963), Todd–Longstaff (1972) and Fayers (1988 and 1994) to describe viscous fingering (displacing fluid tonguing because of viscosity contrast in absence of heterogeneity). These models are all based on a 1-D displacement in the absence of dispersion, using a transversely averaged concentration. Compared to Koval's model, the Todd-Longstaff model uses an additional parameter determined empirically to define the effective viscosity ratio. Fayer's model incorporates additional physics (such as finger width) which requires more parameters determined by fitting experimental or numerical results. The Koval model shows the best results (compared to experimental and numerical simulation results) in moderate to high heterogeneous permeable media, which are more appropriate to reality of the oil reservoirs.

3.6- UTF MATHEMATICAL FORMULATION

3.6.1- Model Assumptions

The general EOR forecasting model is based on the assumption that displacements are locally segregated. "Locally" in this context means on the scale of a

laboratory experiment. Standard theories of displacement (like fractional flow based theories; Buckley 1942) on this scale do not, in general, predict locally segregated. However, in practice local segregation is by far the most common displacement type for light oils, so we assume it to be true from the start. Any deviations from this are accounted for in the Koval approach described below.

There are two advantages of this approach:

1) All of the EOR processes we are to consider behave alike with respect to local behavior. They differ only in the magnitude of the saturations changes (and to be sure their causes).
2) Local segregation renders it unnecessary to know relative permeability data over the complete saturation range. All that is needed are the endpoint relative permeabilities and perhaps a single point on a fractional flow curve. See Lake (1989) for a discussion of the behavior of the local displacements.

In segregated flow, the oil saturation behind the displacing front is reduced to final oil saturation (S_{oF}) while the oil saturation in the unswept zone is S_{oR} which is the oil saturations at the start of the EOR/waterflooding process. We will show that these simplifying assumptions lead to results that agree well with field results and numerical simulation.

Figure 3-7 shows a schematic of a segregated flow displacement when injected fluid displaces the oil. Depending on the process, there may be another constant oil saturation region between S_{oF} and S_{oR}, called the oil bank with saturation S_{oB} that has a constant oil saturation different from (usually higher than) S_{oR} as shown in Figure 3-7 b. Oil bank saturation region usually is created in EOR processes (not waterflooding) and is the result of the miscibility in miscible (solvent) floods or banking of the oil (because of increasing of sweep efficiency) in polymer flooding.

We assume that isothermal and steady state conditions prevail and there is no reaction. Also the initial distribution of the fluids is uniform.

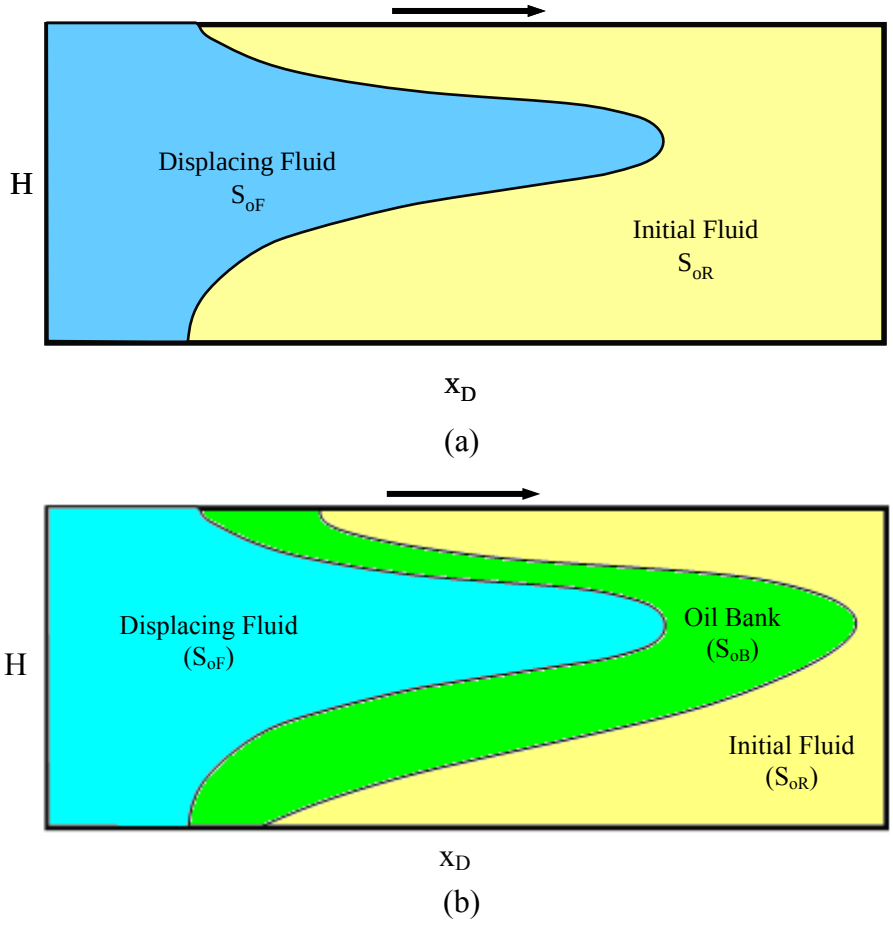

Figure 3-7: Schematic of segregated flow, (a) without oil bank, (b) with oil bank.

3.6.2- One-Front and Multi-Front Displacement Processes

We derive the mathematical model of the general isothermal and waterflood forecasting tool using two approaches. The first approach is the main approach used in development of the UTF (The University of Texas Forecasting Tool). The second

approach is a simpler but heuristic way to describe this model for easier understanding of the model that is explained in section 3.6.4.

The key upgrade from the Koval-based approach is the replacement of a physical dimension, thickness, with storage capacity. Later we show how the flow-storage capacity curve is parameterized with the Koval factor. Figure 3-8 shows the typical storage capacity profile. We differentiate the storage capacity profiles of secondary and tertiary recovery based on the number of constant saturation regions that occur during the flood. For instance, in waterflooding there are two saturation regions of S_{oF} and S_{oR}, depicted in Figure 3-8, the so-called "one-front displacement" case. For EOR recovery methods, such as chemical and gas flooding, an oil bank region is created and there are three saturation regions as shown as S_{oF}, S_{oB} and S_{oR} on Figure 3-10. Therefore, there are two displacing fronts, which is the "two-front displacement" case.

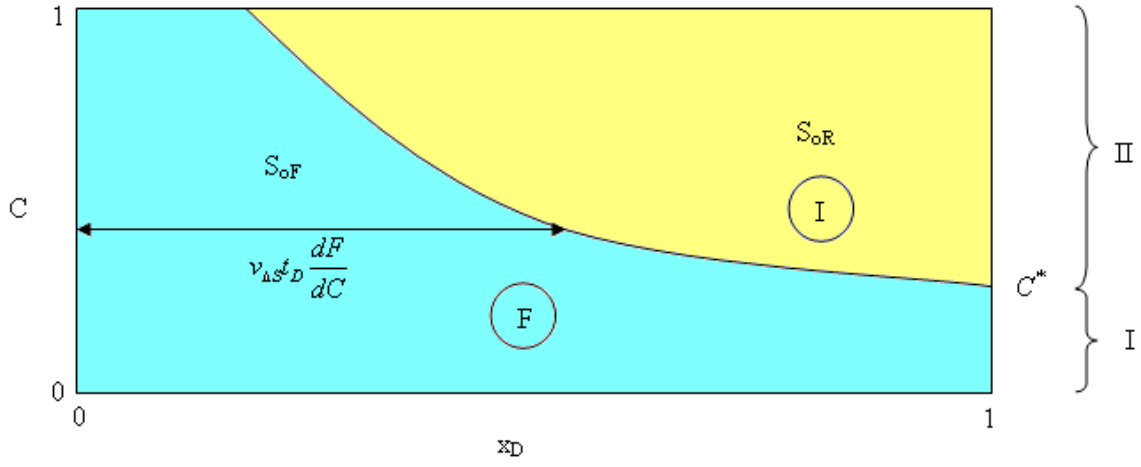

Figure 3-8: Typical storage capacity profile for a one-front displacement after breakthrough of displacing agent (F=Final, I=Initial).

The fraction of injected fluid flowing into a given storage capacity (given layer in case of layered reservoirs) is proportional to (k/φ) of that location and equals to $t_D \frac{dF}{dC}$, where t_D is the total pore volume of injected fluid and $\frac{dF}{dC}$ is derivative of flow capacity (F) to storage capacity (C) defined in Section 3.2 (see Appendix-A for more details). The displacing fluid front location is given by Equation 3-34:

$$x_{D_f} = \begin{cases} 1 & 0 < C < C^* \\ v_{\Delta S} t_D \frac{dF}{dC} & C^* < C < 1 \end{cases} \tag{3-34}$$

where $v_{\Delta S}$ is injected (displacing) fluid dimensionless velocity (specific velocity; velocity normalized by the bulk fluid interstitial velocity), which is constant and is found from fractional flow analysis (construction) and $C^* = C(x_{D_f} = 1; \textit{production point})$.

Oil saturation at a given C (local oil saturation), $S_o\big|_C$, is:

$$\begin{cases} S_o\big|_C = t_D v_{\Delta S} (\frac{dF}{dC}) S_{oF} + \left[1 - t_D v_{\Delta S} (\frac{dF}{dC})\right] S_{oR}, & II \\ S_o\big|_C = S_{oF}, & I \end{cases} \tag{3-35}$$

where I and II are different regions on C-x_D plot depicted on Figure 3-8.

Integrating the local oil saturation, $S_o\big|_C$ with respect to C yields the average oil saturation:

$$\bar{S}_o = \int_{C=0}^{C=1} S_o\big|_C dC = \int_{C=0}^{C=C^*} S_o\big|_C dC + \int_{C=C^*}^{C=1} S_o\big|_C dC = I + II \tag{3-36}$$

This is a step change in solving the ordinary differential equation(s) (ODEs) of the local oil saturation described in Equation 3-35 since we solve directly for average oil saturation of the reservoir, $\bar{S}_o$, by solving the obtained integral equation instead of an ODE (or a set of ODEs for EOR cases). Integral equations are usually easier to solve than differential equations. In addition, upon solving the integral equation, we already solved the up-scaling problem of the fluid flow that could by itself be a very complicated problem. Substituting the terms in Equation 3-36 from Equation 3-35, one can write:

$$\bar{S}_o = S_{oF}C^* + \int_{C=C^*}^{C=1} \left[(S_{oF} - S_{oR}) v_{\Delta S} t_D \frac{dF}{dC} + S_{oR} \right] dC \tag{3-37}$$

Knowing that $F(C=0)=0 \quad and \quad F(C=1)=1$:

$$\bar{S}_o = S_{oR} - \Delta S_o \left[C^* + v_{\Delta S} t_D (1 - F^*) \right], \tag{3-38}$$

$$\Delta S_o = S_{oR} - S_{oF} \qquad and \qquad F^* = F(C^*)$$

at $C^* = 1 \Rightarrow F^* = 1 \Rightarrow \bar{S}_o = S_{oF}$

From the above equation one can see that

$\bar{S}_o = \bar{S}_o(C^*) = \bar{S}_o(C^*(t_D)) = \bar{S}_o(t_D)$

that shows $\bar{S}_o$ is a function of t_D as is C^* (will be proven later in this section).

Solving Equation 3-34 for break through (x_{Df}=1) we can write:

$$\left(\frac{dF}{dC}\right)\Big|_{C^*} = \frac{1}{v_{\Delta S} t_D} \tag{3-39}$$

Up to here, the formulation is general but we must take advantage of an equation to describe the F-C function as F=F(C). We used Koval fractional flux model because of it's abilities, simplicity and wide application even in very heterogeneous permeable media. Using Koval F-C model:

$$F = \frac{1}{1+\frac{1-C}{KC}} \qquad \text{: Koval fractional flux model} \tag{3-40}$$

where K is Koval factor that is a function of both mobility ratio of the phases and reservoir heterogeneity. As did Koval we call it the *Effective Mobility Ratio* since, as we shall see, it is able to capture the effects of reservoir heterogeneity and mobility of the phases effectively even for high heterogeneous permeable media. The conventional mobility ratio defined in literature as ratio of displacing to displaced fluid mobility doesn't include the effects of reservoir heterogeneity.

The derivative of F with respect to C is calculated as:

$$\frac{dF}{dC} = \frac{K}{(1+(K-1)C)^2} \tag{3-41}$$

Substituting in Equation 3-40:

$$\frac{1}{v_{\Delta S} t_D} = \frac{K}{(1+(K-1)C)^2} \tag{3-42}$$

solving Equation 3-42 for C results in C=C^*:

$$C^* = \frac{\sqrt{v_{\Delta S} t_D K} - 1}{K - 1} \tag{3-43}$$

and

$$F^* = F(C^*) = \frac{1}{1 + \frac{1 - C^*}{KC^*}} = \frac{K\left[(v_{\Delta S} t_D K)^{1/2} - 1\right]}{(v_{\Delta S} t_D K)^{1/2}(K - 1)} \tag{3-44}$$

where F^* and C^* are flow capacity and storage capacity at x_D=1.

Equations 3-45 and 3-46 describe F^* and C^* as discontinuous functions of time (t_D).

$$C^* = \begin{cases} 0 & t_D \le t_{D_{BT}} \\ \dfrac{\sqrt{v_{\Delta S} t_D K} - 1}{K - 1} & t_{D_{BT}} < t_D < t_{D_{SW}} \\ 1 & t_{D_{SW}} \le t_D \end{cases} \tag{3-45}$$

$$F^* = \begin{cases} 0 & t_D \le t_{D_{BT}} \\ \dfrac{K\left[(v_{\Delta S} t_D K)^{1/2} - 1\right]}{(v_{\Delta S} t_D K)^{1/2}(K - 1)} & t_{D_{BT}} < t_D < t_{D_{SW}} \\ 1 & t_{D_{SW}} \le t_D \end{cases} \tag{3-46}$$

Figure 3-9 shows a typical F^*-t_D curve.

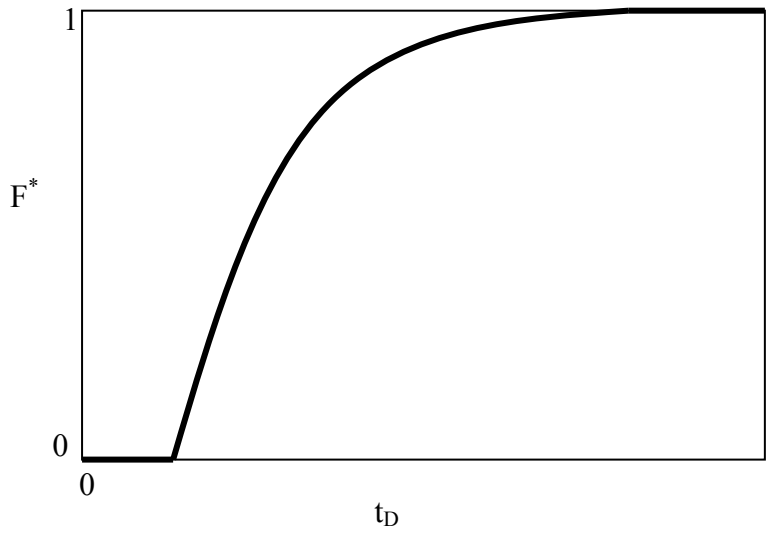

Figure 3-9: Schematic of F^* vs t_D plot.

where:

$$\begin{cases} t_{D_{BT}} \text{ is the break-through time} = \dfrac{1}{v_{\Delta S} K} \\ t_{D_{SW}} \text{ is the sweep out time} = \dfrac{K}{v_{\Delta S}} \end{cases} \tag{3-47}$$

For two-front displacements, as shown in Figure 3-10, (for example when an oil bank region is created as in chemical or solvent EOR flooding, each of the oil bank and displacing fluid fronts are described by separate F-C curves as they have different velocities (because of different mobilities; calculated from fractional flow construction). Equation 3-48 describes the local oil saturation (at a given storage capacity (layer)):

$$\begin{cases} S_o\big|_C = \overbrace{t_D v_C (\frac{dF}{dC})_C}^{\text{F}} S_{oF} + \overbrace{t_D \left[v_B (\frac{dF}{dC})_B - v_C (\frac{dF}{dC})_C \right]}^{\text{B}} S_{oB} + \overbrace{\left[1 - t_D v_B (\frac{dF}{dC})_B \right]}^{\text{I}} S_{oR} , & III \\ S_o\big|_C = t_D v_C (\frac{dF}{dC})_C S_{oF} + \left[1 - t_D v_C (\frac{dF}{dC})_C \right] S_{oB} , & II \\ S_o\big|_C = S_{oF} , & I \end{cases}$$

(3-48)

where subscripts B and C stand for displacing fluid and oil bank, respectively, and $S_o\big|_C$ is local oil saturation at a given C (storage capacity). $(\frac{dF}{dC})_C$ and $(\frac{dF}{dC})_B$ are derivatives of displacing fluid and oil bank flow capacities respect to C which are defined as:

$$F_C = F(K = K_C) = \frac{1}{1 + \frac{1-C}{K_C C}} , \qquad F_B = F(K = K_B) = \frac{1}{1 + \frac{1-C}{K_B C}} \tag{3-49}$$

C_C^* *and* C_B^* for t_D greater than the break through time are defined as:

$$C_C^* = \frac{\sqrt{v_C t_D K_C} - 1}{K_C - 1} , \qquad C_B^* = \frac{\sqrt{v_B t_D K_B} - 1}{K_B - 1} \tag{3-50}$$

Equation 3-48 is a set of ODEs that will be solved with the same procedure as for the one-front displacement (secondary recovery) processes. The solution method includes converting the set of ODEs to integral equations and solving for average oil saturation as function of time, $\bar{S}_o(t_D)$.

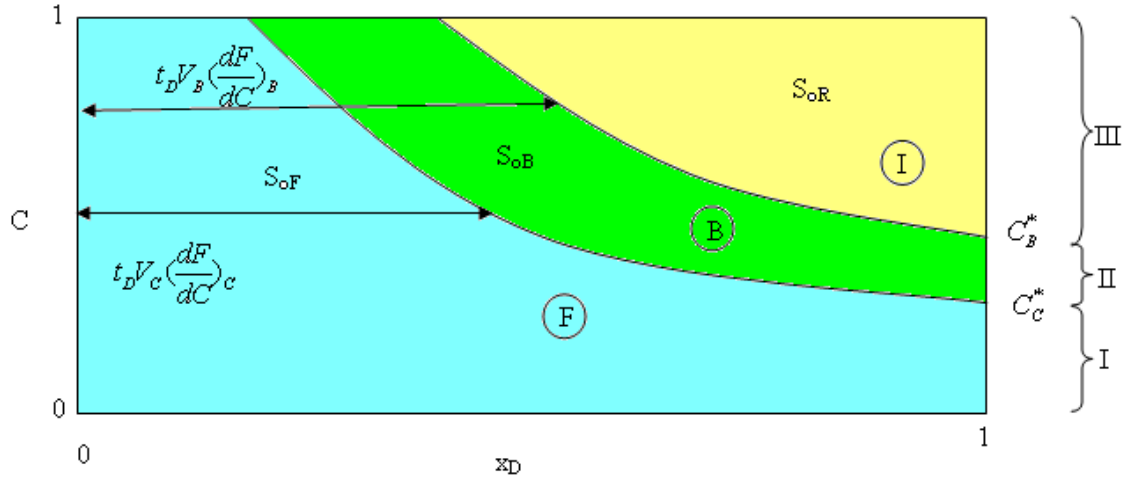

Figure 3-10: Typical storage capacity profile for a two-front displacement after breakthrough of displacing agent (F=Final, B=Bank, I=Initial).

3.6.3- Evaluation of the Forecasting Model at Different Times

Let's consider this problem in different times defined as below:

$$\begin{cases} t_{D_{BT}}^{B} = \dfrac{1}{K_B v_B} & , \text{ Oil Bank Breakthrough} \\ t_{D_{BT}}^{C} = \dfrac{1}{K_C v_C} & , \text{ Displacing Fluid Breakthrough} \\ t_{D_{SW}}^{B} = \dfrac{K_B}{v_B} & , \text{ Oil Bank Sweep out} \\ t_{D_{SW}}^{C} = \dfrac{K_C}{v_C} & , \text{ Displacing Fluid Sweep out} \end{cases} \tag{3-51}$$

1) For $t_D \le t_{D_{BT}}^{B}$ $(C_B^* = 0, C_C^* = 0)$

$$\bar{S}_o = \int_{C=0}^{C=1} S_o dC = \int_{C=0}^{C=C_C^*} S_o dC + \int_{C=C_C^*}^{C=C_B^*} S_o dC + \int_{C=C_B^*}^{C=1} S_o dC$$

$$C_B^* = 0 \text{ and } C_C^* = 0 \Rightarrow \bar{S}_o = \int_{C=0}^{C=1} S_o dC_B = III$$

$$\bar{S}_o = \int_{C=0}^{C=1} S_o dC = t_D v_C S_{oF} \int_{C=0}^{C=1} (\frac{dF}{dC})_C dC + t_D (v_B - v_C) S_{oB} \int_{C=0}^{C=1} (\frac{dF}{dC})_B dC$$
$$- t_D v_B S_{oR} \int_{C=0}^{C=1} (\frac{dF}{dC})_B dC + S_{oR}$$

We know: $\int_{C=0}^{C=1} (\frac{dF}{dC}) dC = 1$

Therefore:

$$\begin{aligned} \bar{S}_o &= t_D v_C S_{oF} + t_D (v_B - v_C) S_{oB} + (1 - t_D v_B) S_{oR} \\ &= v_C (S_{oF} - S_{oB}) + v_B (S_{oB} - S_{oR})\ t_D + S_{oR} \end{aligned} \qquad (3\text{-}52)$$

that is a linear function of t_D ($\bar{S}_o = a t_D + b$)

2) For $t_{D_{BT}}^B \le t_D \le t_{D_{BT}}^C$ $\qquad (0 \le C_B^* \le 1, C_C^* = 0)$

$$\bar{S}_o = \int_{C=0}^{C=1} S_o dC = \int_{C=0}^{C=C_C^*} S_o dC + \int_{C=C_C^*}^{C=C_B^*} S_o dC + \int_{C=C_B^*}^{C=1} S_o dC$$

$$C_C^* = 0 \ \Rightarrow \ \bar{S}_o = \int_{C=0}^{C=C_B^*} S_o dC + \int_{C=C_B^*}^{C=1} S_o dC = II + III$$

$$\bar{S}_o = \int_{C=0}^{C=C_B^*} \left[t_D v_C S_{oF} \left(\frac{dF}{dC}\right)_C + [1 - t_D v_C \left(\frac{dF}{dC}\right)_C] S_{oB} \right] dC +$$
$$\int_{C=C_B^*}^{C=1} \left[t_D v_C S_{oF} \left(\frac{dF}{dC}\right)_C + t_D [v_B \left(\frac{dF}{dC}\right)_B - v_C \left(\frac{dF}{dC}\right)_C] S_{oB} \right] dC$$

$$\bar{S}_o = S_{oB} C_B^* + t_D v_C (S_{oF} - S_{oB}) + S_{oR}(1 - C_B^*) + t_D v_C (1 - F_{C_B}^*) S_{oF} +$$
$$t_D [v_B (1 - F_{B_B}^*) - v_C (1 - F_{C_B}^*)] S_{oB} - t_D v_B (1 - F_{B_B}^*) S_{oR} \qquad (3\text{-}53)$$

$$F_{C_C}^* = F_C(C = C_C^*), \quad F_{C_B}^* = F_C(C = C_B^*), \quad F_{B_B}^* = F_B(C = C_B^*)$$

3) For $t_{D_{BT}}^C \le t_D \le t_{D_{SW}}^B$ $\qquad 0 \le C_B^* \le 1, \;\; 0 \le C_C^* \le 1$

$$\bar{S}_o = \int_{C=0}^{C=1} S_o dC = \int_{C=0}^{C=C_C^*} S_o dC + \int_{C=C_C^*}^{C=C_B^*} S_o dC + \int_{C=C_B^*}^{C=1} S_o dC = I + II + III$$

$$\bar{S}_o = S_{oF} C_C^* + S_{oB}(C_B^* - C_C^*) + t_D v_C (F_{C_B}^* - F_{C_C}^*)(S_{oF} - S_{oB}) + S_{oR}(1 - C_B^*) + t_D v_C (1 - F_{C_B}^*) S_{oF} +$$
$$t_D [v_B (1 - F_{B_B}^*) - v_C (1 - F_{C_B}^*)] S_{oB} - t_D v_B (1 - F_{B_B}^*) S_{oR} \qquad (3\text{-}54)$$

4) For $t_{D_{SW}}^B \le t_D \le t_{D_{SW}}^C$ $\qquad C_B^* = 1, \;\; 0 \le C_C^* \le 1$

$$\bar{S}_o = \int_{C=0}^{C=1} S_o dC = \int_{C=0}^{C=C_C^*} S_o dC + \int_{C=C_C^*}^{C=1} S_o dC = I + II$$

$$\bar{S}_o = S_{oF} C_C^* + S_{oB}(C_B^* - C_C^*) + t_D v_C (F_{C_B}^* - F_{C_C}^*)(S_{oF} - S_{oB}) \qquad (3\text{-}55)$$

5) For $t_{D_{SW}}^C \le t_D$ $\qquad C_B^* = 1, C_C^* = 1$

$$\bar{S}_o = \int_{C=0}^{C=1} S_o dC = \int_{C=0}^{C=1} S_o dC = I$$

$$\bar{S}_o = S_{oF} \tag{3-56}$$

Above equations express average oil saturation ($\bar{S}_o$) as a function of time (t_D). Figure 3-11 shows a typical output of the general EOR forecasting tool (UTF).

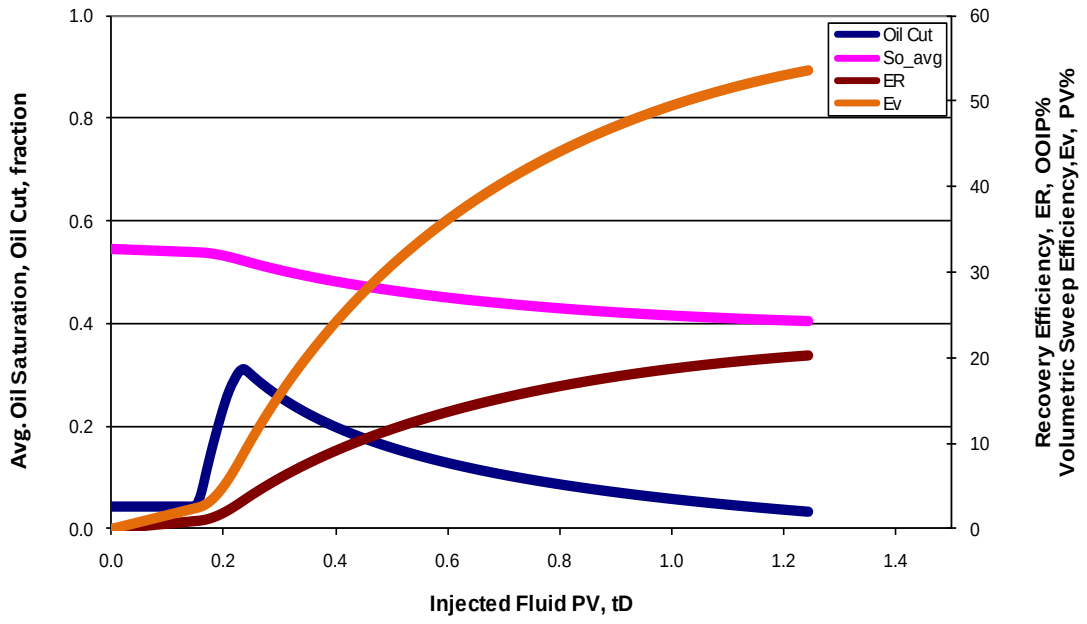

Figure 3-11: Typical output of general isothermal EOR and waterflood forecasting tool (UTF).

3.6.4- Simplified Approach to the Forecasting Model

Based on what we discussed above, a simpler but heuristic approach comes to mind to describe the oil saturation as a step function which starts from S_{oF} at injection

point and propagates toward production point (with saturation of S_{oR}, S_{oB} or S_{oF}) with a combination of waves and shocks as expressed in the following equation:

$$S_o\ x_D,t_D\ = S_{oR} + \ S_{oB} - S_{oI}\ \ C_1\ x_D,t_D\ \ + \ S_{oF} - S_{oB}\ \ C_2\ \ x_D,t_D \tag{3-57}$$

where $C\ x_D,t_D$ works as a transition function here that was calculated in previous approach as:

$$C\ x_D,t_D\ = \begin{cases} 0 & x_D > Kvt_D \\ \dfrac{K\sqrt{\dfrac{t_D v}{Kx_D}} - 1}{K-1} & Kvt_D > x_D > \dfrac{v}{K}t_D \\ 1 & x_D < \dfrac{v}{K}t_D \end{cases} \tag{3-58}$$

where v is velocity (specific velocity) of oil bank or displacing fluid front.

Figure 3-12 shows the schematic average oil saturation profile when there is an oil bank. C_1 and C_2 represent the oil bank and displacing fluid transition functions respectively.

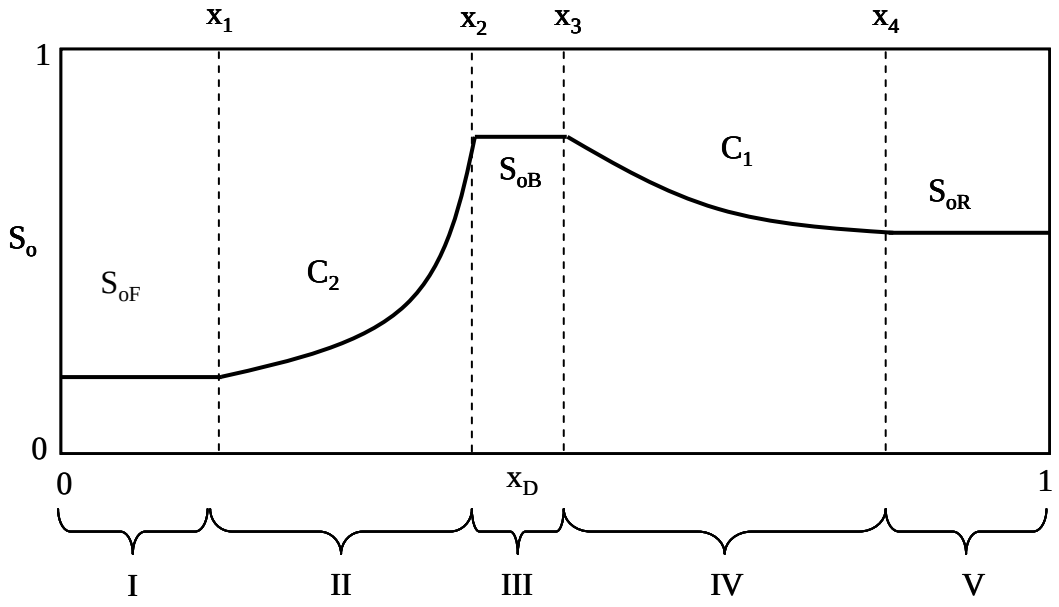

Figure 3-12: Schematic oil saturation profile for a two-front displacement.

The key locations on Figure 6 are:

$$\begin{cases} x_{D1} = \dfrac{v_C}{K_C} t_D, & \text{Injected Fluid Tail} \\ x_{D3} = v_C K_C t_D, & \text{Injected Fluid Front} \\ x_{D1} = \dfrac{v_B}{K_B} t_D, & \text{Oil Bank Tail} \\ x_{D4} = v_B K_B t_D, & \text{Oil Bank Front} \end{cases} \tag{3-59}$$

Intuitively the average oil saturation is calculated as the summation of oil saturation of different regions on Figure 3-12:

$$\bar{S}_o(t_D) = \int_{x_D=0}^{x_D=1} S_o(t_D)\, dx_D = I + II + III + IV + V \tag{3-60}$$

where I, II, III, IV and V are the regions shown in Figure 3-12 and calculated as follow:

Region-I:

$$I = \int_{x_D=0}^{x_D=x_{D1}} S_o(x_D,t_D)\,dx_D = S_{oF}(x_{D1}) = S_{oF}(\frac{v_C}{K_C}t_D) \tag{3-61}$$

Region-II:

$$\int_{x_{D1}}^{x_{D2}} C(x_D,t_D)dx_D = \int_{x_{D1}}^{x_{D2}} \frac{K\sqrt{\frac{t_D v}{Kx_D}}-1}{K-1}\,dx_D = \left[(\frac{1}{K-1})\left(2K\sqrt{\frac{t_D v x_D}{K}}-x_D\right)\right]_{x_{D1}}^{x_{D2}}$$

$$II = \int_{x_D=x_{D1}}^{x_D=x_{D2}} S_o(x_D,t_D)\,dx_D = \int_{x_D=x_{D1}}^{x_D=x_{D2}} S_{oB}+(S_{oF}-S_{oB})C_2(x_D,t_D)\;\;dx_D =$$

$$\left[S_{oB}x_D+(S_{oF}-S_{oB})(\frac{1}{K_C-1})\left(2K_C\sqrt{\frac{t_D v_C x_D}{K_C}}-x_D\right)\right]_{x_{D1}}^{x_{D2}} \tag{3-62}$$

Region-III:

$$III = \int_{x_D=x_{D2}}^{x_D=x_{D3}} S_o(x_D,t_D)\,dx_D = \int_{x_D=x_{D2}}^{x_D=x3}\left[\begin{array}{l} S_{oR}+(S_{oB}-S_{oR})C_1(x_D,t_D)+ \\ (S_{oF}-S_{oB})C_2(x_D,t_D)\end{array}\right]dx_D =$$

$$\left[\begin{array}{l} S_{oR}x_D+(S_{oB}-S_{oR})(\frac{1}{K_B-1})\left(2K_B\sqrt{\frac{t_D v_C x_D}{K_B}}-x_D\right)+ \\ (S_{oF}-S_{oB})(\frac{1}{K_C-1})\left(2K_C\sqrt{\frac{t_D v_C x_D}{K_C}}-x_D\right)\end{array}\right]_{x_{D2}}^{x_{D3}} \tag{3-64}$$

Region-IV:

$$IV = \int_{x_D=x_{D3}}^{x_D=x_{D4}} S_o(x_D,t_D)\,dx_D = \int_{x_D=x_{D3}}^{x_D=x_{D4}} S_{oR} + (S_{oB} - S_{oR})C1(x_D,t_D)\;\; dx_D =$$

$$\left[S_{oR}x_D + (S_{oB} - S_{oR})\left(\frac{1}{K_B - 1}\right)\left(2K_B\sqrt{\frac{t_D v_B x_D}{K_B}} - x_D \right)\right]_{x_{D3}}^{x_{D4}}$$

(3-65)

Region-V:

$$V = \int_{x_D=x_{D4}}^{x_D=1} S_o(x_D,t_D)\,dx_D = S_{oR}(1 - x_{D4}) = S_{oR}(v_B K_B t_D) \tag{3-66}$$

To compute the average oil saturation at a given time we just need to know what regions are still present at that time to be considered in calculations. Therefore, average oil saturation at different times is calculated as follow:

1) For $t_D \le t_{D_{BT}}^B$:

At times before break-through of oil bank all of the five regions pointed above are present, therefore:

$$\bar{S}_o(t_D) = \int_{x_D=0}^{x_D=1} S_o(t_D)\,dx_D = I + II + III + IV + V \tag{3-67}$$

2) For $t_{D_{BT}}^B \le t_D \le t_{D_{BT}}^C$:

The fifth region no longer exists.

$$\bar{S}_o(t_D) = \int_{x_D=0}^{x_D=1} S_o(t_D)\, dx_D = I + II + III + IV \tag{3-68}$$

3) For $t_{D_{BT}}^{C} \le t_D \le t_{D_{SW}}^{B}$:

There will be just regions I, II and III.

$$\bar{S}_o(t_D) = \int_{x_D=0}^{x_D=1} S_o(t_D)\, dx_D = I + II + III \tag{3-69}$$

4) For $t_{D_{SW}}^{B} \le t_D \le t_{D_{SW}}^{C}$:

Regions I and II are the only regions present at these times.

$$\bar{S}_o(t_D) = \int_{x_D=0}^{x_D=1} S_o(t_D)\, dx_D = I + II \tag{3-70}$$

5) For $t_{D_{SW}}^{C} \le t_D$:

Only region I exists.

$$\bar{S}_o(t_D) = \int_{x_D=0}^{x_D=1} S_o(t_D)\, dx_D = I \tag{3-71}$$

As one can see, the above equations describe the average oil saturation as function of time ($\bar{S}_o = \bar{S}_o(t_D)$) for the entire flooding time. This gives us a basis to calculate the main functions for performance evaluation of EOR/waterflood processes which is the subject of the next section.

3.7- MAIN EQUATIONS FOR WATERFLOOD/EOR PERFORMANCE EVALUATION

Using the forecasting model the average oil saturation is calculated as a function of time. Computing the average oil saturation changes with time, the recovery efficiency, cumulative oil production and oil cut (all as functions of time) are calculable as below:

$$E_R(t) = \frac{S_{oR} - \bar{S}_o(t)}{S_{oi}} \tag{3-72}$$

where S_{oi} is original oil saturation of the reservoir, E_R is the recovery efficiency (oil recovered expressed as a fraction of the original oil in place) and t is real or dimensionless time.

$$N_P(t) = E_R(t)(OOIP) \tag{3-73}$$

where N_P is cumulative oil production and OOIP is original oil in place.

Calculating the recovery efficiency enables us to compute the volumetric sweep efficiency, E_v, using ultimate displacement efficiency, E_D. Claridge (1971), Dietz (1952), Dykstra-Parsons (1950), Crane (1963), Stiles (1949) and Johnson (1965) discussed and developed models to predict volumetric sweep efficiencies (areal or vertical). Note that these are a posteriori calculations here; the effects of all of these quantities are subsumed into the Koval factor.

$$E_V(t) = \frac{E_R(t)}{E_D} \tag{3-74}$$

$$E_D = \frac{S_{oR} - S_{or}}{S_{oi}} \tag{3-75}$$

where S_{or} is laboratory (ideal) residual oil saturation to waterflood or EOR process. It's notable that using the E_D (ultimate displacement efficiency) in calculation of E_V

(volumetric sweep efficiency) is compatible with assumption of segregated flow that has been explained before.

Oil cut is calculated using Equation 3-76;

$$Oil\,Cut = f_o = \frac{\Delta \bar{S}_o}{\Delta t_D} = \frac{\bar{S}_o^{n+1} - \bar{S}_o^{n}}{t_D^{n+1} - t_D^{n}} \tag{3-76}$$

where S_o^{n+1}, S_o^n, t_D^{n+1} and t_D^n are average oil saturations and injected fluid pore volumes at subsequent flooding times of t^{n+1} and t^n.

Calculating the oil cut, oil production rate (q_o) is obtained by Equation 3-77:

$$q_o = q_t f_o \tag{3-77}$$

where q_t is the total production rate.

These equations are used for history matching of the field and numerical simulation results of waterflood/EOR projects which is the subject of Chapter 5. Table 3-1 summarizes the main equations of EOR/waterflood performance evaluation.

Output Variable	Equation	Equation#
Recovery Efficiency, E_R	$E_R(t) = \frac{S_{oR} - \bar{S}_o(t)}{S_{oi}}$	3-72
Ultimate Displacement Efficiency, E_D	$E_D = \frac{S_{oR} - S_{or}}{S_{oi}}$	3-75
Volumetric Sweep Efficiency, E_v	$E_V(t) = \frac{E_R(t)}{E_D}$	3-74
Cumulative Oil Recovery, N_p	$N_P(t) = E_R(t)(OOIP)$	3-73
Oil Cut, f_o	$f_o = \frac{\Delta \bar{S}_o}{\Delta t_D} = \frac{\bar{S}_o^{n+1} - \bar{S}_o^n}{t_D^{n+1} - t_D^n}$	3-76
Oil Production Rate, q_o	$q_o = q_t f_o$	3-77

Table 3-1: Summary of main equations for EOR/Waterflood performance evaluation.

Chapter 4: SENSITIVITY ANALYSIS

4.1- INTRODUCTION

Often, the input variables to model have ranges (because of uncertainty) that form statistical distributions. The uncertainty of input variables and the relevant sensitivity of output results to changes in the input make it necessary to study the problem stochastically rather than deterministically. Therefore, we perform a sensitivity analysis (SA) to quantitatively understand the influence of input variables or parameters on the distributions of uncertainty in output results. The results of SA help to identify the most influential input parameters on uncertainty of outputs and provide insight into which input parameters need more attention to better manage the uncertainties.

Sensitivity analysis (SA) is a method to ascertain how each of the model input parameters influences the variations in the model outputs. Generally, SA helps understand:

- How the variation in the output of a model can be apportioned, qualitatively or quantitatively, to different sources of variations.
- How the given model depends on the information that is fed into it.

From a technical point of view, it is important to choose the most accurate and robust SA method that provides both reliable sensitivity measures, is independent of model type, and gives global results.

This chapter starts with preliminary sensitivity analysis using the Chemical Flooding Predictive Model (CFPM). We then perform advanced sensitivity analysis using the Winding Stairs (WS) method. In the final step, the results of SA are used to characterize the most important sources of uncertainty of output variables (such as

ultimate recovery efficiency and peak oil rate). These results help to develop the in-situ correlations of the forecasting model that will be discussed in Chapter 6.

4.2- PRELIMINARY SENSITIVITY ANALYSIS USING CFPM

Chemical EOR, including polymer, surfactant-polymer (SP) and alkaline-surfactant-polymer (ASP) flooding is one of the EOR subsets that has good potentials of oil recovery especially in oil fields with low to moderate oil viscosity, salinity and temperature. SP flooding involves the injection of a surface-active agent (surfactant) to increase oil production by lowering the interfacial tension between oil and water and mobilizing the trapped oil (Lake, 1989). The chemical flood predictive model (CFPM) was developed by Paul et al. (1982) as an analytical model to identify candidate reservoirs for SP flooding. The model predicts the performance of ultimate oil recovery efficiency and oil rate vs. time based on fractional flow theory. It was validated against numerical simulation and field data (Paul et al., 1982).

The CFPM calculates the ultimate recovery efficiency (E_R) as a product of volumetric sweep efficiency (E_V), displacement efficiency (E_D), and efficiency of the mobility buffer (E_{MBe}). In addition, the oil-rate time plot is calculated based on the calculated E_R, the peak oil rate, oil bank arrival time (t_{DB}), peak oil rate time (t_{Ds}), and complete sweep out time (t_{Dsw}). Details of CFPM equations and calculations are given in the original paper by Paul et al. (1982). The discussion below summarizes the most important parts of the CFPM that might be necessary to understand before proceeding.

4.2.1- Mathematical Formulation of Chemical Flood Predictive Model

The ultimate recovery efficiency E_R is calculated as below:

$$E_R = E_V E_D E_{MB} \tag{4-1}$$

where

$$E_V = C_m + \frac{t_{Ds}}{D_s}(1 - F_m) \tag{4-2}$$

where C_m and F_m are coordinates of point m on F-C (fractional flux) curve such that $t_{Dsm}=D_s$. The t_{Ds} in Equation 4-2 is the injected surfactant volume and D_s is the adsorption pore volume as a fraction of the pore volume defined as:

$$D_s = \left(\frac{1-\varphi}{\varphi}\right)\left(\frac{\rho_r a_s}{\rho_s C_s}\right) \tag{4-3}$$

E_D is the ultimate displacement efficiency:

$$E_D = 1 - \frac{S_{or}}{S_{oR}} \tag{4-4}$$

where subscripts o, s and r stand for oil, surfactant and rock respectively, a_s is active surfactant retention, S_{or} is the residual oil saturation after SP flood and S_{oR} is remaining oil saturation at start of SP flood. The mobility buffer efficiency is given by Equation 4-5 and 4-6.

$$E_{MB} = (1 - E_{MBe})\left[1 - \exp\left(\frac{-0.4 t_{DMB}}{E_V^{1.2}}\right)\right] + E_{MBe} \tag{4-5}$$

$$E_{MBe} = 0.71 - 0.6 V_{DP} \tag{4-6}$$

where t_{DMB} is the volume of the mobility buffer as fraction of pore volume, E_{MBe} is the mobility buffer efficiency extended to $t_{DMB}=0$ and V_{DP} known as the Dykstra-Parsons coefficient used for reservoir heterogeneity measurements, which is defined as:

$$V_{DP} = \frac{k_{50} - k_{84.1}}{k_{50}} \tag{4-7}$$

where k_{50} and $k_{84.1}$ are the permeability values at (%>50) and (%>84.1) on straight line fit to a log-probability plot of permeability (Dykstra and Parsons, 1950).

The oil-rate time plot is calculated based on the E_R calculated above. The three important dimensionless times of oil bank arrival time (t_{DB}), peak oil rate time (t_{Ds}), complete sweep out time (t_{Dsw}) and peak oil rate (q_{pk}) are calculated as below such that the same ultimate recovery efficiency is obtained.

$$t_{DB} = \left(\frac{S_{oB} - S_{oI}}{f_{oB} - f_{oI}} \right) t_{Ds} \tag{4-8}$$

where f_{oB} and S_{oB} are oil bank fractional flow and saturation, f_{oI} and S_{oI} are initial (at start of SP flood) oil fractional flow and saturation.

$$t_{Ds} = 1 + D_s - S_{or} \tag{4-9}$$

The corrected breakthrough times accounting for heterogeneity are:

$$\hat{t}_{DB} = \frac{t_{DB}}{H_K} \tag{4-10}$$

$$\hat{t}_{Ds} = \frac{t_{Ds}}{H_K} \tag{4-11}$$

where H_K is the Koval heterogeneity factor related to Dykstra-Parsons coefficient (V_{DP})

$$\log(H_K) = \frac{V_{DP}}{(1 - V_{DP})^{0.2}} \tag{4-12}$$

The sweep out time for heterogeneous media is given by Equation 4-12:

$$\hat{t}_{Dsw} = \hat{t}_{DB} + \frac{2E_R S_{oR}}{\hat{f}_{opk}} \tag{4-13}$$

where $\hat{f}_{opk}$ is the peak oil fractional flow given by

$$\hat{f}_{opk} = \frac{\left(H_K - H_K (\frac{t_{DB}}{t_{Ds}})^{1/2} \right)}{(H_K - 1)} f_{oB} \tag{4-14}$$

The oil rate is calculated using total production rate (q) and oil fractional flow (f_o).

$$q_o = q\hat{f}_o \tag{4-15}$$

Figure 4-1 shows the comparison between the forecasted production data of an SP flood by this method and pilot results (Lake, 1989). The agreement between pilot and predicted results is reasonable.

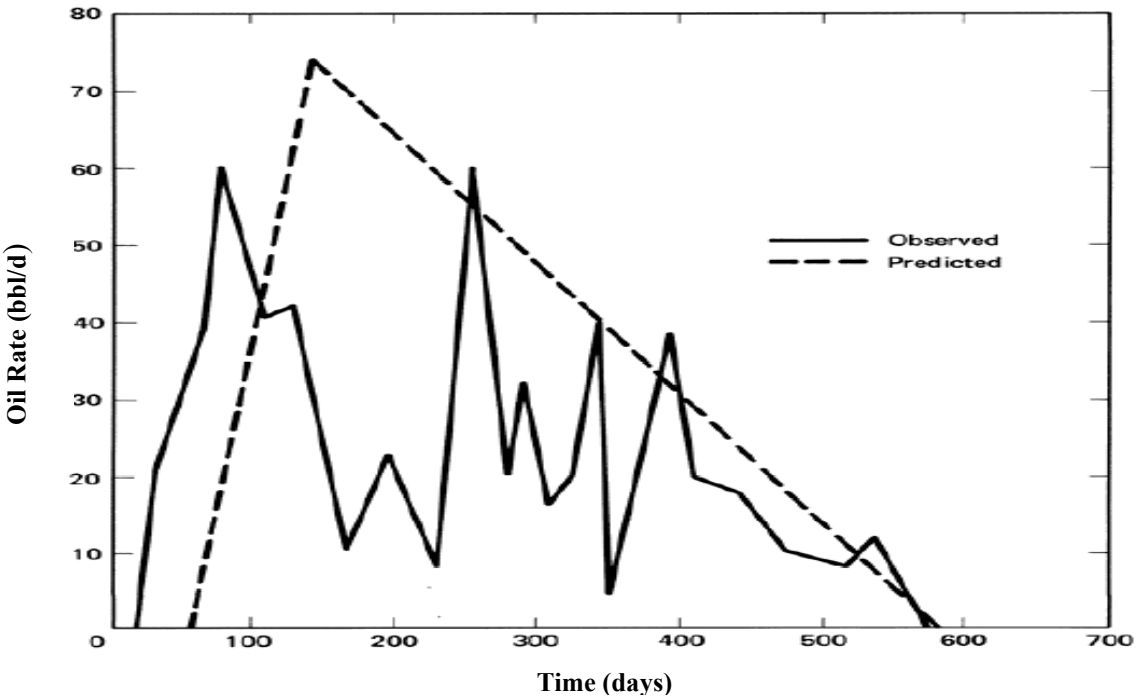

Figure 4-1: Comparison between predicted and observed oil-rate-time responses (Paul et al., 1982).

4.2.2- Field Screening and Forecasting of SP Flood Using CFPM

We modified CFPM from the original model before applying it to the field data for screening/forecasting of SP flooding. The modifications include:

- Modify the capillary number calculations (N_c, to capture multi injection wells and pattern type) that are used to calculate S_{or} on the CDC (capillary desaturation curve).
- Generalize to allow for different CDC curves of oil- and water-wet permeable media including sandstone and carbonate reservoirs.
- Construction of fractional flow curves based on the modified Carman-Kozeny equation (Alpak and Lake, 1999)
- Extension to multiple injectors and producers

- Base the ultimate recovery on the total remaining oil rather than the target oil or the portion previously swept by water.

The CFPM was then applied to numerous oil reservoirs to predict the performance of the SP flooding. The oil reservoir database used in this task was the TORIS (Tertiary Oil Recovery Information System) database, which is a set of 1381 onshore US oil reservoirs collected by DOE (1980). CFPM was developed as spreadsheet and applied to all reservoirs in TORIS database (without the EOR screening for SP flooding) to compare the response of different reservoirs to SP floods. Based on the CFPM calculations, the sum of the SP flood cumulative oil recovery of the TORIS reservoirs database (with their current injection rate reported in the database) would be more than 70 Billion STB which is a great potential for chemical enhanced oil recovery.

Table 4-1 shows the required input and generated output results of CFPM applied to TORIS. Figure 4-2 compares the oil rate-time plots of two cases with the same fluid and reservoir properties but different injection rates. As one can see, increasing the injection rate causes an increase of the peak oil rate and cumulative oil recovery (area under the oil- rate curve) and decreases the flood duration.

Table 4-1: Input parameters and output results of CFPM.

Input Parameters	**Output Results**
Shape Factor, dimensionless	A) Ultimate Recovery Efficiency Calculations
Well Radius, r_w, ft	Productivity Index, STB/day-psi
Skin Factor, dimensionless	Production Rate, STB/day
Porosity, fraction	Surfactant Adsorption, D_s, PV_s/PV_{inj}
Permeability, md	Capillary Number, N_c, Dimensionless

Injectivity Coefficient, C_p, psi/ft	Oil Saturation after SP Flood, S'_{or}, fraction
Depth, ft	Displacement Efficiency, E_D, fraction
Net Pay Thickness, ft	Volumetric Sweep Efficiency, E_v, fraction
Oil Viscosity, μ_o, cp	Efficiency of Mobility Buffer, E_{MB}, fraction
Field Area, acres	Ultimate Recovery Efficiency, E_R, fraction
Oil Saturation at Start of EOR, S_{oR}, fraction	Oil Bank Fractional Flow, f_{oB}, fraction
Dykstra-Parsons Coefficient, V_{DP}, fraction	Oil Bank Saturation, ,S_{oB}, fraction
Wettability	Floodable Pore Volume, V_{pf}-Pattern, STB
Lithology	B) Oil-Rate-Time Calculations
Clay Content, fraction	Oil Bank Arrival Time, $\hat{t}_B$, years
Surfactant Retention, a_s, mg surf/g rock	Peak Oil Fractional Flow, $\hat{f}_{opk}$
Rock Bulk Density, ρ_r, g rock/cc rock	Peak Oil Rate Time, $\hat{t}_s$, years
Cumulative Oil Production, STB	Peak Oil Rate, q_{opk}, STB/day
Initial Oil Saturation, S_{oi}, fraction	Sweep Out Time, $\hat{t}_{sw}$, years
Current Oil Formation Volume Factor, B_{of}, Rb/STB	SP Flood Total Oil Production, N_P/Pattern, STB
Productivity Index, STB/day-psi	
Pressure Difference, ΔP=(Injection -Reservoir Pressure= P_{inj}-P_r), psi	
Injection Rate, bbls/day-well	
Number of Injectors	
Surfactant Slug Size, V_{ps}, fraction PV	
Mobility Buffer Slug Size, t_{DMB}, fraction PV	
Interfacial Tension, σ, mN/m	

Pattern Area, A_p, acres
Surfactant Density, ρ_s, g surf/cc surf
Surfactant Concentration, C_s, cc surf/cc sol

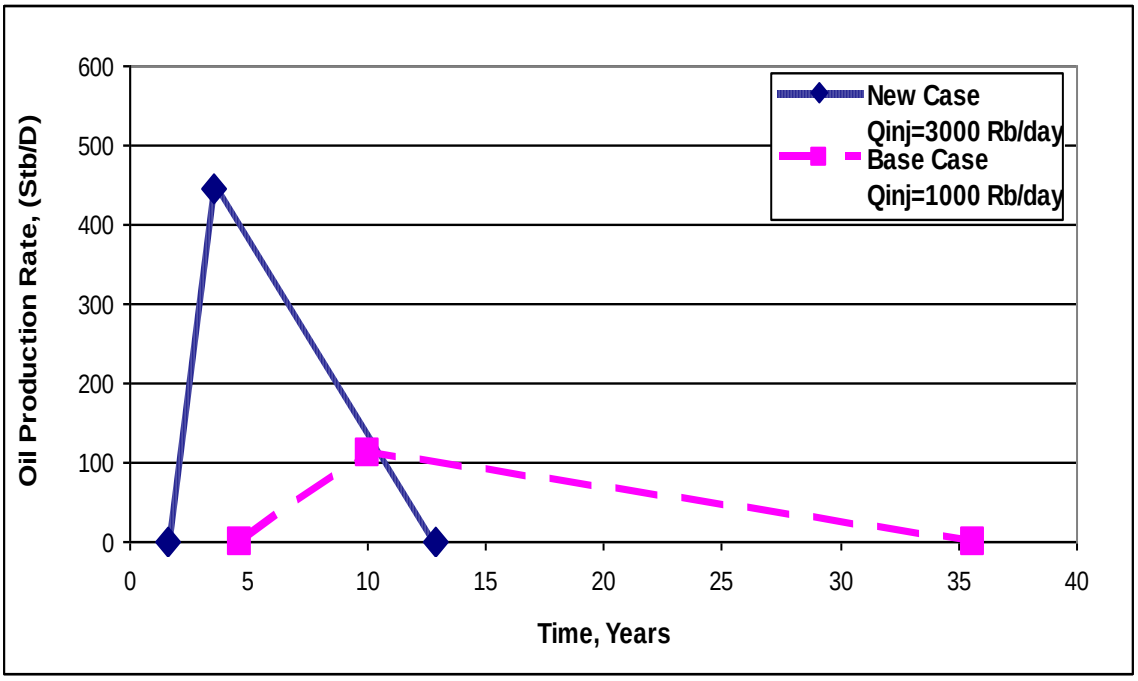

Figure 4-2: Results of SP flood oil rate prediction for two cases with different injection rates. The peak oil rate increases while the duration of flood decreases with increasing the injection rate. The oil and rock properties of Middle Kenai reservoir from the TORIS database have been used (Mollaei, 2010).

Application of SP flood predictive model on the TORIS database shows that reservoirs with higher remaining oil saturation (S_{oR} as oil saturation at start of the SP process), moderate oil viscosity, lower heterogeneity and salinity have larger oil recovery potential by SP flood compared to reservoirs with unfavorable fluid and rock properties.

The response of SP flood to changes of the reservoir and flood design input parameters based on TORIS database are explained as follow.

Table 4-2 summarizes the influence of different reservoir properties and flood design parameters on SP ultimate recovery efficiency and peak oil rate. It is a preliminary sensitivity analysis of SP flooding that changes only one parameter at the time. Section 4.3 shows the results of an advanced SA that also considers changes of different parameters simultaneously. The positive sign "+" indicates a direct relationship between inputs and outputs, which means that increasing the input parameter increases the output value and vice versa. The negative sign "–" indicates an inverse relationship between input and output, meaning that by increasing the input parameter, output decreases and vice versa. "NA" stands for neutral, or no effect, and "Limited" means that the positive or negative effect is limited to a specific range and beyond that the changes in input parameter would have opposite or no effect on the output. For example, increasing the injection rate up to an optimum values (the injection rate that optimizes the oil recovery which depends on reservoir and design parameters) increases the ultimate recovery efficiency but it would cause early break through and a dramatic drop of ultimate recovery efficiency if it was to increases beyond the optimum injection rate. The peak oil rate is not a function of surfactant or polymer (mobility buffer) slug size as long as the slug size is more than adsorbed amount.

Table 4-2: Influence of different input parameters on ultimate recovery efficiency and peak oil rate based on average fluid and rock properties of the TORIS reservoir database ("+": increasing effect, "–": decreasing effect).

Reservoir Parameters	**Ultimate Recovery Efficiency, E_R, fraction**	**Peak Oil Rate, q_{opk}, STB/day**
Shape Factor, dimensionless	+	+
Well Radius, r_w, ft	+	+
Skin Factor, dimensionless	–	–
Porosity, fraction	+	+
Permeability, md	+	+
Injectivity Coefficient, C_p (psi/ft)	+, Limited	+
Depth, ft	+	+
Net Pay Thickness, ft	NA	+
Oil Viscosity, μ_o	–	–
Field Area, acres	NA	NA
Oil Saturation at Start of EOR, S_{oR}, fraction	+	+
Dykstra-Parsons Coefficient, V_{DP}	–	–
Clay Content, fraction	–	–
Surfactant Retention, a_s, mg surf/g rock	–	–
Rock Density, ρ_r, g rock/cc rock	–	–
Pressure Difference, $\Delta P=(P_{inj}-P_r)$, psi	+, Limited	+
Injection Rate, bbls/Well-day	+, Limited	+
Surfactant Slug Size, V_{ps}, PV	+	*NA
Mobility Buffer Slug Size, t_{DMB}, PV	+	*NA

Interfacial Tension, σ, mN/m	–	–, Limited
Pattern Area, A_p, acres	–	–
Surfactant Density, ρ_s, g surf/cc surf	+	+
Surfactant Concentration, C_s, cc surf/cc sol	+	+

*As long as the chemical concentration and slug size exceed the adsorption amount.

4.3- ADVANCED SENSITIVITY ANALYSIS

4.3.1- Fundamentals of Sensitivity Analysis

Sensitivity analysis (SA) helps to quantitatively determine the influence of input variables or parameters on the distributions of uncertainty in output results by systematically changing the input variables. This provides insight to determine the most influential input variables and also helps to better control the uncertainty of output results.

It is desirable to have an SA method that is dimensionless, global, quantitative and model-free as explained below (Salteli et al., 2000a; Salteli, 2002; Lawal, 2007; 2008).

Dimensionless: the calculations of sensitivity indices should be independent of the variable's dimensions.

- Global: The SA method should be global instead of local because global methods characterize input-output sensitivity relationships across the entire specified ranges of the inputs. Regression, correlation and variance decomposition are examples of global SA methods. Sensitivity analysis based on

perturbations of a base case (as in Table 4-1) is local; their results tend to depend on the base case.

- Quantitative: The results of SA should be quantitative rather than qualitative to enable meaningful comparisons.
- Model-free: The desired SA method should be independent of model assumptions.

Amongst the global methods, regression and correlation are model-dependent (by model we mean the fitted model to data as it is used in regression and correlation analysis) and so they are best suited for the SA of linear monotonic models. However, variance-based SA methods that decompose output variance into proportionate sensitivity indices are model-free and do not assume substitute functional relationship for the model under investigation unlike regression and correlation based method. Therefore, variance-based SA methods are suitable for the SA of non-linear non-monotonic models.

4.3.2- Sampling

Sampling is an important step that influences the accuracy of the sampled subset. Many authors have compared different sampling techniques (Tezuka, 1995; Kocis and Whiten, 1997; Joe and Kuo, 2003). Random sampling (Monte-Carlo simulation, MCS) is an inefficient sampling technique because it suffers from disordering and is susceptible to clustering (Fox, 1986). Latin Hypercube Sampling, LHS, a method that partitions the input distributions into equal and non-overlapping grids to achieve a uniform sample of input data, cures some of the problems of random sampling (Stein, 1987; Johnson et al., 1992; Wyss and Jorgensen, 1998; McKay et al., 2000; Helton et al., 2005). LHS performs better than random sampling if the relationship between inputs and outputs is monotonic

(Salteli et al., 2000a; Helton and Davis, 2003). Otherwise LHS is no better than random sampling.

The Sobol LP_T is better than Helton sequences and simple random sampling. The Sobol LP_T method has wide application, relative transparency and ease of implementation. We chose to use this sampling technique with the Winding Stairs (WS, developed by Jansen et al., 1994) SA method as a variance-based SA method. This method decomposes the variance of the Monte Carlo components into:

a) First (Main or Individual) Sensitivity Indices (FSI)

b) Total Sensitivity Indices (TSI)

These indices indicate individual and total effects of the model's inputs (X_i) on the output (Y_i) variance. The difference between the total and individual sensitivities shows the interaction of all other variables on an output variable.

The matrices below show the schematic of the SA matrices by Monte Carlo (MC) and Winding Stairs (WS) methods. Indices "k" and "n+1" stands for the number of variables and number of turns to repeat the cyclic order of "N" realizations, respectively. For the same number of cyclic order of realizations, (n+1), one can see, the number of necessary realizations of WS (N=k(n+1)) is much less than conventional MC (N=k((n-1)k+k)), which makes the WS a robust method compared to MC for SA. For example for k=10 variables and n=1000 cyclic turns of repeat of variables, N (number of necessary realizations) for WS method is about 10,000 while the Monte Carlo (MC) method needs 100,000 realizations. For more details of sensitivity indices calculations refer to Chan et al. (2000) and Lawal (2007 and 2008).

$Y_{WC} =$ [redacted]

$Y_{MC} =$ [redacted]

(4-16)

4.3.3- Mathematical Formulation of WS Sensitivity Analysis Method

The following provides a summary of equations used to perform the WS SA method (Salteli, 2002; Salteli et al., 2000b; Chan et al., 2000; Lawal, 2008)

From statistics, the law of total variance is:

$$V(Y) = V(E(Y|X)) + E(V(Y|X)) \tag{4-17}$$

where X and Y are random variables and Y the output depends on X the input deterministically. For a non-additive model that depends on independent parameters, the

total variance of the output is a sum of partial variances (Salteli et al., 1999; 2000b; Salteli, 2002; Helton et al. 2005). Therefore, Equation 4-17 becomes

$$V(Y) = \sum_{i=1}^{n} V_i + \sum_{i}^{n} \sum_{j=i+1}^{n} V_{ij} + \sum_{i=1}^{n} \sum_{j=i+1}^{n} \sum_{k=j+1}^{n} V_{ijk} + \ldots V_{123\ldots n} \tag{4-18}$$

where

$$\begin{aligned} V_i &= V(E(Y|X_i)) \\ V_{ij} &= V(E(Y|X_i, X_j)) - V_i - V_j \\ V_{ijk} &= V(E(Y|X_i, X_j, X_k)) - V_i - V_j - V_k - V_{ij} - V_{jk} \end{aligned} \tag{4-19}$$

where V is the variance operator, E is the expected value operator and $|$ is the conditional symbol. V(Y) is the total variance and other terms (V_{ij}, V_{ijk},…) are the high-order variances (combined effects or interactions).

The first term in Equation 4-17 is first-order effects, $V(E(Y|X_i))$, resulting from X_i. The second term shows residual effects, expected value of the residual output variance, $E(V(Y|X_i))$, resulting from all other sources other than X_i The residual effects originate from the first-order or main effects of the other input variables excluding X_i, and high-order or joint effects originating from the interactions between input variables (including X_i).

The sensitivity index (S_i) is a measure of first-order or main effects. It is the ratio of the first-order effect (partial variance caused by X_i) to the total variance. Based on these definitions, the sensitivity indices are defined as:

$$S_i = \frac{V(E(Y|X_i))}{V(Y)} \tag{4-20}$$

Dividing the left and right sides of the Equation 4-18 by the total variance V(Y) results in:

$$\sum_{i=1}^{n} S_i + \sum_{i=1}^{n} \sum_{j=i+1}^{n} S_{ij} + \sum_{i=1}^{n} \sum_{j=i+1}^{n} \sum_{k=j+1}^{n} S_{ijk} + \ldots + S_{123\ldots n} = 1 \qquad (4\text{-}21)$$

The total effect of X_i on Y is the sum of its first and higher order effects. According to above equations, the total sensitivity index of variable X_i is defined as:

$$S_{T_i} = S_{x_1} + S_{x_1 x_1} + S_{x_1 x_2} + \ldots + S_{x_1 x_2 \ldots x_i \ldots x_n} \qquad (4\text{-}22)$$

$$S_{T_i} = S_i + \sum_{j \neq i}^{n} S_{ij} + \sum_{j=1}^{n} \sum_{k=j+1}^{n} S_{ijk} + S_{ijk\ldots n} \quad , \quad j,k \neq i;\ j \neq k \qquad (4\text{-}23)$$

In the above equations S_i is the first (main) sensitivity index, S_{Ti} is the total sensitivity index and (S_{Ti} - S_i) gives the sensitivity index because of interactions of variable i with other variables.

From the foregoing, the total effect of X_i on Y, is the sum of its first and high-order effects arising from X_i; which is also (from the law of total variance) the variance of the expectation of Y when all the input factors except X_i (noted by X_{-i}) are kept constant. The total sensitivity index of a variable X_i, is the complementary sum that includes all of the first and high-order sensitivity indices of that variable.

If the first-order sensitivity index (S_i) of the i^{th} input variable is small then the X_i is by itself non-influential or unimportant. If the total sensitivity index (S_{Ti}) is also small, then apart from being unimportant, neither does X_i interact with other variables. Conversely a large S_i shows that X_i has a considerable effect on the uncertainty of Y. Also, a small S_i but large S_{Ti} shows X_i is not important directly but has considerable

effect through interactions with other input variables. The difference between S_{Ti} and S_i indicates the magnitude of the interactions between X_i and other variables (Lawal, 2007; 2008).

4.3.4- CFPM Sensitivity Analysis Results

Winding Stairs (WS) as a variance based SA method was applied to perform detailed SA. As it was explained in Section 4.3.2, WS has the advantage of much less required realizations that makes it an efficient and robust method of SA compared to traditional Monte-Carlo (MC) methods. In addition, as a variance-based SA method, WS decomposes the variance of Monte-Carlo components (elements of Monte Carlo matrices in Equation 4-17 into main and total sensitivity indices. In this way, WS not only decreases the number of necessary realizations (runs) significantly but also identifies the individual and total effects of the model's inputs on the output variance (uncertainty) that helps to recognize the interactions between input parameters. The differences between the total and individual indices are indicators of the magnitude of interactions between input parameters, which is also a source of uncertainty of output results. In other words, WS not only determines the direct influences of variations of input variables on the uncertainty of the output results but also the portion of uncertainty caused by interactions of variables (Salteli, 1999; Chan, 2000).

The word "*interactions*" (first used by Fisher, 1926) means that the relationship between (at least) two variables (e.g. independent and dependent variables) is changed and modified by (at least) another variable. It implies that the strength or the sign (direction) of a relation between (at least) two variables is different depending on the value (level) of some other variable(s) (Statsoft Electronic Statistics Textbook, 2010). In the current research interactions could originate from the correlations between variables

and/or variables appearing in combination of the same function. In cases that significant interaction occurs, it's possible that parameter "A" doesn't cause much uncertainty in output results when we just change that parameter but it causes much more uncertainty when other parameter (parameters) change simultaneously because of interactions with each other through the model equations. For example, the oil viscosity (μ) in the equation of capillary number, $N_{ca} = \frac{\mu v}{\sigma}$, causes more uncertainty to recovery efficiency when it changes simultaneously with other parameters like interfacial tension (σ) and velocity (ν) that includes the permeability variations too.

To calculate the direct and non-direct influences of each input variable (parameter) on uncertainty of output results, two sensitivity indices are defined for each input variable.

c) First (Main or Individual) Sensitivity Indices (S_i or FSI)

d) Total Sensitivity Indices (S_{Ti} or TSI)

These indices indicate individual and total effects of the model's inputs (X_i) on the uncertainty of output (Y_i). The difference shows the interaction of all other variables on output variable.

To apply the Winding Stairs sensitivity analysis (SA) method on CFPM we set up a stochastic type of CFPM in which a common used statistical distribution was assigned to each input parameter (for example a normal distribution for porosity, lognormal for permeability). Numerous realizations and runs were performed and the output results analyzed to calculate sensitivity indices (SI) for each input parameter using the WS SA method. Table 4-3 shows the stochastic input parameters of CFPM and the assigned range of variations for each of the variables. Table 4-4 shows the results of the sensitivity analysis of the CFPM.

CFPM was run under different flow conditions of rate and pressure-constrained modes. Rate-constrained means that the injection rate is specified; pressure-constrained means that the injection well bottomhole pressure is specified. The six output parameters, ultimate oil recovery efficiency, total oil production, maximum (peak) oil production rate, oil bank arrival time (t_B), peak oil rate time (t_s) and sweep out time (t_{sw}), were studied to find the most influential input parameters on the uncertainty of these output results. As discussed earlier, the influence of the variations (uncertainties) of the input parameters on uncertainty of output results can be direct (first SI) or through interactions with other input parameters. For example for the pressure-constrained case, permeability, Dykstra-Parsons coefficient, and porosity have the most direct influences on uncertainty of ultimate recovery efficiency. Permeability and the Dykstra-Parsons coefficient are the two parameters that cause the most uncertainty in ultimate recovery efficiency predictions through interactions with other input parameters.

Table 4-3: CFPM stochastic input parameters and range of variations.

Input Variable	**Min**	**Mean**	**Max**
Porosity, fraction	0.107	0.200	0.319
Initial Oil Saturation, S_{oi}, fraction	0.658	0.700	0.734
Initial Oil Saturation at Start of EOR, S_{oR}, fraction	0.266	0.300	0.334
Heterogeneity, V_{DP}, dimensionless	0.20	0.50	0.87
Shape Factor, C_A, dimensionless	27.77	30.80	34.50
Well Radius, r_w (ft)	0.215	0.250	0.295
Skin Factor, dimensionless	4.0	5.0	6.0
Permeability, k (md)	3.32	98.91	1251.73

Injectivity Coefficient, C_p (psi/ft)	0.269	0.300	0.333
Depth, D (ft)	2382.32	4982.95	9510.62
Net Thickness, H_{net} (ft)	85.05	99.91	118.36
Oil Viscosity, μ_o (cp)	1.36	5.02	17.50
water Viscosity, μ_w (cp)	0.996	1.00	1.003
Field Area, A_f (acre)	3698.42	4001.03	4337.85
Adsorption (mg surf/mg rock)	0.37	0.40	0.44
Rock Density (g/cm^3)	2.62	2.65	2.68
Waterflood Total Oil Production (MMSTB)	119.41	122.53	125.80
Initial Oil Formation Volume Factor, B_{oi} (rb/STB)	1.16	1.30	1.48
Current Oil Formation Volume factor, B_{of} (Rbbl/STB)	1.01	1.20	1.38
Surfactant Slug Size, V_{ps} (PV)	0.093	0.100	0.107
Mobility Buffer Slug Size, t_{DMB} (PV)	0.694	0.700	0.707
Interfacial Tension, σ (mN/m)	0.0009	0.001	0.0011
Pattern Area, A_p (acre)	18.24	19.99	21.67
Surfactant Density, (gr/cm3)	0.960	1.00	1.031
Surfactant Concentration, C_S (cc surf/cc solution)	0.027	0.030	0.034
Original Oil in Place, OOIP (MMSTB)	466.83	500.10	536.86

Table 4-4: Results of CFPM sensitivity analysis.

Pressure-Constrained			**Rate-Constrained**		
Output Parameter	Sen. Index (SI)	Input Parameter	Output Parameter	Sen. Index (SI)	Input Parameter
E_R	First SI	k, V_{DP}, φ	**E_R**	First SI	V_{DP},φ
	Interaction	k, V_{DP}		Interaction	V_{DP},φ
N_p	First SI	OOIP, V_{DP}, k, B_{of}, Φ	**N_p**	First SI	V_{DP}, B_{oi}, B_{of}, Porosity, OOIP
	Interaction	μ_o, OOIP, Φ		Interaction	-
Q_{max}	First SI	k, μ_o	**Q_{max}**	First SI	V_{DP}, Porosity
	Interaction	k, μ_o		Interaction	-
t_B	First SI	k, μ_o, D, C_p, H_{net}	**t_B**	First SI	V_{DP}, B_{oi}
	Interaction	k, μ_o		Interaction	B_{of}, B_{oi}
t_s	First SI	k, μ_o, D, C_p, H_{net}	**t_s**	First SI	V_{DP}, B_{oi}
	Interaction	k, μ_o, V_{DP}		Interaction	-
t_{sw}	First SI	k, μ_o	**t_{sw}**	First SI	B_{oi}, B_{of}
	Interaction	k, μ_o		Interaction	V_{DP}

Figures 4-3 and 4-4 show the calculated main and total sensitivity indices for the ultimate recovery efficiency (E_R) for both pressure and rate-constrained modes. As one can see from the main effects, uncertainties in average permeability (k), heterogeneity (V_{DP}) and porosity are the most important sources of uncertainty for the ultimate recovery efficiency in the pressure-constrained mode. Also, permeability and heterogeneity cause considerable uncertainty on ultimate recovery efficiency (22% and 17% of FSI respectively) through interactions with other parameters as it is clear from the difference of total and main sensitivity indices (SI) of these two parameters. Some of the parameters have negative interactions with other parameters (less TSI than FSI): oil formation volume factor (B_{of}) and oil viscosity (μ_o) in the pressure-constrained mode as Figure 4-3 shows. The total uncertainties caused by these parameters decrease as they interact with changes of other parameters.

In the rate-constrained mode, heterogeneity and porosity cause the most uncertainty in ultimate recovery efficiency through main (direct) effects and also interactions with other parameters. These results provide useful information about the functionality of ultimate recovery efficiency uncertainty (and other output variables such as peak oil rate and oil bank break through time) to different input variables.

Knowing this information helps decrease the uncertainty of output results more efficiently and economically by decreasing the uncertainty of the most important sources of uncertainties instead of decreasing the uncertainty of non-influential parameters. This information can also help to characterize the elements of important dimensionless groups governing the model behavior. Mobility ratio, flow capacity and storage capacity are examples of such dimensionless groups.

Figures 4-5 and 6 illustrate the calculated main and total sensitivity indices for peak oil rate (Q_{max}) in the pressure and rate-constrained modes. Permeability and oil

viscosity are the major causes of uncertainty not only by the main effects but also through the interactions with other parameters in the pressure-constrained mode. Heterogeneity and porosity are the main sources of uncertainty of peak oil rate in the rate-constrained mode through the main effects. There is not considerable uncertainty caused by interactions between parameters in this case. Similar to ultimate recovery efficiency, we have parameters that cause negative interactions with other parameters such as surfactant density and pattern area (Figure 4-5).

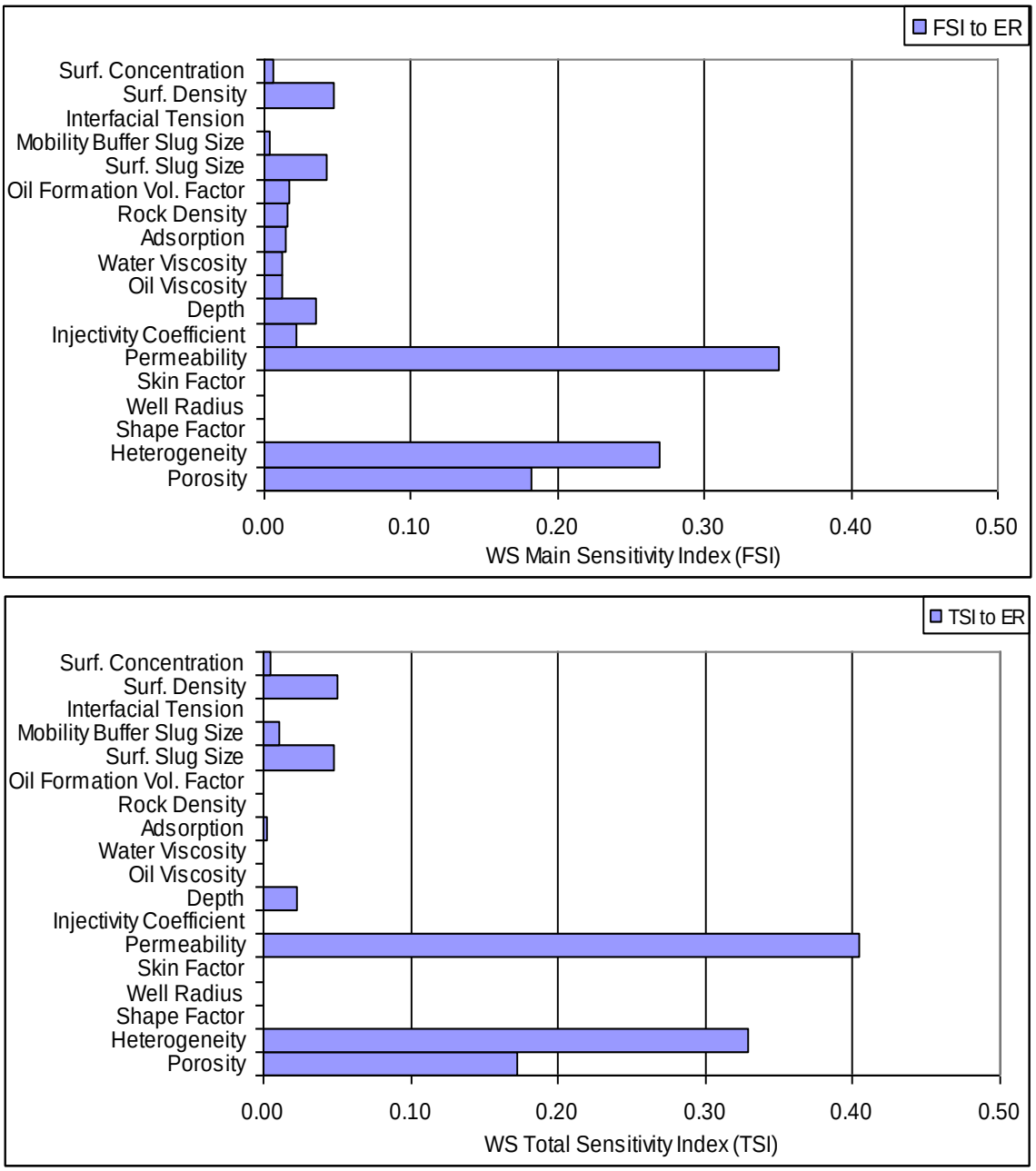

Figure 4-3: Main and total sensitivity indices of ultimate recovery efficiency (E_R) for SP floods in pressure-constrained mode. Plots show the most important sources of uncertainty in ultimate recovery efficiency predictions.

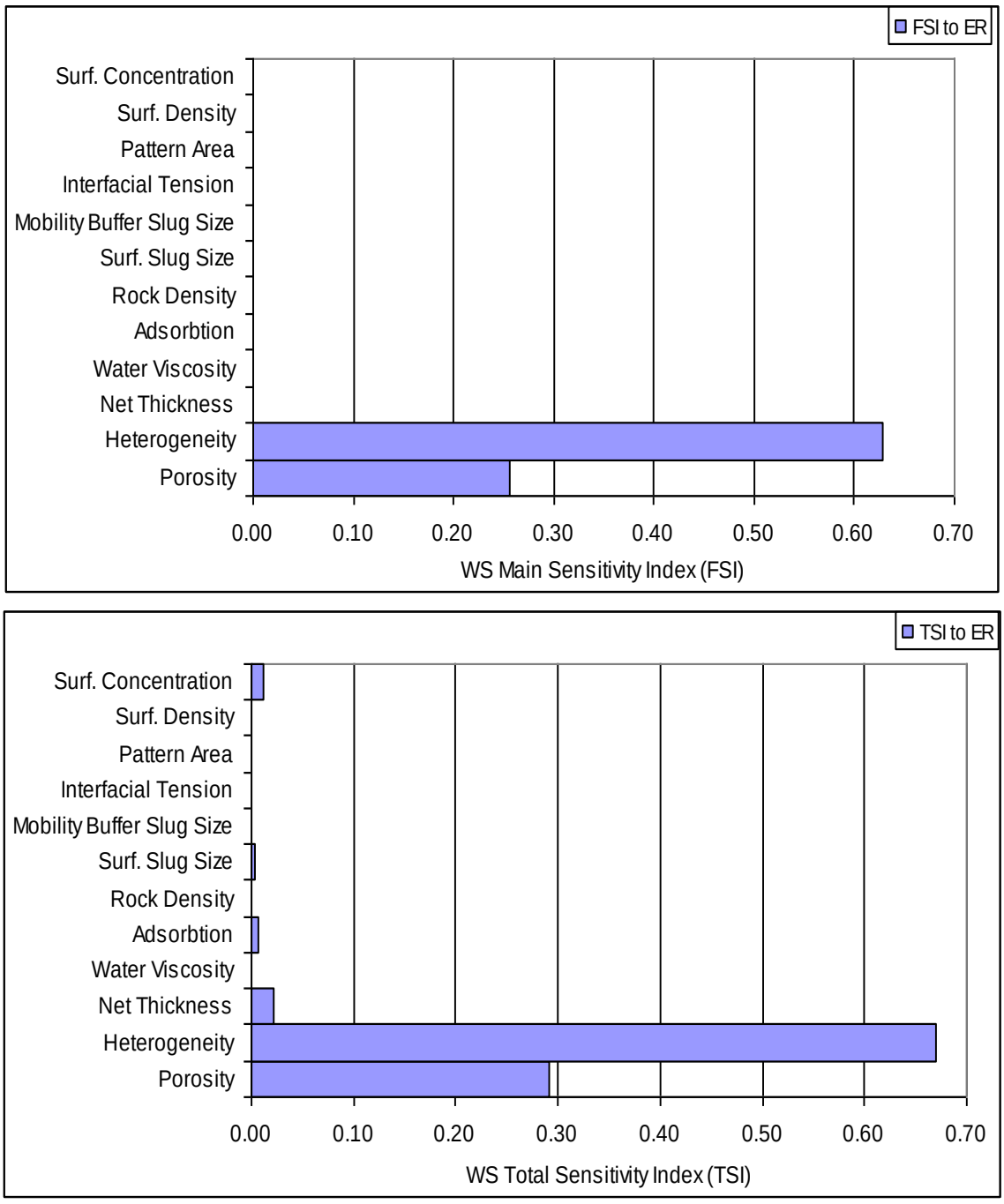

Figure 4-4: Main and total sensitivity indices of ultimate recovery efficiency (E_R) for SP floods in rate-constrained mode. Figure compares the magnitude of sensitivity caused by each input variable.

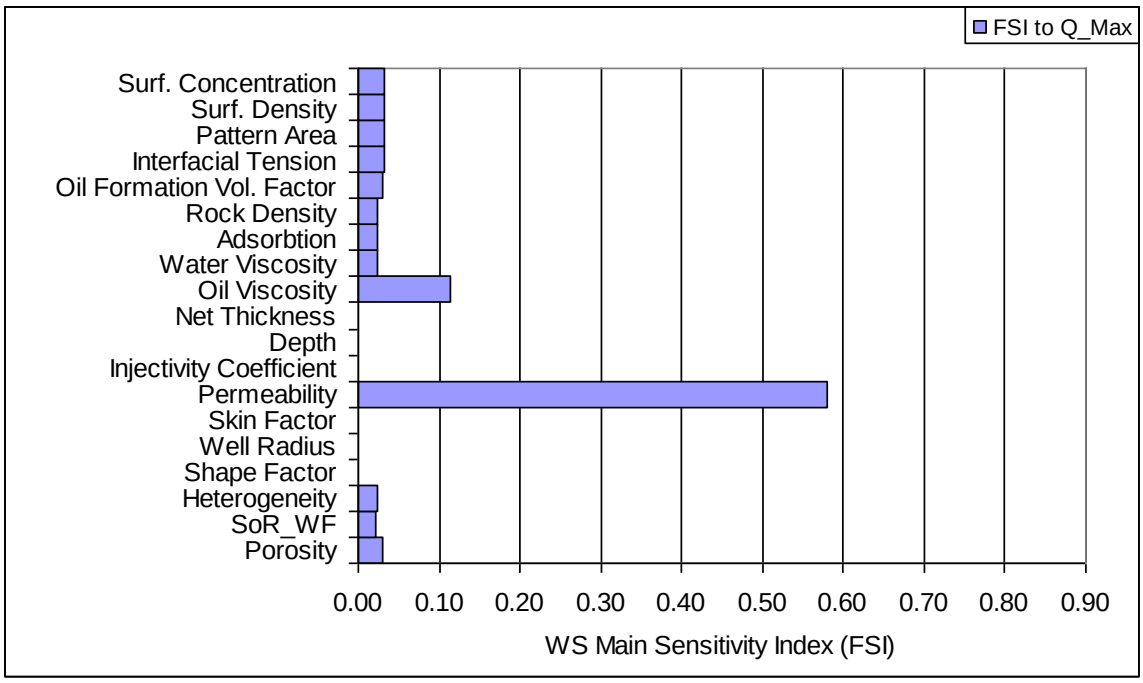

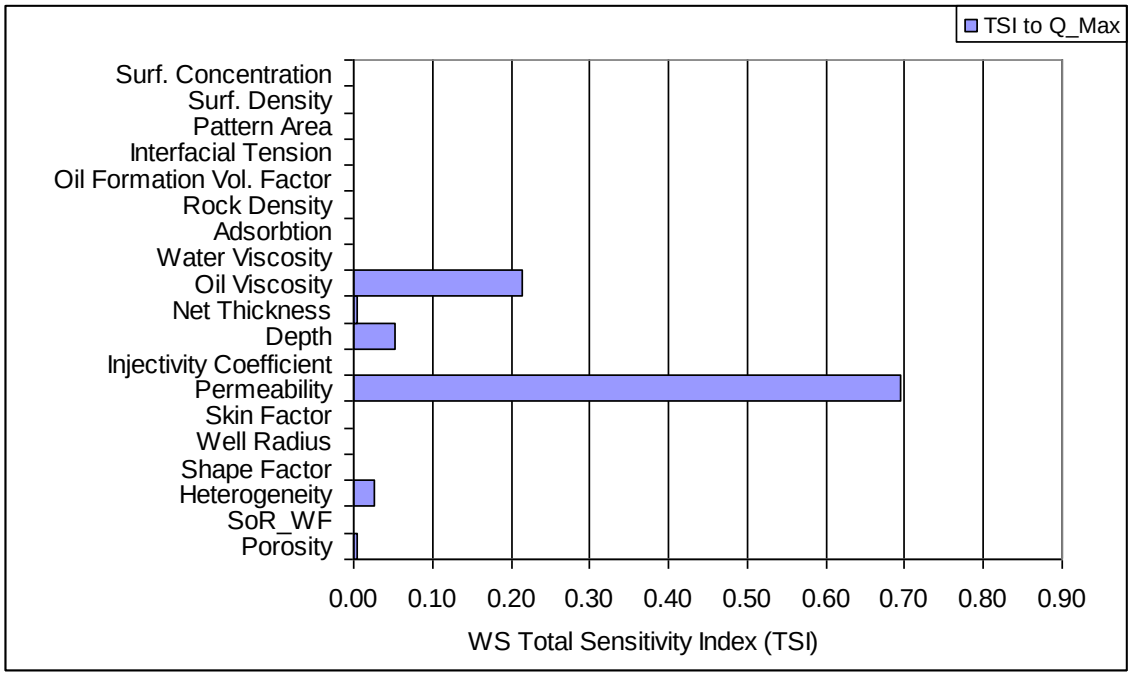

Figure 4-5: Main and total sensitivity indices of peak oil rate for SP floods in pressure-constrained mode. Figure compares the relative importance uncertainty caused by different variables on peak oil rate of SP flooding.

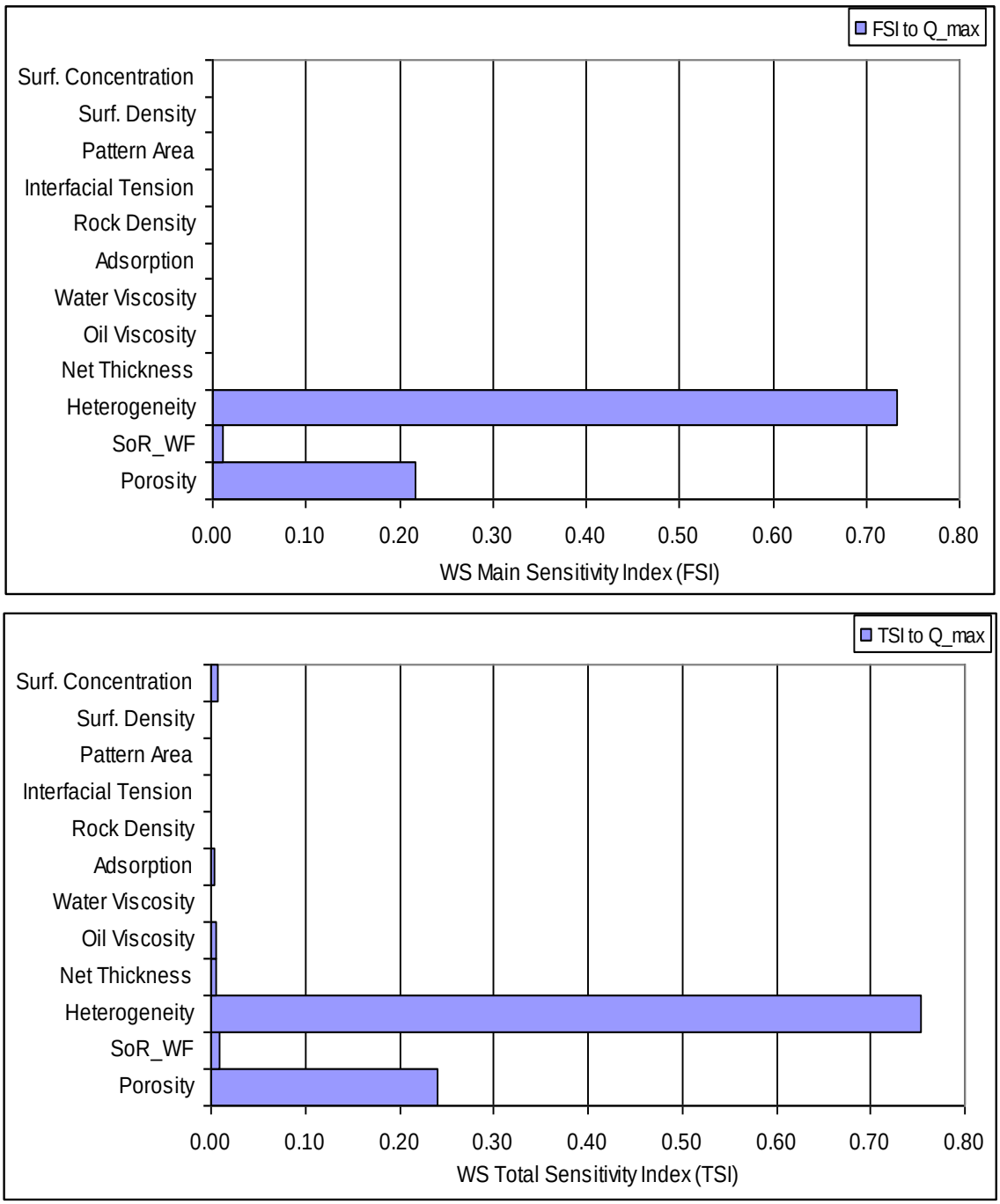

Figure 4-6: Main and total sensitivity indices of the peak oil rate for SP floods in rate-constrained mode. Figure compares the magnitude of uncertainty caused by each input variable.

4.4- DISCUSSIONS

Application of the Chemical Flood Predictive Model to the Tertiary Oil Recovery Information System (TORIS) reservoir database helped identify the SP flood performance and sensitivity.

Generally, reservoir porosity, permeability, well radius, injectivity coefficient, depth, initial oil saturation, pressure difference (between injector and producer), injection rate, surfactant-polymer slug size, surfactant density and concentration are the parameters that have partial or full increasing effect on the ultimate recovery efficiency of SP flood. On the other hand, skin factor, oil viscosity, reservoir heterogeneity, surfactant retention, rock density, clay content, interfacial tension and pattern area have a decreasing effect. Also, the peak oil rate shows similar sensitivity to reservoir and flood parameters except for net pay thickness that has an increasing effect on the peak oil rate while it has no significant impact on the ultimate recovery efficiency (ignoring the gravity effects). The peak oil rate is independent of the SP slug size as long as the slug size is more than adsorption.

The Winding Stairs (WS) sensitivity analysis method was an efficient and robust method of SA compared to traditional Monte-Carlo (MC) methods. As a variance-based SA method, WS decomposes the variance of Monte-Carlo components into main and total sensitivity indices. In this way, WS not only decreases the number of necessary realizations (runs) significantly but also identifies the individual and total effects of the model's inputs on the output variance (uncertainty). The differences between the total and individual indices are indicators of the magnitude of interactions among input parameters, which is also a source of uncertainty of output results. The interactions between variables can be both positive (increasing the uncertainty of output variables) and negative (decreasing the uncertainty of output variables). Knowing the most

important sources of output uncertainty can help to reduce the uncertainty of output results more economically and efficiently.

Sensitivity analysis of SP flood performance based on the CFPM and WS as the SA method shows that uncertainty of reservoir permeability, porosity, heterogeneity and oil viscosity are the most important sources of output uncertainty either directly or through interactions with other parameters. Also, oil viscosity, oil formation volume factor, reservoir depth and thickness cause an increase or decrease in uncertainty through interactions with other input parameters as one can see in Figures 4-3 to 6. This kind of information can not be inferred by simple SA in which only one variable changes at a time as the comparison of the Tables 4-2 and 4-4 shows. Reservoir permeability is not a source of uncertainty in rate-constrained mode since the injection is done with constant rate regardless of reservoir permeability. Generally the rate-constrained mode seems to have fewer variables causing uncertainty in output variables and so less effort (expenses) would be required to reduce the uncertainty of output results.

From the insights provided by SA the following points are important to note:

- Based on preliminary sensitivity analysis (changing one variable at a time), almost every input variable influences the output results. Since these results are qualitative, it is impossible to decide which variables are more influential than others. This limitation suggests the application of modern sensitivity analysis methods.
- Preliminary sensitivity analysis shows that variables such as reservoir porosity, permeability, well radius, initial oil saturation have partial or full increasing effect on the ultimate recovery efficiency of SP flood. On the other hand, oil viscosity, reservoir heterogeneity, surfactant retention have a decreasing effect. The peak oil rate shows similar sensitivity to reservoir and flood parameters.

- Using modern sensitivity analysis, we can calculate the sensitivity of output results to individual variables and also how much of the sensitivity is caused by interaction of variables. This helps to identify the main sources of output uncertainty and gives insights to reduce the uncertainty in a more systematic and efficient way.
- Reservoir permeability, porosity, heterogeneity and oil viscosity are the most important sources of output uncertainty either directly or through interactions with other parameters. To a minor extent, oil formation volume factor, reservoir depth and thickness can cause either an increase or decrease of uncertainty through interactions with other input variables.
- Reservoir permeability is not a source of uncertainty in a rate-constrained mode since the injection rate remains constant regardless of reservoir permeability.
- Generally the rate-constrained mode seems to have fewer variables causing uncertainty in output variables and so less effort (expenses) would be required to reduce the uncertainty of output results.

Chapter 5: VALIDATION OF THE GENERAL ISOTHERMAL EOR AND WATERFLOOD FORECASTING MODEL

Assessing the quality and accuracy of a model is called "*validation*". Validation is something that needs to be done both by model developers and users. Sometimes the word "*validation*" is used along with "*verification*" which is concerned with "*building the model right*". Verification is used in the comparison of the conceptual model to the computer representation that implements that conception to assure that the model is implemented correctly. However, validation is concerned with "*building the right model*". It is used to determine that a model is an accurate representation of the real system. Validation is usually achieved through the calibration of the model, an iterative process of comparing the model to actual system behavior and using the discrepancies between the two, and the insights gained to improve the model. This iterative process in petroleum engineering is called "*history matching*" that includes regenerating the production history of the reservoir such as cumulative oil recovery, oil cut, recovery efficiency and etc.

The objective of this chapter is to develop confidence in the abilities of general isothermal EOR and waterflood forecasting model (UTF; The University of Texas Forecasting Tool) for history matching waterflood and different isothermal EOR processes. We will discuss the basic steps that should be done to apply UTF for history matching of field results. Then examples of field/pilot history matching for each EOR process and waterflooding are presented. The rest of history matching results is provided in Appendix-B.

5.1- MODEL VALIDATION PROCESS

The validation procedure consists of waterflood/EOR field data gathering and matching the production history data with the forecasting model. Following this we go through each stage with examples of history matched fields.

5.1.1- Required Field Data

Waterflood/ EOR field data used in validation of the model was mostly gathered from public sources (such as papers and reports on the performed projects) as listed in the references. This includes 4 field and 15 single well waterfloods, 7 polymer, 20 surfactant-polymer (SP), 4 alkaline-surfactant-polymer (ASP) and 8 solvent floods. The number of field data used for history matching of each EOR process reflects the availability of published data for that EOR process. In addition to field EOR results, laboratory coreflooding results are history matched by the forecasting model and compared to field results.

5.1.2- Preprocessing of the Field Data

In each case the reported production history results (such as cumulative oil recovery, oil cut, recovery efficiency) were digitized and fed into forecasting tool (UTF) spreadsheets for history matching. Figure 5-1 is an example of production history results showing Salem SP flooding pilot results of oil rate, cumulative oil production and oil cut vs. time.

After digitizing the field results and importing into UTF spreadsheets, the data may need some filtering and pre-processing before history matching. The important point is that the forecasting tool must be applied on incremental results of EOR/waterflooding

even though the reported results show a continuous production history of the field from primary to tertiary. For example in case of recovery efficiency (E_R) or cumulative oil recovery, the incremental results of EOR stage must be extracted. Oil cut data doesn't need this treatment but the initial value of oil cut at start of EOR (or waterflood) must be determined from oil cut history results.

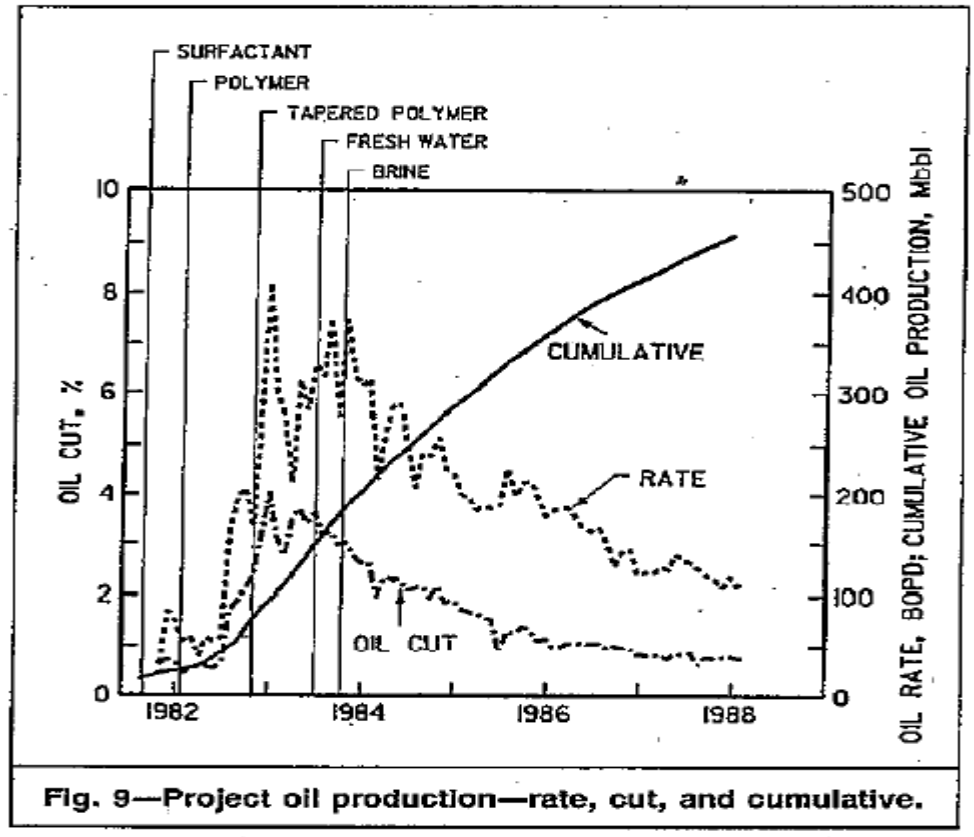

Figure 5-1: Production history results of Salem SP flooding pilot (Widmyer et al., 1988).

The field data may require to be converted from real time to dimensionless time (t_D; injected fluid pore volumes) using Equation 3-11 or in simpler form:

$$t_D = \frac{q_{inj} t}{V_P} \tag{5-1}$$

where q_{inj} is injection rate, t is real time and V_P is field/pilot pore volume. In addition to production history data, we must know the following information about waterflood/EOR project for history matching.

- S_{oR}: Remaining oil saturation at start of the process.
- f_{oi}; Initial oil cut at start of the process
- q_{inj}; Injection rate, for dimensionless time conversion if the reported results are in real time.
- V_P: Field/pilot pore volume, for dimensionless time conversion if the reported results are in real time.

As one can see, UTF needs only very basic information for history matching of the field data, which is one of its advantages compared to history matching using numerical simulation. Before continuing to the history match procedure and results, the basic steps for applying UTF to production history results should be discussed.

5.2- HISTORY MATCHING

After gathering and preparation of the EOR/waterflooding production history data, the forecasting tool (UTF) is applied to match the performance of the EOR/waterflooding results. Following this we explain the procedure and show the results of history matching for waterflooding and different isothermal EOR processes.

5.2.1- Waterflood History Matching

The process of history matching of waterflooding results is easier than EOR processes since there are fewer saturation regions (figure 3-7) and so the formulation is simpler. The results include waterflooding oil cut and cumulative oil recovery of several fields and also single production wells in those fields.

Using UTF, cumulative oil recovery and oil cut results are predicted (forecasted) for each case. History matching is done based on the technique of minimization of error between actual and forecasted data. The error is defined as:

$$Error^2 = \frac{\sum_{i=1}^{n} Actual - Forecasted^{\,2}}{n} \qquad (5\text{-}2)$$

where "Actual" stands for field value, "Forecasted" stands for predicted value by model and "n" is number of data. This error must be minimized to achieve a good match between actual and forecasted results. The matching parameters (variables) for waterflooding are water front Koval factor (K_W) and final average oil saturation (S_{oF}) as explained in Chapter 3. The Koval factor (K_W) controls the shape (behavior) of waterflood performance functions (such as oil cut and recovery efficiency). It is mainly a function of waterflood mobility ratio and reservoir heterogeneity but generally any reservoir/flood property that affects the performance of waterflood. S_{oF} represents the final achievable average oil saturation after injecting many pore volumes of displacing fluid. It accounts for both swept and unswept portions of the reservoir and is an important value in calculating volumetric sweep efficiency and missing (unswept) pore volume of the reservoir. These two variables (K_W and S_{oF}) are adjusted such that a good match

between forecasted and actual results is achieved. The water front velocity is calculated using Equations 3-19 and 20.

The Solver of Microsoft Excel was used successfully to minimize the error and attain a good history match. Note that history matching is conditioned to mathematical and logical limitations of the variables. For example S_{oF} for waterflooding must be greater than or equal to S_{or} (waterflooding laboratory residual oil saturation) and K_W can not be less than 1 (consistent with the Koval model definition). Rarely a user may need to play with matching variables to get a good starting point (first guess) and facilitate Solver job to more easily find the solution.

Figures 5-2 and 5-3 show examples of the forecasted versus actual waterflooding results for a reservoir and single well in a reservoir. The general EOR and waterflood forecasting model fits the field data very well. The rest of waterflooding history match results are provided in Appendix-B.

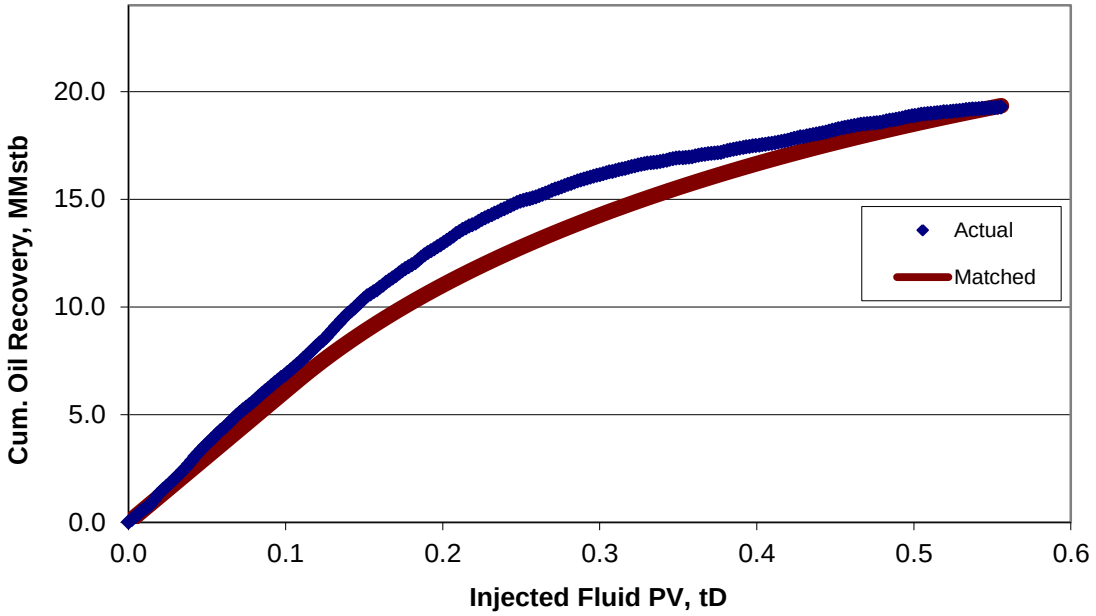

Figure 5-2: Waterflooding history match for whole reservoir (Sand-B).

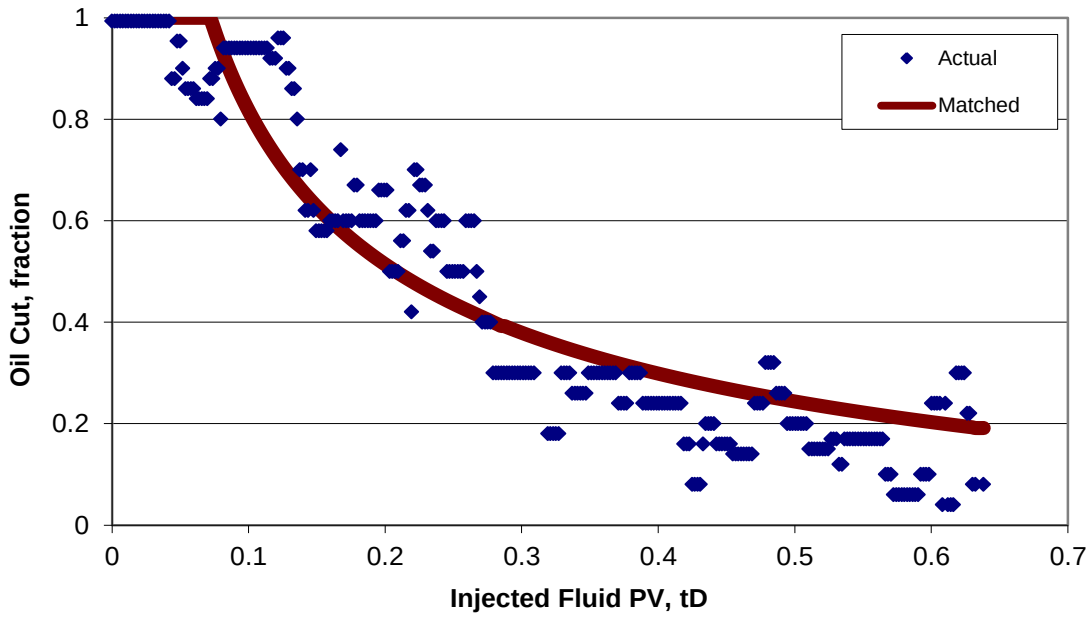

Figure 5-3: Waterflooding oil cut history match for a single well (A-2) in the reservoir (Sand-A).

The obtained Koval factors for field history matching are in between maximum and minimum of single well Koval factors because recovery performance of the field is affected by all of the single wells in the reservoir. Table 5-1 summarizes the Koval factors for waterflooding of different reservoirs and single wells in those reservoirs. The last column in Table 5-1 is the coefficient of determination (square of correlation coefficient, R^2) that is a measure of strength of the history match (fit). The closer the R^2 value to 1 the stronger the fit.

Table 5-1: Summary of fitted Koval factor (K_W) for history match of waterflooding.

Reservoir Name	Well Name	Well Koval Factor	Reservoir Koval Factor	R^2
Sand-A	Well-A1	3.00	7.13	0.992
	Well-A2	5.48		
	Well-A3	2.54		
	Well-A4	8.37		
	Well-A5	3.50		
	Well-A6	4.75		
	Well-A7	15.27		
	Well-A8	12.98		
Sand-B	Well-B1	1.46	3.74	0.949
	Well-B2	10.31		
	Well-B3	2.82		
Sand-C	Well-C1	6.87	4.00	0.899
	Well-C2	1.50		
Sand-D	Well-D1	2.70	4.58	0.887
	Well-D2	5.00		

5.2.2- EOR History Matching

The forecasting model has been validated against all common isothermal EOR processes including chemical EOR: polymer, surfactant-polymer (SP) and alkaline surfactant-polymer (ASP) flooding, and solvent (gas) flooding as well as waterflooding that was represented before. The history match procedure for EOR processes is slightly different compared to waterflooding since there are more different saturation regions (figure 3-7) that signify more complicated mathematical model. Below we explain and show examples of history matching procedure of chemical EOR and then continue to solvent flooding EOR processes. For more examples refer to Appendix-B.

5.2.2.1- Chemical EOR

Chemical EOR has been successfully applied especially in oil fields with small to moderate oil viscosity, salinity and temperature. In chemical EOR different chemicals are injected to control the mobility ratio (between displacing and displaced fluids) by using polymers and/or to decrease the interfacial tension between the phases by using surface-active agents (surfactants; as in SP or ASP flooding) to bring about improved oil recovery (Lake, 1989). The production history data (such as recovery efficiency, cumulative oil recovery, oil cut) of many pilot and field chemical EOR processes including polymer, surfactant-polymer (SP), alkaline surfactant-polymer (ASP) floods were used for history matching and validation of general isothermal EOR forecasting tool. We start with the history match procedure and results of polymer flooding and then continue to SP and ASP flooding.

The history matching procedure for chemical flooding is similar to waterflooding with the exception of one additional matching parameter (variable) because of existence of two displacing fronts. There are three saturation zones for chemical flooding compared to two for water flooding (S_{oR}, S_{oB} and S_{oF}) (one between displacing fluid, the chemical,

and oil bank, the other between oil bank and initial oil). Displacing fluid (chemical) Koval factor (K_C), oil bank Koval factor (K_B) and final average oil saturation (S_{oF}) are adjusted to achieve a good history match of chemical flood performance.

Each matching parameter represents some of the reservoir/process features and characteristics. As explained for waterflooding, the Koval factor describes the shape (curvature) of EOR performance (recovery) functions (oil cut, recovery efficiency, etc.). In case of chemical EOR, in addition to flood mobility ratio and reservoir heterogeneity other factors can influence the recovery of the chemical EOR process such as chemical adsorption and degradation, salinity and inaccessible pore volume. These factors mainly affect the viscosity and relative permeability of the displacing fluid that are accounted in mobility ratio of the flood. S_{oF} represents the final achievable average oil saturation of the process after injecting many pore volumes of displacing fluid. For polymer flood it is conditioned to be more than or equal to S_{or}, the waterflooding laboratory residual oil saturation, but for SP and ASP flooding it ideally is zero because of very low interfacial tension associated with SP and ASP flooding. However S_{oF} never reaches to zero because of oil remained in unswept areas.

These three variables (K_C, K_B and S_{oF}) are adjusted based on error minimization technique (explained in Section 5.2.1) such that a good match between forecasted and actual results is achieved. The velocities of the oil bank and chemical fronts are calculated using Equations 3-21 and 22. S_{oB} (oil bank saturation) can be found by fractional flow construction (as explained in Chapter 3) if there is enough information to build the fractional flow curves, otherwise S_{oB} is a matching parameter.

Error minimization procedure was done using the Solver of Microsoft Excel. Manual adjustment of the matching variables to get a good starting point (first guess) and helping the Solver to more quickly find the solution may help in some cases. Following

this we show some history matching cases of chemical EOR projects including polymer, SP and ASP flooding. Other history matching results are given in Appendix-B.

Polymer Flooding: Daqing Field, Pilot Po

Oil production from the Daqing field comes from sandstone formations of Putaohua and Saertu with the net thicknesses range from 2.3 to 11.6 m (average of 6.1 m) and the in-situ oil viscosity is 9.5 cp. The field was developed by waterflooding in June 1960. Water breakthrough occurred early in producers and the water displacement efficiency was low because of a detrimental water-oil mobility ratio and high inter-layer permeability contrast. Polymer flooding was considered as a mobility control EOR process to increase oil recovery from the field. The Pilot One (PO) polymer flood started in 1990 and ended in 1992. As the result of this successful polymer flooding the average water cut in the pilot unit decreased from 95.2% to 79.4% and the oil recovery was increased by 14% of OOIP. Figure 5-4 shows pilot PO and PT locations in the Daqing field.

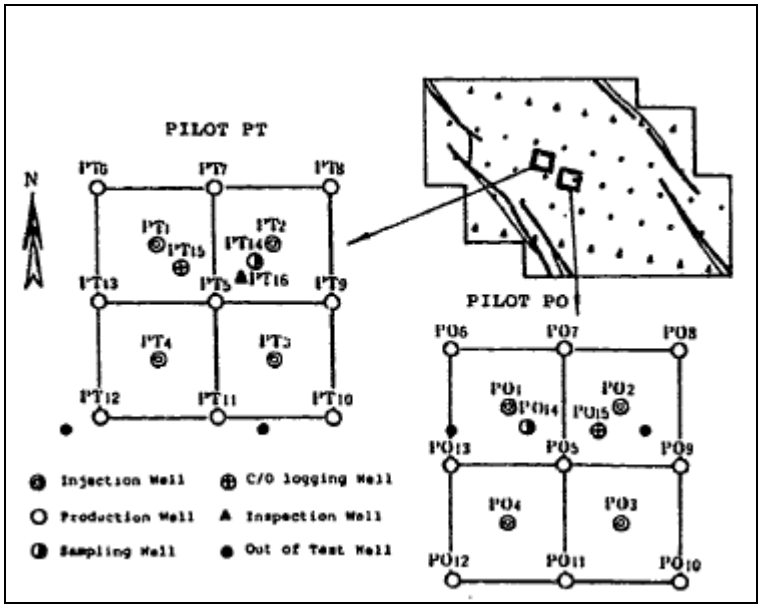

Figure 5-4: Location of polymer flood pilots and wells in Daqing oil field (Wang et al., 1993).

Figure 5-5 shows the history match of cumulative oil recovery of pilot PO. The history match is good; matching parameters are listed in Table 5-2.

Table 5-2: Matching parameters for Daqing field, pilot PO polymer flooding.

Matching Parameter	Value
K_C, Chemical front Koval factor	2.52
K_B, Oil bank front Koval factor	1.27
S_{oF}, Final average oil saturation	0.26

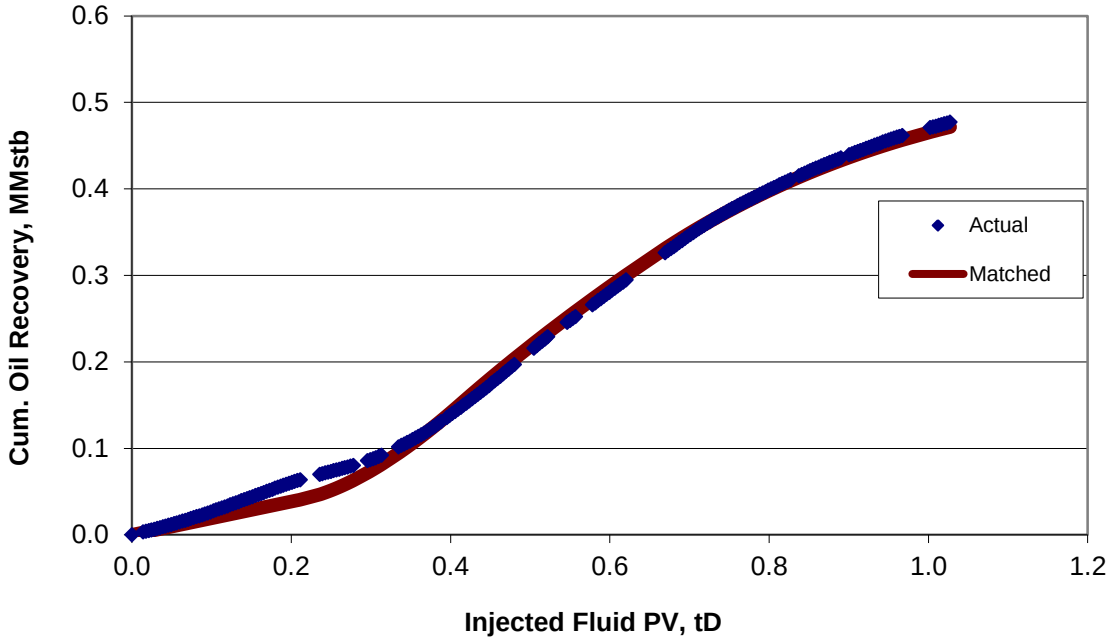

Figure 5-5: Polymer flooding history match of Daqing PO pilot using general isothermal EOR and waterflood forecasting tool (UTF; Wang et al., 1993).

Surfactant-Polymer (SP) Flooding: Wilmington SP Flooding Pilot

The Wilmington field is an asymmetric anticline about 11 miles long by 3 miles wide located along southwestern edge of Los Angeles basin (figure 5-6). The oil producing zones in Wilmington field are unconsolidated sandstones with average permeability of 439 md, ^{o}API oil gravity of 17 and oil viscosity of 25 cp.

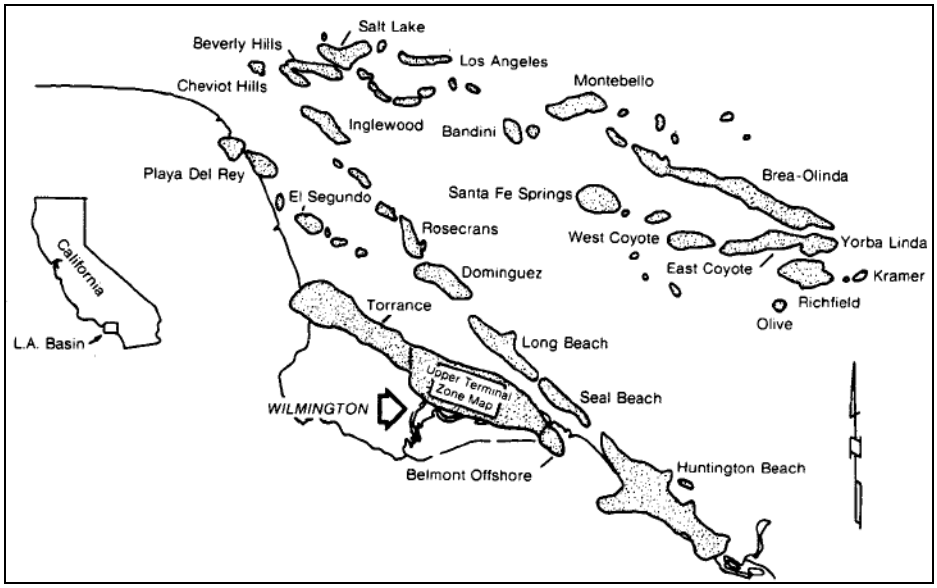

Figure 5-6: Location of Wilmington field in Los Angeles basin (Fanchi, 1988).

Field development started in 1936 and primary production was initiated in 1945. In 1953 gas injection was attempted followed by waterflooding in the same year for the purpose of pressure maintenance. The tertiary SP flood was started with preflush in 1978 followed by surfactant injection in 1979. The SP pilot was performed with 4 injectors and 6 producers as part of US DOE cost-share program (Fanchi et al, 1988; Aguey, 1982). The oil cut at start of the EOR project was about 1.5% and increased to about 8% in the pilot area as the result of SP flooding. Figure 5-7 shows the results of oil cut history match of the Wilmington SP flooding pilot using UTF. The history matching is as strong as for the polymer flood. Table 5-3 summarizes the history matching parameters for the Wilmington SP flood pilot.

Table 5-3: Matching parameters for Wilmington SP flooding pilot.

Matching Parameter	Value
K_C, Chemical front Koval factor	2.622
K_B, Oil bank front Koval factor	1.776
S_{oF}, Final average oil saturation	0.318

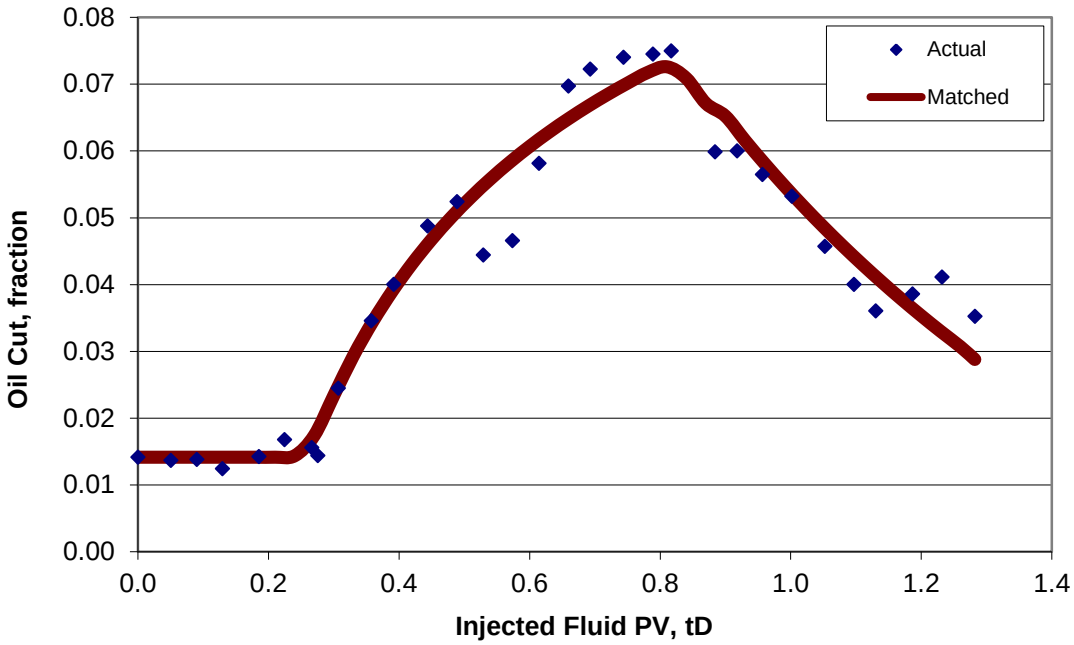

Figure 5-7: History match of Wilmington SP flooding pilot using general isothermal EOR and waterflood forecasting tool (UTF; Fanchi, 1988).

Alkaline Surfactant-Polymer (ASP) Flooding: Daqing Field, Pilot XF

Successful history of polymer flooding in Daqing field with incremental recovery over water flood of more than 12% OOIP motivated the application of SP flooding to further increase recovery. SP flooding was technically successful, but not economical. To

decrease the amount and cost of the expensive surfactants required for chemical flooding, the compatibility of surfactants with alkali was studied.

Several ASP flooding pilots were performed in the Daqing field. Pilot XF consists of one injector and four producers. It is located in the Xingwu region at the south part of the field. The target layer is composed mainly of course sand with permeability of about 600 md and ^{o}API oil gravity of 35. The ASP pilot results showed good performance, increasing the oil cut from 5% to 15%. Figure 5-8 shows the results of oil cut history match of the ASP flooding in pilot XF of the Daqing field. UTF shows a strong ability in history match the ASP results as well as other chemical EOR processes. Table 5-4 lists the summary of matching parameters for the XF Daqing ASP pilot.

Table 5-4: Matching parameters for Daqing ASP flooding, pilot XF.

Matching Parameter	Value
K_C, Chemical front Koval factor	11.123
K_B, Oil bank front Koval factor	2.995
S_{oF}, Final average oil saturation	0.079

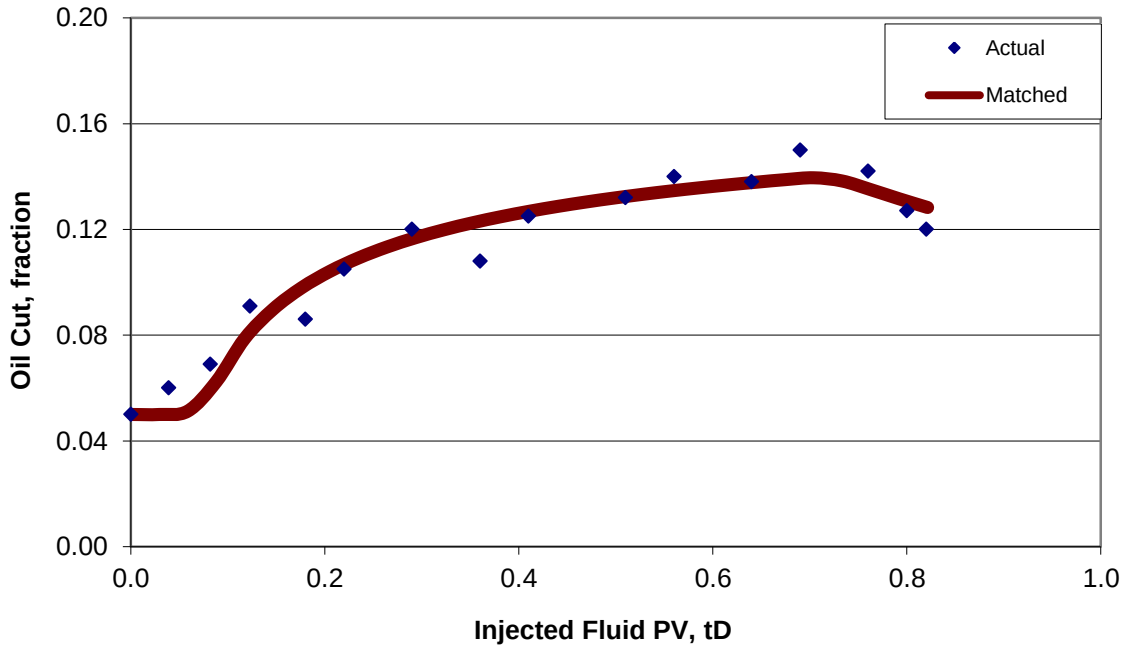

Figure 5-8: Alkaline surfactant-polymer (ASP) flooding history matching of Daqing XF pilot using general isothermal EOR and waterflood forecasting tool (UTF; Demin et al., 1999).

These examples demonstrate the ability of UTF model to closely match chemical EOR field results.

5.2.2.2- Solvent (Gas) Flooding/WAG EOR

Water alternating gas (WAG) field floods have been successfully performed as an EOR method. The main purpose is to increase the sweep efficiency of miscible/ immiscible gas flooding by reducing the mobility ratio between injected gas and the formation oil, which is the major problem in solvent floods with very poor sweep and early gas breakthrough (Mathiassen, 2003; Lake, 2008; Garcia Quijada, 2005; Gaviria Garcia, 2005; Nasir, 2009).

Field results from several CO_2/WAG floods were used to history matching with UTF forecasting model. The history matching procedure is similar to chemical EOR with

the same number of matching parameters (K_S, K_B and S_{oF}). Here we have K_S (solvent front Koval factor) instead of K_C (chemical front Koval factor) that represents the shape and behavior of the solvent-oil bank front mainly controlled by reservoir heterogeneity, pressure, mass transfer between phases and WAG ratio (if it is a water alternative gas flooding instead of continuous gas flooding). S_{oF} characterizes the final achievable average oil saturation of the EOR process after injecting many pore volumes of displacing fluid. Miscible gas flooding can ideally reach to zero oil saturation but this never occurs unless volumetric sweep efficiency (E_V) is 100%. The velocities of oil bank (v_B) and displacing fluid (v_S) fronts are calculated from the fractional flow curve construction (Lake, 1989; Walsh, 1989) using Equations 3-24 and 3-25.

The error minimization technique is applied using K_S, K_B and S_{oF} as matching variables (parameters) to history match the field results. The oil bank saturation (S_{oB}, required for calculation of the velocities) can be found by fractional flow construction (as explained in Chapter 3) if there is enough information to construct the fractional flow curves; otherwise S_{oB} can be used as the matching parameter. Results of several published CO_2/WAG projects were history matched. We only show the history matching results of the SACROC 4PA CO_2 WAG flooding pilot in this chapter. Appendix-B provides history matching of other solvent (gas) flooding projects.

SACROC-Four Pattern (4PA) CO_2/WAG flooding:

The SACROC (Scurry Area Canyon Reef Operators Committee) Unit constitutes the major portion of the Kelly-Snyder Field, a carbonate field discovered in 1948 in Scurry County, Texas. Figure 5-9 shows the map of the SACROC unit in the Kelly-Snyder field with CO_2 flooding patterns. The field has an average porosity of 9.4%, average permeability of 3 md and oil viscosity of 0.35 cp. The field primary recovery under solution gas drive was not significant and waterflooding as the secondary recovery

mechanism was implemented in 1953. Miscible CO_2 flooding started with small amounts in 1976 until 1980 when it began to be widely used.

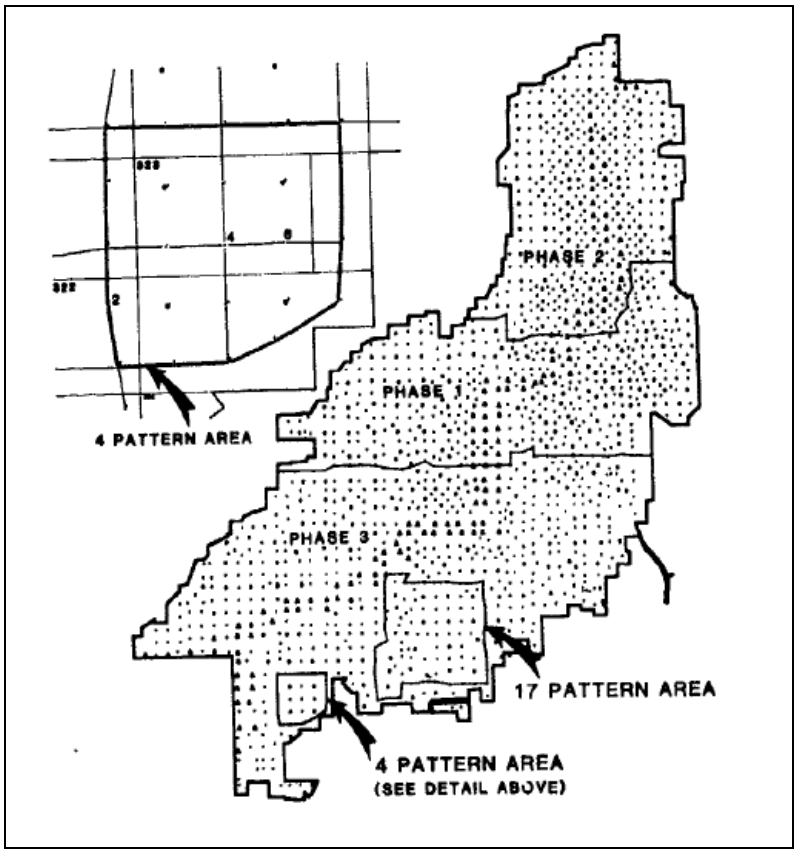

Figure 5-9: Map of SACROC unit in Kelly-Snyder field showing 4 and 17 pattern areas (Langston et al., 1968).

The 4PA pilot is located on the south flank of the field. CO_2 flooding in this pilot started in 1981 with inverted 9-spot patterns. The response to CO_2 flooding was definitive leading the WOR to drop from about 24 at start of the EOR process to about 7 and significant incremental oil recovery of 9% OOIP (Langston et al., 1968).

Figure 5-10 shows the history matching results of the SACROC-Four Pattern (4PA) CO_2/WAG flooding. The history matching is good, showing that the general EOR

and waterflood forecasting model matches the field solvent (gas) flooding EOR as well as it does for the chemical EOR and waterflooding field results. Table 5-5 lists the summary of matching parameters for SACROC 4PA CO_2/WAG project.

Table 5-5: Summary of matching parameters for SACROC 4PA CO_2/WAG flooding.

Matching Parameter	Value
K_S, Solvent front Koval factor	39.557
K_B, Oil bank front Koval factor	7.594
S_{oF}, Final average oil saturation	0.247

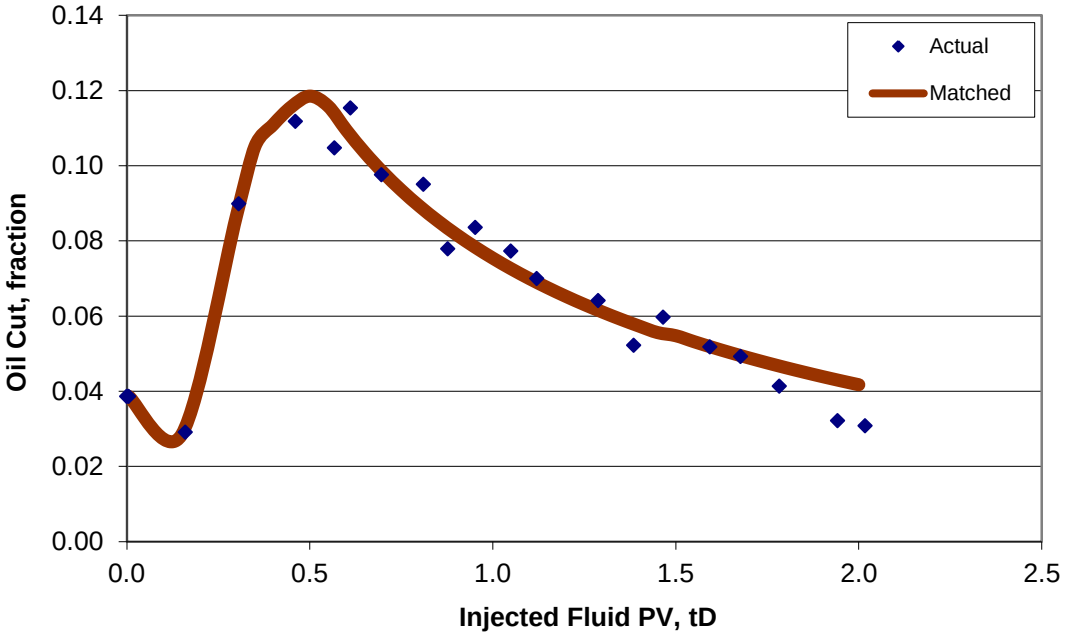

Figure 5-10: CO_2/WAG flooding history matching of SACROC-Four Pattern (4PA) using the general isothermal EOR and waterflood forecasting tool (UTF; Langston et al., 1968).

A summary of field/pilot history matching results with corresponding history matching variables obtained for each field/pilot is shown in Table 5-6. As one can see values of displacing fluid Koval factor (K_1; K_C or K_S) are much larger for solvent/WAG flooding, which reflects the higher mobility ratio of gas compared to chemical EOR that takes advantage of polymer for mobility control. Waterflooding Koval factors (Table 5-1) stand between chemical EOR (K_C) and solvent (gas) flooding (K_S). Oil bank Koval factors (K_2) are usually smaller than displacing fluid Koval factor (K_1) showing that oil bank front is usually more stable than displacing fluid front. The last column in Table 5-6 is the coefficient of determination (square of correlation coefficient, R^2) that is a measure of strength of the history match (fit). The closer the R^2 value to 1 the stronger the fit.

Table 5-6: Summary of Field/pilot history matching variables for different EOR processes.

Field Name	**History Matching Parameters**			
	$^*K_1$	$^*K_2$	$\Delta S_o=S_{oR}-S_{oF}$	R^2
Chateaurenard polymer flood	4.528	1.082	0.305	0.998
Courtenay polymer flood	4.599	2.070	0.274	0.994
Daqing PO polymer flood	1.846	1.751	0.265	0.998
Marmul polymer flood	3.527	1.032	0.500	0.988
Minnelusa polymer flood	5.326	1.320	0.365	0.995
North Burbank polymer flood	2.292	5.014	0.230	0.999
Sleepy Hollow polymer flood	2.870	2.100	0.220	0.997
Benton SP flood	2.471	1.575	0.089	0.852
Sloss SP flood	3.714	2.317	0.204	0.995

Berryhill Pilot SP flood	2.578	2.250	0.066	0.917
Wilmington SP flood	2.622	1.776	0.062	0.950
Borregos SP flood	1.869	1.666	0.061	0.999
Bell Creek SP flood	1.640	1.187	0.054	0.977
Bell Creek Confined SP flood	1.989	1.211	0.158	0.971
Big Muddy Field SP flood	3.432	7.624	0.016	0.956
Big Muddy Pilot SP flood	2.486	1.467	0.110	0.954
Bradford 7 SP flood	7.841	1.997	0.064	0.888
Bradford 8 SP flood	3.907	1.759	0.045	0.965
Manvel SP flood	8.144	4.048	0.057	0.999
North Burbank SP flood	4.430	2.516	0.035	0.913
Berryhill Field SP flood	8.247	3.606	0.077	0.828
1M-2.5 SP flood	2.901	1.454	0.093	0.919
1M-5.0 SP flood	3.551	1.414	0.095	0.997
Salem SP flood	8.019	3.844	0.076	0.823
Chateaurenard SP flood	9.046	2.504	0.409	0.999
Robinson SP flood	4.124	1.584	0.188	0.893
Loudon SP flood	1.696	2.300	0.157	0.960
Daqing XF ASP flood	11.123	2.995	0.361	0.924
Karamay ASP flood	4.951	2.511	0.259	0.894
Cambridge ASP flood	2.402	1.812	0.43	0.993
Tanner ASP flood	13.334	2.126	0.463	0.997
Lost Soldier Tensleep WAG flood	37.930	6.048	0.365	0.957
SACROC 4PA WAG flood	39.557	7.594	0.216	0.925

SACROC 17PA WAG flood	81.883	9.280	0.412	0.998
Wertz Tensleep WAG flood	58.215	10.202	0.284	0.945
West Sussex WAG flood	48.166	14.203	0.056	0.977
Twofreds WAG flood	63.258	5.563	0.212	0.914
Rangely WAG flood	76.795	12.502	0.279	0.998
Slaughter WAG flood	6.891	3.041	0.322	0.883

*K_1 and K_2 are displacing fluid and oil bank front Koval factors respectively.

5.2.3- Coreflood History Matching

In addition to field history matching, we applied UTF on coreflood laboratory experiments of EOR processes. The available coreflood data include SP and ASP coreflood experiments. Table 5-7 summarizes the matching parameters for these experiments.

Table 5-7: History matching parameters for coreflood laboratory experiments (Pope, 2011).

Coreflood#	**History Matching Parameters**			
	$^*K_C$	$^*K_B$	$\Delta S_o=S_{oR}-S_{oF}$	R^2
Core#A: SP flood	1.357	1.001	0.395	0.925
Core#B: ASP flood	1.361	1.001	0.338	0.962
Core#C: ASP flood	1.619	1.118	0.25	0.996
Core#D: ASP flood	1.316	1.001	0.306	0.898
Core#E: ASP flood	1.221	1.030	0.429	0.981

As Table 5-7 shows, both chemical and the oil bank Koval factor (K_C and K_B) values are small and very close to 1 reflecting much less heterogeneity in cores compared to field projects. The saturation difference (ΔS_o) values are relatively larger for corefloods compared to field projects mainly because of larger sweep efficiency of coreflood experiments that are basically 1D displacements. Figure 5-11 shows the results of history matching of ASP coreflooding test on Core#B. Other coreflood history matches are provided in Appendix-B.

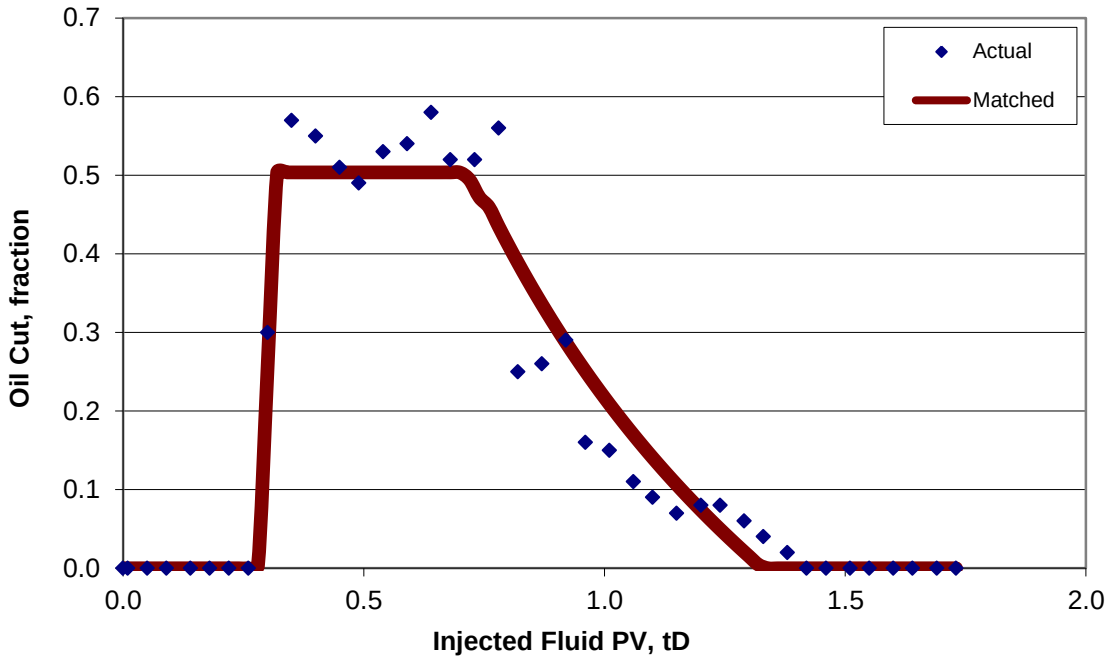

Figure 5-11: ASP coreflood history matching of Core#B using the general isothermal EOR and waterflood forecasting tool (UTF; Pope, 2011).

5.3- DISCUSSIONS

The Koval-based approach described here combines vertical and areal sweep into a single factor, the Koval factor. It is therefore no longer necessary to estimate these effects separately and combine them. The displacement sweep from relative permeability measurements is retained but its complexity is vastly reduced by treating the displacements as locally piston-like. The key upgrade from the Koval-based approach is the replacement of a physical dimension, thickness, with storage capacity. The flow-storage capacity curve is parameterized with the Koval factor.

The forecasting model reproduced well (R^2>0.8) all of the field data we have analyzed and reproduces the simulated data (discussed in Chapter 6) even better. Important insights from the matching are:

- Koval factors (displacing and oil bank fronts; K_1 and K_2) are arranged in order of increasing mobility ratio. Usually, the Koval factor for the oil banks is the smallest of all indicating that the oil banks are usually more stable than that of the displacing fluids.
- Koval factor increases by increasing reservoir heterogeneity (characterized by Dykstra-Parsons coefficient, V_{DP}, and dimensionless geostatistical correlation length (λ), it is discussed more in Chapter 6.
- The Koval factors are usually larger than those inferred from the coreflooding laboratory experiments. This observation is consistent with the following.
- The final average oil saturation in field/pilot projects is larger, sometimes much larger, than what is observed in laboratory experiments. This observation suggests that an important feature of all field displacements is the existence of a missing or lost pore volume, a volume that will never be accessed by displacing fluids (discussed in Chapter 6).

Chapter 6: EOR/WATERFLOOD FORECASTING AND NUMERICAL SIMULATION

6.1- OBJECTIVES

In previous chapters we introduced the mathematical model and showed the history matching abilities of the EOR forecasting model through the validation process. However, the main purpose of the forecasting model (tool) is prediction of the performance of the EOR and waterflooding processes when there is no production/injection history data available and we just have some basic information about the reservoir/recovery process such as reservoir heterogeneity, flood mobility ratio and WAG ratio. By *performance* we mean output results such as recovery efficiency, volumetric sweep efficiency, oil cut, etc. Forecasting is required when we must predict the EOR results for purposes such as quantitative EOR forecasting, EOR screening, EOR evaluation and decision analysis, economical evaluation of EOR/waterflood projects and for an asset of reservoirs or a single pilot/reservoir without relying on the production (injection) history and just using some basic reservoir/recovery process information as mentioned above. We name this type of reservoir performance prediction as "*Forecasting*".

The word "*Forecasting*" is the process of making statements about events whose actual outcomes (typically) have not yet been observed. A commonplace example might be estimation for some results of interest at some specified future date. "Prediction" is a similar, but more general term. An important, albeit often ignored aspect of forecasting, is the relationship it holds with planning. Forecasting can be described as predicting what the future *will* look like, whereas planning predicts what the future *should* look like.

Forecasting methods are divided into qualitative and quantitative techniques.

Qualitative forecasting techniques are subjective, based on the opinion and judgment of consumers and experts; they are appropriate when past data is not available. Whereas quantitative forecasting models are used to estimate the future as a function of past data; they are appropriate when past data is available and we have some information about the system (Anonymous, Forecasting Principles).

To address this issue, we must find the functionality of the forecasting model variables (Koval factors, K_B, K_C and K_S and final average oil saturation S_{oF}) to reservoir/ recovery process variables such as reservoir heterogeneity, mobility ratio, reservoir pressure and WAG ratio. In other words, we must figure out if strong correlations exist between the forecasting model variables and reservoir/ recovery process variables. If the answer to the latter question is yes, then the forecasting model variables can reliably represent the reservoir/ recovery process variables in the forecasting model for forecasting of EOR/waterflooding results.

In this chapter we start with explaining the approach used to develop the response surfaces and in-situ correlations of the forecasting model. Then numerical simulation models and results are presented. Next, the response surface modeling results to describe the forecasting model in-situ correlations are presented. Finally, the forecasting model is applied to predict the volumetric sweep efficiency and missing pore volume of the EOR/waterflooding processes.

6.2- EXPERIMENTAL DESIGN

In general usage, "*Design of Experiments (DOE)*" or "*Experimental Design*" is the design of any information-gathering exercises where variation is present, whether under the full control of the experimenter or not. However, in statistics, these terms are usually

used for controlled experiments. In the Design of Experiments, the experimenter is often interested in the effect of some processes (the "treatment") on some objects, which may be people, groups of people, plants, animals, materials, etc. Design of Experiments is thus a discipline that has very broad application across all the natural and social sciences (Dunn, 1997).

In this work, we applied experimental design approach to find the functionality of the forecasting model variables to reservoir/recovery process variables. For this purpose, comprehensive numerical simulation studies were designed and performed for each secondary and tertiary recovery process based on *Experimental Design & Response Surface Modeling (RSM) technique* that gives the optimum number and design of runs based on the number, type and range of input (reservoir/recovery process) variables. In this way the most efficient number and design of numerical simulations for the purpose of the study is achieved and the unnecessary, exhausting experiments (simulations) are avoided.

The most influential (key) variables that govern the performance of each secondary/tertiary recovery process were selected based on a the detailed sensitivity analysis using *Winding Stairs* sensitivity analysis method, (Mollaei et al., 2011a; Lawal et al., 2007 and 2008, Chan et al., 2000; Salteli et al., 1999) described in Chapter 4, and reservoir engineering knowledge. As the recovery process variables, the endpoint mobility ratio (M^o; mobility ratio of fluids at their endpoint saturation, Kumar et al. 2008) that includes the effects of the viscosity and relative permeability was used for experimental design of chemical EOR and waterflooding processes. For solvent flooding/WAG, WAG ratio (W_R; water to gas injection ratio) and pressure were used for Experimental Design. Reservoir heterogeneity (represented by Dykstra-Parsons coefficient; V_{DP}) and geostatistical dimensionless correlation length (λ, defined in the

reservoir model section) were chosen as reservoir variables in Experimental Design. Tables 6-1 to 6-3 show the ranges of the different variables used for Experimental Design of waterflooding and different EOR processes.

The chosen bottomhole pressure (BHP) range for solvent/WAG EOR varies between MMP (minimum miscibility pressure) of the reservoir fluid (2110 psi) and fracturing pressure of the reservoir. Considering these and to achieve and maintain miscibility during solvent flooding, the BHP (bottomhole pressure) of the pressure-constrained vertical producers varies from 2125 (which is 15 psi greater than the MMP) up to 3500 psi. The range of endpoint mobility ratio for waterflooding and chemical EOR are comprehensive and appropriate to practical field/pilot designs. The range of reservoir heterogeneity variables were selected to cover all possible heterogeneous permeable media.

Table 6-1: Range of variations of reservoir/process variables used for Experimental Design of waterflooding.

Recovery Process/ Reservoir Variable	**Range of Variation**
M^o, dimensionless	0.5 - 50.0
V_{DP}, dimensionless	0.4 - 0.9
λ, dimensionless	0.5 - 10.0

Table 6-2: Range of variations of reservoir/process variables used for Experimental Design of chemical EOR processes.

EOR Process/ Reservoir Variable	**Range of Variation**
M^o, dimensionless	0.1 - 30
V_{DP}, dimensionless	0.4 - 0.9
λ, dimensionless	0.5 - 10.0

Table 6-3: Range of variations of reservoir/process variables used for Experimental Design of solvent (gas) flooding/WAG EOR processes.

EOR Process/ Reservoir Variable	Range of Variations
Water to gas injection ratio, W_R, dimensionless	0.5 - 5.0
(P-MMP)/MMP, dimensionless	1.007 - 1.659
V_{DP}, dimensionless	0.4 - 0.9
λ, dimensionless	0.5 - 10.0

Design of Experiments was done based on the input variable ranges indicated in above tables. The output of the Experimental Design, which gives the optimum design and number of runs, are listed in Appendix-C. The next section describes and explains the reservoir modeling and numerical simulation design for EOR/waterflooding processes.

6.3- RESERVOIR MODELING AND NUMERICAL SIMULATION

The Experimental Design output that suggests the optimum design and number of runs (with different reservoir/recovery process variables) were used for a systematic and comprehensive numerical simulation study of each EOR/waterflood process. We used commercial and in-house reservoir numerical simulators; GEM (general equation of state compositional simulator from CMG simulator package) for solvent (gas) flooding/WAG and UTCHEM (University of Texas Chemical EOR Simulator) for chemical EOR and waterflooding simulations.

6.3.1- Reservoir Model Description

The reservoir model for the Experimental Design simulation study is a five spot pattern pilot surrounded with some quarter of five spots (totally 4 five spot patterns) as shown in Figure 6-1. The model is 2000 ft×2000 ft×100 ft in x, y and z directions

respectively (which covers about 92 acres) and contains 4 pressure constrained production wells and 9 rate constrained injection wells. This reservoir model is similar to the Salem EOR pilot (Strange 1977; Widmyer 1988).

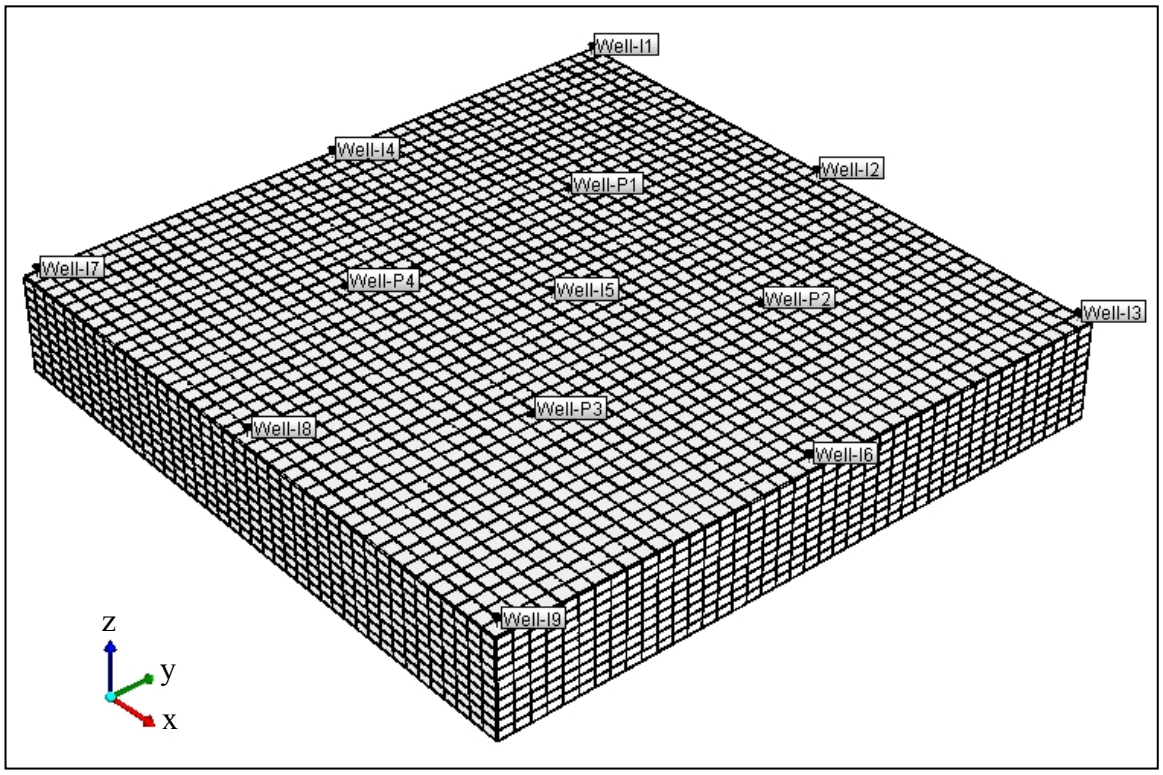

Figure 6-1: The reservoir pilot used for simulation of secondary and EOR processes with surrounding and center vertical injectors and central vertical producers.

Both production and injection wells are vertical and completed in all the layers of the simulation model. Areal gridding sensitivities concluded the proper grid size for the model to be 41×41×10 in x, y and z directions respectively (total grid number of 16,810 cells with 48.78 ft on the sides and 10 ft thick making 10 layers vertically). This grid design showed satisfactory results compared to more finely gridded models (such as 82×82×10).

Reservoir heterogeneity was applied in both the horizontal and vertical directions (k_v/k_h=0.1). This allows different permeabilities for each grid block and is much more realistic than considering constant permeability for whole reservoir or for each layer. To achieve this, we used FFTsim software (Fast Fourier Transform; a reservoir heterogeneity modeling software, Jennings et al., 2002) with a wide range of Dykstra-Parsons coefficient (V_{DP}) along with geostatistical dimensionless correlation length (λ_x or L_x; ratio of the range of the semivariogram to pilot characteristic length in x direction (injector-producer distance). For our models $\lambda_x=\lambda_y$ and λ_z is selected such that represents the number of geological layers. In this work when it is said λ we mean λ_x unless other is specified. These two reservoir variables were also used in Experimental Design along with recovery process variable/s. Reservoir permeability is log normally distributed as it is compatible with reality of the reservoirs. Figure 6-2 shows an example of the permeability field for the case of V_{DP}= 0.8 and λ=10. For each case of simulations a pair of V_{DP} and λ were suggested by Experimental Design and used to generate the permeability field such that represents the desired characteristics. Corey type relative permeability curves were used for water and chemical EOR simulation.

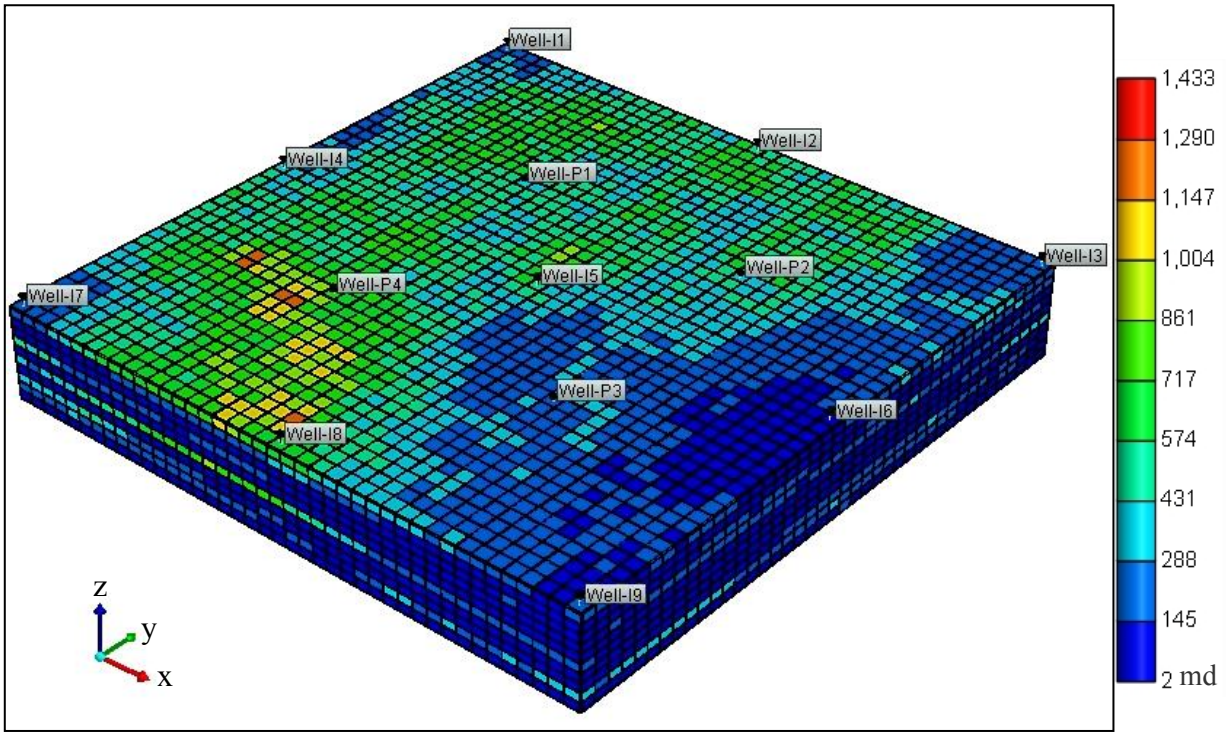

Figure 6-2: Heterogeneous permeability field generated for V_{DP}=0.8 and λ=10. Figure shows heterogeneity applied in both horizontal and vertical directions.

6.3.2- Reservoir Fluid Properties

Proper fluids were used for simulation of different EOR processes and waterflooding. For waterflooding simulation studies the recovery process variable used in Experimental Design is endpoint mobility ratio. To make floods with different endpoint mobility ratios, oils with different viscosities were used. For each waterflooding simulation (listed in Appendix-C) oil viscosity was calculated and applied for whole range of endpoint mobility ratio (M^o of 0.5 to 50) shown in Table 6-1.

In case of chemical EOR, a viscous oil (μ_o= 80 cp) causing an adverse mobility ratio of 100 for waterflooding was selected. Then, the desired mobility ratio of the flood

for each simulation (listed in Appendix-C) was implemented by adjusting the low shear rate polymer viscosity to satisfy the wide range of M^o of 0.1 to 30 used in Experimental Design (Table 6-2).

For solvent/WAG flooding EOR (done as simultaneous water/gas injection), simulations are compositional and more complicated than black oil simulations. The fluid for solvent/WAG flooding EOR simulations was chosen from West Welch reservoir fluid, a Permian Basin field (Taylor et al. 1998). The fluid has API gravity of 32 and small percentage of C_1 and C_{30}^+ compared to intermediate components, which is a typical candidate for CO_2 WAG flooding and has been used in literature for simulation studies (Ghanbarnezhad et al., 2010). In solvent flooding, the recovery process variables used in Experimental Design are pressure, which was explained in Section 6.2, and WAG ratio (W_R). These two variables control the mobility ratio of solvent flooding. WAG ratio was defined in Chapter 3 as the ratio of injection rate of water to solvent. Since solvent (gas) is much less viscous than water, therefore the smaller the WAG ratio the more the fraction of solvent and so the more the mobility ratio and vice versa.

6.3.3- Initial Conditions

The initial status of the reservoir can have a significant effect on the performance of the secondary or tertiary recovery process. We tried to apply the initial conditions as close as possible to practical cases.

For waterflooding, the flow was initiated at a uniform oil saturation of 0.7 followed by injecting 1.5 pore volume of water. The residual oil saturation to waterflood (S_{orw}) is 0.28.

For chemical EOR simulations, the flood was initiated with a uniform oil saturation of 0.7 then followed by injecting 1.0 pore volume of water that causes very

high water cuts (>95%) before starting the injection of chemicals into reservoir. Therefore the chemical EOR is performed as tertiary recovery process.

Solvent flooding also was done as tertiary recovery process. The reservoir was initiated at uniform oil saturation of 0.8 followed by 1.0 PV of waterflooding. When waterflooding is done and water cut peaks to very high values, the solvent/WAG EOR process was initiated. The simulations are isothermal and the reservoir model was initiated at a uniform pressure of 2125 psi for solvent flooding, which is 15 psi above the estimated MMP (minimum miscibility pressure) of 2110 psi.

6.3.4- Numerical Simulation Results and History Matching

After setting up the reservoir models for waterflooding and EOR processes, numerical simulation was performed for all of the different cases suggested by Experimental Design.

For example, for polymer flooding, floods with different M^o (endpoint mobility ratio), reservoir heterogeneity (V_{DP}) and dimensionless correlation length (λ) were simulated with UTCHEM. Results of the simulation were then history matched with the EOR forecasting tool (UTF) to identify and characterize the variations of chemical front Koval factor (K_C), oil bank front Koval factor (K_B) and final average oil saturation (S_{oF}) with changes of process/reservoir variables (M^o, λ and V_{DP}). This helps to describe the forecasting model variables (K_C, K_B and S_{oF}) as functions of recovery process/reservoir variables (M^o, λ and V_{DP}) and see if they are strongly correlated. We based the water and chemical flood history matching on oil cut and solvent/WAG flood on recovery efficiency. Figure 6-3 illustrates an example of polymer flooding simulation and history matching results. The history matching results are strong showing the ability of the

general EOR and waterflood forecasting tool to history match the numerical simulation results.

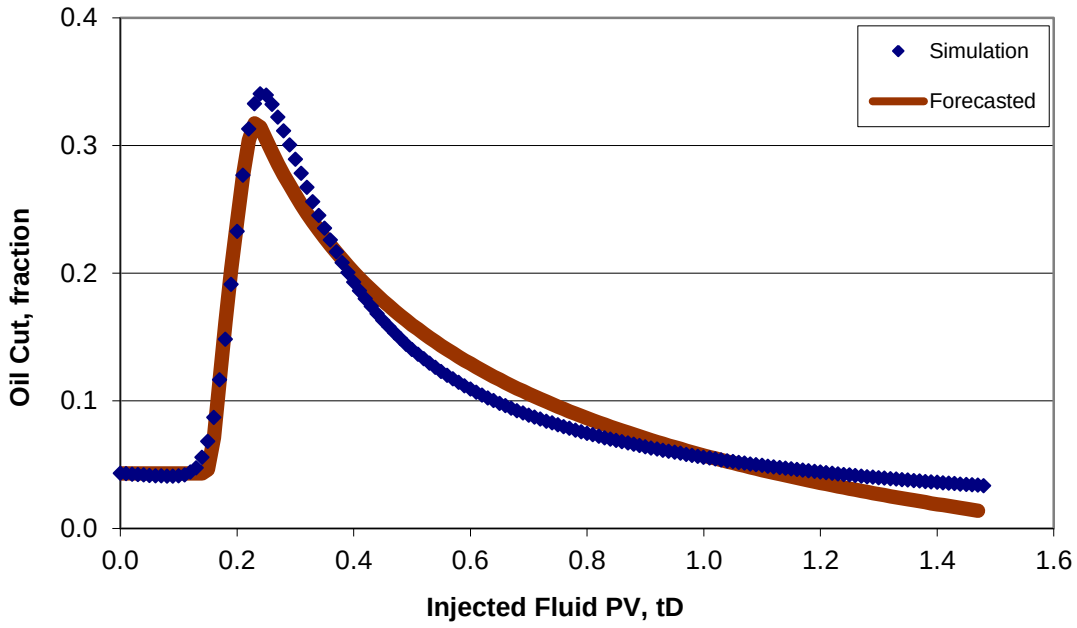

Figure 6-3: History match of Polymer flooding numerical simulation results (M^o= 3, V_{DP}= 0.8, λ_x= 10) using the general isothermal EOR and waterflood forecasting tool (UTF).

Numerical simulation and history matching results of polymer and waterflood show that mobility ratio is the most influential reservoir/recovery process variable that governs the oil recovery efficiency as Figure 6-4 shows. A strong mobility ratio ($M^o < 3$) can substantially compensate for the unfavorable effects of the reservoir heterogeneity. Figure 6-4 summarizes the numerical simulation results of polymer flooding performance in terms of recovery efficiency (E_R). The ellipses on the plot depict the different groups of polymer floods with different recovery efficiency mainly separated by M^o (endpoint

mobility ratio). The legend on the plot shows polymer floods with different sets of (M^o, V_{DP}, λ).

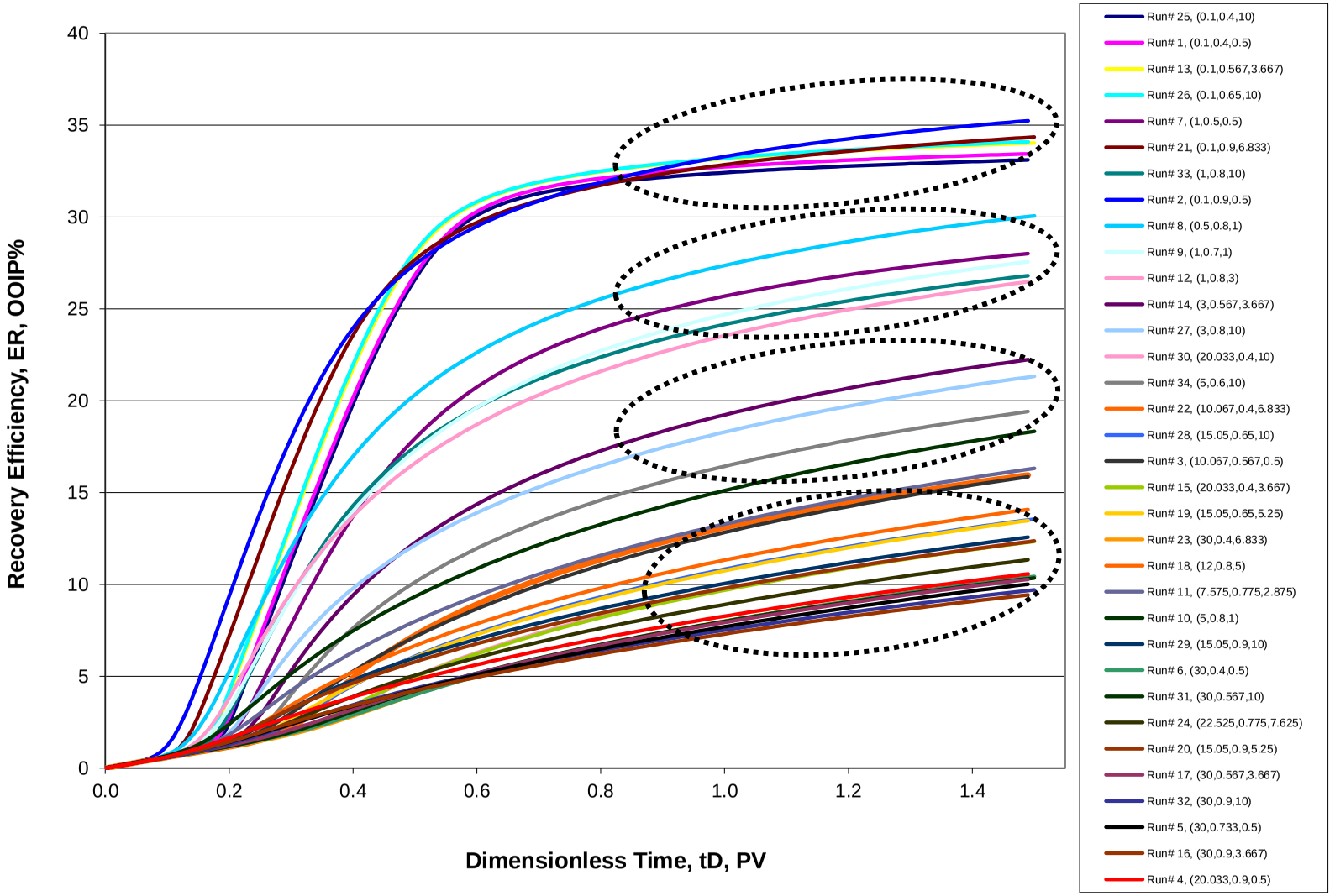

Figure 6-4: Numerical simulation recovery efficiency (E_R) results for polymer flood with different M^o, V_{DP} and λ. Figure shows groups of floods mainly separated by mobility ratio.

WAG numerical simulations were done using CMG-GEM in the form of simultaneous water alternative gas (SWAG) flooding. A similar Experimental Design was done within the extensive range of process/reservoir variables (W_R or WAG ratio), producing bottomhole pressure (BHP), reservoir heterogeneity (V_{DP}) and dimensionless correlation length (λ) shown in Table 6-3. The optimum design and the number of simulations were obtained based on the Experimental Design. The results of the simulation were then history matched (see Chapter 5) using the EOR forecasting tool (UTF) to find the functionality and correlations of solvent front Koval factor (K_S), oil bank front Koval factor (K_B) and final average oil saturation (S_{oF}) with respect to changes of process/reservoir variables (W_R, P, λ and V_{DP}). History matching of WAG numerical simulations shows that in solvent (gas) flooding/WAG, reservoir heterogeneity is the most sensitive governing variable affecting the EOR recovery and sweep efficiency. The unfavorable effect of reservoir heterogeneity worsens substantially for V_{DP} values about or greater than 0.8 such that decreasing WAG ratio (increasing gas injection) can not compensate for that. In such cases, mobility ratio should be decreased using a proper mobility control such as foam. Figure 6-5 illustrates an example of WAG numerical simulation history matching using the EOR forecasting model (UTF). The EOR forecasting model shows good agreement with simulation results. The oscillations of the oil cut curve are related to heterogeneity and high mobility of solvent flooding.

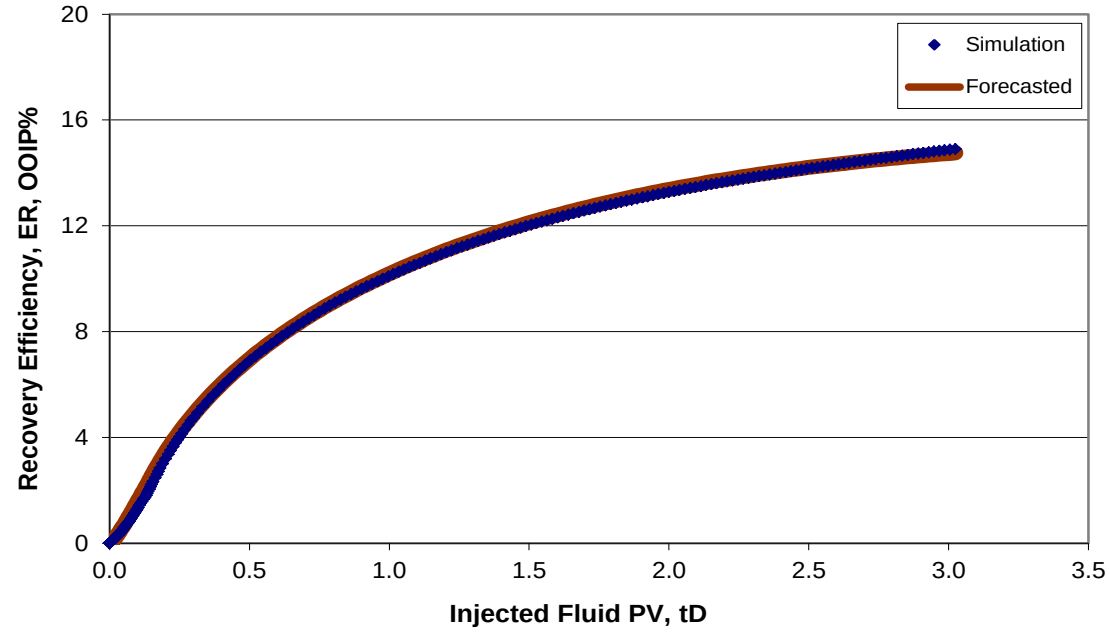

(a)

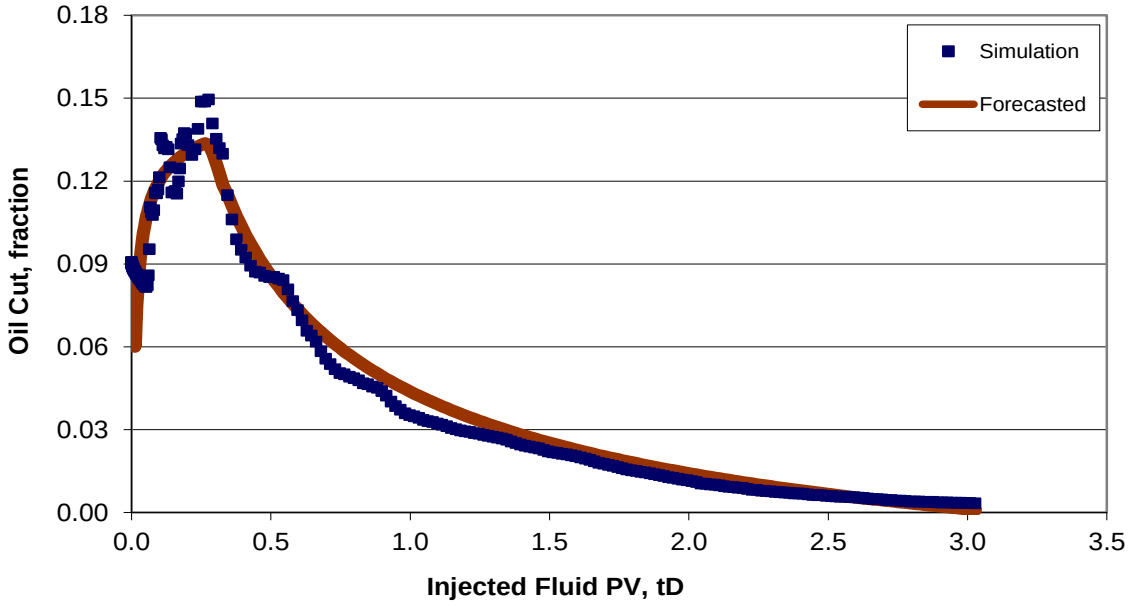

(b)

Figure 6-5: History match of WAG numerical simulation results, (a) recovery efficiency results for W_R=1.04, P=2434 psi, V_{DP}=0.9 and λ=5.34, (b) oil cut results for W_R=2.75, P=2125 psi, V_{DP}=0.8 and λ=5.25 using general isothermal EOR forecasting model (UTF).

To develop the forecasting tool for a secondary recovery processes (waterflooding), a similar procedure of Experimental Design (over an extensive range of recovery process/reservoir variable ranges shown in Table 6-1) and numerical simulations were performed. We used UTCHEM for waterflood simulations. The results of the waterflooding simulations were then history matched using the forecasting tool to correlate the variations of the forecasting model variables (water front Koval factor; K_w and final average oil saturation; S_{oF}) to process/reservoir variables (M^o, V_{DP} and λ). Waterflood simulation results were history matched as well as EOR numerical simulations. Figure 6-6 shows an example of history matching for waterflood numerical simulation results.

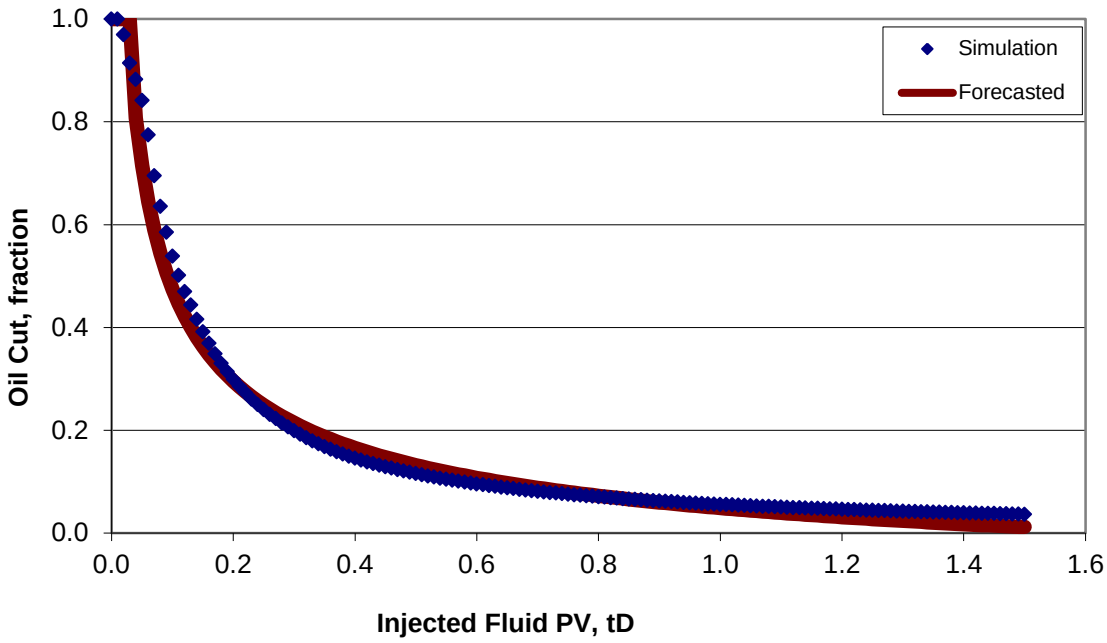

Figure 6-6: History match of Waterflooding numerical simulation results (M^o= 12, V_{DP}= 0.85, λ= 0.5) using general isothermal EOR and waterflood forecasting tool (UTF).

6.4- THE EOR/WATERFLOOD FORECASTING MODEL IN-SITU CORRELATIONS

6.4.1- Response Surface Modeling (RSM)

After history matching all of the numerical simulations for each secondary/tertiary recovery process, we used the *Response Surface Modeling (RSM) Technique* to correlate the forecasting model variables (Koval factors and final average oil saturation) to process/reservoir variables. We have the arrays of Koval factor(s) and S_{oF} related to corresponding process/reservoir variables for waterflooding and EOR processes. The procedure includes multivariate non-linear regression analysis of the data using a cubic RSM model (Mollaei et al., 2011b).

6.4.2- Mathematical Description/ Visualization of In-Situ Correlations and Response Surfaces

For polymer flooding, K_C, K_B and S_{oF} as functions of M^o, λ and V_{DP} are modeled. The strength of the correlations (as measured by R^2, the closer to 1 the stronger the correlation) will tell whether the forecasting model variables can reliably represent the process/ reservoir variables. In other words, the strength of the correlations proves the ability of the forecasting model for forecasting purposes of EOR/waterflooding results. Figure 6-7 a to c show the correlations (response surfaces) describing the chemical (polymer) front Koval factor (K_C), oil bank front Koval factor (K_B) and final average oil saturation (S_{oF}) as functions of M^o and V_{DP} at constant λ. Variations of K_B are much less than K_C. It varies between 1 and 3 and for most cases it is close to one, showing that the oil bank front is mostly more stable than displacing fluid front. Having Koval factors and S_{oF} correlated, average oil saturation ($\bar{S}_o$) is predicted (see Chapter 3) and so recovery efficiency (E_R) can be easily correlated to reservoir/recovery process variables at any time (t_D).

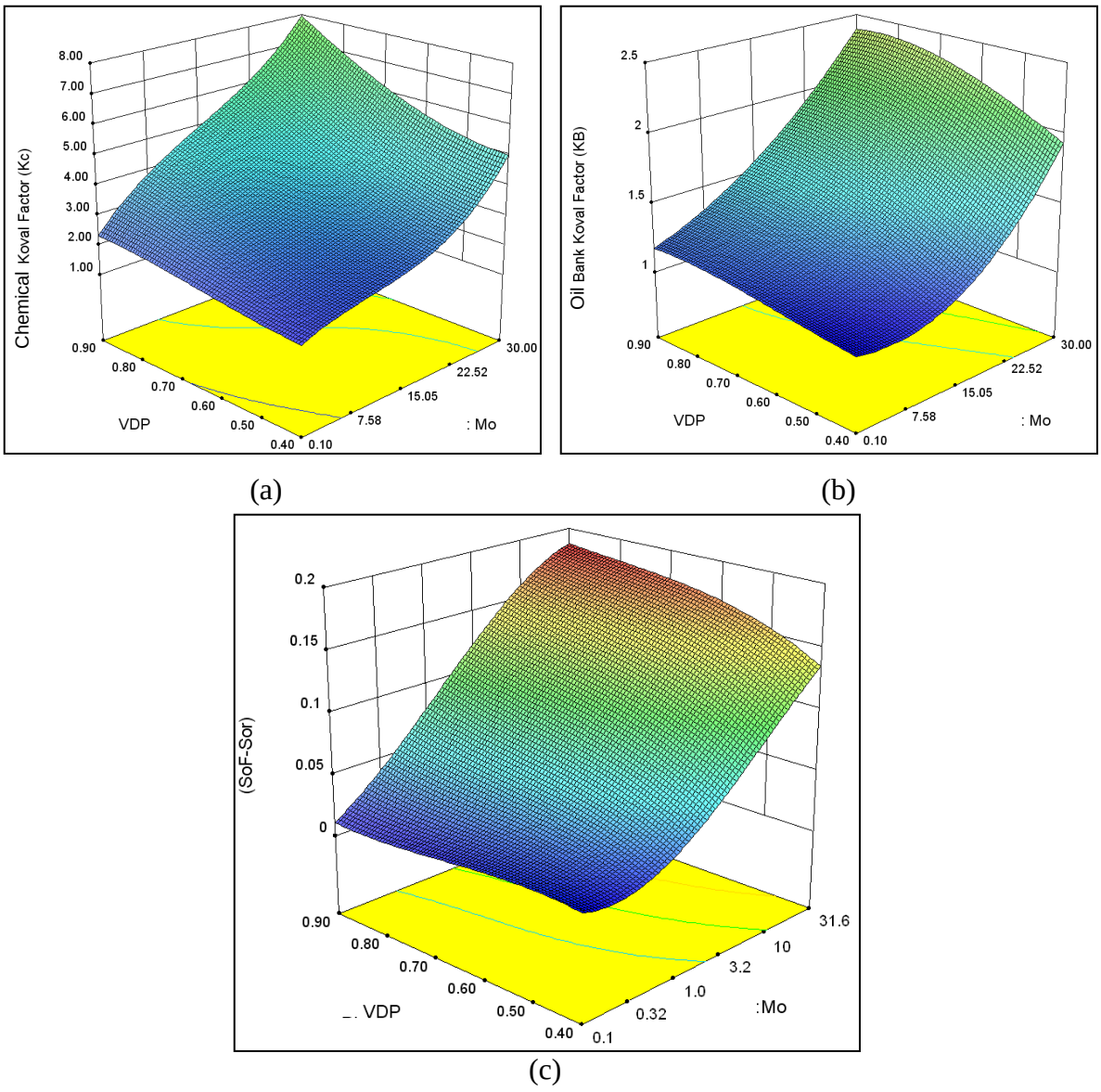

Figure 6-7: Response surfaces for (a) chemical front Koval factor (K_C) correlation, (b) oil bank front Koval factor (K_B) and (c) final average oil saturation correlation (S_{oF}) correlation at λ_x= 10 vs. M^0 and V_{DP}.

Table 6-4 summarizes the obtained correlation coefficient for each response surface. As one can see the R^2 values are very close to 1 proving the existence of strong correlations between the EOR forecasting model variables (K_C, K_B, S_{oF}) and reservoir/process variables (M^o, λ and V_{DP}). This is a major finding of this study that a

variable called *Effective Mobility Ratio* (Koval factor) can couple the effects of the reservoir heterogeneity and mobility ratio of fluids and generates a more efficient and useful dimensionless group for prediction and analysis of secondary/tertiary recovery processes than conventional mobility ratio.

Table 6-4: Correlation coefficients (R^2) for response surfaces of the general isothermal EOR forecasting model (UTF) for polymer floods.

Forecasting Model Variable	**Correlation Coefficient (R^2)**
K_C	0.9953
K_B	0.9913
S_{oF}-S_{or}	0.9981

The mathematical equations describing the K_C, K_B and S_{oF} response surfaces (shown in Figure 6-7) are expressed in Equations 6-1 to 6-3:

$$\begin{aligned} K_C = {} & 6.00761-0.036032(M^o)-21.00500(V_{DP})+0.84725(\lambda_x) \\ & -7.89447\times10^{-3}(M^o)^2+26.96217(V_{DP})^2-0.14320(\lambda_x)^2 \\ & +0.58763(M^o)(V_{DP})-7.96787\times10^{-3}(M^o)(\lambda_x)-0.22240(V_{DP})(\lambda_x) \\ & +2.21500\times10^{-4}(M^o)^3-8.39313(V_{DP})^3+2.53764\times10^{-3}(\lambda_x)^3 \\ & -7.00770\times10^{-3}(M^o)^2(V_{DP})+4.39990\times10^{-4}(M^o)^2(\lambda_x) \\ & +0.29116(M^o)(V_{DP})^2+1.88430\times10^{-3}(M^o)(\lambda_x)^2 \\ & -1.10267(V_{DP})^2(\lambda_x)+0.15292(V_{DP})(\lambda_x)^2 \\ & -0.061770(M^o)(V_{DP})(\lambda_x) \end{aligned} \qquad (6\text{-}1)$$

$$
\begin{aligned}
K_B = {} & 1.88489 - 0.040421(M^o) - 3.87979(V_{DP}) + 0.13111(\lambda_x) \\
& + 1.24441\times10^{-3}(M^o)^2 + 5.44835(V_{DP})^2 - 0.015857(\lambda_x)^2 \\
& + 0.17712(M^o)(V_{DP}) - 3.72354\times10^{-3}(M^o)(\lambda_x) - 0.076050(V_{DP})(\lambda_x) \\
& + 5.23271\times10^{-8}(M^o)^3 - 1.96527(V_{DP})^3 - 4.38018\times10^{-4}(\lambda_x)^3 \\
& - 1.48456\times10^{-3}(M^o)^2(V_{DP}) + 8.27561\times10^{-5}(M^o)^2(\lambda_x) \\
& - 0.053981(M^o)(V_{DP})^2 + 1.87122\times10^{-4}(M^o)(\lambda_x)^2 \\
& - 0.20974(V_{DP})^2(\lambda_x) + 0.032221(V_{DP})(\lambda_x)^2 \\
& - 4.29283\times10^{-3}(M^o)(V_{DP})(\lambda_x)
\end{aligned}
\tag{6-2}
$$

$$
\begin{aligned}
S_{oF} - S_{or} = {} & 0.039817 + 0.038445\,\mathrm{Log}(M^o) + 0.20441(V_{DP}) \\
& - 0.010662(\lambda_x) + 0.032582(\mathrm{Log}(M^o))^2 - 0.54928(V_{DP})^2 \\
& + 2.12965\times10^{-4}(\lambda_x)^2 + 0.10987\,\mathrm{Log}(M^o)(V_{DP}) - 5.03781\times10^{-3}\,\mathrm{Log}(M^o)(\lambda_x) \\
& + 0.042352(V_{DP})(\lambda_x) - 9.87510\times10^{-3}(\mathrm{Log}(M^o))^3 + 0.46141(V_{DP})^3 \\
& - 1.07799\times10^{-4}(\lambda_x)^3 - 0.048555(\mathrm{Log}(M^o))^2(V_{DP}) \\
& + 1.27602\times10^{-3}(\mathrm{Log}(M^o))^2(\lambda_x) - 0.071890\,\mathrm{Log}(M^o)\,(V_{DP})^2 \\
& + 7.81201\times10^{-5}\,\mathrm{Log}(M^o)(\lambda_x)^2 - 0.044982(V_{DP})^2(\lambda_x) \\
& + 1.63135\times10^{-3}(V_{DP})(\lambda_x)^2 + 5.59919\times10^{-3}\,\mathrm{Log}(M^o)(V_{DP})(\lambda_x)
\end{aligned}
\tag{6-3}
$$

where S_{or} is the residual oil saturation to waterflood, a laboratory quantity that is a simulator input.

These equations are of a form that illustrate different orders of interactions in the coefficients of different combination of variables (single terms, binary terms, etc.). For example, the sensitivity of K_C to V_{DP} is adjusted by 21.005. The equations also illustrate the so-called couplings or interactions of variables, those incidents in which the

combination of variables is important. For example the combination of mobility ratio and V_{DP} has 0.58763 as its sensitivity, which is larger than the single-variable sensitivity to mobility ratio. The Koval factor and final average oil saturation capture these intercations (couplings) that more effectively analyze the recovery results than the mobility ratio definition alone.

A similar procedure of *Response Surface Modeling* was performed for solvent (gas) flooding/WAG EOR and waterflooding after history matching of numerical simulation results. The results obtained are as good as for chemical EOR. Tables 6-5 and 6-6 show the obtained correlation coefficients for each forecasting model variable (Koval factor(s) and S_{oF}). As the tables show, the correlation coefficients are very close to 1, supporting the reliability of the general isothermal EOR and waterflood forecasting model for forecasting of EOR/waterflooding results.

Table 6-5: Correlation coefficients (R^2) for response surfaces of the general isothermal EOR forecasting model (UTF) in case solvent flooding/WAG.

Forecasting Model Variable	**Correlation Coefficient (R^2)**
K_S	0.9989
K_B	0.9977
S_{oF}	0.9986

Table 6-6: Correlation coefficients (R^2) for response surfaces of the general isothermal EOR and waterflood forecasting model (UTF) in case of waterflooding.

Forecasting Model Variable	**Correlation Coefficient (R^2)**
K_W	0.9961
S_{oF}-S_{or}	0.9925

Figures 6-8 and 9 show the correlations (response surfaces) of solvent flooding/WAG (including solvent front Koval factor (K_S), oil bank front Koval factor (K_B) and final average oil saturation (S_{oF}) as functions of W_R (WAG ratio), pressure, V_{DP} (Dykstra-Parsons coefficient) and λ (dimensionless correlation length) and waterflooding (including water front Koval factor (K_W) and final average oil saturation (S_{oF}) as functions of M^o, V_{DP} and λ (dimensionless correlation length)). The mathematical description of the response surfaces given below are presented in Equations 6-4 to 8. As one can see, the equations include individual terms (effects) and also interactions between variables through the combination terms. The coefficients are adjusted by sensitivity to the terms by means of non-linear multivariate regression analysis.

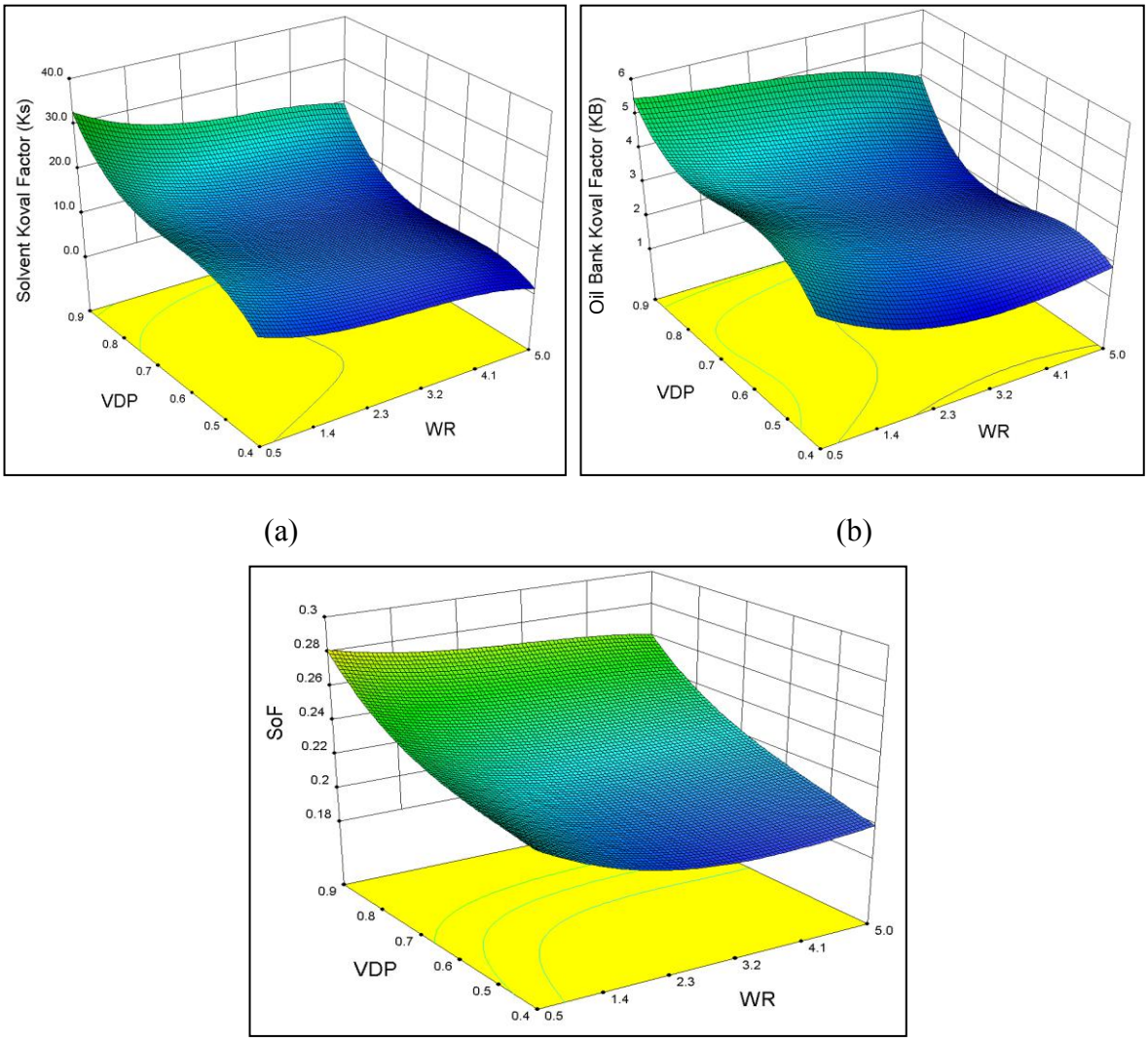

(a) (b)

(c)

Figure 6-8: Solvent front Koval factor (K_S) correlation , (b) oil bank front Koval factor (K_B) correlation and (c) final average oil saturation (S_{oF}) correlation at λ=10 and BHP=2800 psi vs. W_R and V_{DP}.

$$
\begin{aligned}
K_S = {} & -61.07430 - 48.59713(\Delta P_D) - 8.16085(W_R) + 475.83772(V_{DP}) - 3.88420(\lambda_x) \\
& + 9.37539(\Delta P_D)(W_R) + 56.03240(\Delta P_D)(V_{DP}) - 2.80602(\Delta P_D)(\lambda_x) \\
& - 17.66087(W_R)(V_{DP}) + 0.43156(W_R)(\lambda_x) + 17.94027(V_{DP})(\lambda_x) \\
& + 98.11462(\Delta P_D)^2 + 3.18925(W_R)^2 - 887.98935(V_{DP})^2 - 0.23176(\lambda_x)^2 \\
& - 0.57408(\Delta P_D)(W_R)(V_{DP}) + 0.18552(\Delta P_D)(W_R)(\lambda_x) \\
& + 2.19911(\Delta P_D)(V_{DP})(\lambda_x) - 0.078609(W_R)(V_{DP})(\lambda_x) \\
& - 0.76257(\Delta P_D)^2(W_R) - 83.59955(\Delta P_D)^2(V_{DP}) + 3.23717(\Delta P_D)^2(\lambda_x) \\
& - 1.27811(\Delta P_D)(W_R)^2 - 24.53074(\Delta P_D)(V_{DP})^2 - 0.11428(\Delta P_D)(\lambda_x)^2 \\
& + 0.74740(W_R)^2(V_{DP}) - 0.042527(W_R)^2(\lambda_x) + 10.11483(W_R)(V_{DP})^2 \\
& - 0.022650(W_R)(\lambda_x)^2 - 18.97506(V_{DP})^2(\lambda_x) + 0.11332(V_{DP})(\lambda_x)^2 \\
& - 62.71628(\Delta P_D)^3 - 0.30201(W_R)^3 + 582.25048(V_{DP})^3 + 0.018055(\lambda_x)^3
\end{aligned}
\tag{6-4}
$$

$$
\begin{aligned}
K_B = {} & -11.12464 - 7.17701(\Delta P_D) - 1.90115(W_R) + 92.10754(V_{DP}) - 0.57894(\lambda_x) \\
& + 2.10799(\Delta P_D)(W_R) + 0.010050(\Delta P_D)(V_{DP}) - 0.17195(\Delta P_D)(\lambda_x) \\
& - 1.20389(W_R)(V_{DP}) - 0.020569(W_R)(\lambda_x) + 3.20691(V_{DP})(\lambda_x) \\
& + 12.14825(\Delta P_D)^2 + 0.55807(W_R)^2 - 166.99687(V_{DP})^2 - 0.058069(\lambda_x)^2 \\
& + 0.046645(\Delta P_D)(W_R)(V_{DP}) + 0.062301(\Delta P_D)(W_R)(\lambda_x) \\
& + 0.20637(\Delta P_D)(V_{DP})(\lambda_x) - 0.041953(W_R)(V_{DP})(\lambda_x) \\
& - 1.20248(\Delta P_D)^2(W_R) - 17.78302(\Delta P_D)^2(V_{DP}) + 0.37265(\Delta P_D)^2(\lambda_x) \\
& - 0.20701(\Delta P_D)(W_R)^2 + 8.27642(\Delta P_D)(V_{DP})^2 - 0.037474(\Delta P_D)(\lambda_x)^2 \\
& - 0.47201(W_R)^2(V_{DP}) + 6.86096\times10^{-3}(W_R)^2(\lambda_x) + 3.21843(W_R)(V_{DP})^2 \\
& - 2.40465\times10^{-3}(W_R)(\lambda_x)^2 - 3.50423(V_{DP})^2(\lambda_x) + 0.032329(V_{DP})(\lambda_x)^2 \\
& - 0.92882(\Delta P_D)^3 - 0.023072(W_R)^3 + 102.31645(V_{DP})^3 + 4.14120\times10^{-3}(\lambda_x)^3
\end{aligned}
\tag{6-5}
$$

$$
\begin{aligned}
S_{oF} = {} & +0.20012-0.025570(\Delta P_D)-0.037532(W_R)+0.23188(V_{DP})+4.53543E\text{-}003(\lambda_x) \\
& +1.93914\times10^{-3}(\Delta P_D)(W_R)-0.097652(\Delta P_D)(V_{DP})+2.70964\times10^{-3}(\Delta P_D)(\lambda_x) \\
& +0.048883(W_R)(V_{DP})-1.68578\times10^{-3}(W_R)(\lambda_x)+6.42492\times10^{-3}(V_{DP})(\lambda_x) \\
& +8.98656\times10^{-4}(\Delta P_D)^2+7.24988\times10^{-3}(W_R)^2-0.48553(V_{DP})^2-1.11119\times10^{-3}(\lambda_x)^2 \\
& -3.68059\times10^{-3}(\Delta P_D)(W_R)(V_{DP})+1.69708\times10^{-4}(\Delta P_D)(W_R)(\lambda_x) \\
& -8.84339\times10^{-3}(\Delta P_D)(V_{DP})(\lambda_x)+4.79314\times10^{-4}(W_R)(V_{DP})(\lambda_x) \\
& -2.36617\times10^{-3}(\Delta P_D)^2(W_R)-0.11140(\Delta P_D)^2(V_{DP})+1.92949\times10^{-3}(\Delta P_D)^2(\lambda_x) \\
& +3.57839\times10^{-4}(\Delta P_D)(W_R)^2+0.22762(\Delta P_D)(V_{DP})^2-1.58887\times10^{-5}(\Delta P_D)(\lambda_x)^2 \\
& -5.49910\times10^{-3}(W_R)^2(V_{DP})+1.68304\times10^{-4}(W_R)^2(\lambda_x)-0.014068(W_R)(V_{DP})^2 \\
& +2.66040\times10^{-5}(W_R)(\lambda_x)^2-9.90097\times10^{-3}(V_{DP})^2(\lambda_x)+1.88536\times10^{-4}(V_{DP})(\lambda_x)^2 \\
& +0.073288(\Delta P_D)^3-4.34448\times10^{-4}(W_R)^3+0.38523(V_{DP})^3+6.34764\times10^{-5}(\lambda_x)^3
\end{aligned}
\qquad (6\text{-}6)
$$

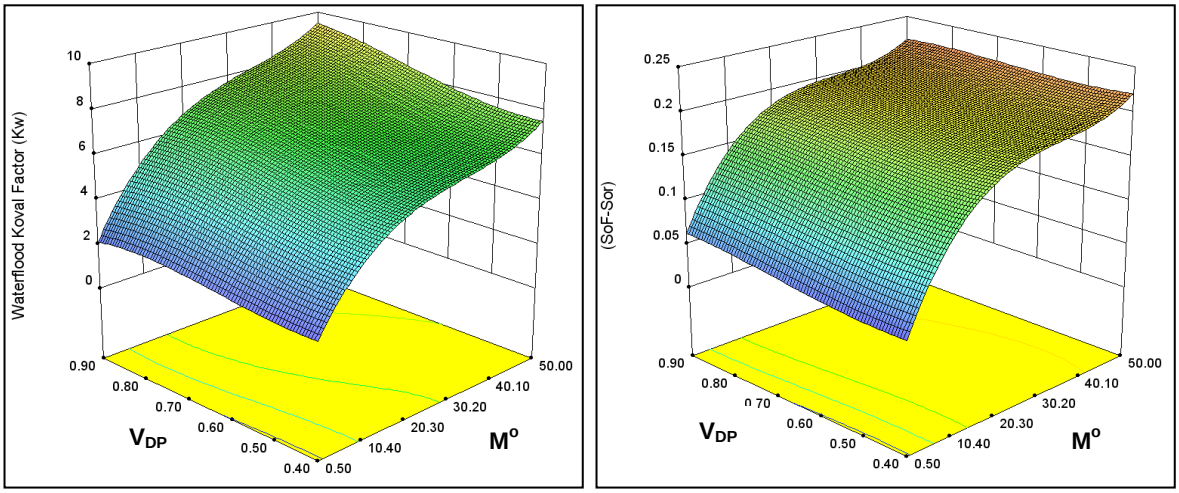

(a) (b)

Figure 6-9: Water front Koval factor (K_W) and final average oil saturation (S_{oF}) correlations at λ=10 vs. M^o and V_{DP}.

$$K_W = 8.52049+0.36214(M^o)-35.73891(V_{DP})-0.24703(\lambda_x)$$
$$-0.010454(M^o)^2+56.16179(V_{DP})^2-4.03542\times10^{-3}(\lambda_x)^2$$
$$+0.058956(M^o)(V_{DP})-2.81600\times10^{-3}(M^o)(\lambda_x)+1.04064(V_{DP})(\lambda_x)$$
$$+1.02571\times10^{-4}(M^o)^3-25.81984(V_{DP})^3+5.38014\times10^{-4}(\lambda_x)^3$$
$$-1.26106\times10^{-3}(M^o)^2(V_{DP})+1.10920\times10^{-4}(M^o)^2(\lambda_x)$$
$$+0.12849(M^o)(V_{DP})^2+1.84360\times10^{-4}(M^o)(\lambda_x)^2$$
$$-0.89478(V_{DP})^2(\lambda_x)-0.010023(V_{DP})(\lambda_x)^2$$
$$-0.010158(M^o)(V_{DP})(\lambda_x) \quad (6\text{-}7)$$

$$S_{oF} - S_{or} = +0.20163+0.012740M^o-0.71847(V_{DP})-0.012360(\lambda_x)$$
$$-3.75107\times10^{-4}(M^o)^2+1.00174(V_{DP})^2+9.58193\times10^{-4}(\lambda_x)^2$$
$$+6.52122\times10^{-4}(M^o)(V_{DP})+4.75905\times10^{-6}(M^o)(\lambda_x)$$
$$+0.026578(V_{DP})(\lambda_x)+3.54335\times10^{-6}(M^o)^3-0.38533(V_{DP})^3$$
$$-5.18925\times10^{-5}(\lambda_x)^3+1.04198\times10^{-5}(M^o)^2(V_{DP})$$
$$+1.36382\times10^{-6}(M^o)^2(\lambda_x)-4.04826\times10^{-4}(M^o)\,(V_{DP})^2$$
$$+3.29316\times10^{-6}(M^o)(\lambda_x)^2-0.021245(V_{DP})^2(\lambda_x)$$
$$-1.81146\times10^{-4}(V_{DP})(\lambda_x)^2-1.47984\times10^{-4}(M^o)(V_{DP})(\lambda_x) \quad (6\text{-}8)$$

6.5- VOLUMETRIC SWEEP EFFICIENCY AND MISSING PORE VOLUME

6.5.1- Definition of Missing and Dynamic Pore Volumes Concepts

The fraction of the reservoir/ pilot that is accessible (sweepable) by the displacing fluid in a secondary or tertiary recovery process has a great impact on recovery efficiency of the process. This fraction is called the volumetric sweep efficiency (E_V, introduced in Chapter 2), which is a function of reservoir heterogeneity and mobility ratio of the fluids (displacing and displaced). E_V measures the ability of the EOR process to contact the

reservoir. In any secondary or tertiary recovery processes there will be unswept regions because of the adverse effects of reservoir heterogeneity and/or unfavorable mobility ratio. Figure 6-10 schematically shows swept and unswept regions of the reservoir during displacement process.

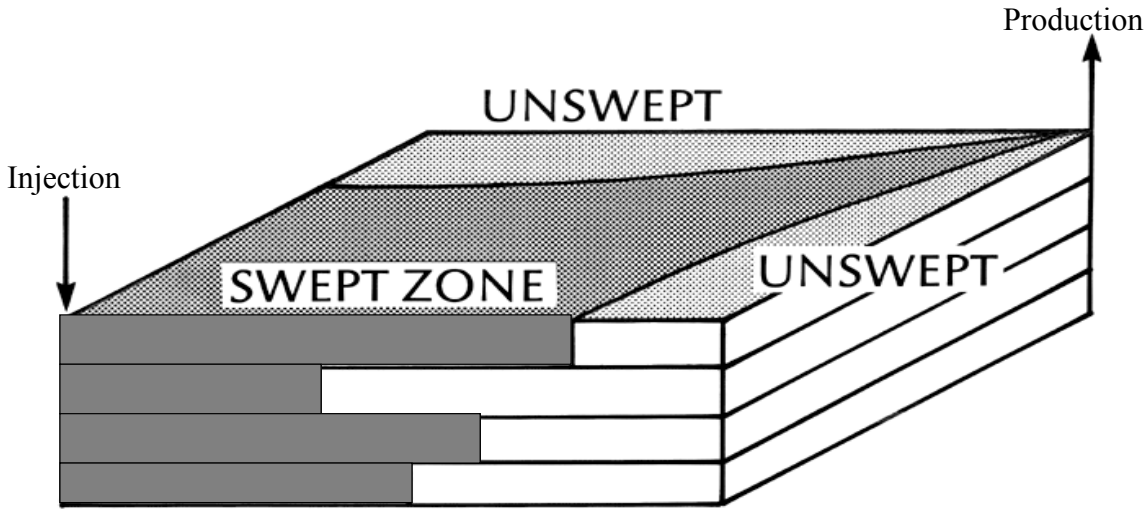

Figure 6-10: 3D schematic of displacement process with swept and unswept regions (Lake, 1989).

Chapter 5 discussed that the final average oil saturation (S_{oF}) is larger, sometimes much larger, than what is observed in laboratory experiments. This observation suggests that an important feature of all field displacements is the existence of a missing or lost pore volume, a volume that will never be accessed by displacing fluids. We name this fraction of the reservoir/pilot static (total) pore volume that remains unswept after injecting many pore volumes of displacing fluid as *missing pore volume*. In the same way, we name the complementary fraction (static PV - missing PV) as *dynamic pore volume (DPV)* which represents the final sweepable fraction of static pore volume after injecting many pore volumes of displacing fluid. It is *dynamic* since it is the pore volume

associated with the recovery process and contributing to the recovery. DPV is a measure of finally achievable volumetric sweep efficiency.

Equations 6-9 and 10 define the static, dynamic and missing pore volumes.

$$Static\,PV = AH_t\phi \tag{6-9}$$

where A is the reservoir/pilot area, H_t is total thickness and ϕ is porosity.

$$Missing\,PV = (Static\,PV) - (Dynamic\,PV) \tag{6-10}$$

The next section explains how we use the EOR and waterflood forecasting model to correlate missing pore volume to reservoir/recovery process variables.

6.5.2- Prediction of Dynamic Pore Volume and Final Volumetric Sweep Efficiency

Equation 6-11 expands the definition of recovery efficiency (E_R) as a function of volumetric sweep (E_V) and displacement efficiencies (E_D):

$$\frac{N_p}{V_p S_{oi}} = E_V \frac{S_{oR} - S_{or}}{S_{oi}} = E_V E_D = E_R \tag{6-11}$$

where S_{oi} is the original oil saturation, S_{oR} is remaining oil saturation at start of secondary/tertiary recovery process, S_{or} is laboratory residual oil saturation, V_P is the static pore volume (PV) and N_p is cumulative oil recovery. By the definition of the dynamic pore volume (DPV), the oil saturation in the swept zone drops to S_{or}, therefore:

$$N_p = PV(S_{oR} - S_{oF}) = DPV(S_{oR} - S_{or})$$

$$\Rightarrow DPV = \frac{PV(S_{oR} - S_{oF})}{S_{oR} - S_{or}} \tag{6-12}$$

This is the key equation to predict the dynamic and missing pore volumes. The only unknown in Equation 6-12 is final average oil saturation (S_{oF}). In section 6.4, it was

discussed how S_{oF} is correlated and described as function of reservoir/recovery process variables for waterflooding and EOR processes. Having S_{oF} identified, we are able to evaluate the dynamic and missing pore volumes.

Figure 6-11 shows correlation (response surface) of dynamic pore volume fraction (fraction of static pore volume, DPV/PV) for waterflooding as function of reservoir heterogeneity and endpoint mobility ratio. The obtained correlation coefficient (R^2) is 0.9925 proving strong correlation between the DPV and reservoir/recovery process variables. As the figure shows there is an inflection point in the increase and drop of sweepable fraction of PV in $M^o \approx 10$. Equation 6-13 represents the mathematical description of the waterflood DPV response surface.

$$\begin{aligned}\frac{DPV}{PV} = {} & +0.51992-0.030333M^o+1.71065(V_{DP})+0.029428(\lambda_x) \\ & +8.93111\times10^{-4}(M^o)^2-2.38508(V_{DP})^2-2.28141\times10^{-3}(\lambda_x)^2 \\ & -1.55267\times10^{-3}(M^o)(V_{DP})-1.13311\times10^{-5}(M^o)(\lambda_x) \\ & -0.063280(V_{DP})(\lambda_x)-8.43655\times10^{-6}(M^o)^3+0.91745(V_{DP})^3 \\ & +1.23554\times10^{-4}(\lambda_x)^3-2.48091\times10^{-5}(M^o)^2(V_{DP}) \\ & -3.24719\times10^{-6}(M^o)^2(\lambda_x)+9.63871\times10^{-4}(M^o)\,(V_{DP})^2 \\ & -7.84086\times10^{-6}(M^o)(\lambda_x)^2+0.050584(V_{DP})^2(\lambda_x) \\ & +4.31301\times10^{-4}(V_{DP})(\lambda_x)^2+3.52342\times10^{-4}(M^o)(V_{DP})(\lambda_x)\end{aligned} \tag{6-13}$$

Correlation (response surface) of dynamic pore volume fraction (DPV/PV) for polymer flooding is depicted in Figure 6-12. Similar to the waterflood, DPV/PV is described as function of reservoir heterogeneity and endpoint mobility ratio. The correlation is strong with correlation coefficient (R^2) of 0.9993. The significantly larger

DPV fraction of polymer flood in comparison with waterflood is obvious, proving the success of application of polymer to control the mobility of the flood and increasing the volumetric sweep efficiency. Equation 6-14 represents the mathematical description of DPV/PV response surface for polymer flood.

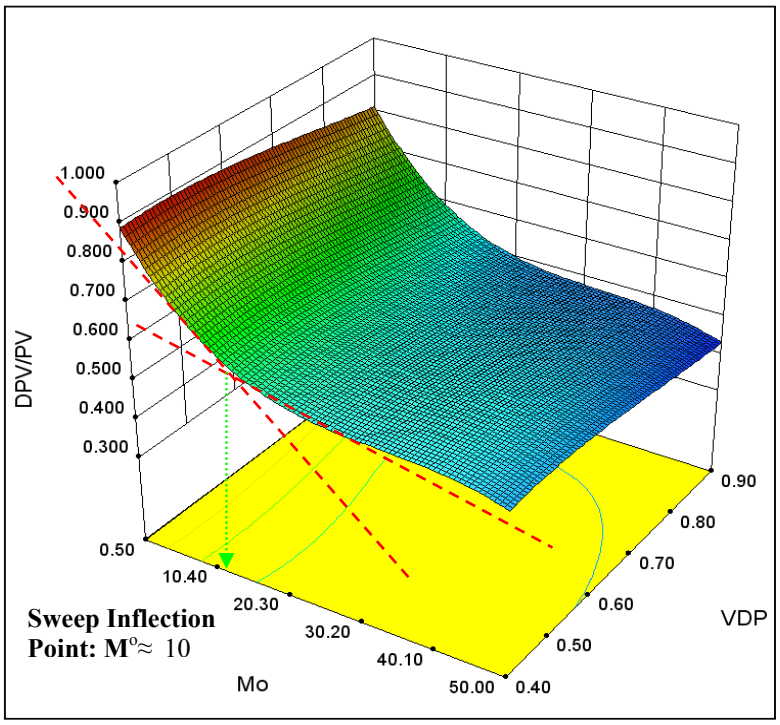

Figure 6-11: Correlation of dynamic pore volume fraction for waterflood at λ=5.

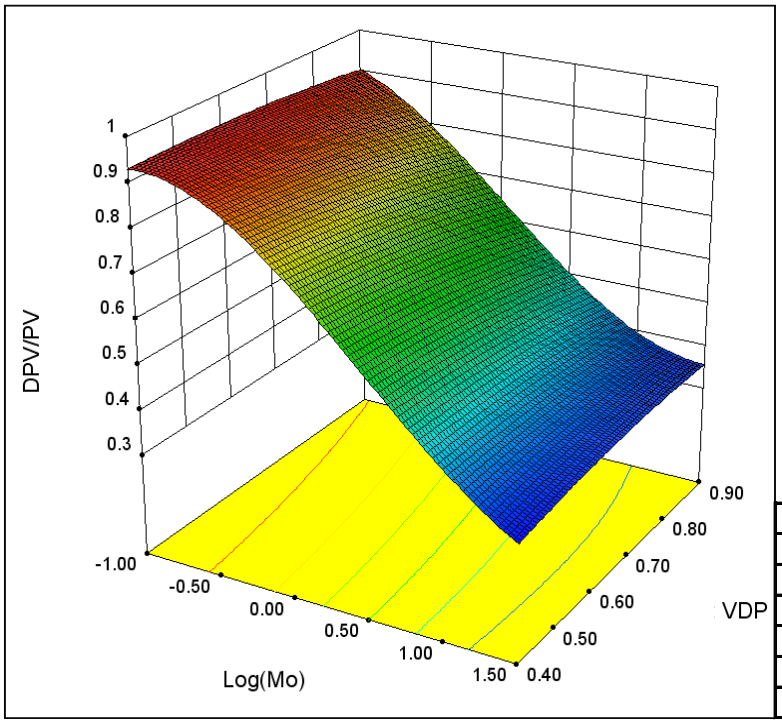

Log(M^o)	M^o
-1.0	0.1
-0.5	0.3
0.0	1.0
0.5	3.2
1.0	10.0
1.5	31.6

Figure 6-12: Correlation of dynamic pore volume fraction for polymer flood at λ=5.

$$\frac{DPV}{PV} = +0.71840-0.31188\text{Log}(M^o)+0.20361(V_{DP})$$
$$+0.020942(\lambda_x)-0.12406(\text{Log}(M^o))^2-0.22065(V_{DP})^2$$
$$-1.18228\times10^{-3}(\lambda_x)^2+0.066256\text{Log}(M^o)(V_{DP})+4.43945\times10^{-3}\text{Log}(M^o)(\lambda_x)$$
$$-0.050454(V_{DP})(\lambda_x)+0.050950(\text{Log}(M^o))^3-0.066546(V_{DP})^3$$
$$+4.32213\times10^{-5}(\lambda_x)^3+0.13503(\text{Log}(M^o))^2(V_{DP})$$
$$-2.31326\times10^{-3}(\text{Log}(M^o))^2(\lambda_x)-0.025708\text{Log}(M^o)(V_{DP})^2$$
$$+1.07231\times10^{-4}\text{Log}(M^o)(\lambda_x)^2+0.027495(V_{DP})^2(\lambda_x)$$
$$+1.32621\times10^{-3}(V_{DP})(\lambda_x)^2-0.011811\text{Log}(M^o)(V_{DP})(\lambda_x)$$

(6-14)

Similar to water and chemical flooding, the dynamic pore volume of the solvent flooding/WAG was successfully correlated to reservoir/recovery process variables with correlation coefficient (R^2) of 0.9971. Figure 6-13 illustrates the response surface (correlation) of DPV/PV fraction as function of reservoir heterogeneity (V_{DP}) and WAG ratio at constant pressure and λ. As figure shows, the values of DPV/PV are substantially smaller for solvent flooding than for water and chemical flooding. It is mainly related to higher (more unfavorable) mobility ratio of solvent flooding processes because of the small gas viscosity. Increasing the WAG ratio can considerably improve the volumetric sweep of solvent flooding processes.

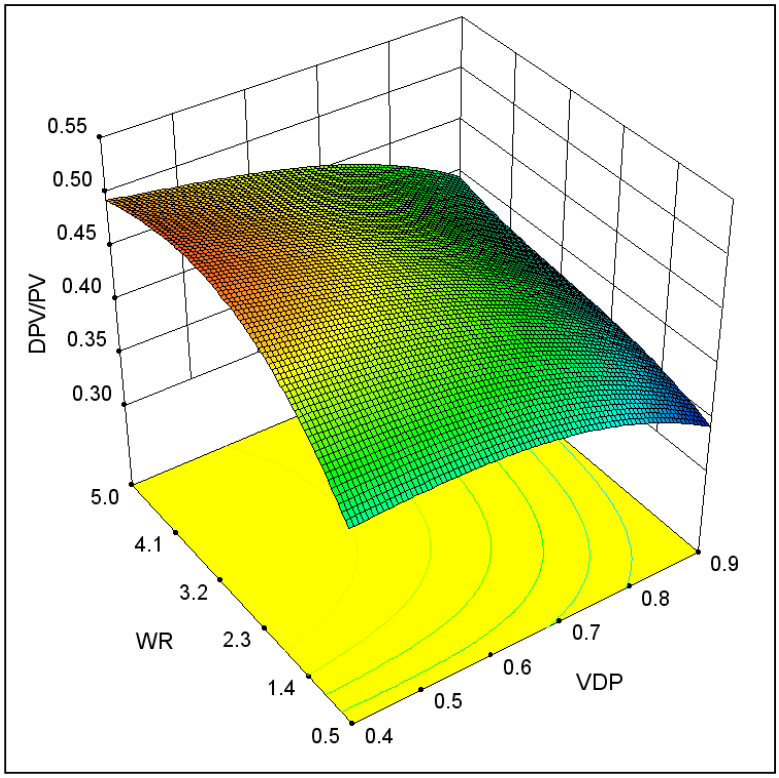

Figure 6-13: Correlation of dynamic pore volume fraction for solvent flooding/WAG at P=2800 psi and λ=10.

The mathematical description of DPV/PV response surface for solvent flooding/WAG is given in Equation 6-15.

$$\frac{DPV}{PV} = +0.40154+0.13613(\Delta P_D)+0.12225(W_R)-0.31086(V_{DP})-0.014193(\lambda_x)$$
$$-0.011033(\Delta P_D)(W_R)+0.24604(\Delta P_D)(V_{DP})-0.012897(\Delta P_D)(\lambda_x)$$
$$-0.16410(W_R)(V_{DP})+6.03951\times10^{-3}(W_R)(\lambda_x)-8.66844\times10^{-3}(V_{DP})(\lambda_x)$$
$$+4.34332\times10^{-4}(\Delta P_D)^2-0.022921(W_R)^2+0.78458(V_{DP})^2+2.84070\times10^{-3}(\lambda_x)^2$$
$$+4.56107\times10^{-3}(\Delta P_D)(W_R)(V_{DP})-5.60777\times10^{-4}(\Delta P_D)(W_R)(\lambda_x)$$
$$+0.028327(\Delta P_D)(V_{DP})(\lambda_x)-1.26702\times10^{-3}(W_R)(V_{DP})(\lambda_x)$$
$$+0.017742(\Delta P_D)^2(W_R)+0.31628(\Delta P_D)^2(V_{DP})+5.53688\times10^{-4}(\Delta P_D)^2(\lambda_x)$$
$$-6.99264\times10^{-4}(\Delta P_D)(W_R)^2-0.64172(\Delta P_D)(V_{DP})^2-1.51674\times10^{-5}(\Delta P_D)(\lambda_x)^2$$
$$+0.020444(W_R)^2(V_{DP})-5.86608\times10^{-4}(W_R)^2(\lambda_x)+0.035813(W_R)(V_{DP})^2$$
$$-1.23746\times10^{-4}(W_R)(\lambda_x)^2-3.75279\times10^{-3}(V_{DP})^2(\lambda_x)+1.15114\times10^{-3}(V_{DP})(\lambda_x)^2$$
$$-0.28107(\Delta P_D)^3+1.17007\times10^{-3}(W_R)^3-0.51429(V_{DP})^3-2.01223\times10^{-4}(\lambda_x)^3$$

(6-15)

6.6- SUMMARY AND DISCUSSIONS

Using Experimental Design and numerical simulation we could successfully generate the in-situ correlations (response surfaces) of the forecasting model. The forecasting model variables are now well correlated to reservoir/recovery process variables and can be reliably used for forecasting when there is no injection/production history. As an extension to the abilities of the forecasting model, these correlations were used for prediction of volumetric sweep efficiency and missing pore volume of EOR and waterflooding processes. Some important insights obtained from this chapter are:

- Generally, the Koval factor (K) and the final average oil saturation (S_{oF}) increase with increasing mobility ratio and reservoir heterogeneity (characterized by the Dykstra-Parsons coefficient, V_{DP}, and dimensionless geostatistical correlation length, λ) causing less oil recovery. Therefore the smaller the Koval factor the more stable the flood (less fingering) and the higher the recovery.

- The Koval factor, the effective mobility ratio, can effectively couple the effects of reservoir heterogeneity and mobility ratio of a flood and create a more efficient and useful dimensionless group for prediction and analysis of secondary/tertiary recovery processes than the conventional mobility ratio.
- In waterflooding and chemical EOR, the mobility ratio is the most influential variable governing the recovery of the flood while solvent/WAG flooding is more affected by reservoir heterogeneity.
- The volumetric sweep and dynamic pore volume of chemical EOR processes are substantially larger than for waterflooding because of mobility control using a polymer solution. Solvent/WAG flooding has the smallest volumetric sweep, which deteriorates in more heterogeneous permeable media.

Chapter 7: SUMMARY, CONCLUSIONS AND RECOMMENDATIONS FOR FUTURE RESEARCH

7.1- SUMMARY OF THE RESEARCH

The main objective of this study was to develop a novel and robust general isothermal EOR and waterflood forecasting model/tool (UTF) for both history matching and forecasting. The UTF conceptual model is based on the fundamental law of material balance, segregated flow and fractional flux theories. Sensitivity analysis study helped to identify the most influential reservoir/process variables for better designing of the forecasting model. The forecasting model generates the key results of isothermal EOR and waterflooding processes including variations of average oil saturation, recovery efficiency, volumetric sweep efficiency, oil cut and oil rate with real or dimensionless time.

The forecasting model was validated against field data and numerical simulation results for isothermal EOR and waterflooding processes. The forecasting model reproduced well (R^2> 0.8) all of the field data and reproduced the simulated data even better.

To develop the UTF for forecasting when there is no injection/production history data, we used experimental design and numerical simulation and successfully generated the in-situ correlations (response surfaces) of the forecasting model variables. The forecasting model variables were proven to be well correlated to reservoir/recovery process variables and can be reliably used for forecasting. As an extension to the abilities of the forecasting model, these correlations were used for prediction of volumetric sweep efficiency and missing/dynamic pore volume of EOR and waterflooding processes.

7.2- CONCLUDING REMARKS

- We successfully developed the general isothermal EOR and waterflood forecasting model. The model is able to match both field and simulation results of EOR processes and waterflooding.
- Sensitivity analysis (SA) helped to calculate the sensitivity of output results to individual variables and also to attribute how much of the sensitivity is caused by interaction of variables. This is useful in identifying the main sources of output uncertainty and also gives insights to reduce the uncertainty in a more systematic and efficient way. Based on this analysis, reservoir permeability, porosity, heterogeneity and oil viscosity are the most important sources of output uncertainty either directly or through interactions with other parameters.
- The Koval-based approach described in this work combines vertical and areal sweep into a single factor, the Koval factor. It is therefore no longer necessary to estimate these effects separately and combine them. The key upgrade from the Koval-based approach is the replacement of a physical dimension, thickness, with storage capacity.
- The Koval factor, the effective mobility ratio, can effectively couple the effects of reservoir heterogeneity and mobility ratio of a flood and create efficient and useful dimensionless variable for prediction and analysis of secondary/tertiary recovery processes than the conventional mobility ratio.
- Koval factors (displacing and oil bank fronts; K_1 and K_2) are arranged in order of increasing mobility ratio. Usually, the Koval factor for the oil banks is the smallest of all indicating that the oil banks are usually more stable (less fingering) than that of the displacing fluids.

- Generally, the Koval factor (K) and the final average oil saturation (S_{oF}) increase with increasing mobility ratio and reservoir heterogeneity (characterized by Dykstra-Parsons coefficient, V_{DP}, and the dimensionless geostatistical correlation length, λ) reducing oil recovery. Therefore the smaller the Koval factor the more stable the flood and the higher the recovery.
- The field/pilot Koval factors are usually larger than those inferred from the coreflooding laboratory experiments. This observation is consistent with the following.
- The final average oil saturation in field/pilot projects is larger, sometimes much larger, than what is observed in laboratory experiments. This observation suggests that an important feature of all field displacements is the existence of a missing or lost pore volume, a volume that will never be accessed by displacing fluids.
- In waterflooding and chemical EOR, the mobility ratio is the most influential variable governing the recovery of the flood while solvent/WAG flooding is more affected by reservoir heterogeneity.
- Generally M^o about 10 is the inflection point of water/polymer flooding sweep efficiency such that above or below that we see tremendous changes in recovery efficiency. An endpoint mobility ratio of equal or less than 3 show good volumetric sweep such that it can compensate the adverse effects of the reservoir heterogeneity.
- The major problem of solvent/WAG flooding is the lack of sweep. Reservoir heterogeneity governs volumetric sweep efficiency and the unfavorable effects of reservoir heterogeneity worsen substantially for V_{DP} values about or greater than 0.8. Alternating with water helps but still needs more (stronger) mobility control such as foam.

- The volumetric sweep and dynamic pore volume of chemical EOR processes are substantially larger than for Solvent/WAG and waterflooding because of mobility control using a polymer solution. Solvent/WAG flooding has the smallest volumetric sweep, which deteriorates in more heterogeneous permeable media.

7.3- RECOMMENDATIONS FOR FUTURE RESEARCH

- The forecasting model was developed for isothermal EOR and waterflooding. A major extension would be developing the model for thermal EOR processes such as steam flooding or in-situ combustion. This will require the application of the energy balance in addition to the mass balances.
- The major problem of solvent/WAG flooding EOR process is the lack of sweep because of adverse mobility ratio (large Koval factors). It is recommended to study and research the application of foam with solvent (gas) flooding in the form of FWAG (foam assisted WAG) and its effects on Koval factors through improvement of mobility ratio and volumetric sweep.
- Capacitance Resistive Model (CRM) is a fast predictive tool for predicting the waterflood production rate and well-to-well connectivities (Sayarpour, 2008). Developing the CRM for EOR processes using UTF would be a great idea to extend the application of CRM to EOR processes.
- Predicting the dynamic pore volume and final volumetric sweep efficiency of EOR and waterflood processes is a major application of the forecasting tool. It is recommended to extend the correlations to estimate sweep efficiency at any time during the flood.

- Prediction of missing/dynamic pore volume for an EOR or waterflood process can be the first ringlet in a chain of efforts to locate the unswept oil. .
- Sensitivity analysis (SA) of the forecasting model (UTF) using the Winding Stairs method is recommended to identify the most influential variables and also the interactions between the variables.
- The two novel concepts introduced and applied in this research are Koval factor (K; the effective mobility ratio) and final average oil saturation (S_{oF}) for more effective analysis of the flood recovery in practical 3D heterogeneous cases. It is strongly recommended to develop and apply these concepts to other areas of reservoir engineering such as water/gas coning and aquifer encroachment.

Appendices

APPENDIX-A: DERIVATION OF INJECTED PORE VOLUME AT A GIVEN STORAGE CAPACITY

The fraction of total pore volume flowing into a given storage capacity (given layer in case of layered reservoirs) is derived by dynamic scaling (or Stiles model; Stiles, 1949) as follow. For discrete layering, strictly KH flow, no mobility contrast and no crossflow:

$$t_{Di} = \frac{\text{cumulative fluid into layer i}}{\text{pore volume of layer i}}$$
$$= \frac{\text{cumulative fluid into reservoir}}{\text{PV of layer i}} \frac{\text{cumulative fluid into layer i}}{\text{cumulative fluid into reservoir}}$$
$$= \frac{\text{cumulative fluid into reservoir}}{\text{PV of layer i}} \frac{\text{kh}_{\text{i}}}{\overline{\text{kH}}}$$

$$\Rightarrow t_{Di} = \frac{\text{cumulative fluid into reservoir}}{\text{PV of reservoir}} \frac{\text{PV of reservoir}}{\text{PV of layer i}} \frac{\text{kh}_{\text{i}}}{\overline{\text{kH}}}$$
$$= \frac{\text{cumulative fluid into reservoir}}{\text{PV of reservoir}} \frac{\text{H}\bar{\phi}}{(\text{h}\phi)_{\text{i}}} \frac{\text{kh}_{\text{i}}}{\overline{\text{kH}}}$$

(A-1)

$$\Rightarrow t_{Di} = t_D \left(\frac{\bar{\phi}}{\bar{\text{k}}} \frac{k_{\text{i}}}{\phi_i} \right) \tag{A-2}$$

As number of layers (N_L) increases, the right side of equation A-1 tends to the derivative of F (flow capacity) with respect to C (storage capacity) for continuous case at the storage capacity.

$$t_D \big|_C = t_D \left(\frac{dF}{dC} \right) \tag{A-3}$$

APPENDIX-B: EOR AND WATERFLOOD HISTORY MATCHING RESULTS

Some examples of EOR and waterflood history matching results were presented in Chapter 5. More examples of history matching results are shown in the following sections.

B.1- Waterflood History Matching

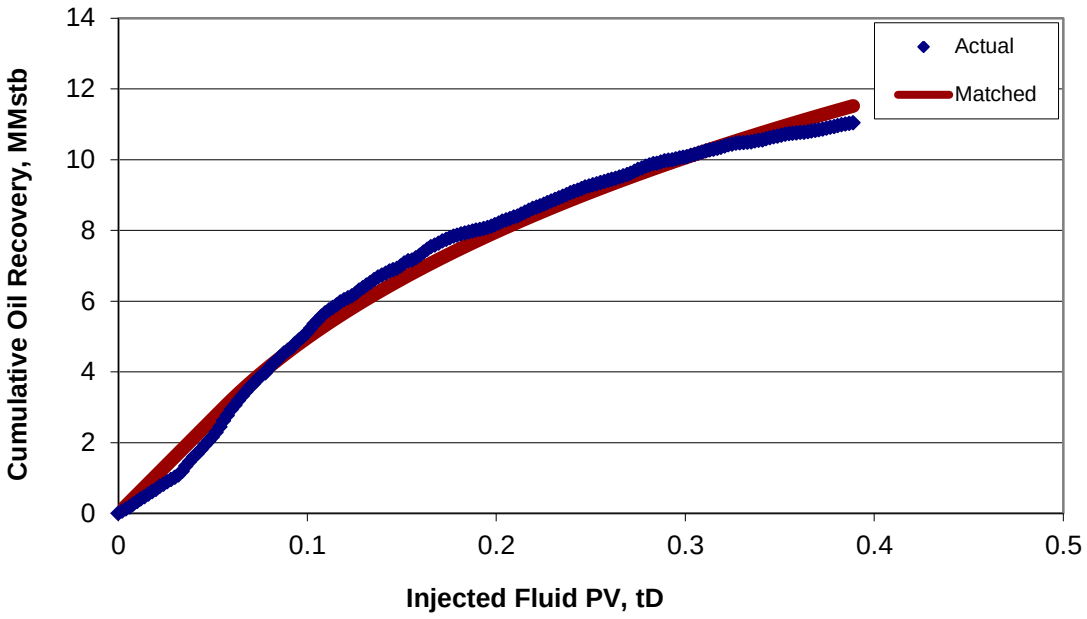

Figure B-1: Waterflooding history match for entire reservoir (Sand-A) using general isothermal EOR and waterflood forecasting tool (UTF).

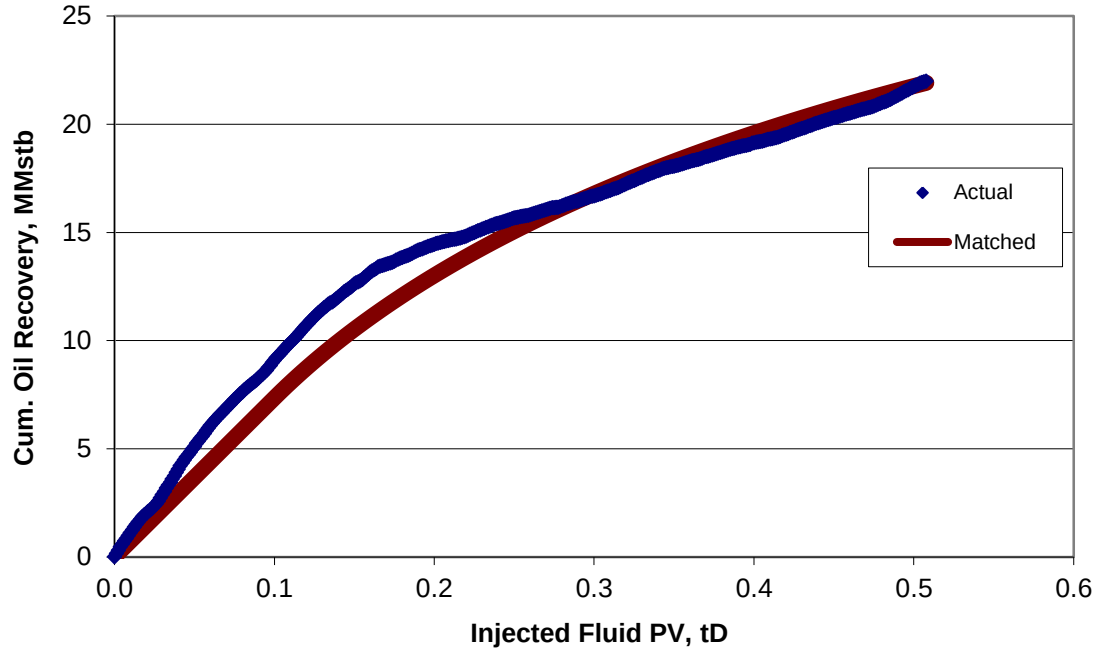

Figure B-2: Waterflooding history match for whole reservoir (Sand-C) using UTF.

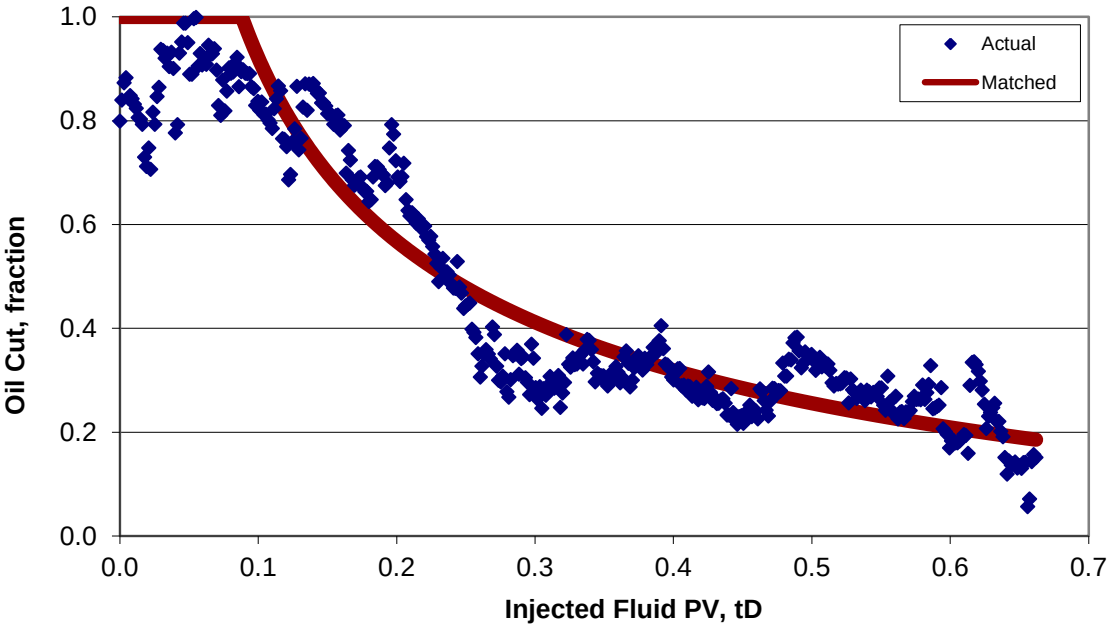

Figure B-3: Waterflooding history match for whole reservoir (Sand-D) using UTF.

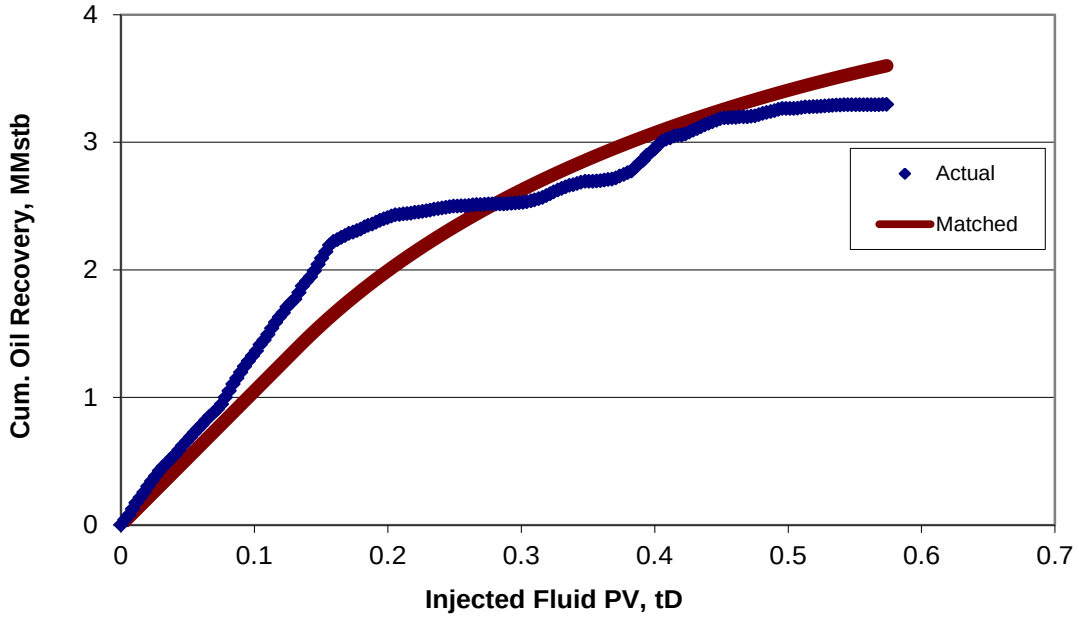

Figure B-4: Waterflooding history match for single well A-1 in the reservoir (Sand-A) using UTF.

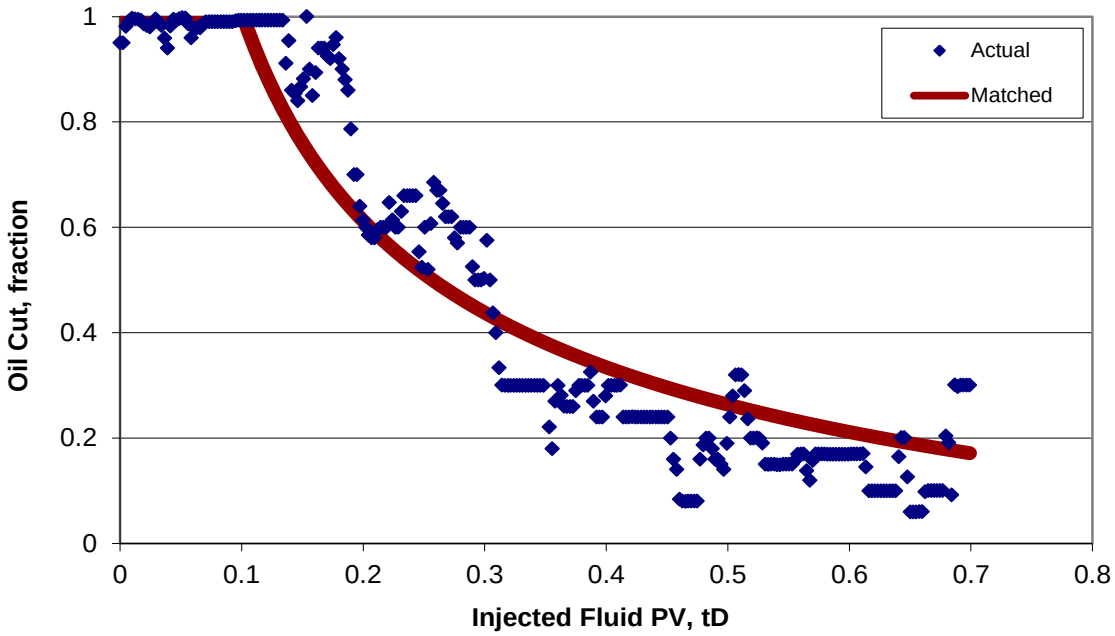

Figure B-5: Waterflooding history match for single well A-3 in the reservoir (Sand-A) using UTF.

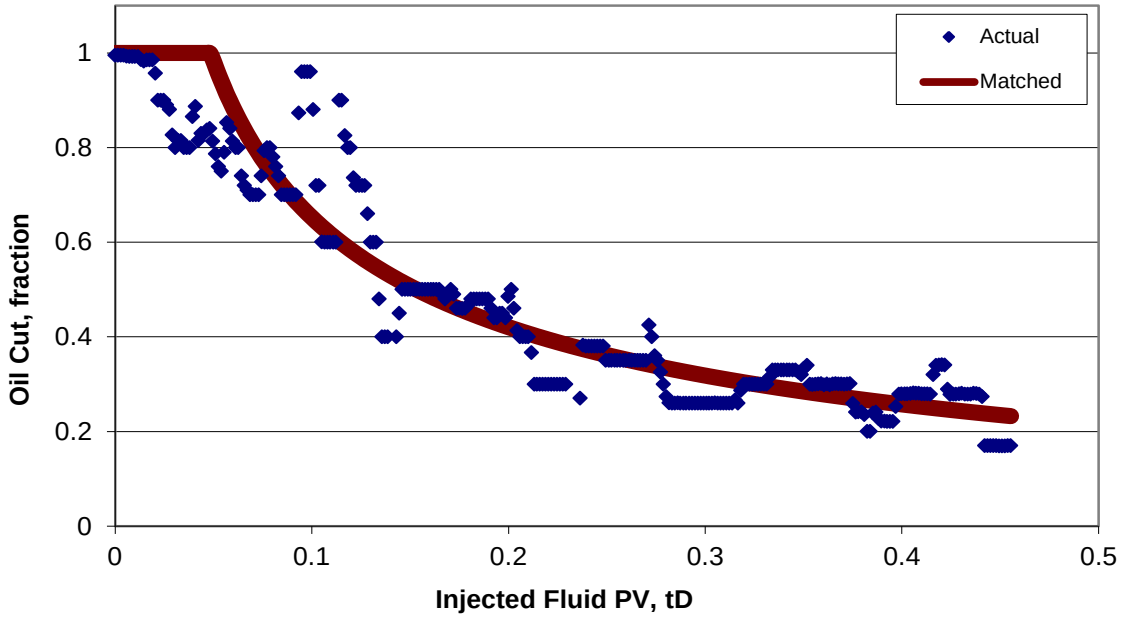

Figure B-6: Waterflooding history match for single well A-4 in the reservoir (Sand-A) using UTF.

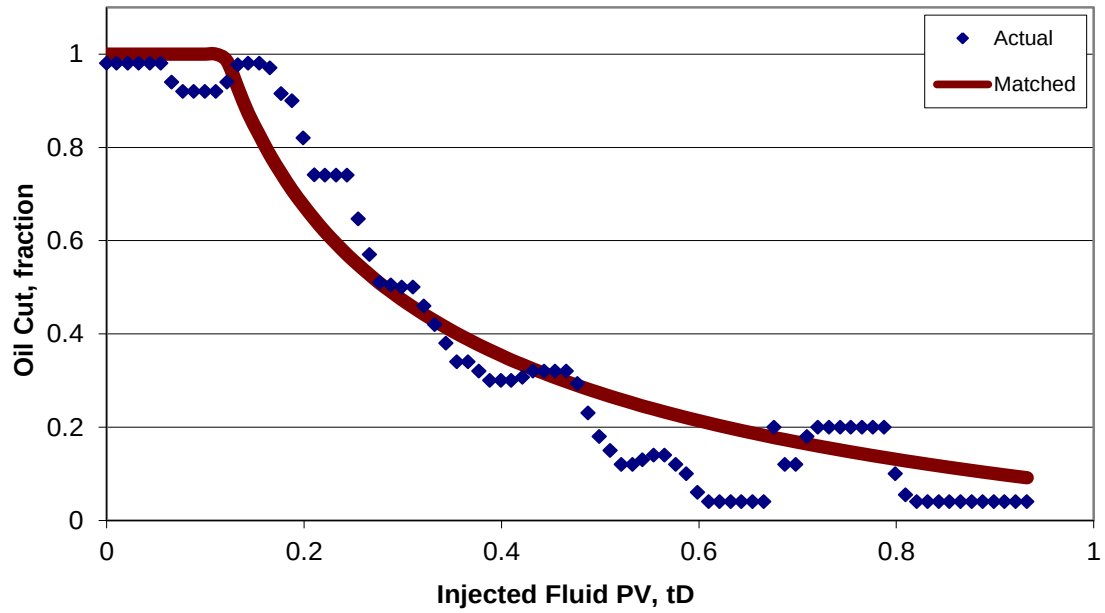

Figure B-7: Waterflooding history match for single well A-5 in the reservoir (Sand-A) using UTF.

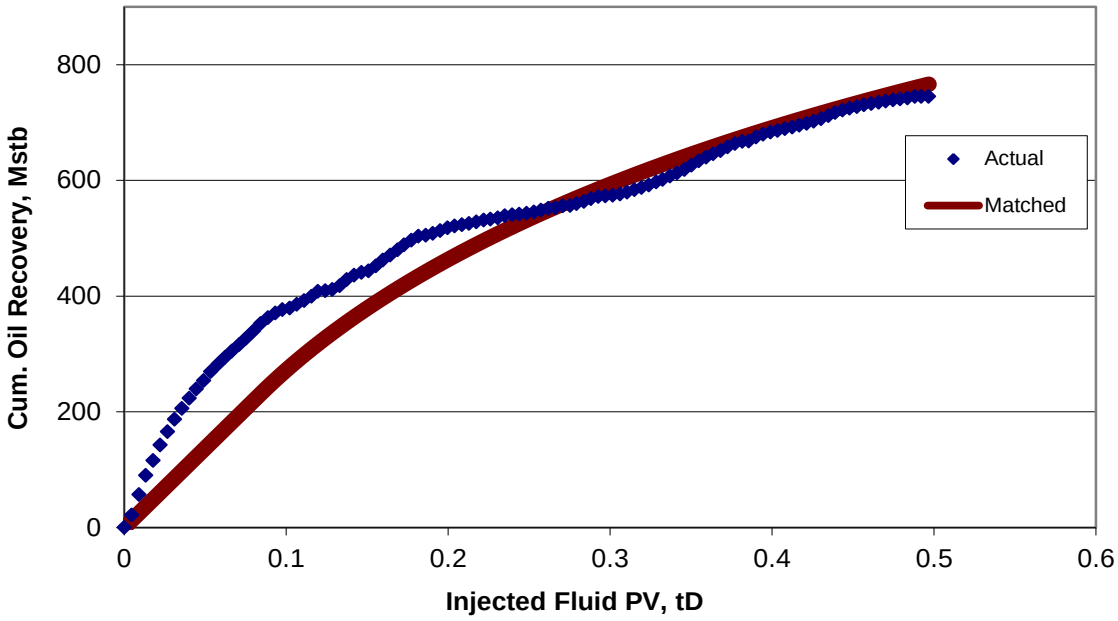

Figure B-8: Waterflooding history match for single well A-6 in the reservoir (Sand-A) using UTF.

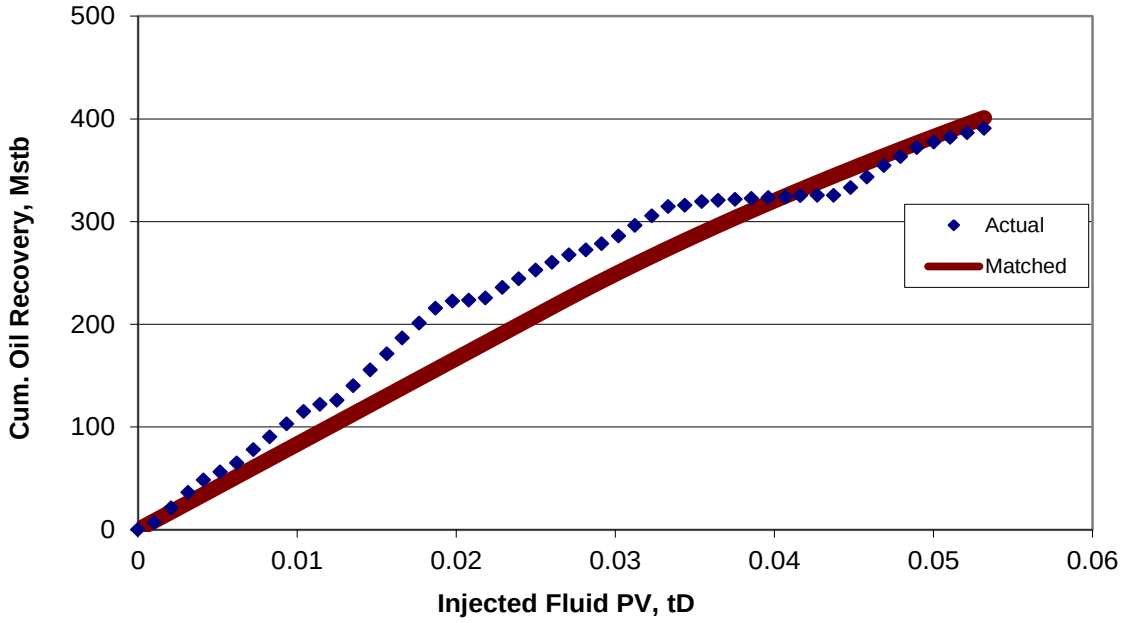

Figure B-9: Waterflooding history match for single well A-7 in the reservoir (Sand-A) using UTF.

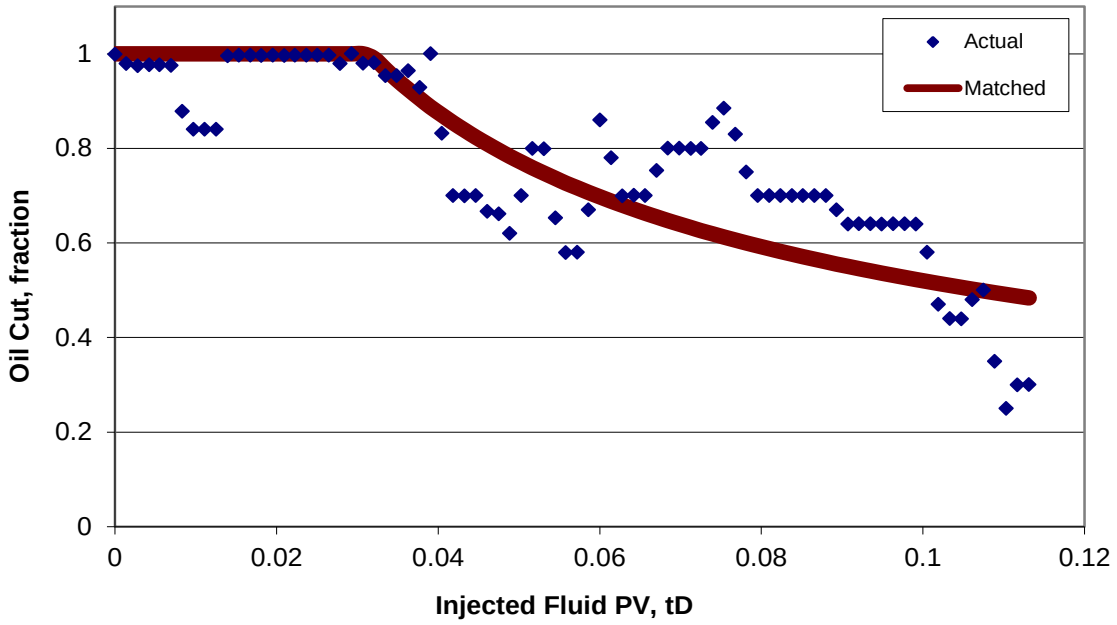

Figure B-10: Waterflooding history match for single well A-8 in the reservoir (Sand-A) using UTF.

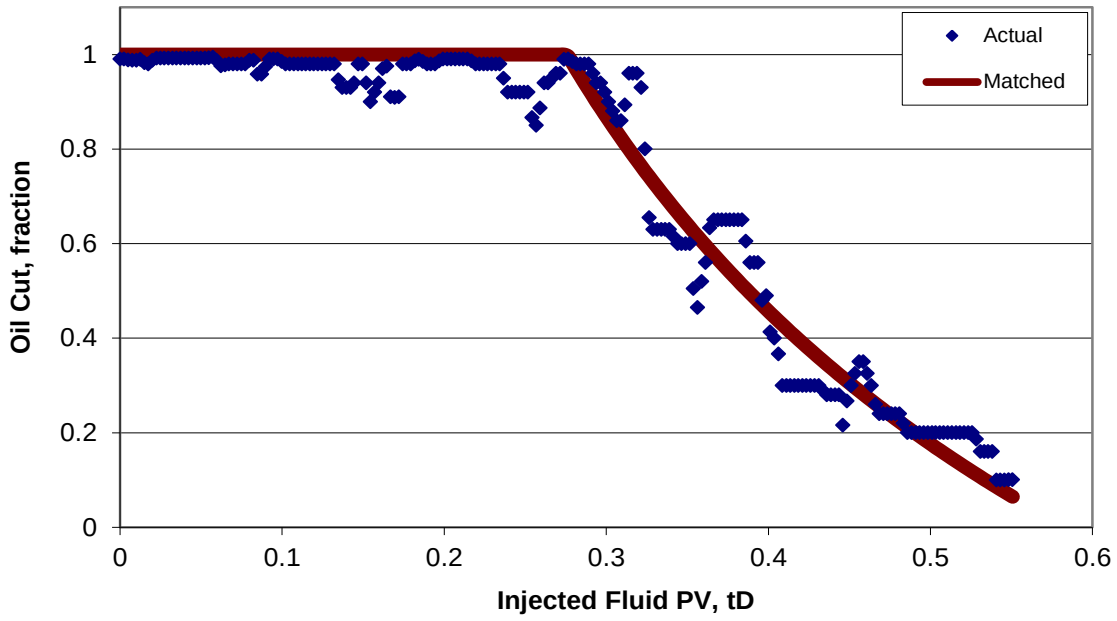

Figure B-11: Waterflooding oil cut history match for well B-1 in reservoir (Sand-B) using UTF.

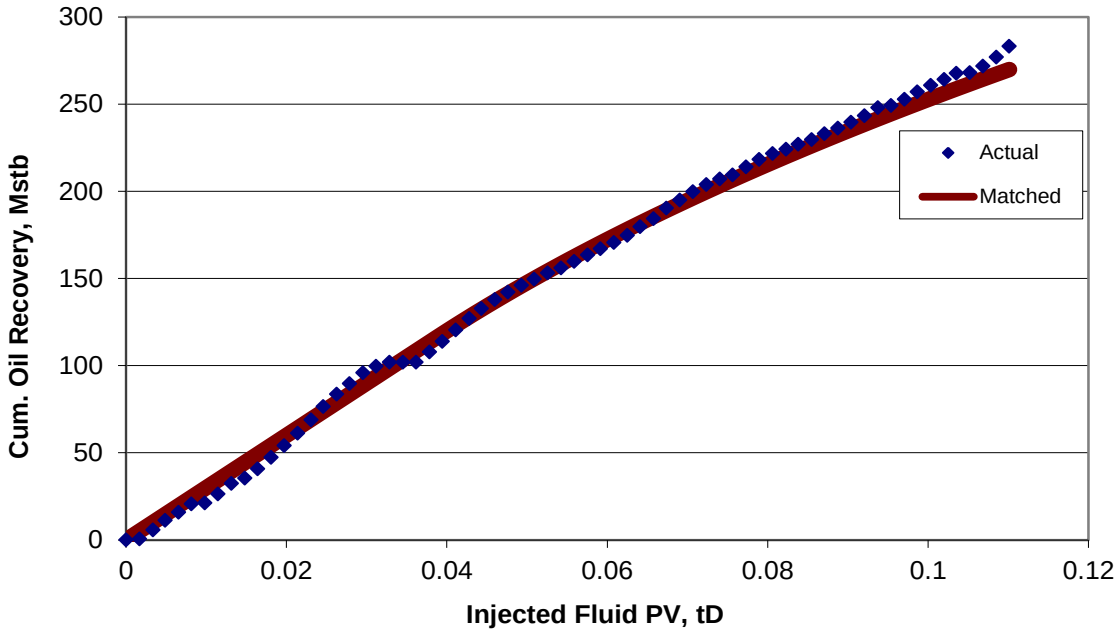

Figure B-12: Waterflooding oil cut history match for well B-2 in reservoir (Sand-B) using UTF.

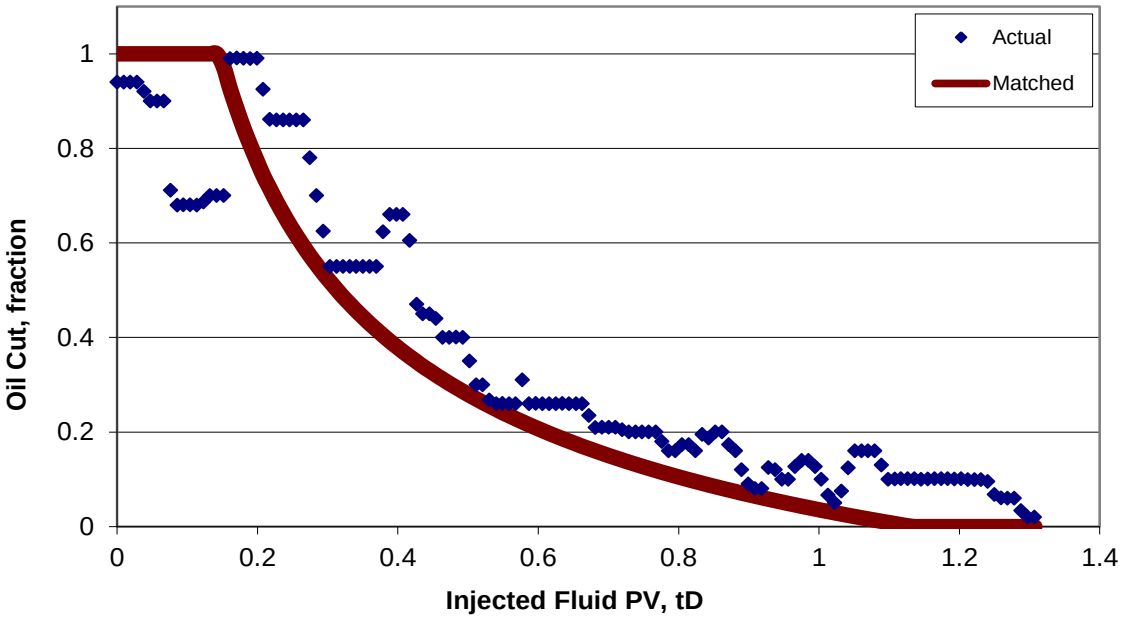

Figure B-13: Waterflooding oil cut history match for well B-3 in reservoir (Sand-B) using UTF.

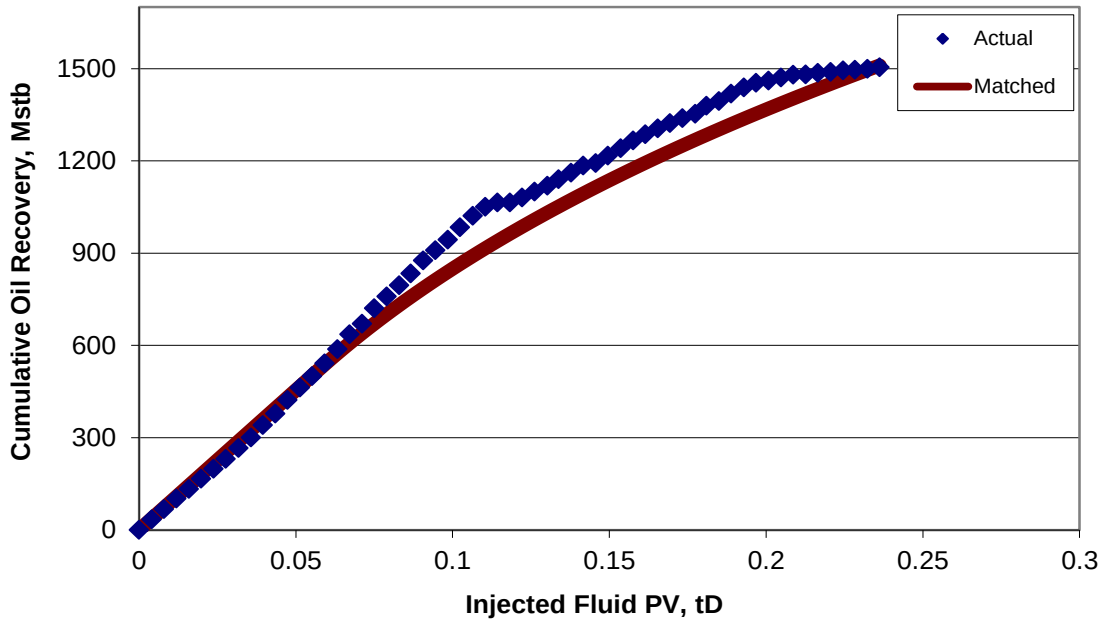

Figure B-14: Waterflooding oil cut history match for well C-1 in reservoir (Sand-C) using UTF.

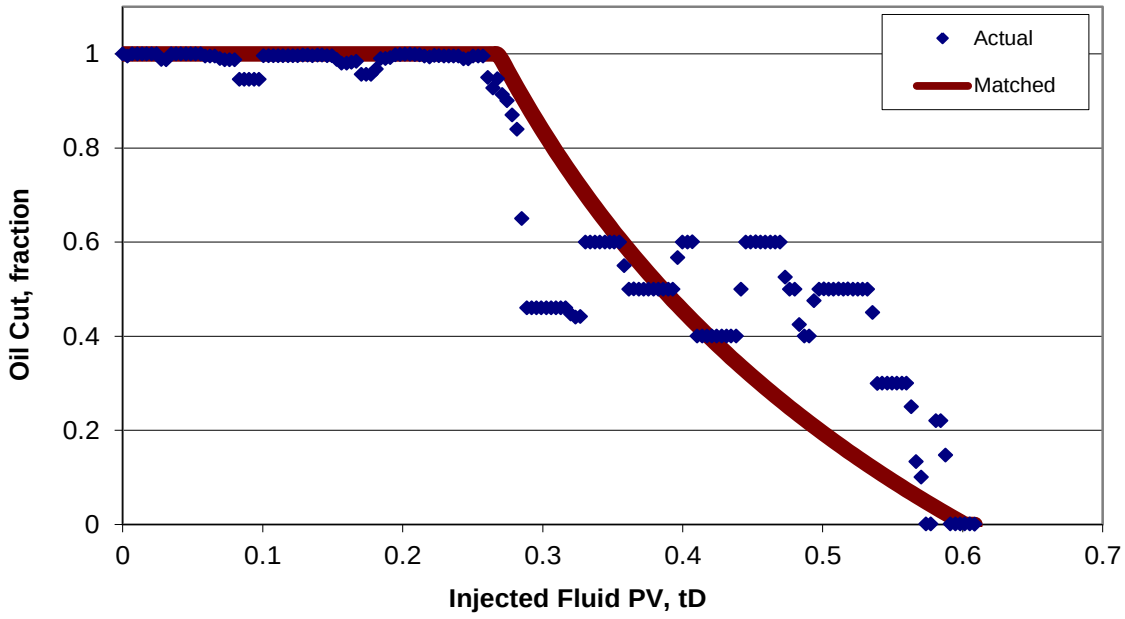

Figure B-15: Waterflooding oil cut history match for well C-2 in reservoir (Sand-C) using UTF.

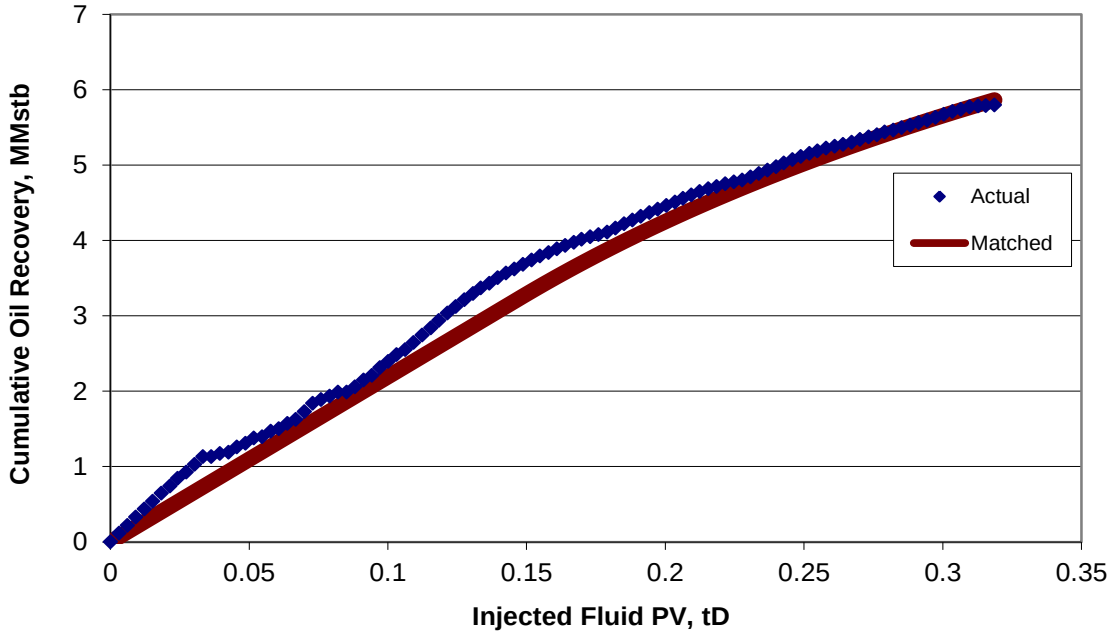

Figure B-16: Waterflooding oil cut history match for well D-1 in reservoir (Sand-D) using UTF.

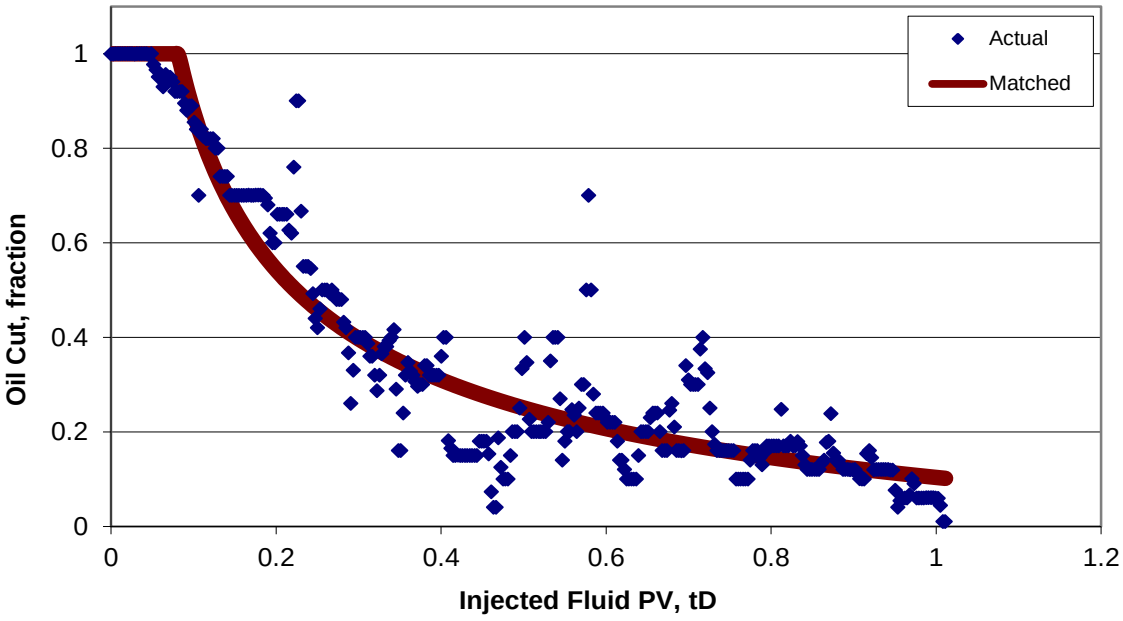

Figure B-17: Waterflooding oil cut history match for well D-2 in reservoir (Sand-D) using UTF.

B.2- EOR History Matching

B.2.1- Polymer Flooding

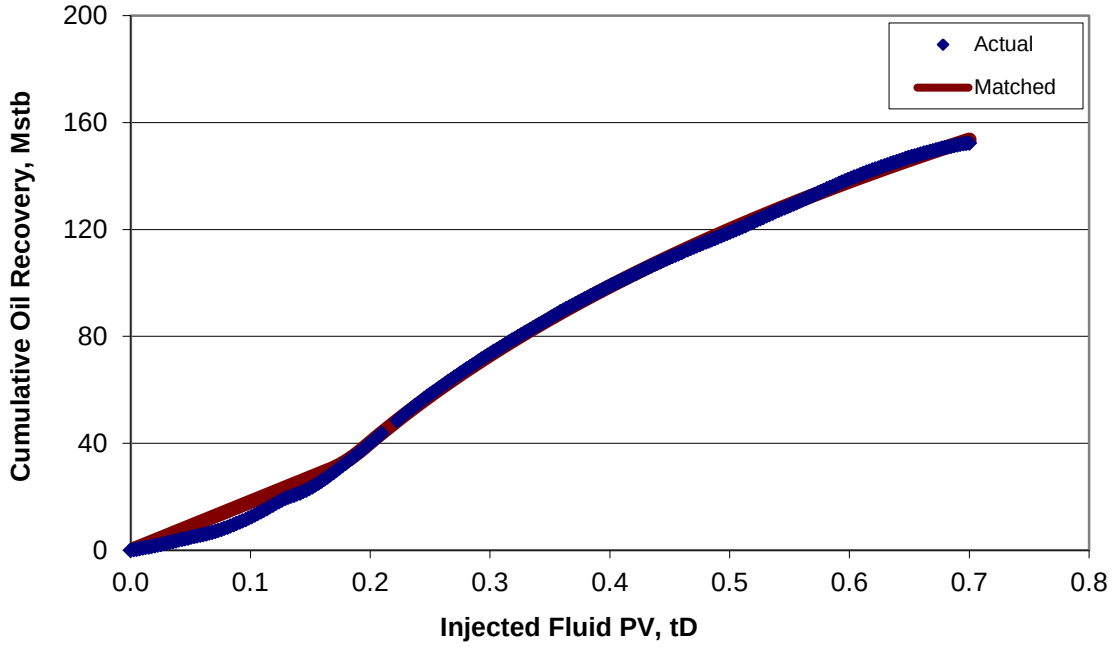

Figure B-8: Polymer flood history match of Chateaurenard using general isothermal EOR and waterflood forecasting tool (UTF; Takaqi et al., 1992).

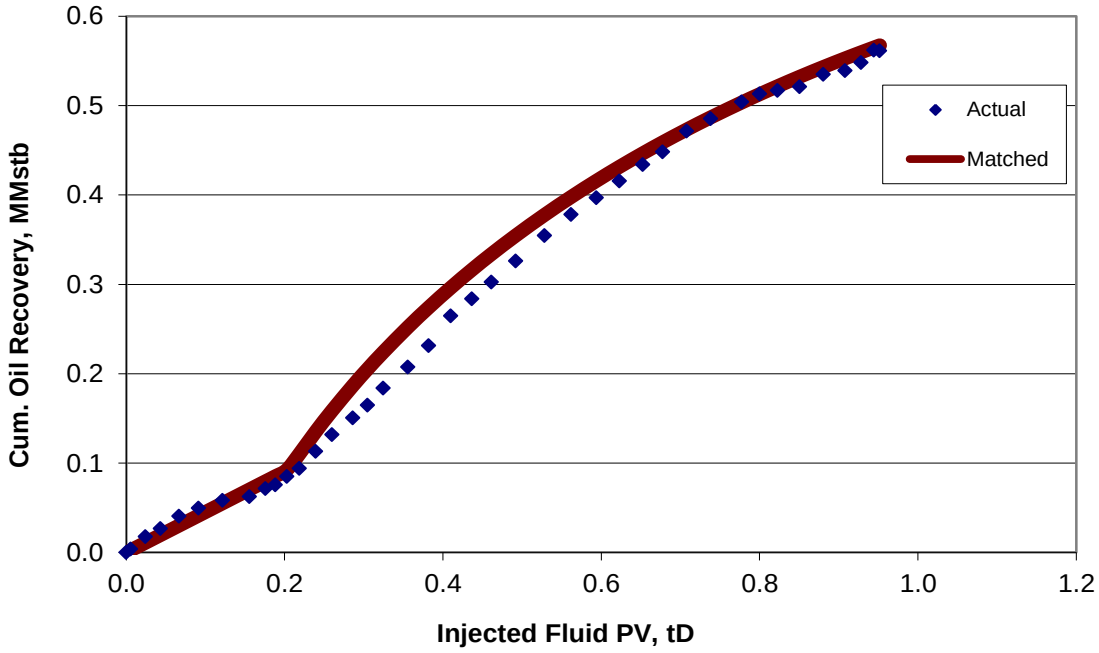

Figure B-9: Polymer flood history match of Marmul using UTF (Koning et al., 1988).

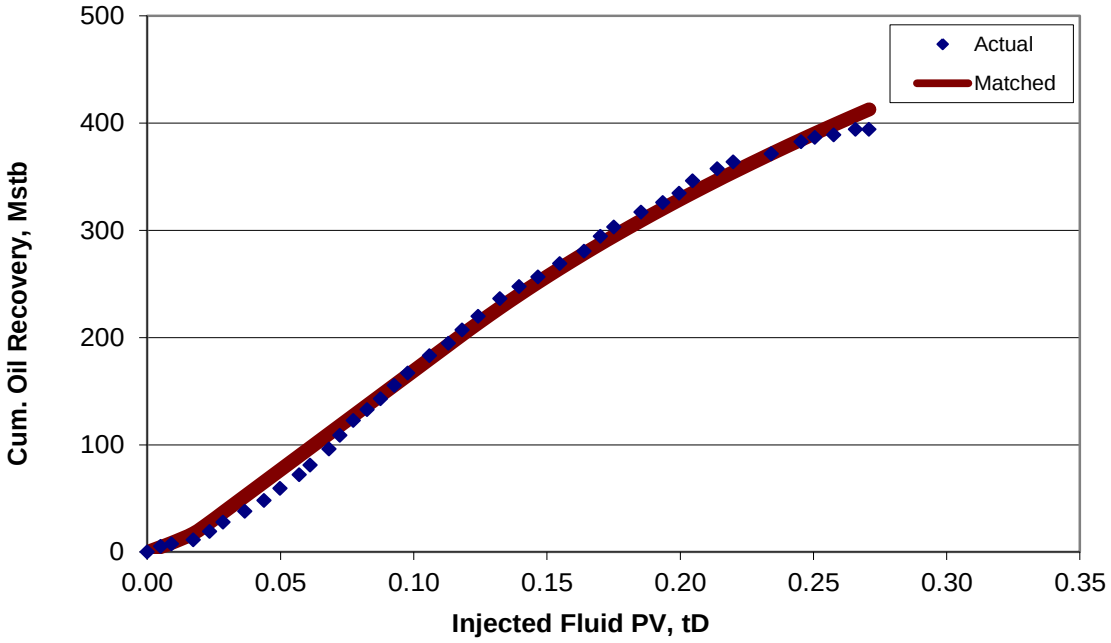

Figure B-10: Polymer flood history match of Minnelusa using UTF (Mack et al., 1984).

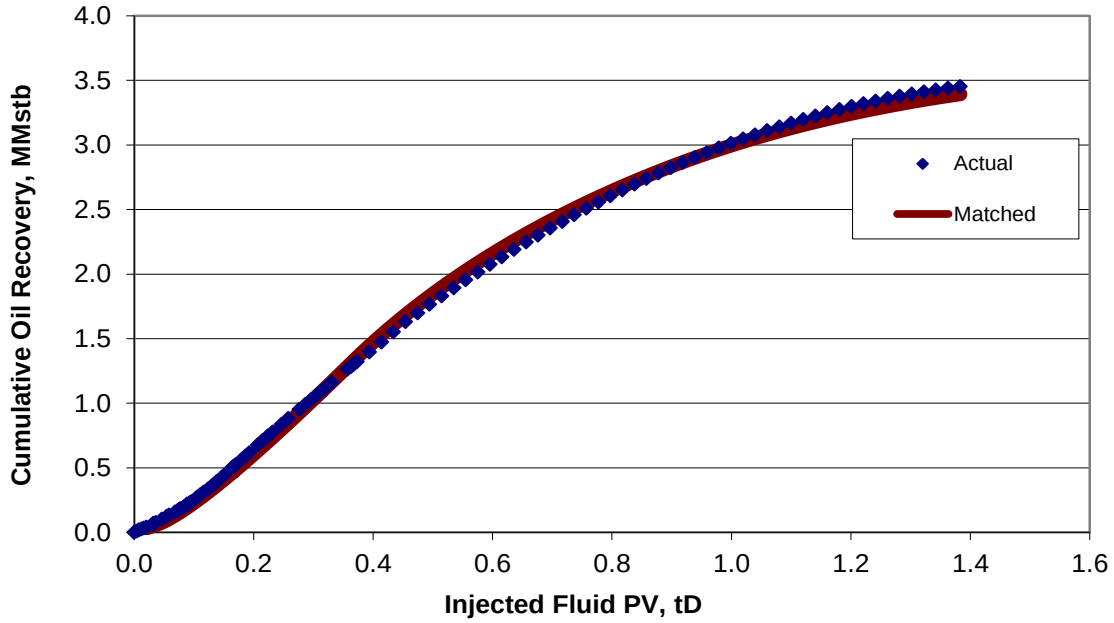

Figure B-11: Polymer flood history match of North Burbank using UTF (Zornes et al., 1986).

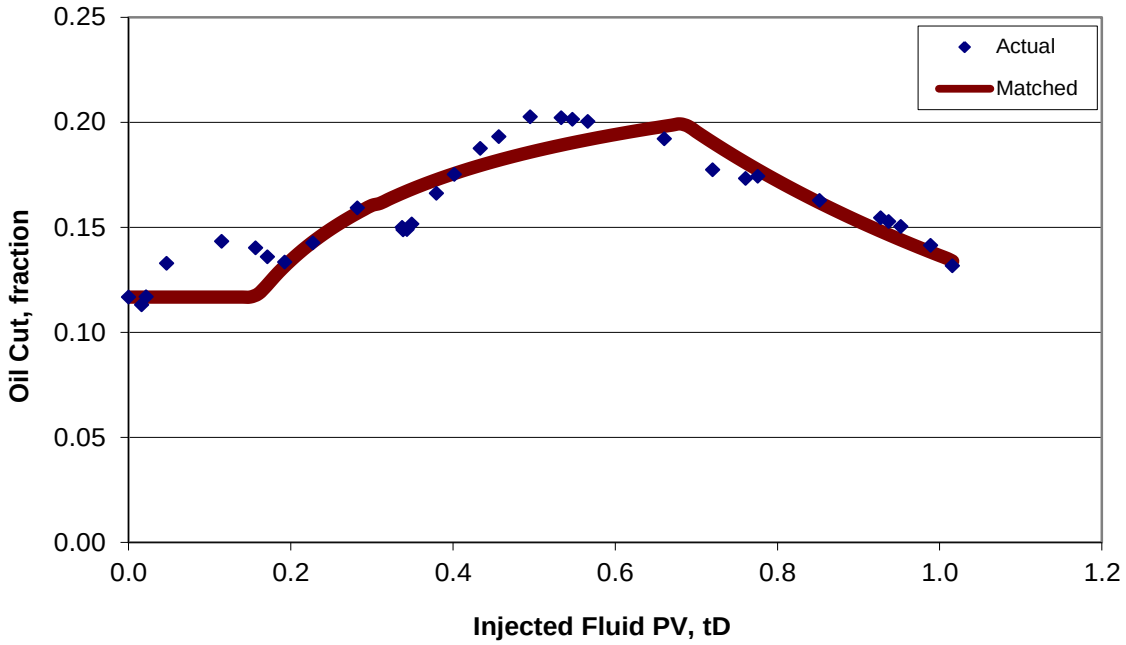

Figure B-12: Polymer flood history match of Courtenay using UTF (Putz et al., 1994).

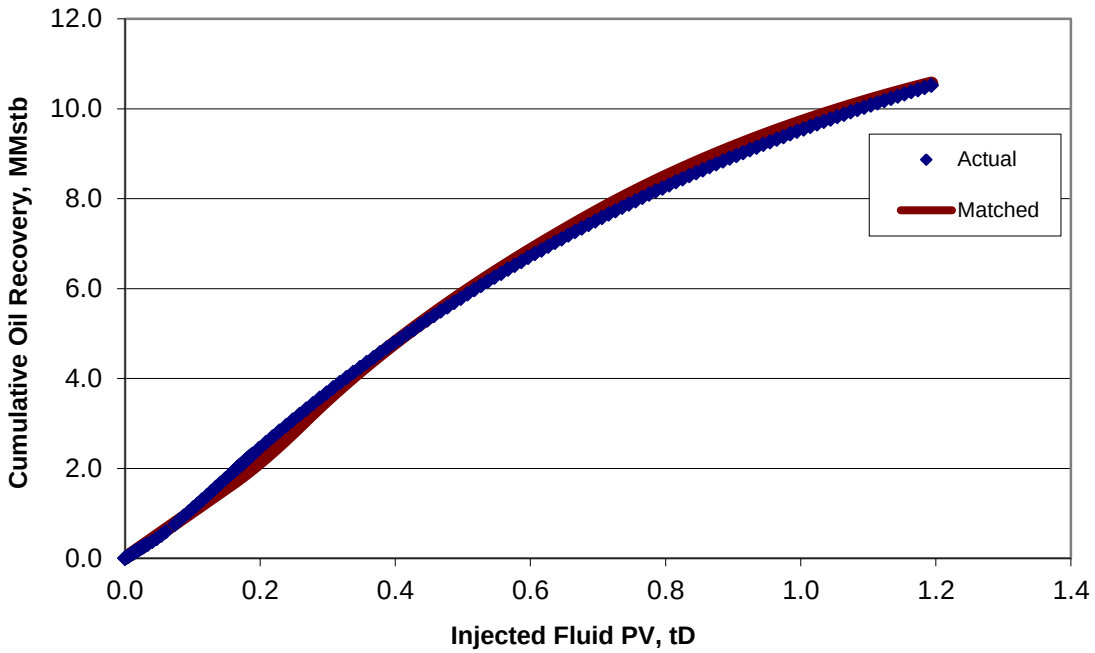

Figure B-13: Polymer flood history match of Sleepy Hollow using UTF (Christopher et al., 1988).

B.2.2- SP Flooding

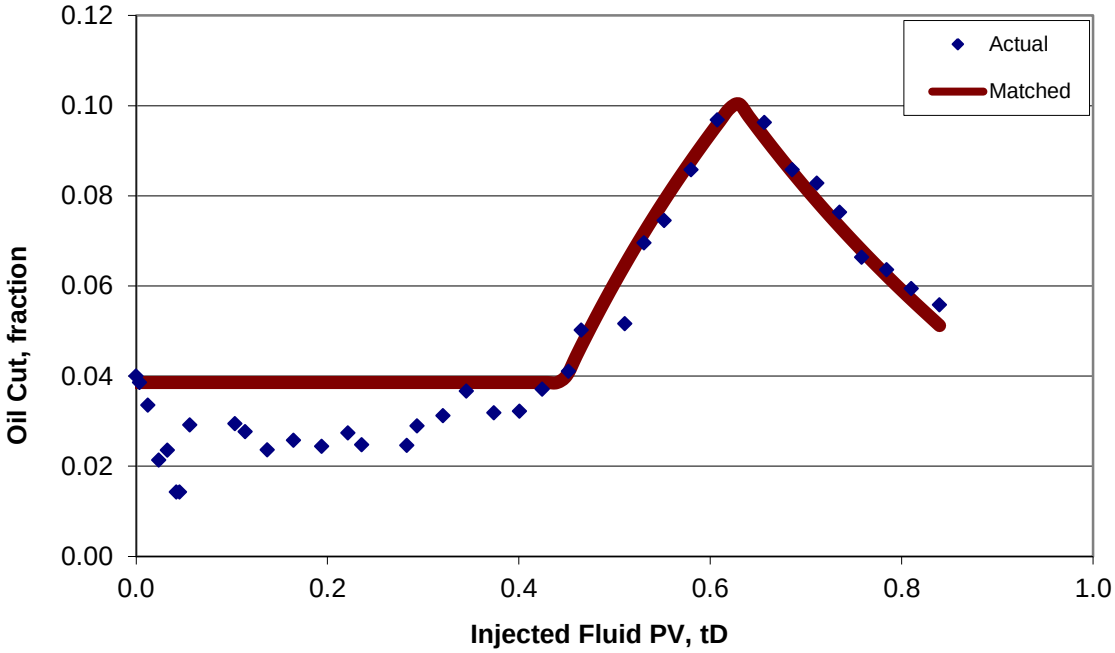

Figure B-14: History match of Bell Creek SP flood pilot using general isothermal EOR and waterflood forecasting tool (UTF; Hartshorne et al., 1984; Vargo, 1978).

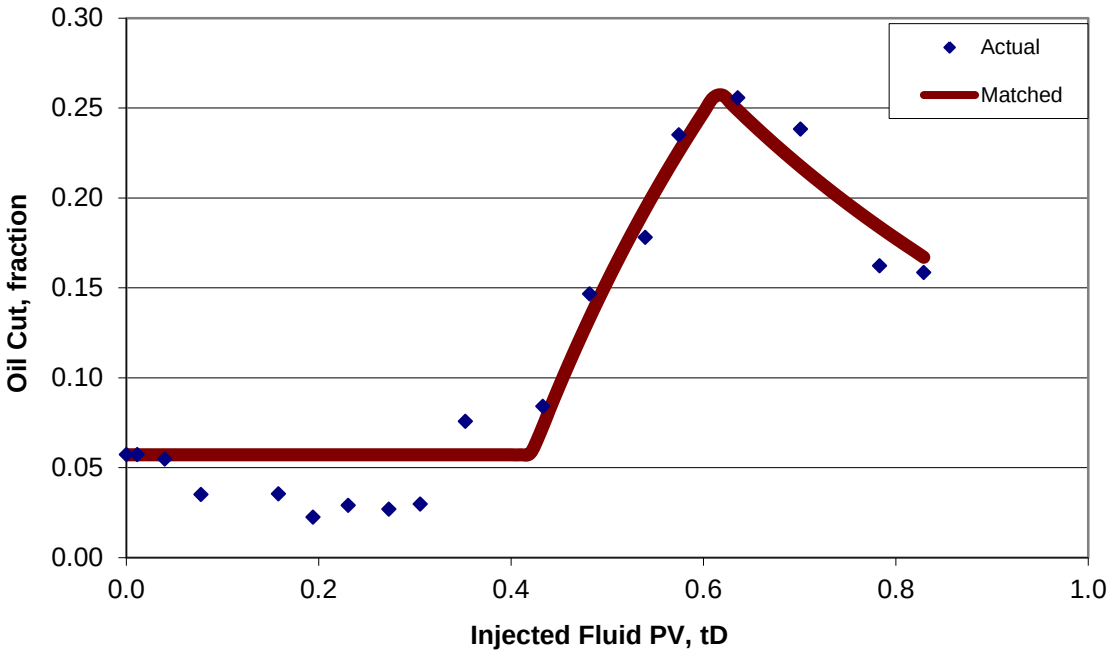

Figure B-15: History match of Bell Creek confined SP flooding pilot using UTF (Hartshorne et al., 1984; Vargo, 1978).

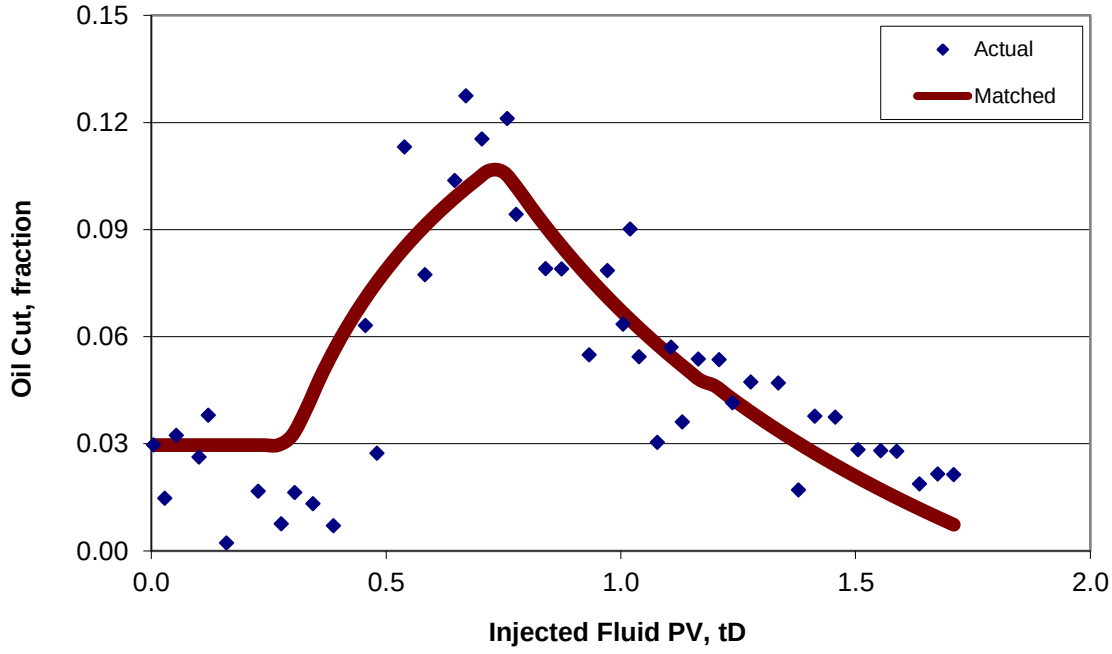

Figure B-16: History match of Benton SP flood pilot using UTF (French et al., 1973).

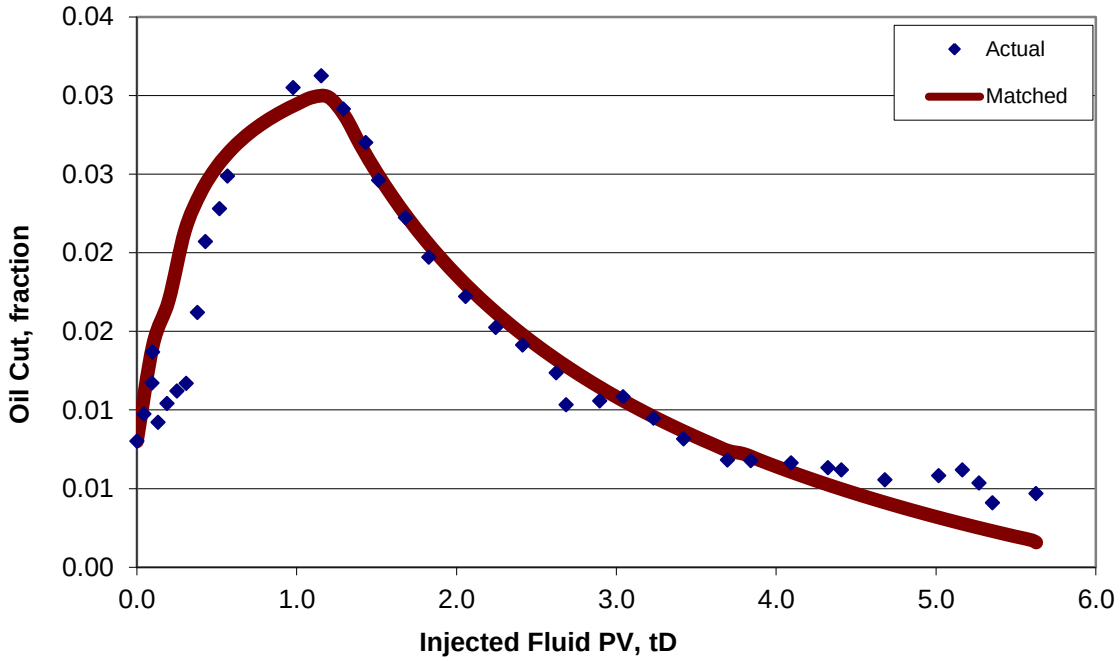

Figure B-17: History match of Berryhill Field SP flood pilot using UTF (Bae, 1995).

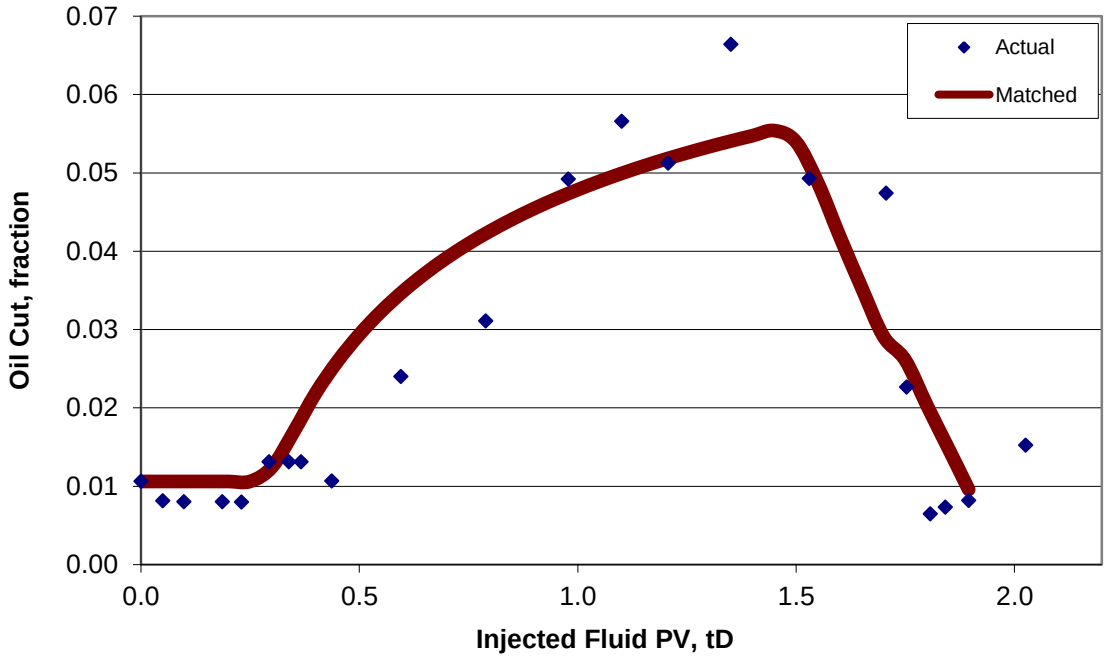

Figure B-17: History match of Berryhill pilot SP flooding using UTF (Bae et al., 1988).

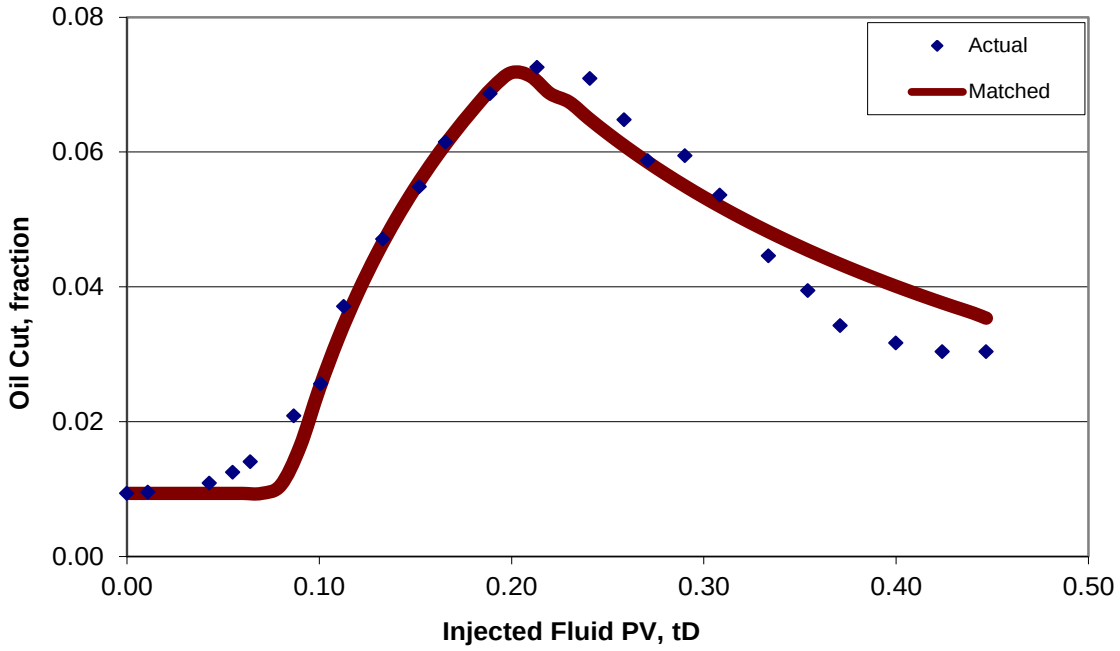

Figure B-18: History match of Big Muddy Field SP flood using UTF (Borah et al., 1988).

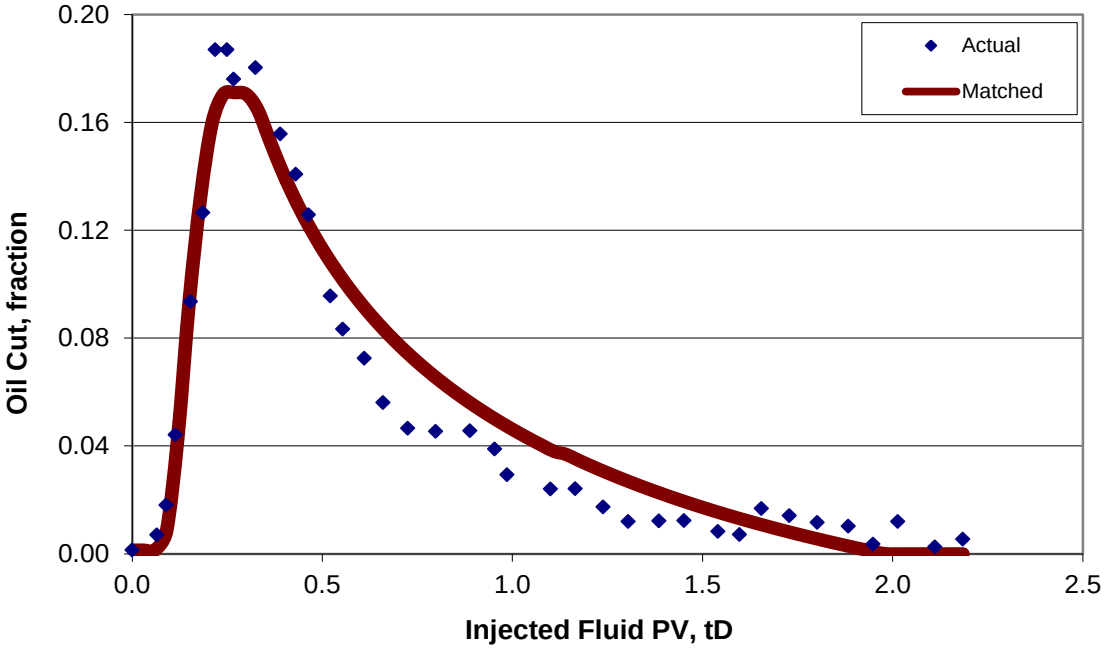

Figure B-19: History match of Big Muddy Pilot SP flood using UTF (Ferrell et al., 1988; Saad et al., 1989).

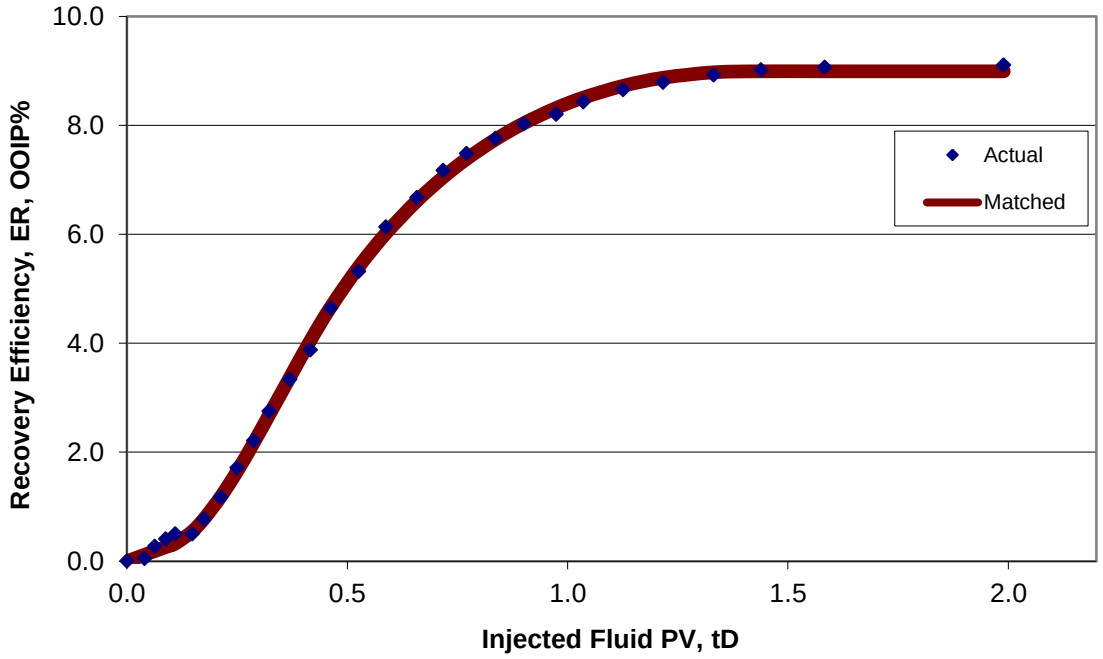

Figure B-20: History match of Borregos SP flood using UTF (Pursley et al., 1975).

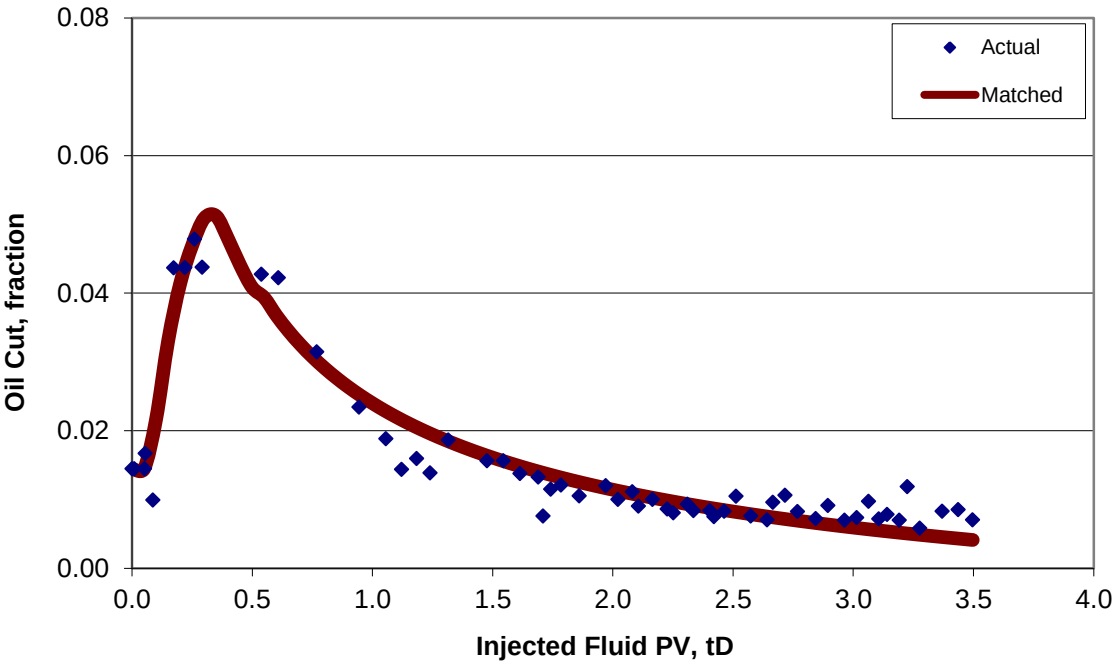

Figure B-20: History match of Bradford-7 Pilot SP flood using UTF (Danielson et al., 1976; Guckert et al., 1982; Ondrusek et al., 1988).

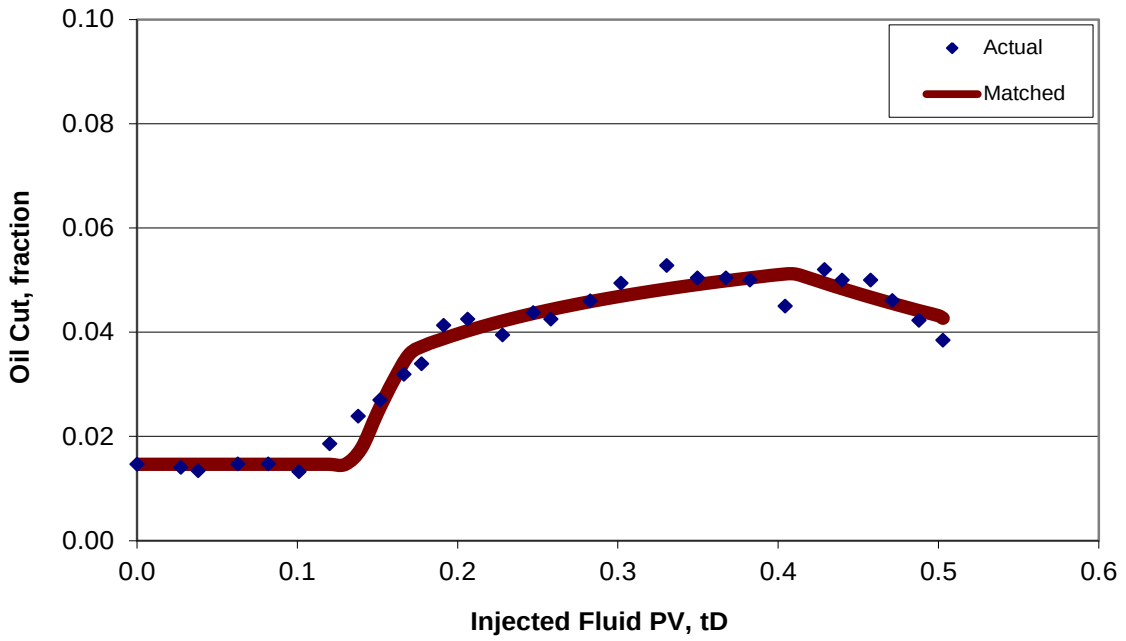

Figure B-21: History match of Bradford-8 Pilot SP flooding using UTF (Danielson et al., 1976; Guckert et al., 1982; Ondrusek et al., 1988).

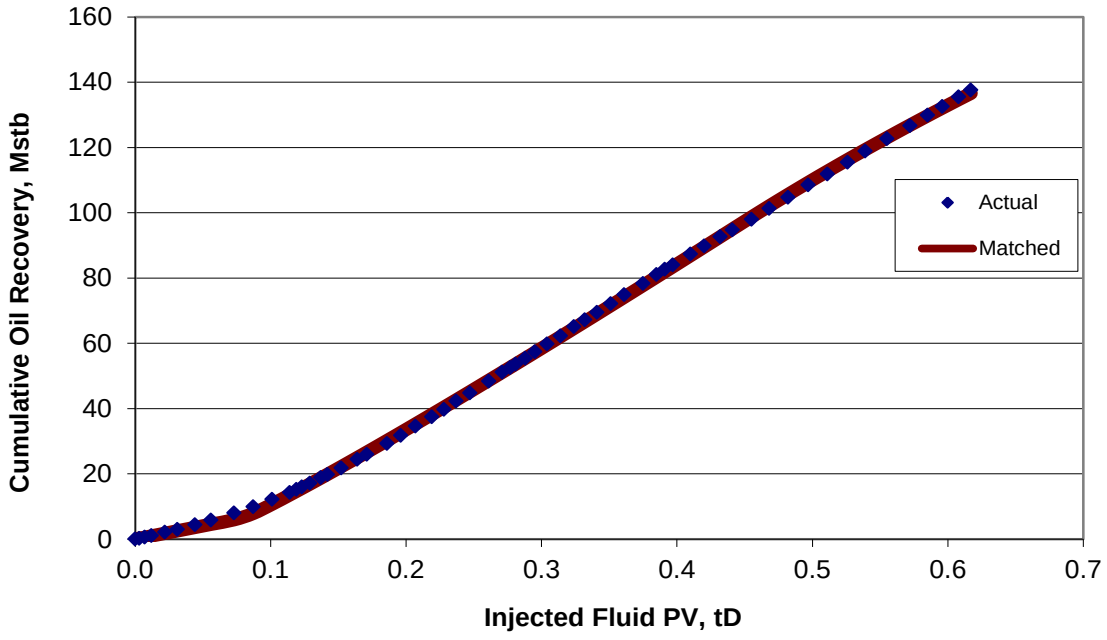

Figure B-22: History match of Chateaurenard Pilot SP flood using UTF (Putz et al., 1981; Chapotin et al., 1986).

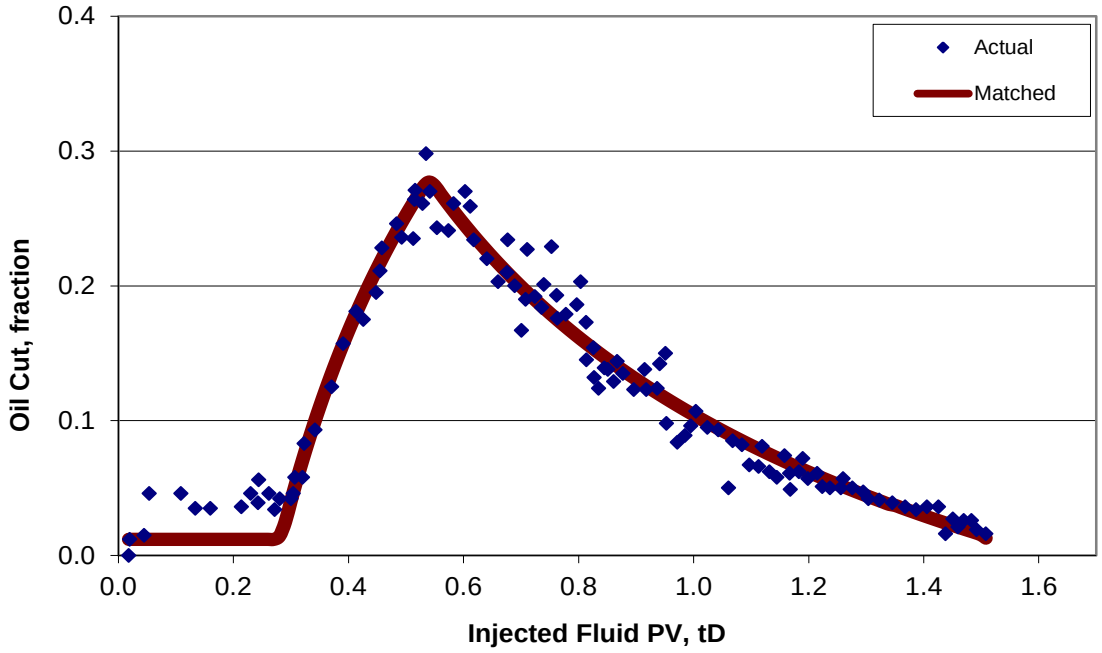

Figure B-23: History match of Loudon Pilot SP flood using UTF (Bragg et al., 1983).

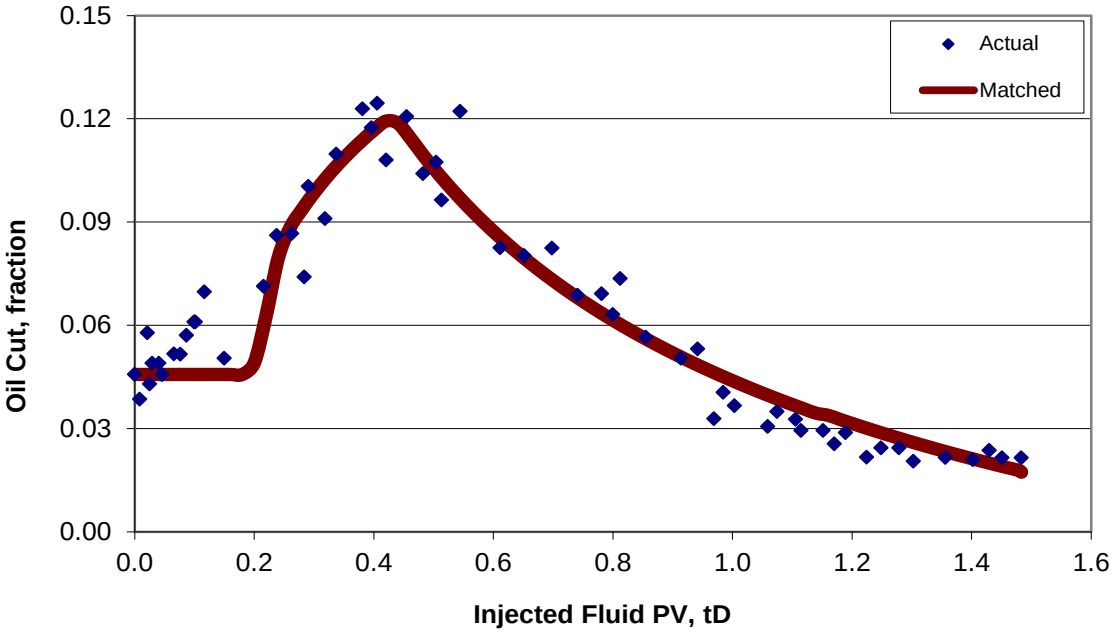

Figure B-24: History match of M1-2.5 Pilot SP flood using general isothermal EOR and waterflood forecasting tool (UTF; Stover, 1988).

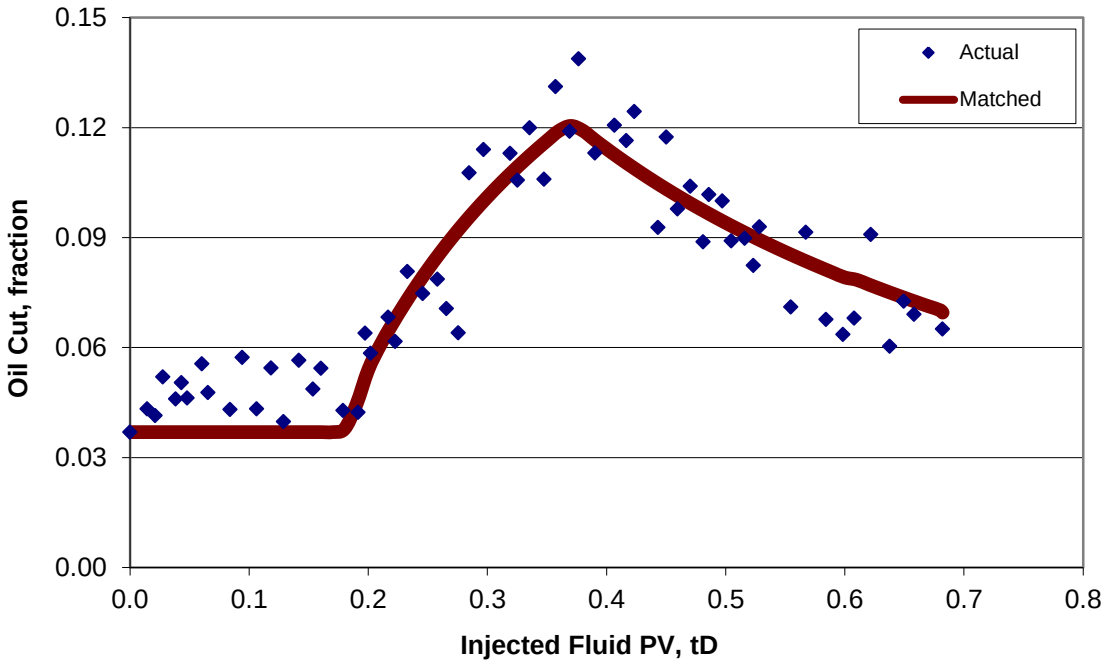

Figure B-25: History match of M1-5 Pilot SP flood using UTF (Stover, 1988).

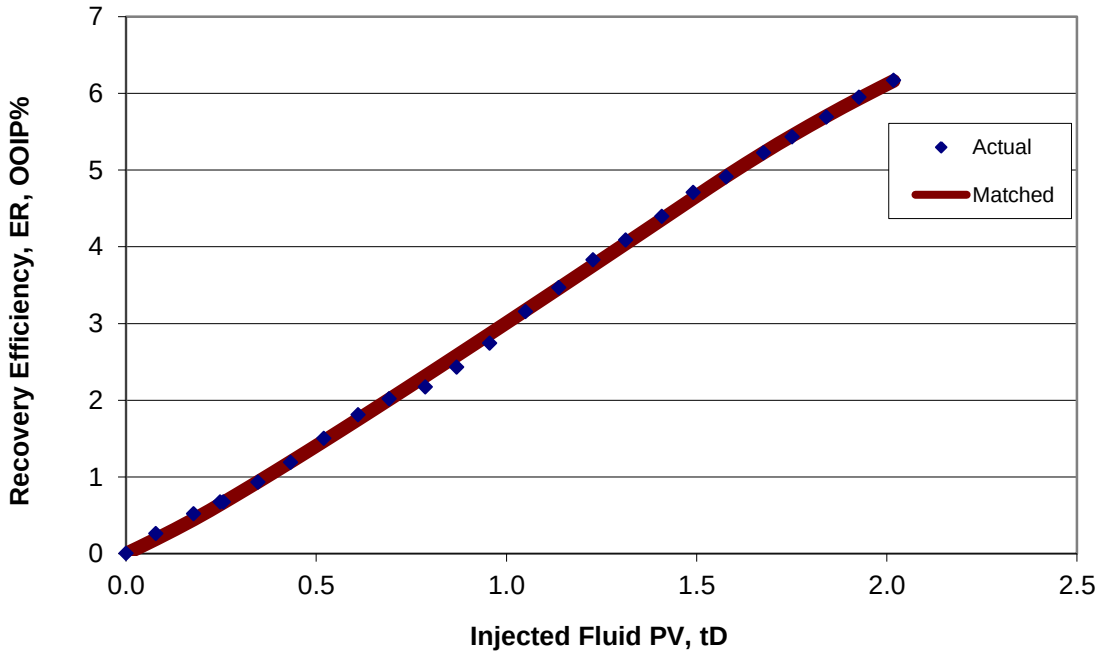

Figure B-26: History match of Manvel Pilot SP flood using UTF (Widmyer et al., 1981).

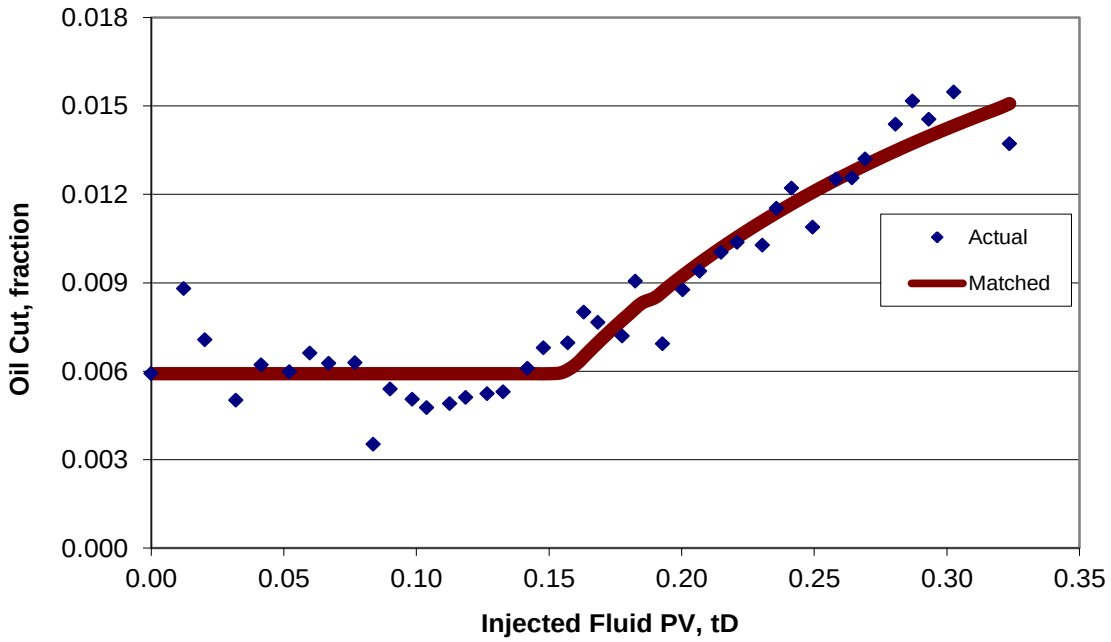

Figure B-27: History match of North Burbank Pilot SP flood using (UTF; Trantham et al., 1978; Trantham, Threlkeld et al., 1980).

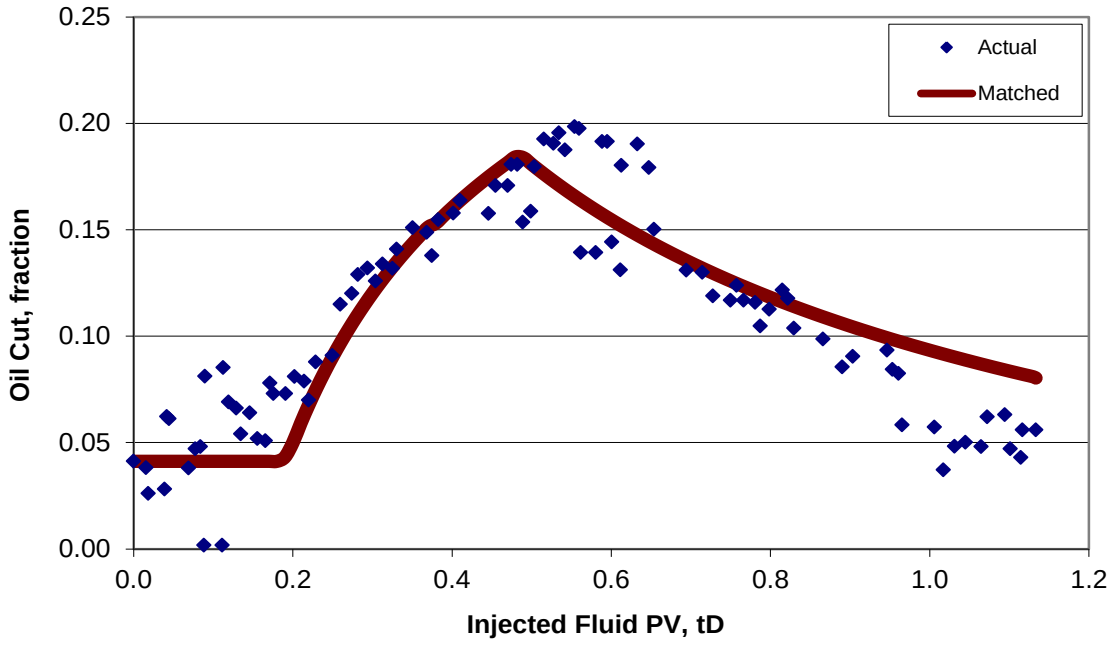

Figure B-28: History match of Robinson Pilot SP flood using UTF (Gogarty et al., 1972).

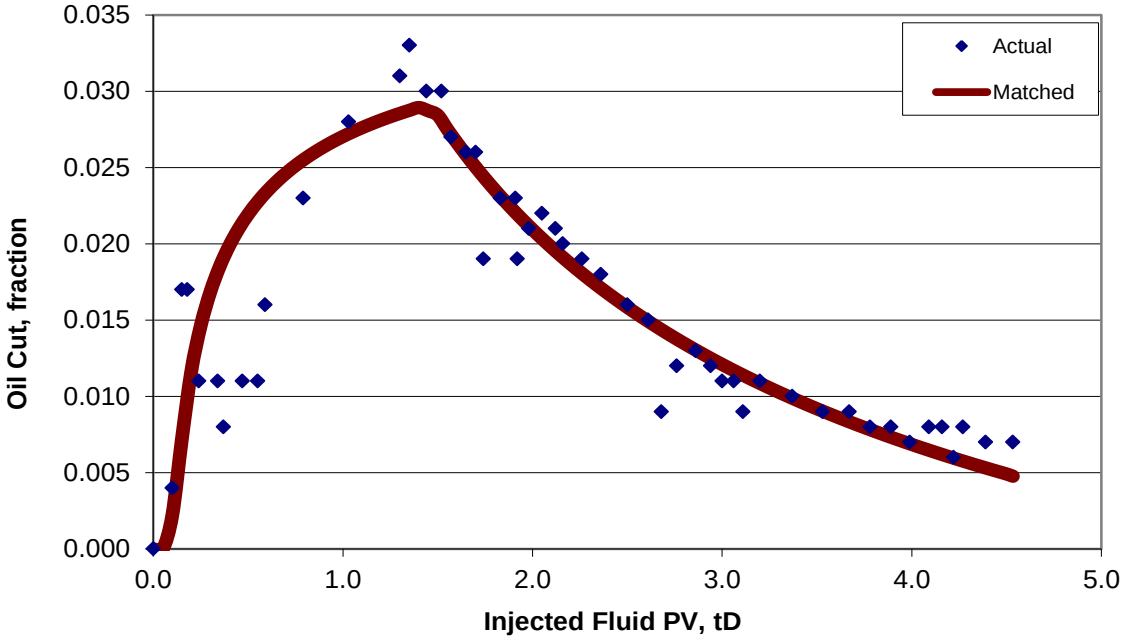

Figure B-29: History match of Salem Pilot SP flood using UTF (Strange et al., 1977; Widmyer et al., 1988).

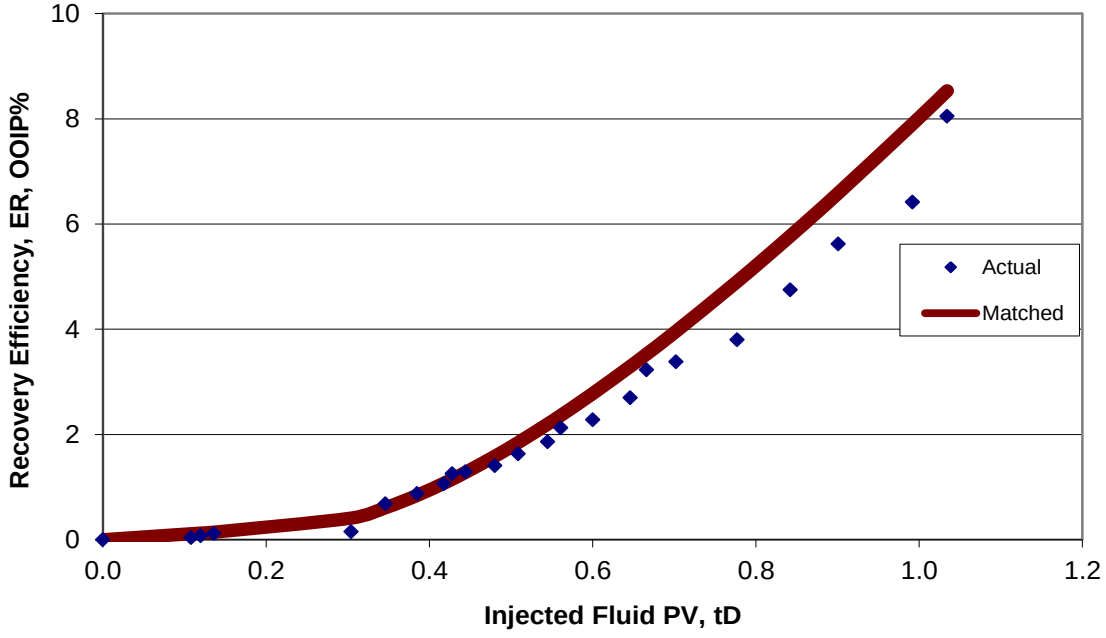

Figure B-30: History match of Sloss Pilot SP flood using UTF (Wanosik et al., 1978).

B.2.3- ASP Flooding

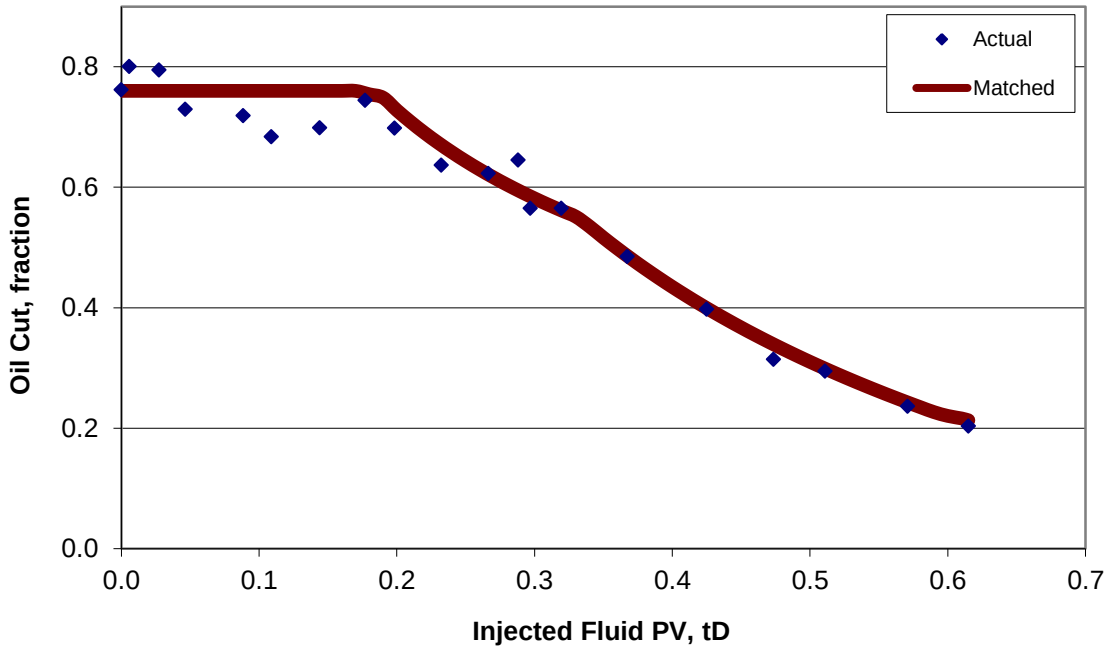

Figure B-31: History match of Cambridge Pilot secondary ASP flood using general isothermal EOR and waterflood forecasting tool (UTF; Vargo et al., 2000).

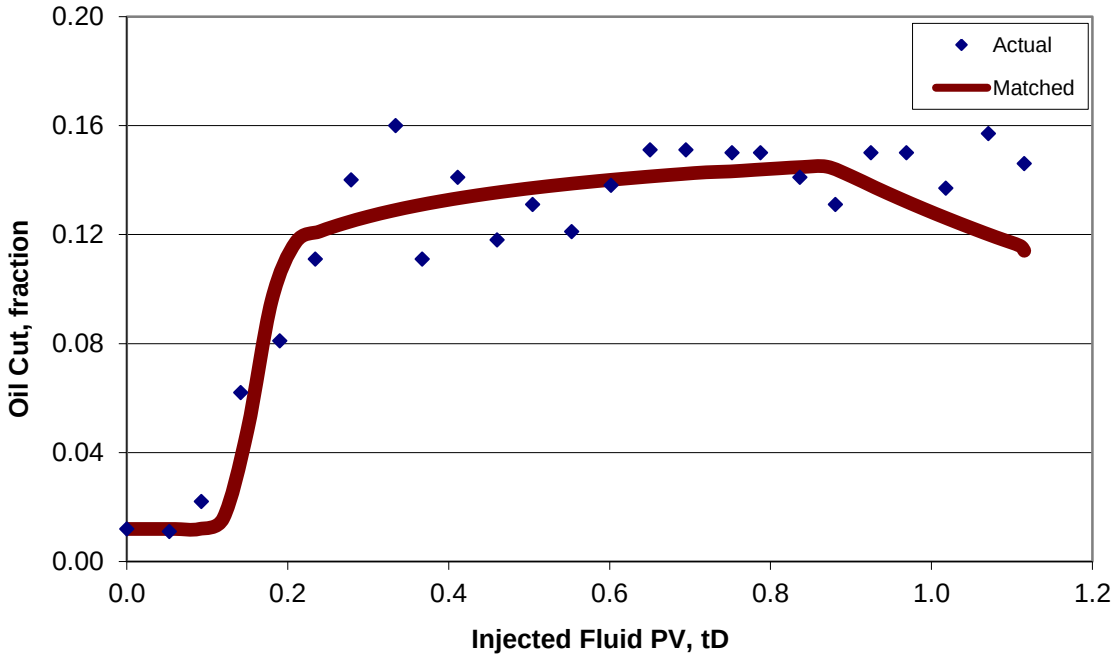

Figure B-32: History match of Karamay Pilot ASP flood using UTF (Qi et al., 2000).

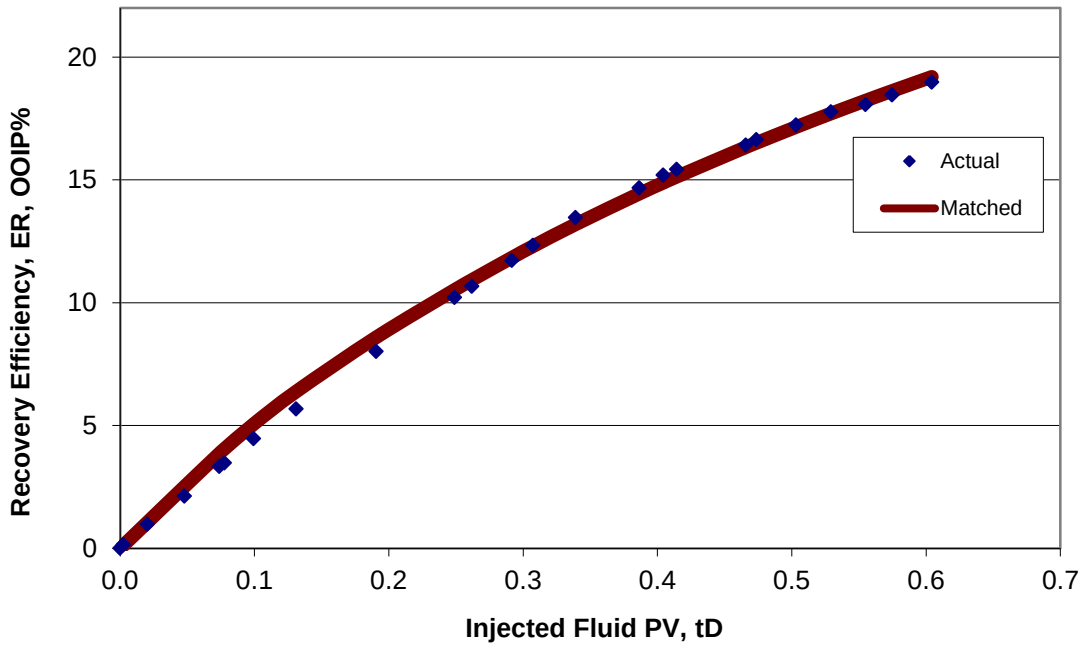

Figure B-33: History match of Tanner Pilot ASP flood using UTF (Pitts et al., 2006).

B.2.4- Solvent/WAG Flooding

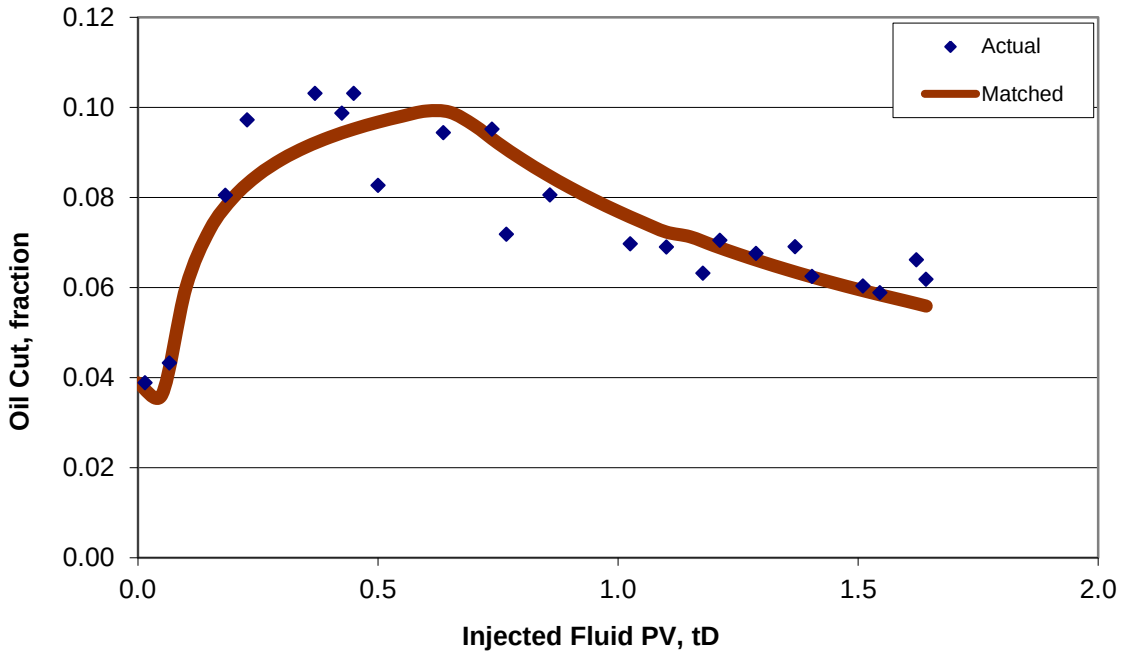

Figure B-34: History match of Lost Soldier CO_2/WAG flood using general isothermal EOR and waterflood forecasting tool (UTF; Brokmeyer et al., 1996).

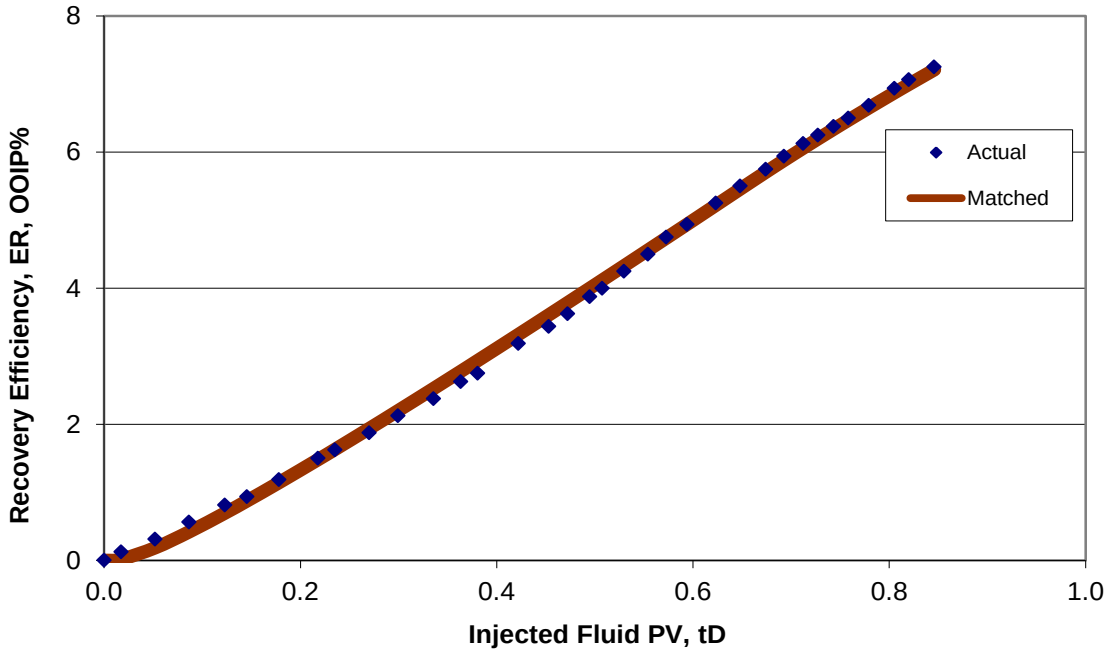

Figure B-35: History match of Rangely CO_2/WAG flood using UTF (Masoner et al., 1995).

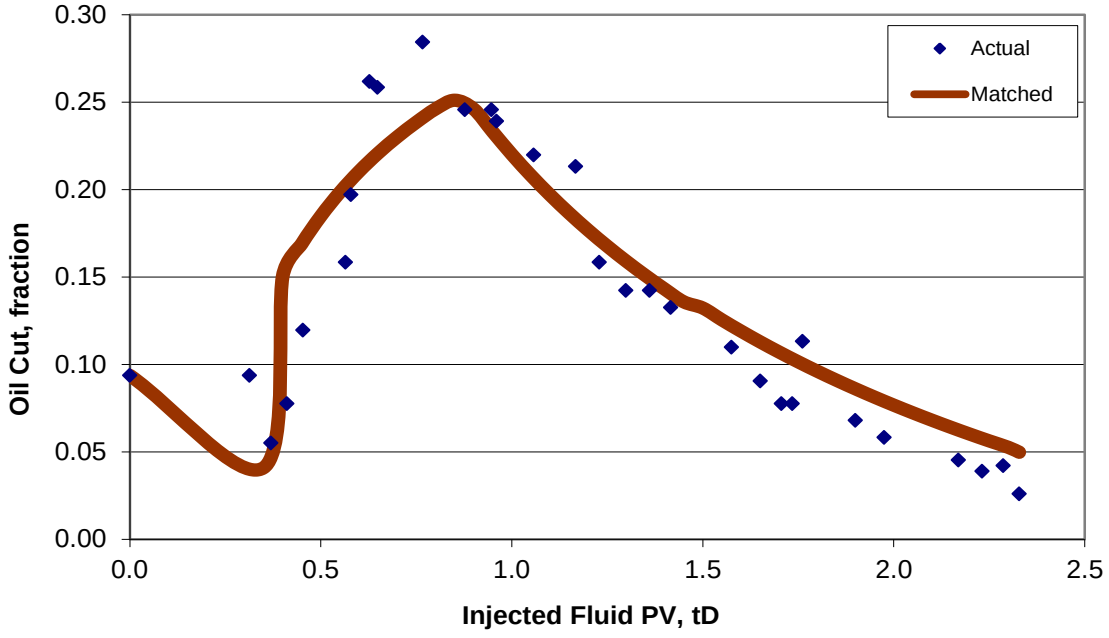

Figure B-36: History match of Slaughter CO_2/WAG flood using UTF (Rowe et al., 1982).

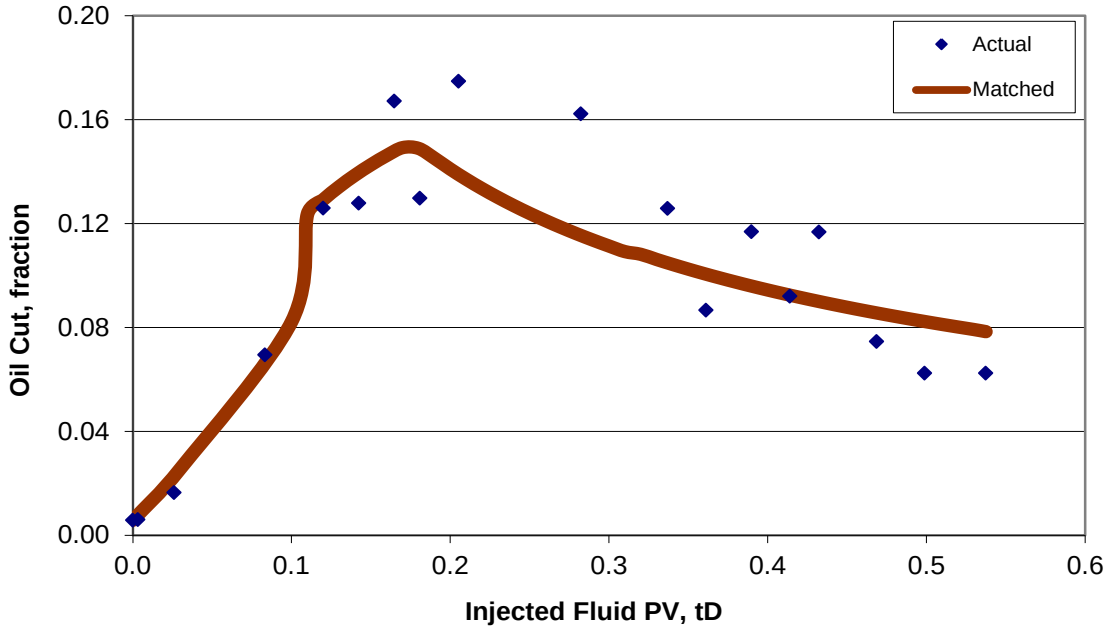

Figure B-37: History match of Twofreds CO_2/WAG flood using UTF (Flanders et al., 1993).

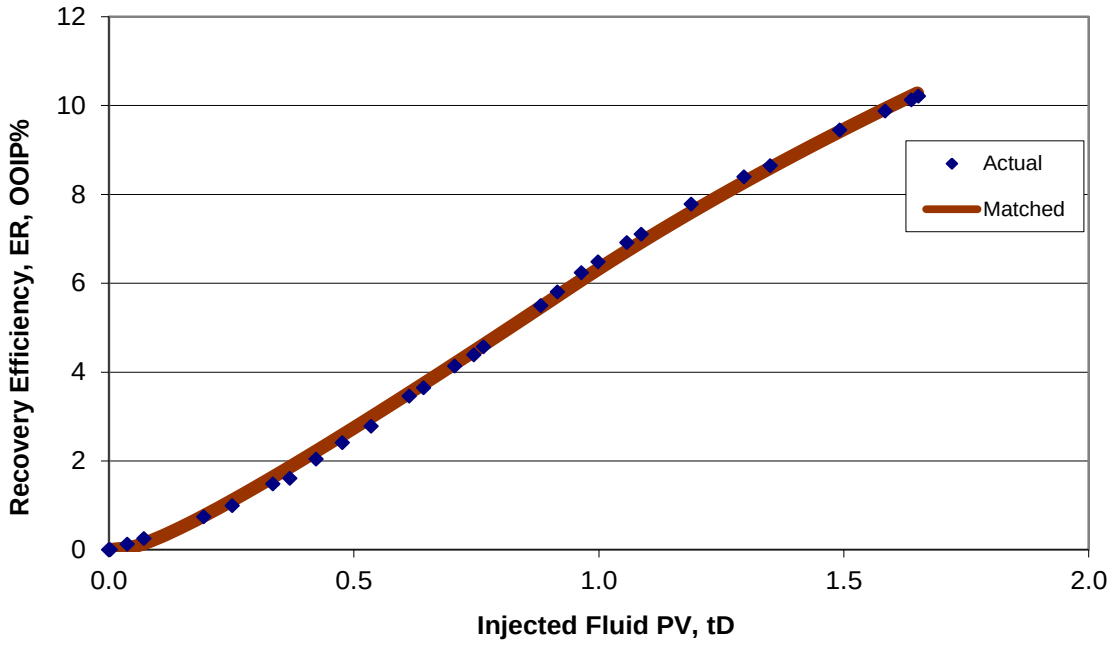

Figure B-38: History match of SACROC-Seventeen Pattern (17PA) CO_2/WAG flood using UTF (Langston et al., 1988).

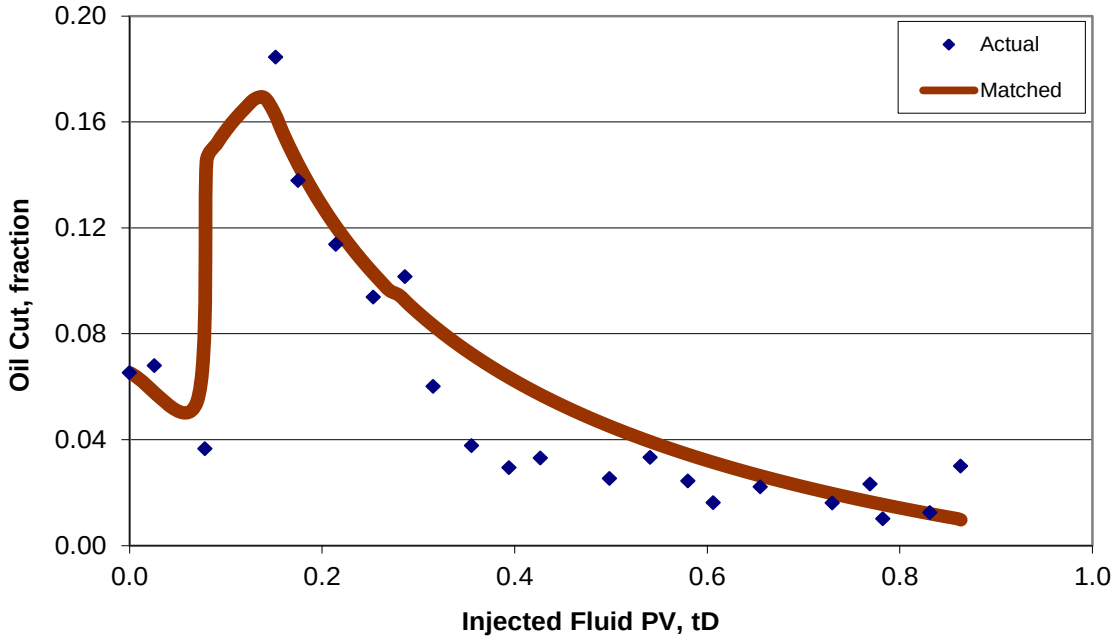

Figure B-39: History match of West Sussex CO_2/WAG flood using UTF (Hoiland et al., 1986).

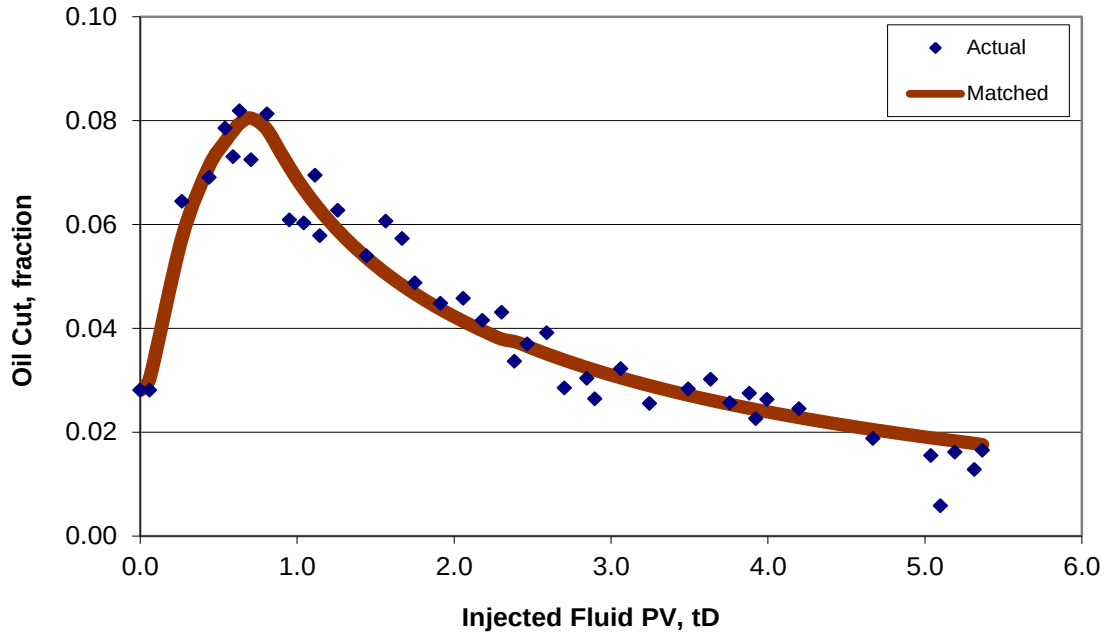

Figure B-40: History match of Wertz CO_2/WAG flood using UTF (Kleinstelber et al., 1990).

B.2.5- Coreflooding Experiments

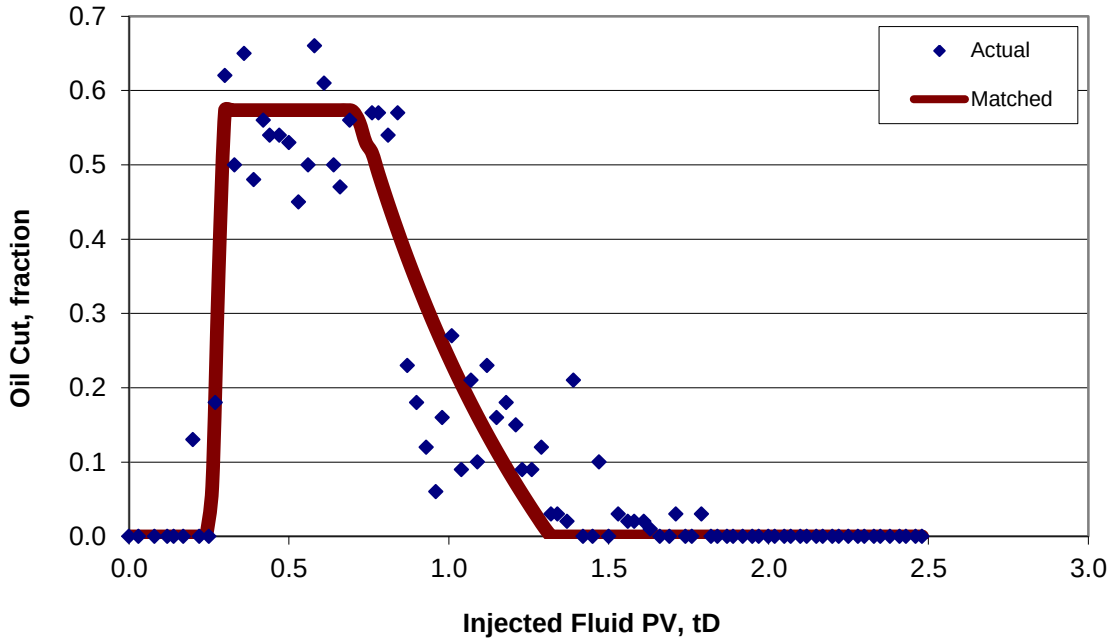

Figure B-41: SP coreflood history matching of Coreflood #A using general isothermal EOR and waterflood forecasting tool (UTF; G.A. Pope, personal communication, 2011).

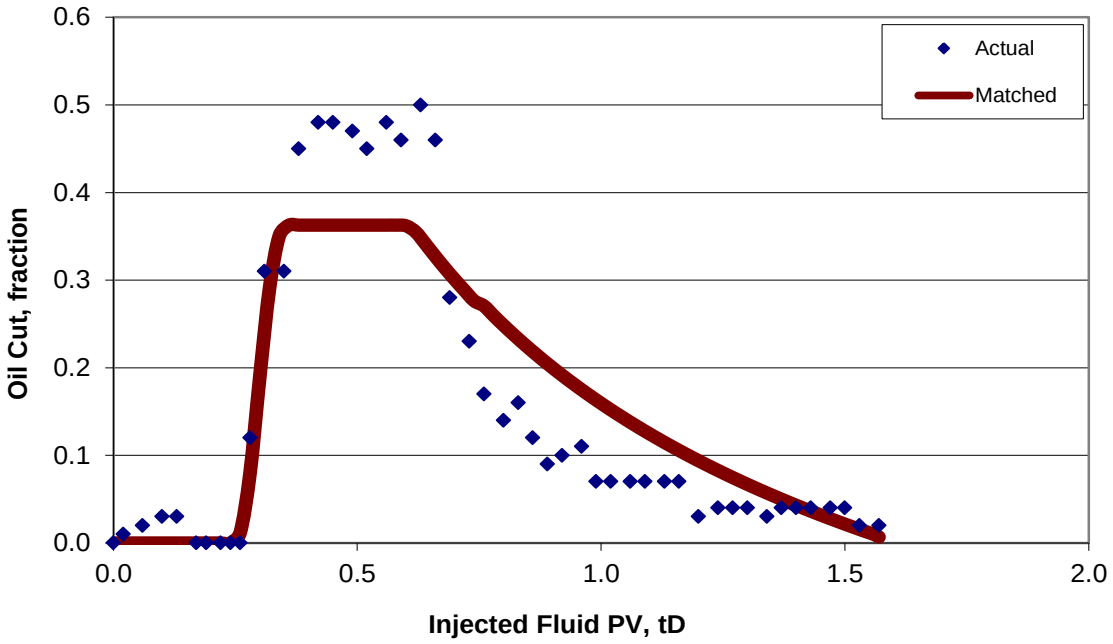

Figure B-42: ASP coreflood history match of Core#C using UTF (G.A. Pope, personal communication, 2011).

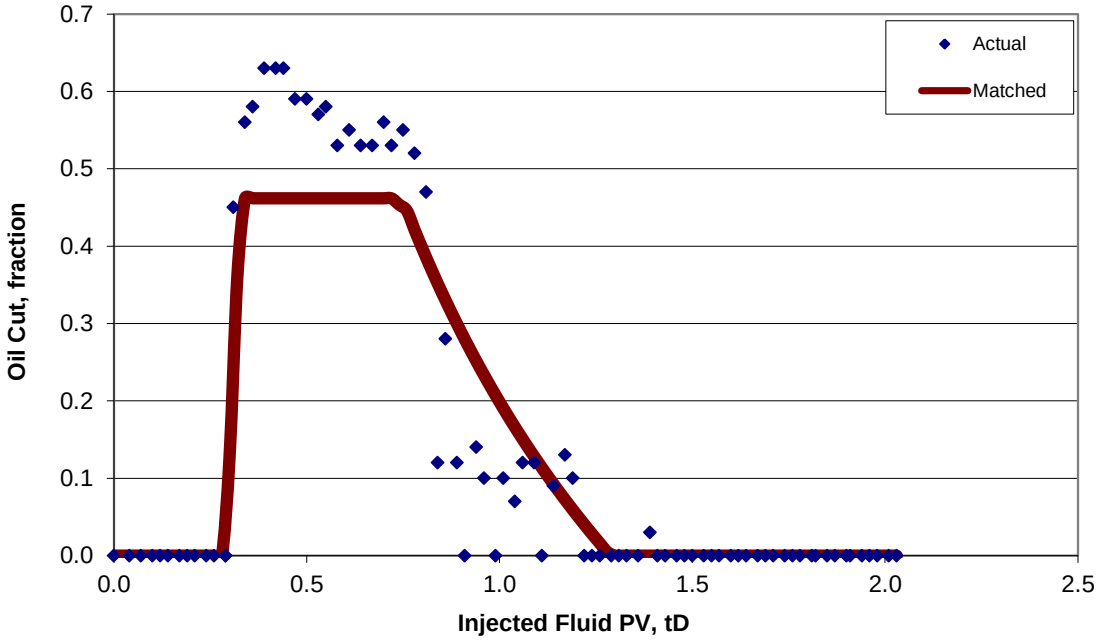

Figure B-43: ASP coreflood history match of Core#D using UTF (G.A. Pope, personal communication, 2011).

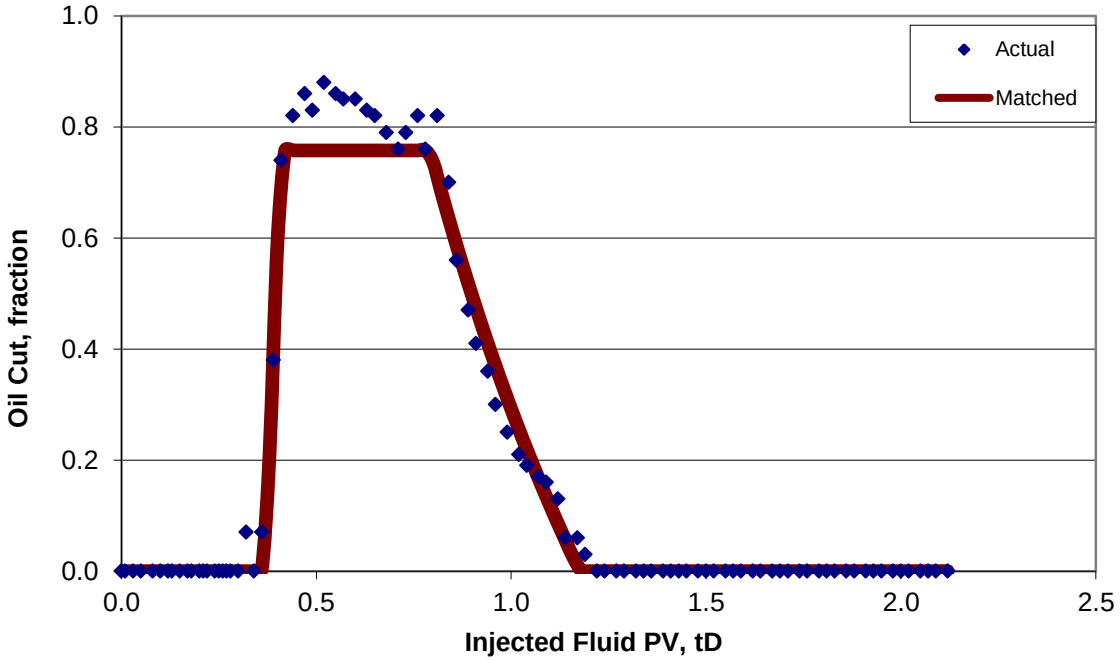

Figure B-44: ASP coreflood history match of Core#E using UTF (G.A. Pope, personal communication, 2011).

APPENDIX-C: TABLES OF NUMERICAL SIMULATION RUNS GENERATED BY EXPERIMENTAL DESIGN

C.1- Waterflooding

Run#	M^o	V_{DP}	λ
1	39.360	0.400	10.000
2	50.000	0.740	10.000
3	6.690	0.400	0.500
4	12.880	0.750	0.840
5	19.060	0.900	10.000
6	0.500	0.800	8.000
7	40.100	0.900	0.500
8	39.360	0.400	10.000
9	15.850	0.580	9.910
10	12.880	0.420	7.010
11	14.360	0.690	5.720
12	0.500	0.570	3.490
13	49.500	0.510	6.720
14	29.460	0.560	6.910
15	15.000	0.400	0.500
16	49.750	0.740	2.780
17	34.660	0.770	7.530
18	50.000	0.900	7.340
19	35.150	0.400	2.980
20	16.590	0.900	3.830
21	15.000	0.900	10.000
22	0.500	0.400	10.000
23	0.500	0.900	0.500
24	50.000	0.800	10.000
25	50.000	0.400	0.500
26	31.690	0.720	1.450
27	35.640	0.540	0.500
28	20.020	0.530	2.970
29	1.000	0.800	10.000
30	5.000	0.870	5.000
31	10.000	0.830	1.000
32	12.000	0.850	0.500
33	15.000	0.700	3.000
34	24.000	0.650	7.000

C.2- Polymer Flooding

Run#	M^o	V_{DP}	λ
1	0.100	0.400	0.500
2	0.100	0.900	0.500
3	10.070	0.570	0.500
4	20.030	0.900	0.500
5	30.000	0.730	0.500
6	30.000	0.400	0.500
7	1.000	0.500	0.500
8	0.500	0.800	1.000
9	1.000	0.700	1.000
10	5.000	0.800	1.000
11	7.580	0.780	2.880
12	1.000	0.800	3.000
13	0.100	0.570	3.670
14	3.000	0.570	3.670
15	20.030	0.400	3.670
16	30.000	0.900	3.670
17	30.000	0.570	3.670
18	12.000	0.800	5.000
19	15.050	0.650	5.250
20	15.050	0.900	5.250
21	0.100	0.900	6.830
22	10.070	0.400	6.830
23	30.000	0.400	6.830
24	22.520	0.780	7.630
25	0.100	0.400	10.000
26	0.100	0.650	10.000
27	3.000	0.800	10.000
28	15.050	0.650	10.000
29	15.050	0.900	10.000
30	20.030	0.400	10.000
31	30.000	0.570	10.000
32	30.000	0.900	10.000
33	1.000	0.800	10.000
34	5.000	0.600	10.000

C.3- Solvent/WAG Flooding

Run#	ΔP_D	W_R	V_{DP}	λ
1	0.007	1.805	0.570	7.435
2	0.333	2.750	0.650	5.250
3	0.659	0.500	0.400	0.500
4	0.161	4.078	0.580	10.000
5	0.007	2.750	0.650	5.250
6	0.053	5.000	0.560	0.500
7	0.007	5.000	0.900	0.500
8	0.659	3.560	0.790	7.757
9	0.395	0.500	0.485	8.005
10	0.659	5.000	0.818	0.500
11	0.154	1.040	0.900	5.345
12	0.255	5.000	0.800	7.768
13	0.581	0.550	0.738	3.350
14	0.659	5.000	0.400	0.500
15	0.007	4.415	0.725	3.113
16	0.007	3.425	0.423	0.500
17	0.346	0.725	0.723	6.960
18	0.007	0.500	0.400	3.833
19	0.659	1.243	0.588	10.000
20	0.441	1.940	0.853	9.824
21	0.007	2.750	0.800	5.250
22	0.463	4.235	0.900	3.214
23	0.626	5.000	0.548	4.775
24	0.626	3.268	0.545	0.722
25	0.515	4.370	0.400	9.240
26	0.398	1.963	0.675	0.500
27	0.154	4.280	0.413	4.775
28	0.141	0.680	0.575	0.975
29	0.659	5.000	0.900	10.000
30	0.007	5.000	0.400	9.715
31	0.043	0.500	0.770	10.000
32	0.333	2.750	0.650	10.000
33	0.659	1.918	0.400	5.393
34	0.128	1.783	0.400	10.000
35	0.346	5.000	0.573	0.548
36	0.333	1.000	0.650	5.250
37	0.421	1.715	0.400	1.545
38	0.659	0.500	0.900	8.955
39	0.375	5.000	0.575	7.382
40	0.146	2.818	0.825	0.747

41	0.395	0.500	0.900	0.500
42	0.007	3.650	0.900	9.145

Nomenclature

A= Area, acres
a_s= Active surfactant retention, mg/g rock
ASP= Alkaline-Surfactant-Polymer
BHP= Bottom hole pressure, psia
C= Storage capacity, fraction
C_A= Shape factor, dimensionless
C_s= Surfactant concentration, cc surf/cc sol
CDC= Capillary desaturation curve
CFPM= Chemical flood predictive model
C_m , F_m= Coordinates of point m on a F-C curve, fraction
C_p= Injectivity coefficient, psi/ft
D= Depth, ft
D_s= Adsorption pore volume, dimensionless
E_D= Displacement efficiency, fraction
E_{MBe}= Mobility buffer efficiency, fraction
E_V= Volumetric sweep efficiency, fraction
E_R= Ultimate recovery efficiency, fraction
E( )= Expected value operator
F= Flow capacity, fraction
f= Fractional flow, fraction
f_o= oil cut, fraction
FSI (S_i)= First (main or individual) sensitivity index
H= Thickness (total), ft
h= Layer thickness, ft
H_K= Koval heterogeneity factor, dimensionless
K= Koval factor, dimensionless
k= Permeability, md
LHS= Latin hypercube sampling
M^o= Endpoint mobility ratio, dimensionless
MC= Monte Carlo Simulation
MMP= Minimum miscibility pressure, psia
MP= Micellar-Polymer
N_c= Capillary number
N_p= Oil production, STB
OOIP= Original oil in place, STB
P= Pressure, psi
q= Flow rate, bbl/day
R^2= Correlation Coefficient, dimensionless
Rb= Reservoir barrels

r_w= Radius, ft
S_{or}= Residual oil saturation after EOR, fraction
S_{oR}= Remaining oil saturation at start of EOR or Waterflood, fraction
SA= Sensitivity analysis
SP= Surfactant-Polymer
STB= Stock tank barrel
t_D= Dimensionless time, dimensionless
t_{DB}= Dimensionless oil bank break through time, dimensionless
t_{DMB}= Mobility buffer slug size, dimensionless
t_{Ds}= Dimensionless peak oil rate time, dimensionless
t_{Dsw}= Dimensionless sweep out time, dimensionless
TORIS= Tertiary oil recovery information system
TSI (S_{Ti})= Total sensitivity index
V_{DP}= Dykstra-Parsons coefficient dimensionless
V_p= Pore volume, dimensionless
V( )= Variance operator, units depend on argument
W_R= WAG ratio, dimensionless
WS= Winding stairs
x_D: Dimensionless distance, dimensionless

Greek Symbols

φ= Porosity, fraction
ρ= Density, gr/cm^3
μ= Viscosity, cp
σ= Interfacial tension, mN/m
v= Specific velocity, dimensionless
λ= Geostatistical dimensionless correlation length, dimensionless

Subscripts and Superscripts

B= Oil bank
BT= Break through
C= Chemical or displacing agent
F=Final
f= front
I= Initial
i= original
J= Injection
MB= Mobility buffer
o= Oil
p= Pattern

pk= Peak
r= Rock
S= Surfactant, Solvent
SW= Sweep-out
w= Water
^= Heterogeneous media

References

Alpak, F and Lake, L., "Validation of a Modified Carman-Kozeny Equation to Model Two-Phase Relative Permeabilities. SPE paper 56479 presented at Society of Petroleum Engineers Annual Technical Conference and Exhibition held in Houston, Texas, USA, October 3-6, 1999.

Anada, H.R. and Watts, R.J., "Sate of The Art Review of Nitrogen and Flue Gas Flooding in Enhanced Oil Recovery", DOE report, DOE/MC/08333-2, December 1980.

Bae, J.H., "Glenn Pool Surfactant Flood Expansion Project: A Technical Summary", SPE Reservoir Engineering, 1995, 10, No. 2, 123-128.

Bae, J.H., and E.U. Syed., "Glenn Pool Surfactant Flood Pilot Test: Part 2-Field Operations", SPE Reservoir Engineering 3, No. 3 (1988): 771-777.

Boehm, B.W., *Software Engineering Economics*, Prentice Hall, Englewood Cliffs, NJ, 1981.

Borah, M.T., and M.D. Gregory, "A Summary of the Big Muddy Field Low-Tension Flood Demonstration", SPE paper 17536 presented at the SPE Rocky Mountain Regional Meeting, held in Caspar, WY, May 11-13, 1988.

Box, G.E.P. and Draper, N.R., *Empirical Model-Building and Response Surfaces*, John Wiley and Sons, New York, 1987, p. 424.

Bragg, J.R., Gale, W.W. and Canning, J.W., "Loudon Surfactant Flood Pilot-Overview and Update", SPE paper 11505 presented at the SPE Middle East Oil Technical Conference, Manama, Bahrain, 14-17 March, 1983.

Brokmeyer, R.J., Borling, D.C. and Pierson, W.T., "Lost Soldier Tensleep CO_2 Tertiary Project, Performance Case History; Bairoil, Wyoming", SPE paper 35191 presented at the Permian Basin Oil and Gas Recovery Conference, Midland, TX 27-29 March, 1996.

Buckley, S.E. and Leverett., M.C., "Mechanism of Fluid Displacements in Sands", Transactions of the AIME, Vol. 146, 1942, 107–116.

Caudle, B.H. and Dyes, A.B., "Improving Miscible Displacement by Gas-Water Injection", Transactions of AIME, 1959, 213, 281-284.

Chan, K., Salteli, A. and Tarantola, S., "Winding Stairs: A Sampling Tool to Compute Sensitivity Indices", Statistics and Computing, Vol. 10, 2000, 187-196.

Chang, S.H., Owusu, L.A., French, S.B. and Kovarik, F.S., “The Effect of Microscopic heterogeneity on CO_2-Foam Mobility: Part 2-Mechanistic Foam Simulation”, SPE

paper 20191 presented at the SPE/DOE seventh Symposium on Enhanced Oil Recovery held in Tulsa, Oklahoma, April 22-25, 1990.

Chapotin, D., Lomer, J. and Putz, A., "Chateaurenard (France) Industrial Microemulsion Pilot Design and Performance", SPE paper 14955 presentated at the SPE/DOE Fifth Symposium on Enhanced Oil Recovery of the Society of Petroleum Engineers and the Department of Energy held in Tulsa, OK, April 20-23, 1986.

Chen, G., Han, P., Shao, Z., Zhang, X., Ma, M., Lu, K. and Wei, C., "History Matching Method for High Concentration Viscoelasticity Polymer Flood Pilot in Daqing Oilfield", SPE paper 144538 presented at the SPE Enhanced Oil Recovery Conference held in Kuala Lumpur, Malaysia, July 19-21, 2011.

Christensen, J R, Stenby, E H, and Skauge, A, "Review of the WAG field experience", SPE paper 71203 presented at the SPE International petroleum conference and exhibition, Mexico, Villhermosa, March 3-5, 1998.

Christopher, C.A., Clark, T.J. and Gibson, D.H., "Performance and Operation of a Successful Polymer Flood in the Sleepy Hollow Reagan Unit", SPE paper 17395 presented at the SPE/DOE Enhanced Oil Recovery Srymposium held in Tulsa, Oklahoma, April 17-20, 1988.

Claridge, E.L., "Prediction of Recovery in Unstable Miscible Flooding", Paper SPE 2930, SPE Journal, September 1971.

Clark, S.R., Pitts, M.J. and Smith, S.M., "Design and Application of Alkaline-Surfactant-Polymer Recovery System to the West Kiehl", SPE Advanced Technology Series, 1993, Vol. 1, No. 1, 172-179.

Craig, F. F., Geffen, T. M. and Morse, R. A., *Oil Recovery Performance Of Pattern Gas Or Water Injection Operations From Model Tests*, Petroleum Transactions, AIME, 1955, Vol. 204, 7-15.

Crane, F.E., Kendal, H.A. and Gardner, G.H.F., "Some Experiments on the low of Miscible Fluids of Unequal Density Through Porous Media", SPE paper 535, SPEJ, November 1963.

Dake, L.P., *Fundamentals of Reservoir Engineering*", "Elsevier/North-Holland Inc., New York, 1979.

Danielson, H.H., Paynter, W.T. and Milton, H.W., "Tertiary Recovery by the Maraflood Process in the Bradford Field." Journal of Petroleum Technology, 1976, 28, No. 2, 129-138.

Demin, W., Jiecheng, C., Junzheng, W., Zhenyu, Y., Yuming, Y. and Hongfu, L., "Summary of ASP Pilots in Daqing Oil Field", SPE paper 57288, presented at SPE Asia Pacific Improved Oil Recovery Conference to be held in Kuala Lumpur, Malaysia, 25–26 October, 1999.

Dietz, D.N., "A Theoretical Approach to the Problem of Encroaching and By-Passing Edge Water. Akad. Van Watenschappen, Amsterdam Proceeding, 1953, 56-B, 83-92.

Dao, E.K., Lewis, E. and Mohanty, K.K., "Multicontact Miscible Flooding in a High-Pressure Quarter Five-Spot Model", SPE paper 97198 presented at the SPE Annual technical Conference and Exhibition held in Dallas, Texas, October 9-12, 2005.

Duane, N.C. and Dauben, D.L., "Evaluation of the Coalinga Polymer Demonstration Project", DOE report, DOE/BC/10033-7, April 1983.

Dunn, P., "James Lind (1716-94) of Edinburgh and the treatment of scurvy", Archive of Disease in Childhood Fetal Neonatal, United Kingdom, British Medical Journal Publishing Group, January 1997, 76, No. 1, 64–65.

Dyes, A. B., Caudle, B. H. and Erikson, R.A., *Oil Production After Breakthrough As Influenced By Mobility Ratio*, Petroleum Transactions, AIME, April 1954, 27-32.

Dykstra, H., and Parsons, R.L., "The Prediction of Oil Recovery by Water Flood", Secondary Recovery of Oil in the United States, 2nd ed., API (1950) 160-174.

Fanchi, J.R. and Carroll, H.B., "Evaluation of the Wilmington Field Micellar/Polymer Project", SPE Reservoir Eng., May 1988, 609-616.

Farajzadeh, R., Matsuura, T., Van Batenburg, D., Dijk, H., and Rijswijk, B.V., "Detailed Modeling of the Alkali Surfactant Polymer (ASP) Process by Coupling a Multi-purpose Reservoir Simulator to the Chemistry Package PHREEQC", Paper SPE 143671 presented at the SPE Enhanced Oil Recovery Conference held in Kuala Lumpur, Malaysia, July 19-21, 2011.

Fayers, F.J., "An Approximate Model with Physically Interpretable Parameters for Representing Viscous Fingering", SPE Reservoir Eng. Journal, 1988, 551–558.

Fayers, F.J., Jouaux F., and Tchelepi H.A., "An Improved Macroscopic Model For Viscous Fingering And Its Validation for 2D and 3D Flows-I. Non-gravity Flows", In Situ,1994, 18, 43–78.

Ferrell, H.H., King, D.W. and Sheely, C.Q., "Analysis of the Low-Tension Pilot at Big Muddy Field, Wyoming", SPE Formation Evaluation, 1988, 3, No. 2, 315-321.

Fisher, R. A., "The Arrangement Of Field Experiments", Journal of the Ministry of Agriculture of Great Britain, 1926, 33, 503-513.

Flanders, W.A. and DePauw, R.M., "Update Case History: Performance of the Twofreds Tertiary CO_2 Project", SPE paper 26614 presented at the annual Technical Conference and Exhibition of the Society of Petroloum Engineers held in Houston, TX, October 3-6, 1993.

Fox, B. L., "Algorithm 647: Quasirandom Sequence Generators", ACM Transactions on Mathematical Software, December 1986, 12, No. 4, 363-376.

French, M.S., Stegemeier, G.L., Ueber, R.C., Abrams, A. and Hill, H.J., "Field Test of an Aqueous Surfactant System for Oil Recovery, Benton Field, Illinois", Journal of Petroleum Technology, 1973, 25, No. 2, 195-204.

Garcia Quijada, M., "Optimization of a CO_2 Flood Design, Wasson Field-West Texas", Master Thesis, Texas A&M University, 2005.

Gaviria Garcia, R., "Reservoir Simulation of CO_2 Sequestration and Enhanced Oil Recovery in the Tensleep Formation, Teapot Dome Field", Master Thesis, Texas A&M University, 2005.

Ghanbarnezhad, R. and Lake, L.W., "Simultaneous Water-Gas-Injection Performance Under Loss of Miscibility", Paper SPE 129966 presented at the SPE Improved Oil Recovery Symposium, Tulsa, Oklahoma, USA, 24-28 April, 2010.

Giordano, R.M., "Estimating Field-Scale Micellar/Polymer Performance", SPE paper 16731, presented at society of petroleum engineers annual technical conference held in Dallas, Texas USA, 27-30 September 1987.

Gogarty, W.B., and Surkalo, H., "A Field Test of Micellar Solution Flooding", Journal of Petroleum Technology, 1972, 24, No. 9, 1161-1169.

Green D.W., and Wilhite G.P, *Enhanced Oil Recovery*, SPE, Richardson, Texas, 1998.

Guckert, L. G. and Paynter, W.T., "Micellar-Polymer Flooding Projects in the Bradford Field", SPE paper 10027 presented at International Petroleum Exhibition and Technical Symposium of Society of Petroleum Engineers held in Beijing, China, March 18-26, 1982.

Hartshorne, J.M. and Nikonchik, J.S., "Micellar/Polymer Flood Shows Success in Bell Creek Field", SPE paper 13122 presented at the SPE 59th annual Technical Conference and Exhibition held in Houston, Texas, U.S.A., September 15-19, 1984.

Helton, J. C. and Davis, F. J., "Latin Hypercube Sampling and the Propagation of Uncertainty in Analyses of Complex Systems", Reliability Engineering and System Safety, 2003, 81, 23–69.

Helton, J. C. Oberkampf, W. L., and Johnson, J. D., "Competing Failure Risk Analysis Using Evidence Theory", Risk Analysis, 2005, 25, No. 4, 973-994.

Hirasaki, G. and Zhang, D. L., "Surface Chemistry of Oil Recovery From Fractured, Oil-Wet, Carbonate Formations", SPE Journal, 2004, 22, No. 9, 151-62.

Hoiland, R.C., Joyner, H.D.and Stalder, J.L., "Case History of a Successful Rocky Mountain Pilot CO_2 Flood", SPE paper 14939 presented at SPE/DOE Fifth Symposiumon Enhanced Oil Recovery, Tulsa, Oklahoma, April 20-23, 1986.

Jansen, M. J. W., Rossing, W. A. H., and Daamen, R. A., "Monte Carlo Estimation of Uncertainty Contributions from Several Independent Multivariate Sources, in: Predictability and Nonlinear Modeling in Natural Sciences and Economics", Gasman, J. and van Straten, G. eds. Kluwer Academic Publishers, 1994, 334–343.

Jarrel, P.M., Fox, C.E., Stein., M.H. and Webb, S., *Practical Aspects of CO_2 Flooding*, Monograph Series, SPE, Richardson, Texas, 2002.

Jennings, J.W., Ruppel, S.C. and Ward, W.B., "Geostatistical Analysis of Fluid-Flow Effects in Carbonate Outcrops", SPE Res Eval & Eng, 2002, 3, 292.

Jensen, T.B., Harpole, K.J., Osthus, A., "EOR Screening for Ekofisk", SPE paper65124 presented at the SPE European Petroleum Conference held in Paris, France, 24-25 October, 2000.

Joe, S. and Kuo, F. Y., "Remark on Algorithm 659: Implementing Sobol's Quasirandom Sequence Generator", ACM Trans. on Mathematical Software, 2003, 29 (1) March, 49–57.

Johnson, N. L., Kotz, S., and Kemp, A. W., "Univariate Discrete Distributions", second edition, John Wiley and Sons, New York, 1992.

Johnson, J.P., "Predicting Waterflood Performance by the Graphical Representation of Porosity and Permeability Distribution", SPE paper 918, SPE Reservoir Engineering, November 1965.

Jones, R.S., Pope, G.A., Ford, H.J. and Lake, L.W., "A Predictive Model for Water And Polymer Flooding", SPE paper 12653 presented at the SPE/DOE Fourth Symposium on Enhanced Oil Recovery held in Tulsa, OK, April 15-18, 1984.

Kocis, L. and Whiten, W. J., "Computational Investigations of Low-Discrepancy Sequences", ACM Transactions on Mathematical Software, 1997, 23 (2) June: 266-294.

Kleinstelber, S.W., "The Wertz Tensleep CO_2 Flood: Design and Initial Performance", Journal of Petroleum Technology, 1990, 42, No. 5, 630-636.

Koning, E.J.L., Mentzer, E. and Heemskerk, J., "Evaluation of a Pilot Polymer Flood in the Marmul Field, Oman", SPE paper 18092 presented at the annual Technical Conference and Exhibition of the Society of Petroloum Engineers held in Houston, TX, October 2-5, 1988.

Koval, E.J., "A Method for Predicting the Performance of Unstable Miscible Displacement in Heterogeneous Media", Paper SPE 450, SPE Journal, June 1963.

Krumrine, P.H. and Boyce, S.D., "Profile Modification and Water Control With Silica Gel-Based Systems", SPE paper 13578 presented at the SPE Oilfield and Geothermal Chemistry Symposium held in Phoenix, Arizona, March 9-11, 1985.

Kumar, M., Hoang, V., Satik, C. and Rojas, D., "High-Mobility-Ratio-Waterflood Performance Prediction: Challenges and New Insights", SPE Reservoir Evaluation & Engineering Journal, February 2008, 11, No. 1, 186-196.

Lake, L.W., *Enhanced Oil Recovery*, Prentice-Hall, Inc., Upper Saddle River, New Jersey, 1989.

Lake, L.W., Stock, L.G. and Lawson, J.B., "Screening Estimation of Recovery Efficiency and Chemical Requirements for Chemical Flooding", SPE paper 7069, presented at fifth symposium of improved oil recovery of the society of petroleum engineers held in Tulsa, Oklahoma USA, 16-19 April 1978.

Lake, L.W. and Walsh, M.P., "Enhanced Oil Recovery (EOR) Field Data Literature Search ", Technical Report, The University of Texas at Austin, 2008.

Langston, M.V., S.F. Hoadley, and D.N. Young, "Definitive CO_2 Flooding Response in the SACROC Unit", Paper SPE 17321 presented at the SPE Enhanced Oil Recovery Symposium, Tulsa, Oklohoma, USA, 17-20 April 1988.

Lawal, A., "Application of Sensitivity analysis in Petroleum Engineering", Master Thesis, The University of Texas at Austin, 2007.

Lawal, A. and Lake, L.W., "Sensitivity Analyses of Production and Recovery Forecasts Using Variance-Based Methods", SPE paper 110846, presented at Society of Petroleum Engineers joint meeting held in Bakersfield, California USA, 31 March- 2 April 2008.

Lazar, I., I.G. Petrisor, and T.E. Yen, "Microbial Enhanced Oil Recovery (MEOR)", Journal of Petroleum Science and Technology, 2007, 25(11-12), 1353-1366.

Mack, J.C and Duvall, M.L., "Performance and Economics of Minnelusa Polymer Floods", SPE paper 12929 presented at the Rocky Mountain Regional Meeting of the Society of Petroloum Engineers held in Casper, WY, May 21-23, 1984.

Masoner, L.O. and Wackowski, R.K., "Rangely Weber Sand Unit CO_2 Project Update", SPE Reservoir Engineering, 1995, 10, No. 3, 203-207.

Martin, F.D. and Taber, J.J., "Carbon Dioxide Flooding", SPE Technology Today Series April 1992, 396 -400.

Mathiassen, O.M., "CO_2 as Injection Gas for Enhanced Oil Recovery and Estimation of the Potential on the Norwegian Continental Shelf", Master Thesis, Norwegian University of Science and Technology (NTNU), 2003.

McKay, M. D., Beckman, R. J., and Conover, W. J., "A Comparison of Three Methods for Selecting Values of Input Variables in The Analysis of Output From Computer Code", Technometrics 42 (1), special 40th anniversary issue, 2000, February: 55-61.

Mohammadi, H., "Mechanistic Modeling, Design, and Optimization of Alkaline/Surfactant/Polymer Flooding", PhD dissertation, The University of Texas at Austin, 2008.

Mollaei, A. and Delshad, M. 2011, "General Isothermal Enhanced Oil Recovery and Waterflood Forecasting Model", SPE paper 143925 presented at the 86th Annual Technical Conference and Exhibition of the Society of Petroleum Engineers held in Denver, Colorado, October 30-Novemebr 2, 2011b.

Mollaei, A., Lake, L.W. and Delshad, M., "Application and Variance Based Sensitivity Analysis of Surfactant-Polymer Flood", Journal of Petroleum Science and Engineering, 79, Issues 1-2, 25-36, 2011a.

Nasir, F.M. and Chong, Y.Y., "The Effect of Different Carbon Dioxide Injection Modes on Oil Recovery", International Journal of Engineering and Technology (IJET), 29, No. 10, 66-72, 2009.

Nelson, R.C., "The Salinity Requirement Diagram-A Useful Tool In Chemical Flooding Research And Development", SPE Journal, 1982, 259-270.

Ondrusek, P.S., "Micellar/Polymer Flooding in the Bradford Field", Journal of Petroleum Technology, 1988, 40, No. 8, 1061-1067.

Patton, J.T., "Prediction of Polymer Flood Performance", SPE paper 2546, presented at society of petroleum engineers annual technical conference held in Denver, Colorado USA, 28 October 1969.

Paul, W., Lake, L.W., Pope, G.A. and Young, G.B., "A Simplified Predictive Model for Micellar-Polymer Flooding", SPE paper 10733, presented at regional meeting of Society Of Petroleum Engineers held in California USA, 24-26 March 1982.

Paul, W., Lake, L.W. and Gould, T.L., "A Simplified Predictive Model for CO_2 Miscible Flooding", SPE paper 13238, presented at annual technical conference of Society Of Petroleum Engineers held in Houston, Texas USA, 16-19 September 1984.

Peters, E., *Petrophysics*, In Press, The University of Texas at Austin, 2012.

Pitts, M.J., P. Dowling, K. Wyatt, H. Surkalo, and C. Adams, "Alkaline-Surfactant-Polymer Flood of the Tanner Field", SPE paper 100004 presented at SPE/DOE Symposium on Improved Oil Recovery, Tulsa, Oklahoma, April 22-26, 2006.

Pope, G.A., "The Application of Fractional Flow Theory to Enhanced Oil Recovery", SPE Journal, 1980, 20, No. 3: 191-205.

Pope, G.A., chemical EOR laboratory coreflooding data, September 2011.

Pursley, S.A. and Graham, H.L., "Borregos Field Surfactant Pilot Test", Journal of Petroleum Technology, 1975, 27, No. 6, 695-700.

Putz, A.G., Bazin, B. and Pedron, B.M., "Commercial Polymer Injection in the Courtenay Field, 1994 Update", SPE paper 28601 presented at the SPE 69th

annual Technical Conference and Exhibition held in New Orleans, LA, U.S.A., September 25-28, 1994.

Putz, A., Chevalier, J.P., Stock, G. and Philippot, J., "A Field Test of Microemulsion Flooding, Chateaurenard Field, France", Journal of Petroleum Technology, 1981, 33, No. 4, 710-718.

Qi, Q., Hongjun, G., Dongwen, L. and Ling., D., "The Pilot Test of ASP Combination Flooding in Karamay Oil Field" SPE paper 64726, presented at International Oil and Gas Conference and Exhibition held in Beijing, China, 7-10 November 2000.

Rowe, H.G., York, D.S. and Ader, J.C., "Slaughter Estate Unit Tertiary Pilot Performance", Journal of Petroleum Technology, 1982, 34, No. 3, 613-620.

Saad, N., Pope, G.A. and Sepehrnoori, K., "Simulation of Big Muddy Surfactant Pilot", SPE Reservoir Engineering, 1989, 4, No. 1, 24-34.

Salteli, A., "Sensitivity Analysis for Importance Assessment", Risk Analysis, 22 (3): 579-590, www.ce.ncsu.edu/risk/pdf/saltelli.pdf, December 2009.

Salteli, A., Chan, K. and Scott, E. M., *Sensitivity Analysis*, Wiley series in probability and statistics, John Wiley and Sons Ltd, 2000a.

Salteli, A., Tarantola, S. and Chan, K.: "A Quantitative Model-Independent Method of Global Sensitivity Analysis of Model Output" Technometrics, Risk Analysis, Vol. 41, No. 1, February 1999.

Salteli, A., Tarantola, S., Campolongo, F. and Ratto, M., *Sensitivity Analysis in Practice: A Guide to Assessing Scientific Models*, John Wiley and Sons Ltd., New York, 2000b.

Sanchez, N.L., "Management of Water Alternating (WAG) Injection Projects", SPE paper 53714 presented at the Latin American and Caribbean Petroleum Engineering Conference, Caracas, Venezuela, 21-23 April, 1999.

Sayarpour, M., "Development and Application of Capacitance-Resistive Models to Water/CO_2 Floods", PhD Dissertation, The University of Texas at Austin, 2008.

Sayarpour, M., C. S. Kabir and L. W. Lake, "Field Applications of Capacitance Resistive Models in Waterfloods", paper SPE 114983, presented at Society of Petroleum Engineers Annual Technical Conference and Exhibition held in Denver, Colorado, USA, 21-24 September, 2008.

Simon, R. and Graue, D.J., "Generalized Correlations for Predicting Solubility, Swelling and Viscosity Behavior of CO_2-Crude Oil Systems", Journal of Petrol Technology., 1965, 17(1), 102-106.

Sorbie, K., *Polymer Improved Oil Recovery*, Blackie and Son Ltd, Glasgow, 1991.

Sobol, I. M., "On the Systematic Search in a Hypercube", SIAM J. of Numerical Analysis, 1979, 16 (5): 790-793.

Stein, M., "Large Sample Properties of Simulations Using Latin Hypercube Sampling", Technometrics, 1987, 29 (2), 143-151.

Stiles, W.E., "Use of Permeability Distribution in Water Flood Calculations", Petroleum Transcripts, AIME, January 1949.

Stover, D.F., "Commercial Scale demonstration enhanced oil recovery by micellar-polymer flood", DOE report, DOE/ET/13077-130, November 1988.

Strange, L.K. and Talash, A.W., "Analysis of Salem Low-Tension Waterflood Test", Journal of Petroleum 29, No. 11 (1977): 1380-1384.

Taber, J.J., Martin, F.D. and Seright, R.S., "EOR Screening Criteria Revisited-Part 1: Introduction to Screening Criteria and Enhanced Recovery Field Projects", SPE Reservoir Engineering, 1997, Vol. 12, Number 3, 189-198.

Takaqi, S., Pope, G.A. and Sepehrnoori, K., "Simulation of a Successful Polymer Flood in the Chateaurenard Field", Paper SPE 24931 presented at the 67th Annual Technical Conference and Exhibition of the Society of Petroleum Engineers held in Washington, DC, October 4-7, 1992.

Taylor, A. R., Hinterlong, G.H. and Kumar, K.H., "West Welch CO_2 Flood Simulation with an Equation of State and Mixed Wettability", Paper SPE 39808 presented at the SPE Permian basin Oil and Gas recovery Conference, Midland, Texas, USA, 25-27 March, 1998.

Tezuka, S., *Uniform Random Numbers: Theory and Practice*, Kluwer International Series in Engineering and Computer Science, Kluwer Academic Publishers, Dordrecht, Netherlands, 1995.

Todd, M.R. and Longstaff, W.J., "The Development, Testing, And Application of A Numerical Simulator For Predicting Miscible Flood Performance", Journal of Petroleum Technology, 1972, 874–882.

TORIS, "Tertiary Oil Recovery Information System", TORIS Data Preparation Guidelines, Management and Operating Contract for the Department of Energy's National Oil and Related Programs, http://www.netl.doe.gov/KMD/cds/disk41/Disk41.html, 1995.

Trantham, J.C., and Patterson, H.L., "The North Burbank Unit, Tract 97 Surfactant/Polymer Pilot Operation and Control", Journal of Petroleum Technology, 1978, 30, No. 7, 1068-1074.

Trantham, J.C., Threlkeld, C.B. and Patterson, H.L., "Reservoir Description for a Surfactant/ Polymer Pilot in a Fractured, Oil-Wet Reservoir-North Burbank Unit Tract 97", Journal of Petroleum Technology, 1980, 32, No. 9, 1647-1656.

Tzimas, E., Georgakaki, A., Garcia Cortes, C. and Peteves., S.D., "Enhanced Oil Recovery using Carbon Dioxide in the European Energy System", European Commission Joint Research Center, 2005.

Vargo, J.J., "Site Selection, Reservoir Definition and Estimation of Tertiary Target Oil for the Bell Creek Unit "A" Micellar-Polymer Project", SPE paper 7072 presented at the fifth Sympoalumon Improved Methods for oil Recovery of the Society of Petroleum Engineers of AIME held in Tulsa,Oklahoma, April16-19,1978.

Vargo, J., Turner, J., Vergnani, B, Pitts, M.J., Wyatt, K., Surkalo, H. and Patterson, D., "Alkaline-Surfactant-Polymer Flooding of the Cambridge Minnelusa Field", SPE Reservoir Evaluation & Engineering, 2000, 3, No. 6, 552-558.

Wang, D. and Hao, Y., " Results of Two Polymer Flooding Pilots in the Central Area of Daqing oil Field", SPE paper 26401, presented at the 68th Annual Technical Conference and Exhibition of the Society of Petroleum Engineers held In Houston, Texas, 3-6 October 1993.

Walsh, M. P. and Lake, L. W., 1989, "Applying Fractional Flow Theory to Solvent Flooding and Chase Fluids", Journal of Petroleum and Science Engineering, 2 (44).

Wanosik, J.L., L.E. Treiber, L.E., Myal, F.R. and Calvin, J.W., "Sloss Micellar Pilot: Project Design and Performance", SPE paper 7092 presented at the Fifth Symposium on Imroved Methods for Oil Recovery of the Society of Petroleum Engineers of AIME held in Tulsa, Oklahoma, April l6-19, 1978.

Welge, H.J., "A Simplified Method for Computing Oil Recovery by Gas or Water Drive" Trans. AIME, 1952, 195: 91-98.

Widmyer, R.H, D.B. Williams, and J.W. Ware., "Performance Evaluation of the Salem Unit Surfactant/Polymer Pilot", Journal of Petroleum Technology, 1988, 40, No. 9, 1217-1226.

Widmyer, R.G. and Pindell, R.G., "Manvel Enhanced Recovery Pilot Performance Evaluation", SPE paper 9793 presented at the SPE/DOE Enhanced Oil Recovery Symposium, Tulsa, Oklahoma, April 5-8, 1981.

Wyatt, K., Pitts, M. and Surkalo, H., "Economics of Field Proven Chemical Flooding Technologies", SPE paper 113126 presented at the SPE/DOE Improved Oil recovery Symposium held in Tulsa, Oklahoma, April 19-23, 2008.

Wyss, G. D. and Jorgensen, K. H., "A User's Guide to LHS: Sandia's Latin Hypercube Sampling Software", SAND Report, SAND98-0210 Distribution, Unlimited Release Category UC-505, February. Risk Assessment and Systems Modeling Department, Sandia national laboratories, 1998.

Yang, Z.M., Yortsos, Y.C., Salin, D., "Asymptotic Regimes In Unstable Miscible Displacements In Random Porous Media", Advances in Water Resources, 2002, 25, 885–898.

Zornes, D.R., Cornelius, A.J. and Long. H.Q., "An Overview and Evaluation of the North Burbank Unit Block A Polymer Flood Project, Osage County, Oklahoma", SPE

paper 14113 presented at the SPE International Meeting on Petroleum Engineering held in Beijing, China, March 17-20, 1986.

Anonymous, "A Cookbook for Applying Sensitivity Analysis in Practical Cases of Modeling", http://webfarm.jrc.cec.eu.int/uasa/cookbook.pdf. May 2005 .

Anonymous, "Electronic Statistics Textbook from StatSoft Inc.", http://www.statsoft.com/textbook/, June 2010.

Anonymous: "Assumptions, Models, and the Scientific Method", Genesis Journal, Cosmic Chemistry: Cosmogony, Appendix B, from: "http://genesismission.jpl.nasa.gov/educate/scimodule/Cosmogony/CosmogonyPDF/AppendixB.pdf", August 2011.

Anonymous, "Forecasting Principles", http://www.forecastingprinciples.com/index.php?option=com_content&task=view&id=3&Itemid=3, October 2011.

Vita

Alireza Mollaei was born in Iran. He obtained his BSc and MSc in petroleum engineering from Petroleum University of Technology (Iran) and MEng from University of Calgary (Canada) in 2003 and 2005 respectively before enrolling in The University of Texas at Austin for PhD in Spring of 2008. He worked as reservoir engineer in some oil companies such as Chevron and Occidental and accomplished his PhD in Fall of 2011.

Email: armollaei@gmail.com

This dissertation was typed by Alireza Mollaei.